UNIVERSITÀ DEGLI STUDI DI PADOVA

DIPARTIMENTO DI GEOSCIENZE

SCUOLA DI DOTTORATO DI RICERCA IN SCIENZE DELLA TERRA

CICLO XXIII

GEOCHEMICAL AND ISOTOPIC TRACERS IN COPPER DEPOSITS AND ANCIENT ARTIFACTS: A DATABASE FOR PROVENANCE

Direttore della Scuola: Ch.mo Prof. Gilberto Artioli

Supervisore: Ch.mo Prof. Gilberto Artioli

Ch.mo Prof. Paolo Nimis

Dottorando: Ilaria Giunti

Index

Abstract

The provenance of metal artifacts in the early history of metallurgy has been a major question in archaeology for many decades. Pb isotope ratios ($^{206}Pb/^{204}Pb$, $^{207}Pb/^{204}Pb$, $^{208}Pb/^{204}Pb$) are commonly used for provenancing in archaeometry, but interpretations are hardly debated and sometimes ambiguous because natural ore deposits frequently show overlapping Pb isotopic compositions. The first way to reduce observed overlaps is by improving the analytical precision. The second way to reduce ambiguities is to combine the lead isotopic signature with other geochemical indicators, e.g. minor and trace elements or other isotopic data. Extraction of reliable provenance information from a combination of several geochemical tracers, however, requires sophisticated statistical analysis. Here, more than 350 samples were collected from 50 mining areas. Some of the most important copper districts in the central-eastern Southern Alps (*Variscan basement and Permian-Triassic cover, Carnic Alps*), in the Western Alps (*Piedmont Zone, Ligurian Briançonnais, Gran Paradiso nappe, Argentera*), in the Ligurian Apennines (*Libiola, Monte Loreto*) and the Southern Tuscany (*Isola d'Elba, "Colline metallifere" and Montecatini Val di Cecina*). About 270 samples of primary (copper and copper-iron sulfides and copper sulphosalts) and secondary (supergenic copper carbonates and oxides and native copper) raw minerals and archaeological finds (slags, copper and bronze artifacts of Chalcolithic to Late Bronze Age) were analyzed for lead isotopes and minor and trace elements (including most transition metals and chalcophile elements and the REE). Moreover, the feasibility of the routine measurement of the $^{65}Cu/^{63}Cu$ isotope ratio and its use as a possible ore tracer was also tested. An advanced statistical investigation (PCA, PLS-DA, NPC) has been carried out on the database to provide discriminant statistic tools for metal provenancing.

The samples were first characterized mineralogically and petrologically (XRD, RL-OM), and then analysed by ICP-QMS (Inductively Coupled Plasma-Quadrupolar Mass Spectrometry) for trace elements and $^{65}Cu/^{63}Cu$ isotopic ratios. Multicollector ICP mass spectrometry (MC-ICP-MS) was used to determine precise Pb isotopic ratios ($^{206}Pb/^{204}Pb$, $^{207}Pb/^{204}Pb$, $^{208}Pb/^{204}Pb$).

The chemical/isotopic dataset of the mines was analysed with Principal Component Analysis (PCA) and Partial least Square-Discriminant Analysis (PLS-DA). The chemical and isotopic data were arranged into a bidimensional matrix characterized by samples (objects) in the rows and the chemical measurement as the variables in the columns. The dataset was also analysed with the Nonparametric Combination (NPC) test, which is an inferential multivariate nonparametric method that frees from the stringent assumptions of parametric methods (such as *t* and *F* test) and allows a more flexible analysis both in terms of specification of multivariate hypotheses and in terms of the nature of the variables involved. One of the most important advantages of applying nonparametric statistics like permutation tests, is that it allows one to relax the assumption of normality of response variables. Moreover, the NPC Test does not requires modelling of dependence among variables and is not affected by the problem of loss of degrees of freedom when the number of variables is large compared to sample size. Results of NPC

Test analysis were obtained using the free software NPC Test R10, where as test statistic we used the F-test and as combining function we used the Fisher combining function (Pesarin, 2001). The results can be graphically represented by PCA.

The availability of an unprecedented and comprehensive amount of geochemical data for Alpine copper deposits yielded information relevant to their metallogenic interpretation. In particular, the isotopic compositions of trace lead in copper-bearing hydrothermal sulphide deposits from the central-eastern Southalpine region were combined with existing lead isotope data for hydrothermal polymetallic deposits in the same area and compared with the isotopic compositions of potential lead sources. Copper and polymetallic pre-Variscan (Late Ordovician–Early Silurian) stratiform, post-Variscan (Permian to Triassic) vein, and stratabound sediment-hosted (Permian to Early Triassic) deposits, are characterized by highly variable ratios of radiogenic to non-radiogenic lead, but show very similar, high, time-integrated μ (= $^{238}U/^{204}Pb$) and W (= $^{232}Th/^{204}Pb$) values. A progressive relative increase in radiogenic lead is observed from (i) pre-Variscan deposits to (ii) post-Variscan sulphide-rich veins in the Variscan metamorphic basement and in the lower–intermediate units of the Early Permian volcanic sequence to (iii) post-Variscan sulphide-rich and fluorite-rich veins in the upper units of the Early Permian volcanic sequence to (iv) post-Variscan fluorite-rich veins cutting the overlying Late Permian sediments and mid-Triassic mafic dikes. The dominant lead sources for all these deposits were Cambrian–Devonian (meta)sediments of the Variscan basement. Contributions from Permian and Triassic igneous rocks were of minor importance, if any, even for vein deposits which were evidently related to Permian magmatism

While Pb isotopic fingerprinting could potentially help identify the likely provenance of an archeological object, there are a number of related difficulties. First of all, natural ore deposits frequently have overlapping Pb isotopic compositions. So, trace elements, Rare Earth Elements and $^{65}Cu/^{63}Cu$ isotopic ratios were investigated in addition to lead isotopes.

Copper $^{63}Cu/^{65}Cu$ isotopic ratio is sensitive to the temperature of mineral segregation; therefore, it provides information on the nature of the mineral used for the object manufacturing. A statistical selection was carried out to detect the variables that more effectively distinguish the investigated ores. This was achieved using a PLS-DA strategy. This technique is a classification method that models the differences between two classes. The PLS method calculates a linear regression model between the predictors matrix (X) and the response vector (Y): in this particular case the Y vector is expressed with the binary code. The model provides scores and loading plots as well as the regression coefficient for each variable. An estimate of the statistical significance of these regression coefficients is also provided.

The statistical relevance of the variables was tested through the Martens Uncertainty test. The study of the correlation loadings and the model coefficients led to the definition of a variable subset capable to discriminate the samples coming from the different mining sites/areas. A single model was not sufficient and a multi-step exclusion strategy was required to attain a satisfactory discrimination. The procedure adopted can be summarized as follows: 1) the whole data set is taken into account and a PCA model is built. Through the study of the score plots generated by the combination of the first principal

components (usually PC1 to PC4) the most effectively discriminated locality is chosen for the exclusion process; 2) the next step is the variable selection in order to emphasize the differences between the selected locality and all other localities: the aim is to build a simple discriminant model using only PC1 or no more than two PCs; 3) the data related to the selected locality are excluded from the original matrix and the whole process is then repeated on this reduced matrix initially considering again all the variables.

The discriminating power of the database was tested for the provenancing of copper metals and slags from the Agordo area (BL) and of prehistoric copper fragment and slags from Millan (Bressanone, BZ). The samples were projected onto an existing PCA model, and their position compared with the position of the samples used to build the model. The same projection method was also used for the validation of the multiple step exclusion strategy.

Data for copper artifacts and slags from the Agordo area show that the discriminant model that best identifies the Agordo ores is perfectly applicable to the objects, clearly indicating that the metal was extracted from the local ores.

For the Millan case, the discriminating model of the deposits that best describes the copper fragment is the one that identifies the Val Venosta area (Oris, Val Martello, and Stelvio mines), located 80 km to the west of the archaeometallurgical site of Millan. This result suggests that the copper sample is genetically unrelated to the large amount of associated slags produced during the smelting of copper from local sphalerite/galena-rich chalcopyrite ores, which have a significantly different mineralogical and geochemical character.

A successful strategy to characterize copper ores and to trace the provenance of copper minerals and ancient copper objects was presented. A whole analytical protocol starting from the sampling to the quantitative analysis was developed to ensure geologically sound and good quality analytical data. The measurements of a wide group of elements including the Rare-Earth Elements (REE) together with the lead and copper isotopic ratio in Cu minerals allowed a full geochemical characterization of the investigated Cu-ores. The data collected were used to build a database that can be used as the fundamental reference frame for tracing of metal extraction and diffusion in the past. Application of advanced statistical techniques to the geochemical and isotopic data proved to be a powerful tool to discriminate the ore source areas. The presented applications to copper metal samples and slags seem to confirm that the analysis can be successfully performed on archaeometallurgical specimens. The availability of such an unprecedented and comprehensive amount of data for Alpine copper deposits also yield interesting information for their geochemical and metallogenic interpretation. In particular, the high μ and W values of the deposits from the central-eastern Southalpine are consistent with regional isotopic patterns of Pb–Zn-rich deposits in more northerly and easterly sectors of the Eastern Alps (Austroalpine, eastern Southalpine) and of several circum-Mediterranean Pb–Zn and polymetallic deposits of Paleozoic to Triassic age (Sardinia; Betic Cordillera) or derived from remobilization of Paleozoic deposits (Tuscany). This isotopic uniformity suggests the existence of an isotopic province characterized by the dominance of old (Early Proterozoic to Archean) detrital source material, extending across a relatively wide portion of the former north-Gondwanan margin.

Riassunto

La provenienza di manufatti metallici nella prima storia della metallurgia è stata il maggiore problema in archeologia per molte decadi. I rapporti isotopici del Pb ($^{206}Pb/^{204}Pb$, $^{207}Pb/^{204}Pb$, $^{208}Pb/^{204}Pb$) sono comunemente usati per definire la provenienza dei manufatti in archeometria, ma le interpretazioni sono fortemente dibattute e qualche volta ambigue dal momento che i depositi naturali mostrano di frequente composizioni isotopiche del Pb sovrapposte. Il primo modo di ridurre le sovrapposizioni osservate è di aumentare la precisione analitica. Il secondo modo di ridurre le ambiguità è di combinare la segnatura isotopica del piombo con altri indicatori geochimici, ad esempio con altri dati isotopici o di elementi minori e in traccia. L'estrazione di un'informazione di provenienza affidabile dalla combinazione di numerosi traccianti geochimici, tuttavia, richiede analisi statistiche sofisticate. Qui più di 350 campioni sono stati raccolti da 50 aree minerarie. Alcuni dei più importanti distretti di rame nella porzione centro-orientale delle Alpi meridionali (Alpi Carniche, copertura Permo-Triassica e basamento Varisico), nelle Alpi occidentali (Zona Pedemontana, Brianzonese Ligure, nappe del Gran Paradiso, Argentera), negli Appennini Liguri (Libiola, Monte Loreto) e nella Toscana meridionale (Isola d'Elba, "Colline metallifere" and Montecatini Val di Cecina). Sono stati analizzati circa 270 campioni di minerali grezzi primari (rame, solfuri di rame-ferro e solfo-sali di rame) e secondari (carbonati e ossidi di rame supergenico e rame nativo) e ritrovati archeologici (scorie, manufatti di rame e bronzo di età da Calcolitica a Tardo Bronzo) per analisi degli isotopi del piombo e degli minori e in tracce (inclusi la maggior parte dei metalli di transizione, elementi calcofili e terre rare). Inoltre è stata testata la fattibilità di misure di routine del rapporto isotopico del Cu ($^{65}Cu/^{63}Cu$) e del suo possibile uso come tracciante delle miniere. E' stata eseguita un'avanzata analisi statistica (PCA, PLS-DA, NPC) su un database per ottenere strumenti statistici discriminanti per la provenienza dei metalli.

I campioni sono stati prima caratterizzati mineralogicamente e petrologicamente (XRD e RL-OM) e successivamente analizzati mediante tecnica ICP-QMS (Spettrometri di Massa Quadrupolare mediante Plasma accoppiato induttivamente) per gli elementi in tracce e i rapporto isotopico $^{65}Cu/^{63}Cu$. E' stata usata la spettrometria di massa multicolletore (MC-ICP-MS) per la determinazione precisa dei rapporti isotopici del piombo ($^{206}Pb/^{204}Pb$, $^{207}Pb/^{204}Pb$, $^{208}Pb/^{204}Pb$).

L'insieme di dati chimico/isotopico delle miniere è stato analizzato con l'Analisi delle Componenti Principali (PCA) e con l'Analisi Discriminante dei minimi quadrati parziali (PLS-DA). I dati chimici e isotopici sono stati inseriti in una matrice bidimensionale caratterizzata dai campioni (manufatti) nelle righe della matrice e le analisi chimiche come variabili nelle colonne. L'insieme dei dati è stato inoltre analizzato con il test della Combinazione non-parametrica (NPC), che è un metodo non-parametrico multivariato inferenziale che libera dalle stringenti assunzioni dei metodi parametrici (come il t e F test) e permette un'analisi più flessibile sia in termini della specificazione di ipotesi multivariate, sia in termini della natura della variabili in causa. Uno dei più importanti vantaggi dell'applicare statistiche non-parametriche come i test di permutazione, è che

permette di lasciare libera l'assunzione di normalità delle variabili di risposta. Inoltre, il Test NPC non richiede la modellazione della dipendenza tra le variabili e non è affetta da problemi di perdita di gradi di libertà quando il numero di variabili è grande comparato al numero dei campioni. I risultati dell'analisi del Test NPC sono stati ottenuti usando il programma libero NPC Test R10, dove abbiamo usato l'F-test come test statistico e la funzione di combinazione Fisher come funzione combinante. I risultati possono essere rappresentati graficamente mediante la PCA.

La disponibilità di una comprensiva e senza precedenti quantità di dati geochimici per i depositi Alpine di rame ha dato informazioni rilevanti per la loro interpretazione metallo genica. In particolare, le composizioni isotopiche delle tracce di piombo nelle mineralizzazione a rame in depositi di solfuri idrotermali della regione sudalpina centro-orientale sono state combinate con i dati degli isotopi del piombo di depositi poli-metallici idrotermali esistenti nella stessa area, e comparati con le composizioni isotopiche di potenziali sorgenti di piombo. Depositi stratiformi di rame e poli-metallici pre-Varisici (tardo Ordoviciano - primo Siluriano), depositi a vene post-Varisiche (da Permiano a Triassico) e depositi a stratabound ospitati in sedimenti (da Permiano al primo Triassico) sono caratterizzati da rapporti altamente variabili di piombo radiogenico e non, ma mostrano valori di μ (= $^{238}U/^{204}Pb$) e W (= $^{232}Th/^{204}Pb$) molto simili e alti. Si osserva un relativo progressivo aumento in piombo radiogenico dai (i) depositi pre-Varisici alle (ii) vene ricche di solfuri post-Varisiche presenti nel basamento metamorfico Varisico e nelle unità inferiori-intermedie della sequenza vulcanica per primo Permiano alle (iii) vene post-Varisiche ricche in fluorite e solfuri nelle unità superiori della sequenza vulcanica del primo Permiano alla (iv) vene post-Varisiche ricche in fluorite che tagliano i sovrastanti sedimenti tardo-permiani e i dicchi mafici medio-triassici. Le sorgenti di piombo dominanti per tutti questi depositi sono i (meta)sedimenti del Cambriano-Devoniano del basamento Varisico. Contributi da rocce ignee permiane e triassiche sono di minore importanza, se presenti, anche per depositi di vena che sono evidentemente correlati con il magmatismo permiano.

Mentre l'impronta isotopica del Pb potrebbe potenzialmente aiutare la probabile provenienza del manufatto archeologico, ci sono numerose difficoltà correlate. Prima di tutto, i depositi naturali hanno frequentemente composizioni isotopiche del Pb sovrapposte. Così in aggiunta agli isotopi del Pb sono stati analizzati gli elementi in tracce, terre rare e rapporti isotopici del rame ($^{65}Cu/^{63}Cu$).

Il rapporto isotopico del rame $^{65}Cu/^{63}Cu$ è sensibile alla temperature di segregazione del minerale; quindi fornisce informazioni sulla natura del minerale usato per la produzione del manufatto. E' stata operato una selezione statistica per identificare le variabili che più effettivamente distinguono le miniere investigate. Questo è stato raggiunto usando una strategia PLS-DA. Questa tecnica è un metodo di classificazione che modella le differenze tra due classi. Il metodo PLS calcola un modello di regressione lineare tra la matrice dei predittori (X) e il vettore risposta (Y): in questo particolare caso il vettore Y è espresso con un codice binario. Il modello restituisce *scores and loading plots* così come il coefficiente di regressione per ogni variabile. Viene inoltre fornito una stima del significanza statistica di questo coefficienti di regressione.

La rilevanza statistica delle variabili è stata testata attraverso il Martens Uncertainty test. Lo studio delle matrici di correlazione e dei coefficienti del modello permette di definire un sotto-insieme di variabili in grado di discriminare i campioni provenienti dalla differenti aree/siti. Un singolo modello non è stato sufficiente ed è stata richiesta una strategia di esclusione a più passaggi per ottenere una discriminazione soddisfacente. La procedura adottata può essere schematizzata come segue:
1) l'intero insieme di dati è preso in considerazione e viene creato un modello PCA. Attraverso lo studio dei *score plots* generato dalla combinazione delle prime componenti principali (in genere da PC1 a PC4) la località maggiormente discriminante viene scelta per il processo di esclusione;
2) il passo successivo la selezione della variabile con l'intento di enfatizzare le differenza tra la località selezionata e tutte le altre località: l'obiettivo è costruire un semplice modello discriminante usando solo PC1 o non più di due PCs:
3) i dati correlati alla località selezionata sono esclusi dalla matrice originale e l'intero processo è quindi ripetuto su questa matrice ridotta inizialmente considerando di nuovo tutte le variabili.
Il potere discriminante del database è stato testato sulla provenienza di metalli e scorie di rame provenienti dall'area di Agordo (Belluno) e di frammenti e scorie di rame preistorici provenienti da Millan (Bressanone, Bolzano). I campioni sono stati proiettati in un modello PCA esistente, e la loro posizione comparata con la posizione dei campioni usati per costruire il modello. Lo stesso metodo di proiezione è stato inoltre usato per la validazione della strategia di esclusione a passaggi multipli.
I dati per manufatti e scorie di rame proveniente dall'area di Agordo mostrano che il modello discriminante che meglio identifica le miniere di Agordo è perfettamente applicabile ai manufatti, indicando chiaramente che il metallo è stato estratto dalle miniere locali.
Per il caso di Millan, il modello discriminante dei depositi che meglio descrive il frammento di rame è quello che identifica l'area della Val Venosta (miniere di Oris, Val Martello e dello Stelvio), localizzate 80 km a ovest del sito archeometallurgico di Millan. Questo risultato suggerisce che il campione di rame è geneticamente non correlato alla grande quantità di scorie associate prodotte durante il processo di *smelting* del rame provenienti dalle locali miniere di calcopirite ricche di sfalerite e galena, che hanno un carattere mineralogico e geochimico significativamente differente.
E' presentata una strategia vincente per caratterizzare miniere di rame e per tracciare la provenienza di minerali e antichi manufatti di rame. E' stato sviluppato un intero protocollo di controllo, che parte dal campionamento all'analisi quantitativa, per assicurare una corrispondenza geologica e una buona qualità dei dati analitici. Le misure di un vasto numero di elementi che include le terre rare (REE) insieme con i rapporti isotopici del rame e del piombo in minerali di rame ha permesso una completa caratterizzazione geochimica delle miniere a rame investigate. I dati raccolti sono stati usati per costruire un database che può essere usato come riferimento fondamentale per tracciare l'estrazione del metallo e la sua diffusione in passato. L'applicazione di avanzate tecniche statistiche ai dati geochimici e isotopici fornisce uno strumento potente per discriminare le aree delle miniere sorgenti. Le applicazioni presentate relativamente ai

campioni e scorie di rame sembrano confermare che le analisi possono essere operate con successo su campioni archeometallurgici. La disponibilità di un tale ammontare di dati esaustivo e senza precedenti per i depositi di rame alpini inoltre da informazioni interessanti per la loro interpretazione geochimica e metallogenica. In particolare, gli alti valori di μ e W dei depositi del sud-alpino centro-orientale sono consistenti con andamenti isotopici regionali dei depositi a Pb-Zn in settori più settentrionali e orientali delle Alpi orientali (Australoalpino, Sudalpino orientale) e di numerosi depositi metallici e a Pb-Zn dell'area mediterranea di età paleozoica fino a triassica (Sardegna, Cordigliera Betica) o derivati da rimobilizzazione di depositi paleozoici (Toscana). Questa uniformità isotopica suggerisce l'esistenza di una provincia isotopica caratterizzata da una preponderanza di vecchio materiale sorgente detritico (primo Proterozoico fino ad Archeano), che si estende attraverso una relativamente estesa porzione di un più recente margine nord-Gondwaniano.

Part I

INTRODUCTION TO THE DATABASE

1. Lead Isotopes Theory

Isotopes are atoms of the same chemical element with different masses: they are composed of varying numbers of neutrons and a fixed number of protons. In the case of lead isotopes, this variability in the number of neutrons is related to the origin of lead. This is either primitive (that is to say that it is present since the formation of the Earth): the isotope ^{204}Pb; or radiogenic isotopes ^{206}Pb, ^{207}Pb and ^{208}Pb.
Radiogenic isotopes are the result of radioactive decay:

- **^{235}U ⇒ ^{207}Pb**
- **^{238}U ⇒ ^{206}Pb**
- **^{232}Th ⇒ ^{208}Pb**

In other words, the amount of ^{204}Pb does not change since the formation of Earth, unlike isotopes ^{206}Pb, ^{207}Pb and ^{208}Pb, whose amount increases with the decay of ^{235}U, ^{238}U and ^{232}Th. There are other isotopes of Pb, unstable, but too short lived to be interesting for the study of geological events (Houtermans et al., 1946).
These four isotopes give information on the age and source of lead to mineralization. The age assessment of mineralization based on the radioactive decay of ^{235}U and ^{238}U ^{206}Pb and ^{207}Pb fathers son. Indeed, these two isotopes of uranium have similar physical and chemical behavior and therefore a report ^{235}U/^{238}U identical in all reservoirs. This ratio is changing over time because these two isotopes have different half-life. Currently, the ratio rises to ^{235}U/^{238}U 1/137.88. Basing itself that on the isotopes ^{235}U, ^{238}U and ^{206}Pb, ^{207}Pb and by eliminating all the variables relating to disintegration of ^{232}Th in ^{208}Pb, we can determine the age of a rock.
To determine the source of lead is based on radioactive isotopes ^{238}U and ^{232}Th, because they have different physical and chemical behavior: thorium is less mobile

than uranium under oxidizing conditions, which is why the U/Th is not constant from one container to another, their relationship is so characteristic of the different environments. To facilitate the interpretation of isotopic data, three different ratios were determined (Faure, 1986) to describe the geological source of Lead analyzed. They are μ (= $^{238}U/^{204}Pb$), ω (= $^{232}Th/^{204}Pb$) and κ (= $^{232}Th/^{238}U$).

1.1 Methodologies

In the present work, the age and source of mineralization is determined by different types of lead-bearing minerals at the time of crystallization. At the time of formation, minerals therefore adopt the lead isotope signature typical of mineralizing fluid which they are derived. The isotopic signature is then frozen, while the rock continues to evolve based on the decay of uranium and thorium. We can determine the age of crystallization of minerals and the source of lead, if we know the conditions under which the formation of lead 206, 207 and 208 is submitted. Several models have been developed to interpret these isotopic signatures. In my opinion, the interpretation must be made on two distinct levels:

- *Global approach.* It is based partly on the laws of decay of thorium and uranium and the other on the Earth's history and major tectonic events. Faure and Mensing (2005) and Dickin (2005) describe several models (Stacey and Kramers, 1975; Cumming and Richards 1975), still often used today. The interpretations derived from these models have an imprecision for many fields, the calculated age of introduction of mineralization corresponds to a date in the future. The model of Kramers and Tolstikhin (1997) tries to overcome this paradox, called "paradox of the future."
- *Local factors.* If the influence of rock leached (washed) by the mineralizing fluid is important, the Kramers and Tolstikhin model (1997) gives no acceptable solution, and interpretation at the local level is essential. There is to evaluate the influence of rock and minerals leached on the isotopic signature of mineralization analyzed.

1.1.1 Global approach: galena models

In the galena method, a phase that contains no U is analyzed, so there is no problem associated with loss of U (Dickin, 2005). A brief description of the most important models is reported here in chronological order.

Holmes-Houtermans model (1946). Holmes (1946) and Houtermans (1946) divided the isotopic evolution of galena into two parts. The first was assumed to be a rock system, which must have remained closed to U and Pb from the formation of the Earth until galena separation. The second was in the galena itself, which must contain no significant amounts of uranium. To apply the Holmes–Houtermans model, the galena source rock is assumed to be a closed system with a ‘single-stage’ Pb isotope history.

A growth curve is then constructed for this galena source, which runs from the primordial Pb composition to that of the analysed galena, and is calibrated for various values of t (t=age of galena). The shape of the growth curve is determined by the two uranium decay constants, and its trajectory by the $^{238}U/^{204}Pb$ or 'μ' value of the closed-system galena source. For the single-stage model described, it is called the μ_1 value and would normally be between 7 and 9. According to the Holmes–Houtermans model, not every galena source rock need have the same growth curve, defined by the same μ value (Dickin, 2005). The problem encountered using the Holmes–Houtermans model was that, as more galenas were analysed, they were found to scatter more and more widely on the Pb–Pb isochron diagram. Some of the ages determined were clearly erroneous, since they were in the future. Others, which were outliers to the main trend, often gave ages that could be shown to be geologically impossible. Since galenas of these two types contradicted the Holmes–Houtermans model, they were called 'anomalous leads'.

Stanton and Russell model (1959). Given the complexity of the Earth's evolution, it was realised even in the 1950s that the host rock source of a given galena ore was unlikely to have been a closed system since the formation of the Earth (Dickin, 2005). Stanton and Russell analyzed sulphides associated with sediments and volcanics in greenstone belts and island arcs, which were structurally conformable with the host rocks; they regarded these ores as being formed by syngenetic deposition in sedimentary basins associated with volcanic centres, and therefore as representing galena derived directly from the upper mantle without crustal contamination. Nine deposits of various ages were selected, and a single stage growth curve (upper mantle) with a μ_1 value of 9 was proposed. These ores were termed 'conformable' leads because of their structural occurrence, and all galenas that didn't fit this curve were by inference 'anomalous'. Anomalous leads were divided into groups such as 'J-type leads' after a deposit at Joplin, Missouri, which gave ages in the future, and some other types such as the 'B' type, which gave ages in the past. Unfortunately, due to the mobility of Pb during crustal processes, it is difficult to develop *a priori* criteria to recognise galenas that will fit the conformable Pb evolution model. Therefore, the galena method is largely discredited as a dating tool.

In the early 1970s, new measurements of the uranium decay constants (Jaffey et al., 1971) and a better estimate of primordial Pb from Canyon Diablo necessitated a re-examination of the conformable Pb model. For example, using the new values, a curve calculated to yield a reasonable fit to conformable galenas gave a low apparent age for the Earth of 4.43 Byr (Doe and Stacey, 1974). Alternatively, a terrestrial age of 4.57 Byr based on Pb–Pb dating of meteorites (Tatsumoto et al., 1973) caused the Geochron to lie to the left of most Phanerozoic galenas and young oceanic volcanics. This problem became known as the 'Pb paradox' and meant that single-stage Pb models gave 'future ages' up to 1 Byr in error for Phanerozoic rocks (Dickins, 2005).

Cumming and Richards Model (1975). To rectify these problems, Oversby (1974) proposed a model for an evolving (mantle) source of galena Pb with a progressive increase in μ value over time (approximated by a series of small increments in μ). This model was elaborated upon by Cumming and Richards (1975), who modelled a galena source with a linear increase in μ value. Surprisingly perhaps, Cumming and Richards regarded the galena source as a regional average of the crust. However, this might not be as strange as it sounds, since later work would show that mantle and crustal Pb

evolution are in fact coupled together, and that upper-mantle Pb is largely buffered by the crust. The model of Cumming and Richards yields a good fit to the ages of selected galena data, but still implies a young apparent age for the Earth of 4.50 Byr.

Stacey and Kramers model (1975). They proposed that Pb in ore deposits is formed by a two-stage process. Stacey and Kramers used Canyon Diablo Pb and average modern Pb (from a mixture of manganese nodules, ocean sediments and island-arc rocks) to anchor the ends of a composite growth curve. This curve was produced by two closed systems (stage 1 and 2) with different μ values (μ_1 and μ_2), separated in time by a world-wide differentiation event (Figure 1.1).
The first stage started at T = 4.57 × 10^9 y with primeval Pb in a reservoir having μ = 7.192 and ω= 32.208, and ended at T'= Q = 3.70 ×10^9 y when μ increased to 9.735 and ω to 36.837 because of a geochemical differentiation (Faure and Mensing, 2005). Lead evolution then continued to point P, representing average crustal Pb.
The closed systems consisted of a combination of the upper mantle and upper crust (lower crust, lower mantle and core being isolated). The model gave the best fit to a selection of conformable galenas dated by the enclosing sediments when μ_1 = 7.2, μ_2 = 9.7 and the event was at 3.7 Byr. Stacey and Kramers noted that their model was only an approximation of Pb isotope evolution in the real Earth. For example, the discrete event at 3.7 Byr in the model might actually represent a slow change in the Earth's evolution during the Early Archean. The above observations suggested that the galena source evolved for the last 3.8 Byr along a higher-μ growth curve than the geochron, but the reason for this behaviour was not clear. However, the two-stage model of Stacey and Kramers (1975) provides a simple and still widely used reference that facilitates comparison of the different isotopic signatures.

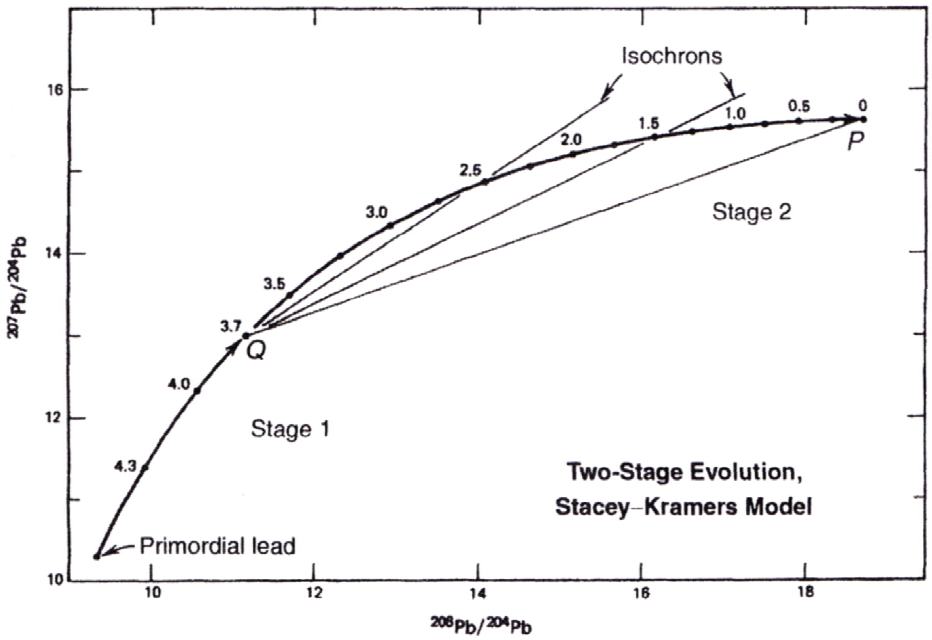

Figure 1.1 – Two stage Pb model of Stacey and Kramers (1975) reported by Faure and Mensing (2005)

1.1.2 Global approach: The model of Kramers and Tolstikhin (1997)

To give a better solution to the paradox of the future Kramers and Tolstikhin (1997) model in some detail the exchange of lead between the different major reservoirs, including the most important events in the history of the Earth. They are based on the following principles:

1. Initially, during the formation of Earth's core, most of the lead which is siderophile, concentrates in the nucleus: its content was depleted in other reservoirs (see principle 2). At this time, there is very little radiogenic lead, therefore the isotope ^{204}Pb mostly enriches. Uranium and thorium, the father of radiogenic lead components, are lithophile (which tend to bind to oxygen, such as silicon and aluminum), which is why they are enriched in other reservoirs . In other words, the lead content of the nucleus doesn't change very much during the history of the Earth (so the ratio $\mu = {}^{238}U/{}^{204}Pb$ is low), since very little is enriched in radiogenic lead, unlike other tanks.
2. The most important lead tanks are: the continental crust, upper mantle and lower mantle the core (Table 1.1). For the formation of lead deposits on the surface of the Earth, lead contribution of the lower mantle is probably insignificant, since the exchange between the upper and lower mantle is small. In the same way, the exchange between the lower mantle and the core is small. Only rocks of the continental crust and upper mantle have a significant role in the formation of lead deposits.

RESERVOIR	U	Th	Pb	μ	k
Upper mantle/ source of MORB	0.005-0.007	0.0127-0.019	0.03-0.05	10.1	2.66
Bulk continental crust	1.7	8.5	14.8	9.58±0.9	4.55±0.3
Lower crust	0.28-1.1	1.06-6.6	4.0-12.5		
Upper crust	2.2-3.94	9.5-14.8	15.0-23.1	11.08	3.88

Table-1.1 Estimates for U, Th, and Pb isotope abundances in terrestrial reservoirs (Kramers and Tolstikhin, 1997). Concentrations (ppm) of the elements and concentration ratios (μ and k).

3. The continental crust is divided into four parts of equal mass to better reflect its diversity relative to its age and composition. These are: the young upper crust, the old upper crust, the young lower crust and the old lower crust. They are differentiated according to several criteria:

   Upper crust and lower crust are distinguished by the geological process of partial melting, that is to say by the merger of minerals in successive magma formation. Specifically, the liquid magma, created by partial melting, is added to the young upper crust. This simulates three intracrustal processes: first the primary fractionation is the basis for the distinction mafic rocks (rocks containing minerals rich in iron and magnesium) - felsic rocks (rocks containing minerals rich in silicon and aluminum); then the anatexis (complete fusion of rock) of the felsic crust lying at depth because of orogenesis

(mountain building); and finally the transfer of uranium fluids during metamorphism. In other words, in these three processes, uranium and thorium, associated with felsic rock, are transported to the upper crust: it is characterized by a μ high, unlike the lower crust: the upper crust evolves from a perspective enriched in radiogenic lead isotope.

The young and the old crust are characterized by the geological process of erosion. In fact, according to a law of erosion, young crust is more easily eroded than the old (Kramers and Tolstikhin, 1997). In addition, it affects only the upper crust. To keep constant the mass ratios between the four crustal domains, some of the lower crust is transferred to the upper crust: the process models the movements associated with isostasy. Finally, by erosion, this model also takes into account the transport of uranium to the oceanic crust, which is significantly larger than that of lead and thorium because of the solubility of uranium. In other words, the young upper crust is, in relation to the old upper crust, slightly less rich in thorium and uranium, transported to the oceanic crust: it is characterized by a slightly less μ higher than that of the old upper crust.

Specifically, KRAMERS and TOLSTIKHIN (1997) calculate five lines of evolution type for five available tanks. They are descending in function of $\mu = {}^{238}U/{}^{204}Pb$ (^{238}U is the father of the ^{206}Pb element): the old upper crust, the young upper crust, mantle, crustal young and the old lower crust.

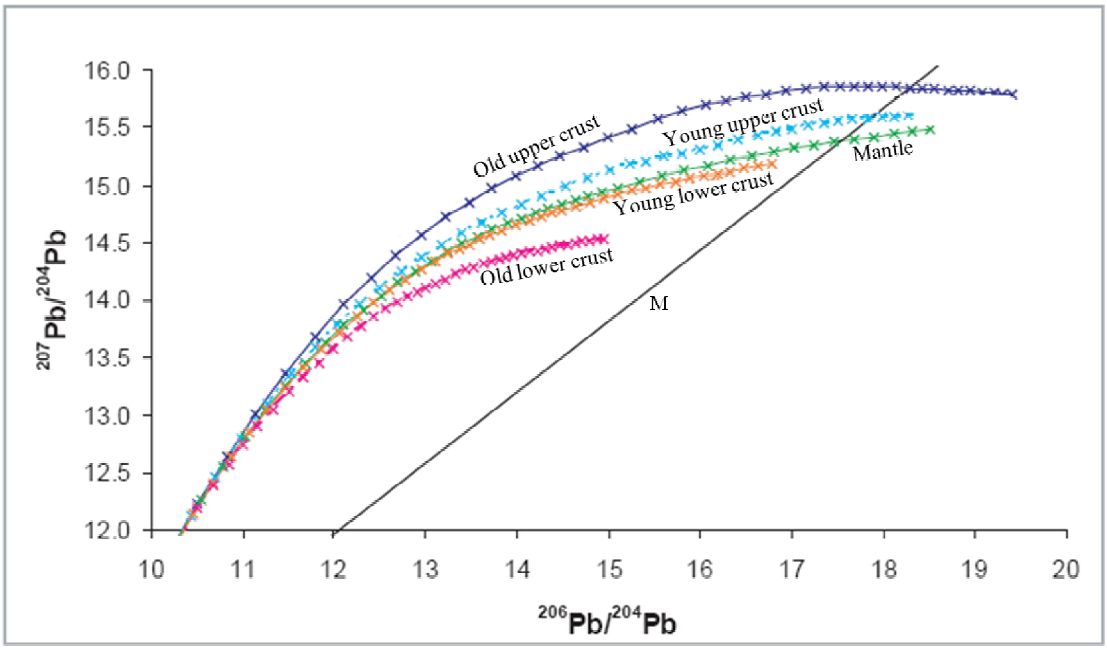

Figure 1.2 Evolution of lead isotopic compositions. Calculated evolution for mantle and four crustal reservoirs up to age zero (t = 4.55 Ga) compared to observed evolution. Time difference between symbols is 200 Ma.

There (figure 1.2) points straight end of these lines of evolution, representing currently trained minerals stop sharply to the right of the geochron. This also named geochron Isochron meteoric, is defined by a former model right ("single stage model", Faure 1986). It indicates the current age of Rock formed at the beginning of the formation of Earth independently reservoir has come. This age is valid only for the rocks have undergone a single phase therefore enrichment or impoverishment in radiogenic or radioactive elements. Kramers and Tolstikhin model (1997) provides a marked improvement compared to previous models: the paradox of the future is solved for mineralization which have not undergone the influence of a radiogenic lead-rich rock.

1.1.3 Local factors: the mobility of lead

The model of Kramers and Tolstikhin (1997) does not explain the isotopic signature of all mineralization. Despite the clear improvement over previous models, some deposits have still a future isotopic signature, so they have a signature too radiogenic for which the model chosen does not provide an explanation. Kramers and Tolstikhin consider only major earth movements and not the local influence of the host rock. Leached by hydrothermal fluids, it enriches them according to its lead content, but also of the structural position of lead in different minerals of which it is formed.
Silicate rocks have a high lead content (Marcoux, 1986) (Table 1.2) which increases with the percentage of potassium silicate, including microcline and orthoclase (Table 1.3).

Igneus Rocks	**Lead content**	**Sedimentary Rocks**	**Lead content**
Peridotites	<0.3 ppm	Sandstones	10 ppm
Gabbros	3 ppm	Pelites	23 ppm
Basalts	4 ppm	Black schists	29 ppm
Andesites-Diorites	6 ppm	Metapelites	34 ppm
Phonilites	14 ppm	Carbonates	5 ppm
Granites	20-50 ppm	Evaporites	<1 ppm
Granodiorites	12-20 ppm	**Metamorphic Rocks**	**Lead content**
Dacites	15 ppm	Gneiss	20 ppm
Rhyolites	24 ppm	Granulites	19 ppm

Table 1.2 Average lead content of the main common rocks, according to Marcoux (1986).

Among sedimentary rocks, sandstones, black shales and oil shales in particular, through the clay minerals and iron oxides used in their composition, have a great capacity to absorb lead and have therefore a potential uranium leaded and above average sedimentary rocks. The lead content shows wide variations between 10 and 34 ppm in these rocks.
The contribution of lead from a rock in a hydrothermal leaching is not proportional to its content. Indeed, Sahl et al. (1973) studied several cases and found that a representative average rock of the continental crust (40% and 20% plagioclase

feldspar), lead drift to 11 ppm (ppm = 53 * 20%) of feldspar and for 2 ppm plagioclase. However, this assessment is in contradiction to the lead content of these two minerals (Table 1.1.3): it should be 8 ppm (19ppm * = 40%) of plagioclase. In plagioclase, lead crystal is in position identical to that of feldspar, but its large size relative to atoms substituted (Ca, Na) imprison in the network. The feldspars are more easily leached than plagioclase. Micas have a minimal contribution, since the interlayer atoms K^{+} and Pb^{2+}, the lead is taken away prematurely, in terms of alteration of feldspar (Marcoux 1986).

The contribution of accessory minerals in hydrothermal leaching depends on their mineralogical stability. Thus, zircon and monazite by example are very resistant to dissolution by hydrothermal fluids and therefore almost inert, unlike uraninite and thorianite, easily mobilized. They bring the radiogenic lead to these solutions.

Minerals	Lead content	Minerals	Lead content
Orthoclase	53 ppm	Biotite	21 ppm
Microcline	98 ppm	Amphibole	15 ppm
Plagioclase	19 ppm	Quartz	<3 ppm
Muscovite	26 ppm		

Table 1.3 Average lead content of the main common silicates, according to Marcoux (1986).

1.2 Analysis tools for isotopic data

For isotope analysis, we measure the amount of each isotope, that is to say, we count the number of each isotope of lead present in a sample. However, to avoid having to take into account the absolute lead content of each element, isotopes are expressed in general form of isotope ratio, specifically reports $^{206}Pb/^{204}Pb$, $^{207}Pb/^{204}Pb$, $^{208}Pb/^{204}Pb$ or ^{207}Pb / ^{206}Pb and $^{208}Pb/^{206}Pb$.

These ratios are shown in different diagrams (Figure 1.3), which each have their advantages and disadvantages:

- *$^{207}Pb/^{204}Pb$ vs $^{206}Pb/^{204}Pb$ diagram: <u>the age index</u>* - The isotope ^{207}Pb comes from the radioactive decay of ^{235}U, ^{206}Pb isotope that of ^{238}U. These two radioactive atoms have physicochemical properties very similar and thus show similar behavior in the various reservoirs. This property eliminates several other factors needed to calculate the age of mineralization (Faure 1986). This diagram can more easily estimate the age of the establishment of mineralization.
- *$^{208}Pb/^{204}Pb$ vs $^{206}Pb/^{204}Pb$ diagram: <u>Lead geological source index</u>* - The isotope ^{208}Pb is derived from the decay of ^{232}Th, ^{206}Pb on the ^{238}U. These are elements with different physical and chemical behavior. Their combination can be used to characterize different metallogenic sources. However, this is only possible if we analyze lead having suffered a single training session (single stage model,

Faure 1986): The thorium content varies greatly from one rock to another because this component shows a very complex physicochemical behavior.

- *$^{208}Pb/^{206}Pb$ vs $^{207}Pb/^{206}Pb$ diagram: precision index* - The error induced in the other three types of representations of isotopic data is due to ^{204}Pb. This measure is difficult for two reasons. ^{204}Pb measurement can be problematic because of its low relative abundance. It is currently 1.4%, that of ^{206}Pb by 25%, 21.6% of the ^{207}Pb and ^{208}Pb by 52% on average. Second, having the same weight isotopes, ^{204}Pb interferes with ^{204}Hg, often present in very small quantities in the gas used for analysis (e.g. argon), in the mineralizations or in some archaeological artifacts. This interference requires a sensitive enough correction. The advantage of this representation is to eliminate all problems related to measuring the isotope ^{204}Pb, it is thus particularly precise: from 0.001% when measured with TIMS and from 0.0001% when measured with ICP -MS. However, it is almost impossible to obtain a geological interpretation: only the position of the points is useful.
- *$^{206}Pb/^{204}Pb$ vs $^{207}Pb/^{206}Pb$ diagram: archaeological index* - This representation, like the previous chart, the accuracy is often used in archaeology. This diagram tries to keep a maximum of precision, while integrating the isotope ^{204}Pb problematic. But like the diagram of precision, geological interpretation is not possible. In addition, data produce a straight line: the diagram contains much less information because the data cover only a linear and non-dimensional space.

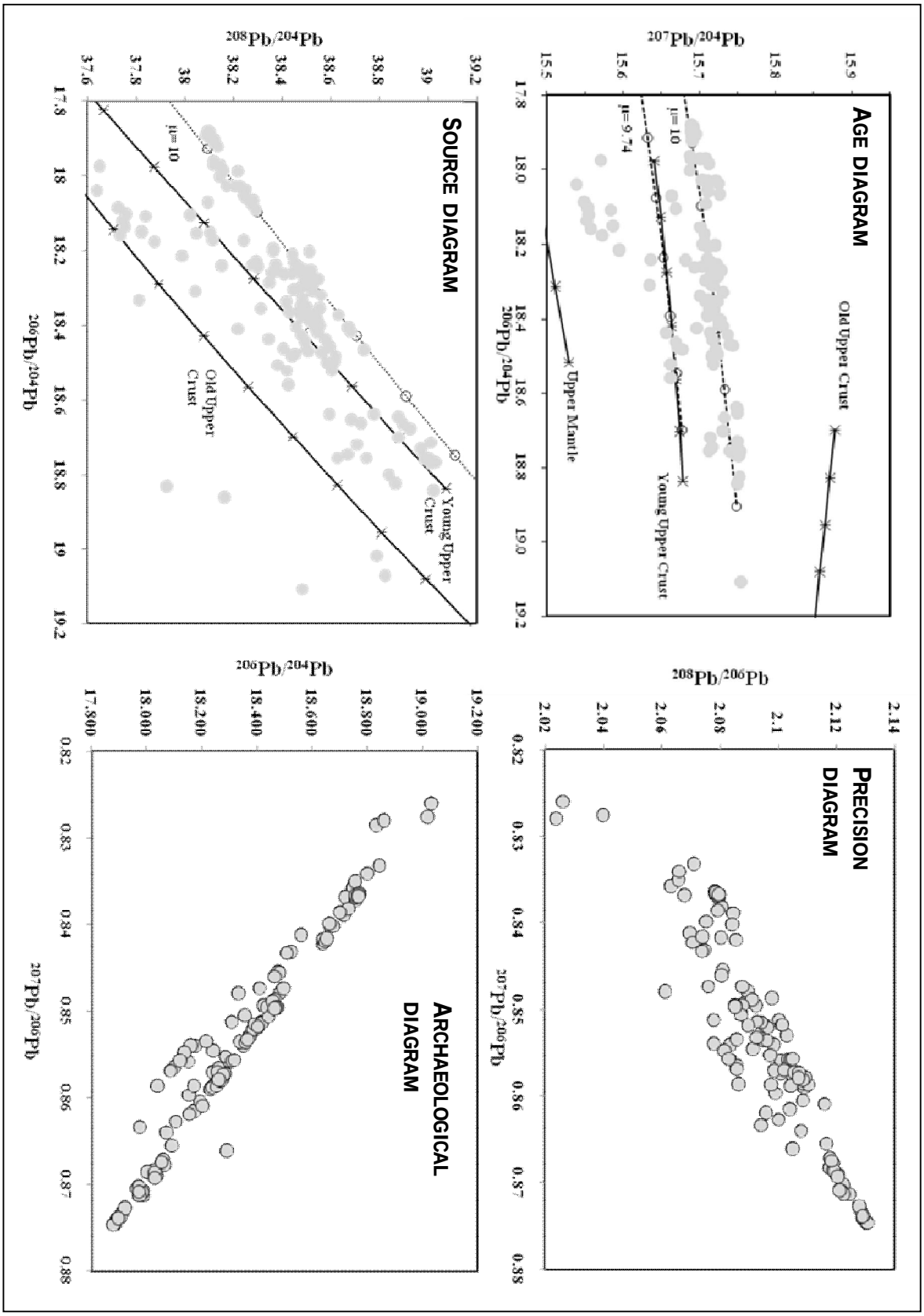

Figure 1.3 Average lead content of the main common silicates, according to Marcoux (1986).

In the diagram *age index*, two types of lines have meaning. These two lines also exist in the diagram that indicate the *geological source*, but they are not represented here, since they are difficult to interpret for the reasons given above.
The *evolution curves* (see Figures 1.1.1) are the first one and have been computed by Kramers and TOLSTIKHIN (1997). These curves show the temporal evolution of a lead from five different geological sources, namely: the upper mantle, the young upper crust, the old upper crust, the young and the old lower crust. The points indicated on the curves are weights specific age (time: 200 Ma). The lines that connect points of the same age but from different sources are not isochronous, but lines of miscibility between two leads of the same age but from different sources.
The *trend line of a ore deposit* is the second type. It shows the development trend of the isotopic signature of all samples from a mine. Opinions are divided on its meaning:

I. The line represents the isotope fractionation. The slope (m) of this line corresponds to the difference in isotopic weight of the two isotopes that have their ratio shown on the y axis divided by the weight difference of the two isotopes with isotopic ratio on the axis x.

   That is, in age index diagram, we have:

$$m = \Delta(207/204) / \Delta(206/204) = 3 / 2 = 1.5$$

   and for the geological source diagram, we have:

$$m = \Delta(208/204) / \Delta(206/204) = 4 / 2 = 2$$

   The slope of this trend line is always the same for each deposit.

II. The line is a line of miscibility between a original lead and a leached rocks lead. It assesses the influence of rock. It corresponds to the regression analysis for a given mineralization. A mine can be formed of several mineralization: we must define a regression line for each mineralization.

1.3 Interpretation of isotopic data

The interpretation of isotopic data focuses on three different factors:

- The age of mineralization (see age diagram in figure 1.3). It can be evaluated by the intersection of the trend line of a reservoir and a line of evolution calculated by Kramers and Tolstikhin (1997). The age needs, in some cases, to be corrected according to the nature of the rock. This correction uses two knowledges. First, it requires a good understanding of the stratigraphy,

specifically the lead content of the rock covered by the mineralizing fluid. Secondly, the age of the mineralization must be correlated with the age of a magmatic intrusion or metamorphism may be the source of this mineralization.

- The source of lead (source diagram in fig. 1.3). The source of the mineralizing fluid can be assessed approximate by the geological source of lead diagram. It is estimated based on the proximity of an evolution curve point analyzed in Kramers and Tolostikhin (1997).
- The isotopic signature of a deposit. Every isotopic ratio analyzed is important to characterize a deposit peculiarity. Ideally, two separate diagrams are used: the age index diagram and the precision diagram. This choice would best explain the geological interpretations based on the first diagram, while enjoying the high precision of analysis given by the second one. This characterization is based on a graphical evaluation.

1.4 Lead isotopes in archaeological metal objects

The provenance of metal artifacts in the early history of metallurgy has been a major question in archeology for many decades. Pb isotope ratios are commonly used for provenancing in archaeometry (Gale & Stos-Gale, 2000; Hauptman, 2007; Villa, 2009), but interpretations are hardly debated (see Pollard, 2009, and Gale, 2009) and sometimes ambiguous because natural ore deposits frequently show overlapping Pb isotopic compositions. The first way to reduce observed overlaps is by improving the analytical precision. Two values are said to be statistically indistinguishable when their difference is smaller than the sum of the analytical uncertainties with which they were measured. Thus, it may be impossible to tell apart two values if the measurement precision is low, but it may be possible to resolve them if the precision increases (Villa, 2009). The second way to reduce ambiguities is to combine the lead isotopic signature with other geochemical indicators, e.g. minor and trace elements (Ixer, 1999; Pernicka, 1999) or other isotopic data.

Moreover we have to assume that Pb doesn't fractionate through the metallurgical process. There are many experimental works in literature that exclude the lead isotopes fractionation during the metallurgical phases (Barnes et al., 1978; MacFarlane, 1999; Cui and Wai, 2010).

Supposed that fractionation is absent, we have to consider another factor: the possible mixing phenomena. Mixing can be caused by: two different mineral charges, different metal objects recycling or the addition of flux agents during smelting (Attanasio et al., 2001).

The second way to reduce ambiguities is to enlarge the context with other indicators. As was mentioned above, trace element concentrations vary as metallurgy evolves;

however, because of similarities in the chemical behavior of element groups that are related in the periodic system, the metallurgical processing affects certain element ratios much less than the individual element concentrations. Thus, by a judicious investigation of the multielement abundance patterns, some characteristics that discriminate among different ore bodies can be retraced in the metallic artifacts (cf., Pernicka 1999; see also, Artioli et al. 2008).

2. Copper isotopes

A large number of transition metal stable isotopes, such as lead, chromium, iron or copper, can be used as geochemical tracers to investigate ore formation processes, ore ages or to characterize elemental ore composition. The variation of isotopic ratios for these metals are quite scattered on a range of several per mil and the difference between ores depend mainly on formation temperature, abiotic or biotic process and redox state during mineral formation processes. In this respect copper isotopic ratio has increased in importance not only as a geochemical tracer for natural processes but also as a tracer in archaeometry along with lead isotopes (Gale et al., 1999). Copper has only two stable natural isotopes: ^{63}Cu (62.9296 a.m.u.) and ^{65}Cu (64.9278 a.m.u.). Their accepted natural abundances are 69.17% and 30.83% respectively and the isotopic ratio ^{63}Cu/^{65}Cu keep at a value of 2.244 (Murphy et al., 1964). For copper ore bodies, the isotopic data show a variation in ^{63}Cu/^{65}Cu ratio on a regional scale that mainly depends on ore formation temperature.

This leads to a δ63 variation that ranges between -4, -6 ‰ to +2, +3‰ (with respect to SRM NIST 976) (Zhu et al., 2000). This kind of information can be used to make provenance studies on minerals and also on artefacts coming from the early bronze age through a fingerprinting of the geographical localization of the ores. However, variations of δ63 values in the range of ±1–2‰ are also observed on a local scale inside every single ore (Mathur et al., 2009; Asael et al., 2007) From a provenance-tracking point of view, these in-ore fluctuations of ^{63}Cu/^{65}Cu ratios surely represent a source of noise that cannot be avoided. From an analytical point of view, these fluctuations could lead to the conclusion that the utilization of a highly precise method

for isotopic ratio measurements is not mandatory for obtaining meaningful information regarding provenance.

The reported natural variation of the ratio of the stable copper isotopes 63Cu and 65Cu is up to 9‰ (Walker et al., 1958; Shields et al., 1965; Marechal et al., 1999; Marechal and Sheppard, 2002; Johnson et al., 2004; Zhu et al., 2000; Rouxel et al., 2004), where δ is defined as δ^{65}Cu

$$\delta^{65}\mathrm{Cu} = \left(\frac{65\mathrm{Cu}/63\mathrm{Cu}_{\mathrm{sample}}}{65\mathrm{Cu}/63\mathrm{Cu}_{\mathrm{std}}} - 1\right) * 1000$$

δ65Cu values are reported relative to the standard NIST SRM-976. In chondrites, the maximum variation does not exceed 1.5‰, but three reservoirs presumably formed at high temperatures with significantly different compositions could be identified (Luck et al., 2003). These data together with oxygen isotopes and element ratios support the presence of isotopically distinct Cu components in the Solar System, which indicates that relatively high-temperature processes may be capable of altering Cu isotope compositions significantly. Similarly, Zhu et al. (2000) found for hydrothermal vents on the ocean floor a range of δ65Cu values between_0.5 and +1.2&. However, magmatic processes do not appear to produce significant copper isotope fractionation, although Zhu et al. (2002) showed that significant iron isotope fractionation occurs up to 1000 °C. Rouxel et al. (2004), however, explained the large δ65Cu variation in seafloor sulfide deposits by low-temperature secondary processes after sulfide deposition, while the primary, high-temperature (about 350 _C) precipitation did not lead to significant variation in d65Cu. In hydrothermal copper deposits formed between 150 and 290 °C, Jiang et al. (2002) report a variation in δ65Cu for chalcopyrite between -3.7 and +0.3‰.

The natural variation of copper isotope ratios has been attributed to a number of processes such as liquid–vapor separation, multi-step equilibrium processes, redox reactions or involvement of organisms (Marechal et al., 1999; Zhu et al., 2000, 2002; Jiang et al., 2002; Larson et al., 2003; Graham et al., 2004; Rouxel et al., 2004; Ehrlich et al., 2005). Zhu et al. (2000) have shown that even samples of the same mineral from the same locality may exhibit large variations of copper isotope ratios. All workers agree that both biological and inorganic processes can cause significant shifts in copper isotope ratios at low temperatures (Gale et al., 1999; Marechal et al., 1999; Zhu et al., 2000, 2002; O'Nions and Zhu, 2002; Riuz et al., 2002; Marechal and Albarede, 2002; Larson et al., 2003; Graham et al., 2004). The details of the processes causing the δ65Cu variations are not yet clear in every case, but Graham et al. (2004) inferred for the Grasberg deposit, Australia, that selective metamorphic overprinting on the microscale was responsible for the variations in Cu and Fe isotope values observed. Their data indicate that variations of δ65Cu values in magmatic–hydrothermal porphyry copper systems and associated skarns range between 0 and 1.3‰ and that there is a distinctive evolution of Cu isotope values with magmatic differentiation. The authors related this evolution to either fractionation during distillation of the Cu from an underlying source or to fractionation within the evolving hydrothermal fluid. However, despite obvious clustering of the δ65Cu values of single intrusions within the composite complex investigated by Graham et al. (2004), which allows tracing the evolution of copper isotope values with time and differentiation, there is still considerable overlap of the data among various intrusions effectively preventing a single analysis being related to a specific source. Furthermore, their data stem from a relatively small group of samples which renders their interpretation more difficult.

3. Trace and Rare Earth elements

3.1 Trace elements

For igneous and metamorphic systems, an operational definition might be as follows: trace elements are those elements that are not stoichiometric constituents of phases in the system of interest. Clearly this definition is a bit fuzzy: a trace element in one system is not one in another. For example, potassium never forms its own phase in mid-ocean ridge basalts (MORB), its concentration rarely exceeding 1500 ppm; but K is certainly not a trace element in granites. For most silicate rocks, O, Si, Al, Na, Mg, Ca, and Fe are ‘major elements’. H, C, S, K, P, Ti, Cr, and Mn are sometimes ‘major elements’ in the sense that they can be stoichiometric constituents of phases. These are often referred to as ‘minor elements’. All the remaining elements are always trace elements, with the exception of a important circumstances such as pegmatites and ore deposits. The above definition breaks down entirely for fluids and natural waters since there is only one phase, namely the fluid, and it's not stoichiometric. Trace elements in seawater and in rocks do have one thing in common: neither affect the chemical or physical properties of the system as a whole to a significant extent. This might serve as

a definition. However, trace (or at least minor) elements can determine the color of a mineral (e.g., the green color of chrome diopside), so even this definition has problems. And CO_2, with a concentration in the atmosphere of only 360 ppm, profoundly affects the transparency of the atmosphere to infrared radiation, and, as a result, Earth's climate. At even lower concentrations, ozone in the upper atmosphere controls the atmospheric transparency to ultraviolet radiation. So this definition is not satisfactory either.

Yet another possible definition of a trace element is: an element whose activity obeys Henry's Law in the system of interest. This implies sufficiently dilute concentrations that for trace element A and major component B, A-A interactions are not significant compared to A-B interactions. There is perhaps no satisfactory quantitative definition of a trace element that will work in every situation. For our present purposes, any of these definitions might do, but bear in mind that a trace element in one system need not be a trace element in another.

No matter how we define the term "trace element", most elements will fall into this category. That being the case, this is a good place to consider the geochemical characteristics of the elements. Goldschmidt recognized four broad categories: atmophile, lithophile, chalcophile, and siderophile. Atmophile elements are generally extremely volatile (i.e., they form gases or liquids at the surface of the Earth) and are concentrated in the atmosphere and hydrosphere.

Lithophile, siderophile and chalcophile refer to the tendency of the element to partition into

a silicate, metal, or sulfide liquid respectively. Lithophile elements are those showing an affinity for silicate phases and are concentrated in the silicate portion (crust and mantle) of the earth. Siderophile elements have an affinity for a metallic liquid phase. They are depleted in the silicate portion of the earth and presumably concentrated in the core. Chalcophile elements have an affinity for a sulfide liquid phase. They are also depleted in the silicate earth and may be concentrated in the core. Many sulfide ore deposits originated from aqueous fluids rather than sulfide liquid. A chalcophile element need not necessarily be concentrated in such deposits. As it works out, however, they generally are. Most elements that are siderophile are usually also somewhat chalcophile and vice versa. There is some basis for Goldschmidt's classification in the chemistry of the elements. The lithophile elements occur mainly at either end of the periodic table, siderophile elements are mainly group 8, 9 & 10 elements (and their neighbors), chalcophile elements are mainly group 11, 12 and the heavier group 13-16 elements, while the atmophile elements are mainly the noble gases. The distribution of the electropositive elements (those that give up an electron more readily than they accept one) among metal, sulfide, and silicate phases is controlled by the free energies of formation of the corresponding sulfides and silicates. By comparing the free energies of formation with those of ferrous sulfide and ferrous silicate, it is possible to deduce which elements are siderophile, those which are chalcophile and which are lithophile. For historical reasons, namely lack of ΔG_f^o data on silicates, the point is generally illustrated using the enthalpy of formation, ΔH_f, of the oxide. Since 'oxyphile' could arguably be a better term than lithophile, this is not such a bad thing. Elements whose oxides have high $-\Delta G_f$ are lithophile. Why this is the case should be clear from our understanding of thermodynamics. States with the lowest free energy are the most stable: a high $-\Delta G_f$ indicates the oxide is much more stable than the metal. Elements whose oxides have $-\Delta G_f$ similar to that FeO combine with oxygen only about as readily as Fe, and are generally siderophile. Those elements whose oxides have low $|\Delta G^\circ|$ are generally chalcophile.

Lithophile elements also have either very low electronegativities or very high ones and tend to form ionic bonds (although the basic silicate bond, the Si—O bond, is only about 50% ionic, metal–oxygen bonds in silicates are dominantly ionic). Siderophile and chalcophile elements have intermediate electronegativities and tend to form covalent or metallic bonds.

3.2 Rare Earth Elements

The rare earths are the two rows of elements commonly shown at the bottom of the periodic table. The first row is the lanthanide rare earths, the second is the actinide rare earths. However, the term “rare earths” is often used in geochemistry to refer to only to the lanthanide rare earths. We will follow that practice in this book, though we will discuss both the actinide and lanthanides in this section. Only two of the actinides, U and Th, have nuclei stable enough to survive over the history of the Earth. Y shares the same chemical properties, including charge and ionic radius, as the heavier rare earths, and as a result behaves much like them.

As the alkalis and alkaline earths, the rare earths and Y are strongly electropositive; the lanthanide have electronegativities of 1.2 or less, the actinides U and Th have slightly higher electronegativities. As a result, they form predominantly ionic bonds, and the hard charged sphere again provides a good model of their behavior. The lanthanide rare earths are in the +3 valence state over a wide range of oxygen fugacities. At the oxygen fugacity of the Earth’s surface, however, Ce can be partly or wholly in the +4 state and Eu can be partly in the +2 state at the low oxygen fugacities of the Earth’s interior. Th is always in a +4 valence state, but U may be in a +4 or +6 valence state, depending on oxygen fugacity. Unlike the alkali and alkaline earth elements, they are relatively insoluble in aqueous solutions, a consequence of their higher charge and high ionic potential and resulting need to be coordinated by anions. The one exception is U in its fully oxidized U^{6+} form, which forms a soluble oxyanion complex.

The rare earths are transition metals. In the transition metals, the s orbital of the outermost shell is filled before filling of lower electron shells is complete. In atoms of the period 6 transition elements, the 6s orbital is filled before the 5d and 4f orbitals. In the lanthanide rare earths, it is the 4f orbitals that are being filled, so the configuration of the valence electrons is similar in all the rare earth, hence all exhibit similar chemical behavior. Ionic radius, which decreases progressively from La^{3+} (115 pm) to Lu^{3+} (93 pm), is thus the characteristic that governs their relative behavior. Because of their high charge and large radii, the rare earths are incompatible elements. The degree of incompatibilities varies, however. Highly charged U and Th are highly incompatible elements, as are the lightest rare earths. However, the heavy rare earths have sufficiently small radii that they can be accommodated to some degree in many common minerals. The heaviest rare earths readily substitute for Al^{3+} in garnet, and hence can be concentrated by it. Eu, when in its 2+ state, substitutes for Ca^{2+} in plagioclase feldspar more readily than the other rare earths. Thus plagioclase is often anomalously rich in Eu compared to the other rare earths, and other phases in equilibrium with plagioclase become relatively depleted in Eu as a consequence. The systematic variation in lanthanide rare earth behavior is best illustrated by plotting the log of the relative abundances as a function of atomic number (this sort of plot is

sometimes called a Masuda, Masuda-Coryell, or Coryell plot, but most often is simply termed a rare earth plot or diagram). Relative abundances are calculated by dividing the concentration of each rare earth by its concentration in a set of normalizing values, such as the concentrations of rare earths in chondritic meteorites. Abundances generally decrease with increasing atomic number. Thus a simple plot of abundances produces a saw tooth pattern of decreasing abundances. This can be seen in Figure 3.1, which shows rare earth abundances in the CI chondrite Orgueil (CI chondrites are a class of meteorites that are taken to be the best representative of the average concentrations of non-volatile elements in the solar system).

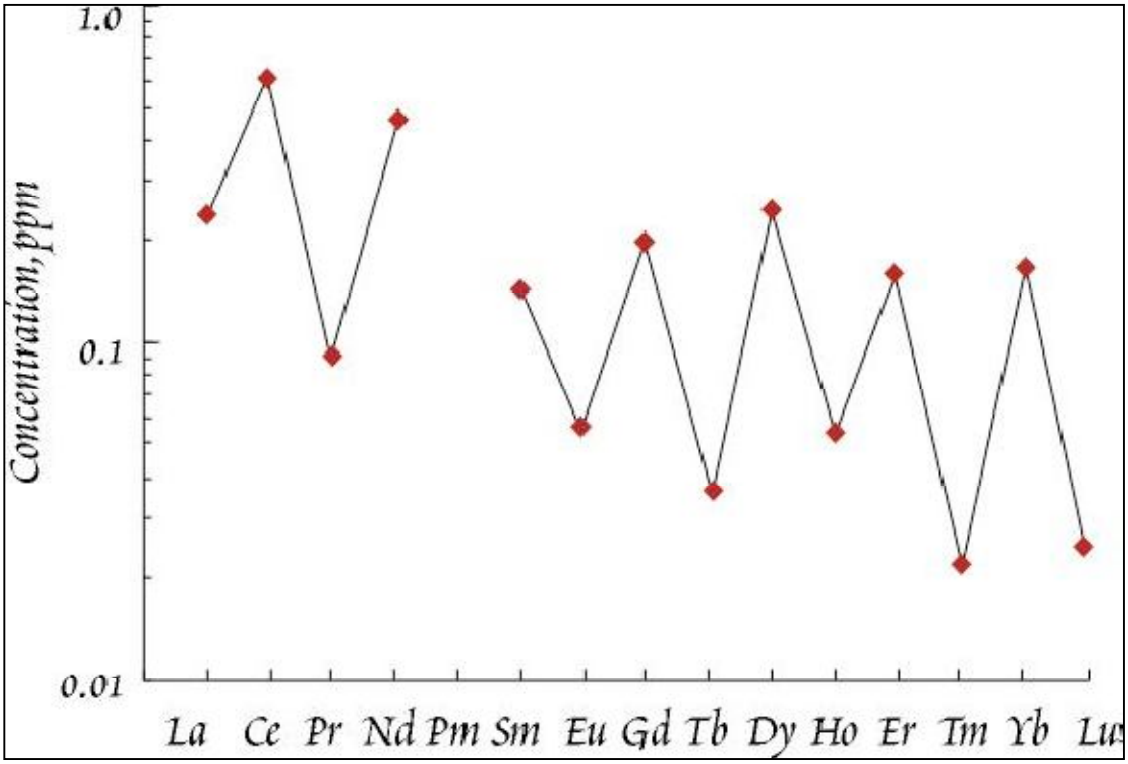

Fig. 3.1 Concentrations of the rare earths in the carbonaceous chondritic meteorite Orgueil

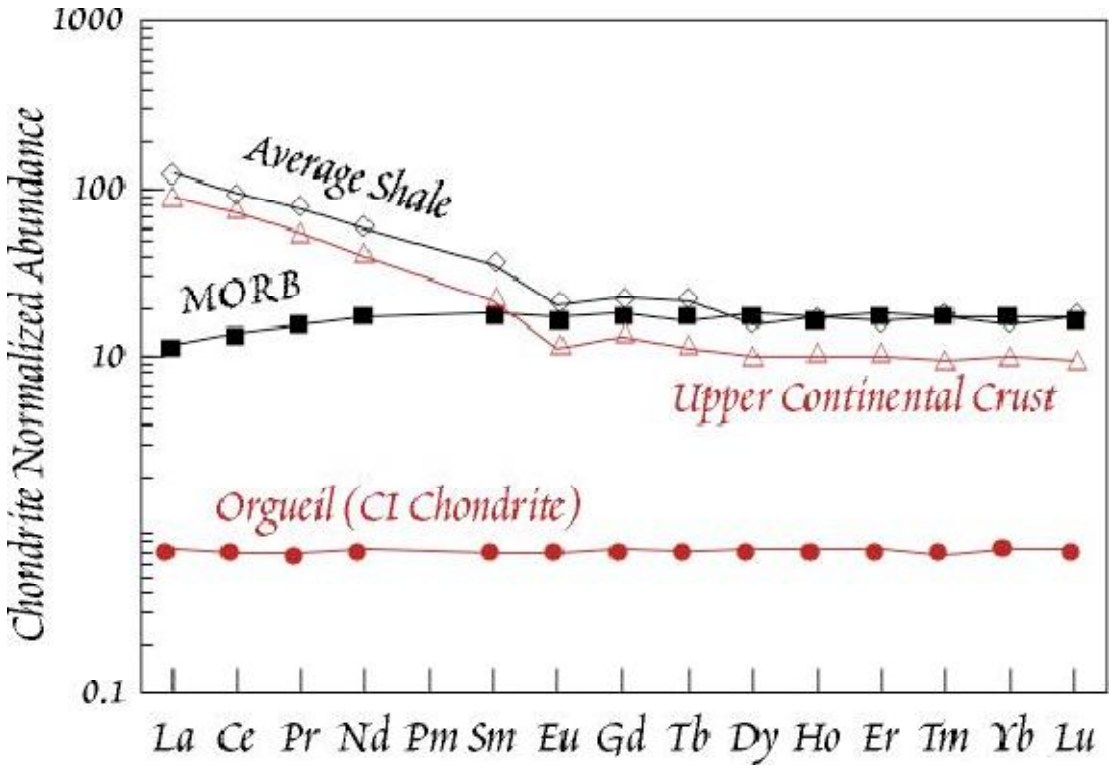

Fig. 3.4 A rare earth plot showing rare earth patterns for average upper continental crust (Rudnick and Fountain, 1995), average shale, average mid-ocean ridge basalt, and the meteorite Orgueil. As a carbonaceous chondrite, Orgueil has lower rare earth concentrations than the average of ordinary chondrites used for normalization.

"Normalizing" the rare earth abundances to those of chondritic meteorites eliminates effects related to nuclear stability and nucleosynthesis and produces a smooth pattern, such as those seen in Figure 3.2. Though all igneous geochemists normalize rare earth abundances to some set of chondritic values, there is no uniformity in the set chosen. Popular normalization schemes include the CI chondrite Orgueil, an average of 20 ordinary chondrites reported by Nakamura (1974), and the chondritic meteorite Leedy (Masuda et al., 1973). Although the absolute values of the normalizing values vary (for example, the Nakamura values are about 28% higher than those of Orgueil), the relative abundances are essentially the same. Thus the normalized rare earth pattern should be the same regardless of normalizing values. A complete tabulation can be found in Rollinson (1993). Rare earth patterns for upper continental crust and average mid-ocean ridge basalt (MORB) are also shown in Figure 3.1. MORB exhibits a light rare earth-depleted pattern; upper continental crust is light rare earth-enriched with a negative 'Eu anomaly'. The light rare earth depletion of MORB reflects the incompatible element-depleted nature of the upper mantle from which these magmas are derived. This incompatible element depletion of the mantle is generally thought to have resulted from extraction of partial melts, in which the incompatible elements were concentrated. Those partial melts have crystallized to form the continental crust. If this is so, the complementary nature of the rare earth patterns of MORB and continental crust is not coincidental. There are good reasons to believe that the relative abundances of rare earths in the Earth as a whole are similar to those of chondrites, i.e., the rare earth pattern of the Earth should be flat. Mass balance therefore requires the sum of all the various rare earth reservoirs in the Earth have a flat rare earth pattern. If we assume the continental crust and the mantle are the only two reservoirs with significant concentrations of rare earth elements, and if the continental crust is

light rare earth-enriched, then the mantle should be light rare earth-depleted. A negative Eu anomaly is typical of many continental rocks, as well as most sediments and seawater. The Eu anomaly probably arises because many crustal rocks of granitic and granodioritic composition were produced by intracrustal partial melting. The residues of those melts were rich in plagioclase, hence retaining somewhat more of the Eu in the lower crust, and creating a complimentary Eu depleted upper crust. Sediments and seawater inherit this Eu anomaly from their source rocks in the upper continental crust. Many sedimentary rocks, and seawater, have rare earth patterns that are similar to each other, and to that of the continental crust. To accentuate the difference in rare earth patterns between sediments, low temperature geochemists often normalize rare earth abundances to the concentrations in average shale. Again, there are several sets of normalizing values (Rollinson, 1993), but the relative abundances are all similar. Because the rare earths are highly insoluble and immobile, rare earth patterns often remain unchanged during metamorphism. Hence rare earth patterns can provide information on the premetamorphic history of a rock. Indeed, even during the production of sediment from crystalline rock, the rare earth patterns often remain little changed, and rare earth patterns have been used to identify the provenance, i.e., the source, of sedimentary rocks. Rare earth patterns have also become useful tools in chemical oceanography, now that modern analytical techniques allow their accurate determination despite concentrations in the parts per trillion range.

3.3 The First Series Transition Metals

The chemistry of the transition elements is considerably more complex. There are several reasons for this. First, many of the transition elements have two or more valence states in nature. Second, the transition metals have higher electronegativity than the alkali and alkaline earths, so that covalent bonding plays a more important role in their behavior. Bonding with oxygen in oxides and silicates is still predominantly ionic, but bonding with other nonmetals,
such as sulfur, can be largely covalent. A final complicating factor is the geometry of the d orbitals, which are highly directional and thus bestow upon the transition metals specific preferences for the geometry of coordinating anions, or ligands.
The solubility of the transition metals, though generally lower than that of the alkalis and alkaline earths, is quite variable and depends upon valence state and the availability of anions with which they can form soluble coordination complexes. Their behavior in magmas is also variable. They range from moderately incompatible (e.g., Ti, Cu, Zn) to very compatible (e.g., Cr, Ni, Co), but their exact behavior is generally a stronger function of composition (of both solid and melt phases) than that of the highly incompatible elements. With the exception of Mn, the first transition series metals are also siderophile and/or chalcophile.

3.4 The Noble Metals

The platinum group elements (Rh, Ru, Pd, Os, Ir, Pt) plus gold are often collectively called the noble metals. These metals are so called for two reasons: first they are rare, second they are unreactive and quite stable in metallic form. Their rarity is in part a consequence of their highly siderophilic character. The concentration of these elements in the silicate Earth is only about 1% of their concentrations inchondrites. Presumably, the bulk of the Earth's inventory of these elements is in the core. As a result of their low concentrations, their behavior is still poorly understood. These elements are all also chalcophile (i.e., all are enriched in sulfide liquids relative to silicate liquids), although to varying degrees. Ir appears to be the most chalcophile, Pt and Au the least. Considering the associations of their ore deposits, the platinum group elements (PGE) may be divided into two subgroups: the Ir group (Ir, Os, and Ru) and the Pd group (Rh, Pd, Pt). The former are often associated with chromites (chromite is $(Fe,Mg)Cr_2O_4$, part of the spinel solid solution) in ultramafic rocks as native metal alloys or sulfide (e.g., the Stillwater Complex of Montana), while the latter are associated with magmatic sulfides of Fe, Ni, and Cu associated with gabbros (e.g., the Sudbury Complex of Ontario).

Besides forming compounds with sulfur, these elements form a variety of chloride and other

halide complexes. These complexes may play an important role in the formation of some PGE deposits and certainly do in many gold deposits. These elements are transition elements and, like the first transition series, can exist in multiple valence states, ranging from 0 to +8, and have bonding behavior influenced by the d-orbitals. Thus their chemistry is complex. When in high valence states, some, Os and Ru for example, form oxides that are highly volatile.

The nature of the host phase for these elements in the mantle is unclear. Mitchell and Keays (1981) found that they were concentrated in minerals in the order garnet<olivine<orthopyroxene <clinopyroxene<spinel, but that the total inventory in all minerals was less than that in the bulk rock. They concluded that 60-80% of the PGE's were present in intergranular sulfides. An alternative host is native metal grains, such as osmiridium (an approximately 50-50 Os-Ir alloy), which have been found in peridotites. A study by Brügmann et al. (1987) of komatiites revealed that the concentrations of Au and Pd increased with decreasing MgO while those of Ru, Os, and Ir decreased with decreasing MgO concentrations.

This suggested that Au and Pd are moderately incompatible elements while are Ru, Os, and Ir are highly compatible. Subsequent work has confirmed this conclusion and shown that Rh is compatible while Pt is incompatible. Recent studies suggest that the elements dissolve in silicate melts in low valence states, +2 for Ir (and perhaps Os), and +1 for the other elements. The solubility of these elements in silicate melts, relative to native metal alloys, appears to be quite low, but is probably not exceeded in nature. In a manner analogous to the rare earths, PGE data are sometimes presented as plots of the chondrite-normalized abundance. In this case, however, elements are not ordered by atomic number, but rather by decreasing melting point. This, as it turns out, places them in order of decreasing compatibility.

Part II

NORTHERN ITALY COPPER MINES

1. Copper mineralogy

Copper is a salmon pink or reddish element with a bright metallic luster. It is malleable, ductile, and a good conductor of heat and electricity, which is one of the principal reason for its extensive use today. Like silver and gold, copper is a face-centered cubic metal (Scott, 2002).

The chemical symbol for copper is Cu, the element is the number 29 in the periodic table, and it has an atomic weight of 63.546. Cu has two natural isotopes, ^{63}Cu and ^{65}Cu, with relative natural abundances of 69.17% and 30.83% respectively.

Copper abundances in rocks are reported in table 1.1. Table 1.2 lists the most common copper ore minerals although more than one hundred and fifty copper minerals are known.

Mean abundance	ppm
Silicatic Crust	30
Continental Crust	25
Ultramafic rocks	10
Basalts	87
Andesites	54
Diorites	35
Granites	10
Sienites	5
Schists	45
Shales	250
Carbonates	4
Greywackes	45
Soils	20

Table 1.1 – Cu abundances in rocks (Brigo and Montanari, 2006)

The most common and used copper mineral is chalcopyrite; bornite, covellite and chalcocite are also important. Many deposits are also rich in secondary mineral phases such as malachite, azurite, cuprite, tenorite and native copper.

Electrical conductivity of pure copper and other physical properties are influenced by elemental impurities. These impurities are:

- As: the most frequent impurity in copper together with O. As-bearing Cu (0.1-0.5%) has better thermal resistance.

- Sb: it does not influence mechanic features up to 0.5% in weight.
- Ag: it is soluble in Cu up to 3%. it doesn't influence copper
- Be: it strongly decreases electric conductivity
- Bi: it makes hot worked Cu, very brittle.
- Cd: small amounts of Cd are soluble in copper, with an improvement of mechanic characteristics of Cu.
- Fe: it is soluble up to 3% in copper, improving mechanic characteristics to the detriment of ductility.
- Ca, P and Li: very usefull to outgas and deposit copper. High percentages of P make copper brittle.
- Mn: it improves mechanic characteristics of copper to the detriment of ductility
- Ni: it improves mechanic characteristics of copper even if in small amounts
- Pb: it is little soluble in copper (0.1%) and it makes hot-worked copper brittle. This problem is solved if As is added (0.3-0.4%)
- S: even small percentages of S (0.1%) make copper brittle.
- Sn: it is very soluble in copper and it is used for bronze production.
- Ti: it is soluble up to 0.23% in Cu. It makes it harder but tenacity decreases.
- Zn: it is very soluble in copper and it is used for brass production.

Mineral		Chemical formula	%Cu	Density	Mohs Hardness
Native el.	Native copper	Cu	99.52	8.9	2.5-3
Sulfides and sulfosalts	Chalcopyrite	$CuFeS_2$	34.63	4.1-4.3	3.5
	Chalcocite	Cu_2S	84.8	5.5-5.8	2.5-3
	Bornite	Cu_5FeS_4	50.7	5.06-5.08	3
	Covellite	CuS	66	4.6-4.76	1.5-2
	Enargite	$Cu_3(As,Sb)S_4$	46.8	4.43-4.45	3
	Tetrahedrite	Cu_3SbS_3	52.1	4.6-5.1	3-4.5
	Tennantite	Cu_3AsS_3	57	4.6-5.1	3-4.5
	Bournonite	$2PbSCu_2SSb_2S_3$	12.7	5.8-5.9	2.5-3
Oxides	Cuprite	Cu_2O	88.8	6	3.5-4
	Tenorite	CuO	79.8	5.8-6.4	3-4
Carbonates	Malachite	$Cu_2[(OH)_2CO_3]$	57.3	3.9-4.03	3.4-4
	Azurite	$Cu_3[(OH)CO_3]_2$	55.16	3.77	3.5-4
Sulfates	Antlerite	$Cu_3[(OH)_4SO_4]$	53.74	3.9	3
	Brochantite	$Cu_4[(OH)_6SO_4]$	56.2	3.9	3.5-4
Silicates	Chrysocolla	$Cu_4[(OH)_8Si_4O_{10}]$	40	2-2.4	2-4
Chlorides	Atacamite	$Cu_2(OH)_3Cl$	59.4	3.75-3.77	3-3.5

Table 1.2 – Most common copper minerals (Brigo and Montanari, 2006)

1.1 Copper Deposits

Copper is distributed fairly regularly in various geological eras, however, important concentrations began to form in the Proterozoic. In particular the Upper Proterozoic is characterized by the development of large sulfides deposits both with dominant Cu (e.g. Zambian Copper Belt) and with Pb-Zn-Cu (many examples in Australia). Another enrichment step occurs in the Phanerozoic, both in oceanic environments and in continental convergent margins (Andean type). Here the main copper deposit types are reported.

Orthomagmatic deposits. Orthomagmatic deposits are deposits that form during the normal processes of magmatic differentiation. In most cases, concentration of metals appears to be the result of different processes combination. Depending on these factors we have different types of deposit.
First type is Ni (Cu,PGE) sulfide deposit in komatitic lavas, that can be of two types: i) stratiform at the lava flow base ii) disseminated within cumulitic peridotitic levels. Paragenesis is given by pyrrhotite, pentlandite and pyrite with subordinate chalcopyrite.
Second type is Cu-Ni deposit associated to basic and ultrabasic intrusions, that represent the intrusive equivalent of deposits associated to komatitic flows. Paragenesis is given by pyrrhotite with chalcopyrite, pentlandite and cubanite.
Last type of deposit is that associated to stratified intrusive complexes. These deposits are stratiform. Stratified basic complexes are typically associated with mineralization in chromite, PGM (Platinum-Group Minerals), Ni and Cu sulfides and, in most differentiated portions, ilmenite and Ti-V bearing magnetite. The layered complexes are generally located in cratonic or continental areas.

Deposits associated with acid and intermediate plutonic complex. These deposits change their characteristics depending on the stage of granitic melt evolution sequence (pegmatitic, pneumatolitic and hydrothermal stages). Factor that most influences mineralizations formation is the intrusion depth. Copper deposits are relevant in *Skarn* type deposits. These are epigenetic/metasomatic bodies with irregular shape, formed at the contact between carbonatic rocks (limestones, dolomites) and intrusive granitoids, such as granodiorite, diorite, monzonite, at a depth ranging from 1 to a few km. In particular, acid calcalcaline intrusions are associated to Cu (Pb-Zn) skarn.
Meso-and epithermal deposits. The hydrothermal fluids are primarily responsible for the formation of a wide variety of deposits, not necessarily linked to the presence of magma. Depending on the depth of emplacement, the temperature of the fluids and the origin of water that generated them, hydrothermal deposits can be qualitatively divided into several classes. *Porphyry Coppers* belong to this deposit typology; they are linked to intrusive magmatism (acid to intermediate) along continental margins. They are fine grain sulfide disseminations (mainly chalcopyrite and pyrite), that develop at the top of granodioritic and quartz-dioritic plutons. Porphyry coppers are associated with characteristics

hydrothermal alteration facies caused by circulation of metal-bearing magmatic-hydrothermal fluids. The prevalent age of these deposits is Cenozoic.

Stratiform and strata-bound ore deposits associated with volcanic and sedimentary rocks.
Exhalative processes constitute the expression of supergenic hydrothermal activity. The resulting metal deposits are typically syngenetic with sedimentary formations in the basin, and they themselves largely derived from the deposition of sedimentary processes (chemical and partly mechanical), which are originated by the interaction between hydrothermal solutions and seawater.
The metallic deposits are often associated with volcanic rocks (volcanogenic massive sulfides, VMS), but in some cases are totally contained within sedimentary sequences (sedimentary-exhalative, *Sedex*) and show no apparent relation with volcanites.
VMS deposits that appear on the continents have a lenticular shape, more or less thick up to almost stratiform. Generally deposits show a mineralized zone at the base with disseminations and veins (*stringer zone*), characterized by the presence of a network of fractures (*stockwork*), in seabed rocks and these veins allow the going up of hydrothermal solutions. The typical mineralogy is given by sulfides, which generally consists of more than 90% pyrite, possibly associated with sulfates and oxides In general, volcanogenic massive sulfides deposits can be classified on the basis of their average composition and the nature of associated sedimentary and/or volcanic rocks. In terms of compositional relations, Cu-Zn-Pb ratios allow detection of two major groups of deposits: (1) Cu-Zn deposits and Zn-Pb-Cu deposits.
Sedex deposits are stratiform deposits and they are formed in sedimentary basins on continental rift zones seabed, aulacogens or epicontinental seas, as a result of exhalative hydrothermal activity. The main distinctive factor is the absence of genetic relationships with volcanic rocks and, therefore, the absence of a magmatic chamber as the main engine of the convective circulation of hydrothermal fluids. They are especially associated with early Proterozoic rocks, but can occur during rocks of any age.
Sedex deposits are generally made up of several overlapping lenticular mineralized bodies. Sulfides (mainly galena and sphalerite) are finely stratified and often interspersed with sediments.
Stratiform copper deposits in sedimentary rocks are typically associated with bituminous and pyritic shales, expression of reducing anoxic sedimentary environments, at the contact with oxidized red continental clastic sediments. Most important deposits are age ranging from Upper Proterozoic to Upper Paleozoic, and they formed in areas with arid or semi-arid climate at continental rift zone or in epicontinental seas. The mineralization can be formed in syngenetic conditions up to late diagenetic The characteristic minerals include native copper, chalcocite, bornite, chalcopyrite, galena, sphalerite and pyrite.
Mississippi Valley Type Deposits (MVT) are epigenetic mineral deposits far from any bodies of igneous rock. They are commonly found on continental platform deposits of dolostones and limestones. Deposits are not strictly stratiform piles (stratabound), with metasomatic replacement bodies, veins and stockworks. Paragenesis is given by sphalerite, galena, pyrite and marcasite, with subordinate chalcopyrite.

2. Geological setting and sampling of Alpine copper mines

In this work some of the most important copper districts in Northern and Central Italy have been studied (fig. 2.1). Form a geological point of view the study covered four main areas: the central-eastern Southern Alps (*Variscan basement and Permian-Triassic cover, Carnic Alps*), the Western Alps (*Piedmont Zone, Ligurian Briançonnais, Gran Paradiso nappe, Argentera*), the Ligurian Apennines (*Libiola, Monte Loreto*) and Southern Tuscany-Elba (*Isola d'Elba, "Colline metallifere" and Montecatini Val di Cecina*).

2.1 Western Alps

Deposits that we studied in Western Alps are in penninic units (Piedmont zone, Briançonnais and Gran Paradiso) and helvetic unit (Argentera) (see fig.2.1).

2.1.1 Upper penninic nappes: Piedmont zone

The Upper Penninic nappes are predominantly derived from the Piedmont-Liguria Ocean (Alpine Tethys) and pieces of exhumed sub continental mantle of the immediately adjacent distal margin of Apulia (Schmid et al., 2004).

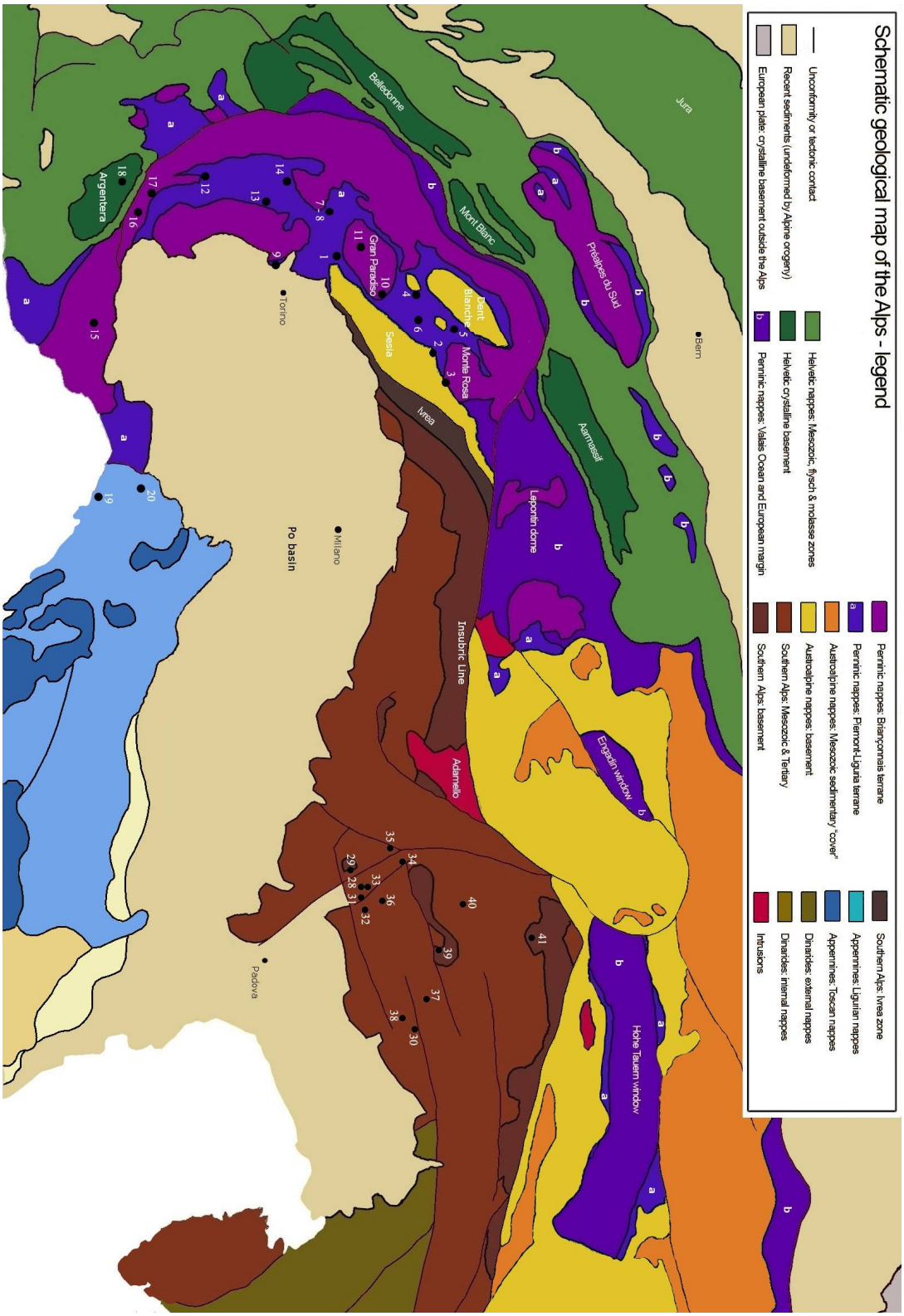

Fig. 2.1 – Schematic geological map of the Alps (modified after Schmid et al., 2004). Mines investigated are reported with a catalogue number (see table 2.1)

These units consist of (i) ophiolites, often grading into distal continental margin units (i.e. Manatschal & Nievergelt, 1997); (ii) Bündnerschiefer (i.e. "Avers Bündnerschiefer"; Oberhänsli, 1978) or Schistes Lustrés (i.e. Escher et al., 1997), often containing ophiolitic slices or olistoliths; (iii) nonmetamorphic cover nappes of very internal, but not exclusively oceanic origin, such as the Helminthoid flysch of the Embrunais-Ubaye cover nappes (i.e. Kerkhove, 1969) or the Nappes Supérieures of the Préalpes of Western Switzerland and adjacent France (i.e. Caron et al., 1989), respectively; (iv) and finally, ophiolitic mélanges such as the Matrei zone found at the rim of the Tauern window (see paragraph 2.4.3) (Frisch et al., 1989; Kurz et al., 1998).
The Piedmont Zone, forming a very large part of the internal Western Alps, was mostly overprinted by subduction-related, Tertiary-age, pressure-dominated metamorphism (i.e. Gebauer, 1999) and associated deformation. Oceanic units that make up the Piedmont area is also known as the zone of "calcescisti con pietre verdi". It includes fragments of oceanic crust and Mesozoic sedimentary cover that is characterized by calcschists (the "Schistes Lustrés" in french literature). In the Piedmont Zone several stratiform copper-bearing pyrite deposits (with chalcopyrite, sphalerite and other sulfides) are found in ophiolitic metamorphites (mainly prasinites) (Bottino et al. 1975).

2.1.2 Middle Penninic nappes: Ligurian Briançonnais Zone and Gran Paradiso internal massif

These units are part of the "Briançonnais terrane". A subdivision into a more internal "Briançonnais" and a more external "Subbriançonnais" paleogeographical domain is only possible where cover sequences are well preserved (Shmid et al. 2004).
The Middle Penninic basement nappes partly consist of a pre-Late Carboniferous basement exhibiting pre-alpine metamorphism, and partly of mono metamorphic Permo-Carboniferous fill (e.g. Baudin et al. 1993). This unit comprises all basement nappes whose origin is known or interpreted to have been part of the Briançonnais terrane. This attribution is well established in case of the basement slices that make up the former Bernhard nappe and its equivalents in the Western Alpine Arc (i.e. Gouffon 1993; Escher et al. 1997).
The "Internal Massifs", i.e. the Dora Maira, Gran Paradiso and Monte Rosa nappes, belong to the Briançonnais terrane (Keller & Schmid 2001). Detached Middle Penninic cover nappes of the Western Alps are found at the front of the Western Alps, together with Upper Penninic cover nappes.
Deposits studied in the present work are located in Ligurian Briançonnais Zone and Gran Paradiso internal massif.
Ligurian Briançonnais Zone: in the Ligurian Alps, the Briançonnais Zone is composed of a relatively chaotic stacking of tectonic units wich were in origin in paleogeographic continuity. Three sectors are recognized, inner, middle an outer, each of them being composed of a crystalline basement and a Permo-Carboniferous cover (Rossetti and Ferrero, 2008).
Gran Paradiso internal massif: The eclogitic internal massif is continental exotic block, underplated in the accretionary complex and subsequently mixed with oceanic elements

in a westward tectonic escape movement during their extrusion. It's constituted by metagranites and gneisses with metabasites, in which we can find Cu, Pb, Sb mixed sulfides.

2.1.3 Helvetic unit: Argentera massif

The Helvetic unit represents the Europe paleomargin and is the outer-most domain present in the Piedmont Alps. In Piedmontit it is represented by the Argentera massif which is made up of a nucleus of Hercynian granite, augen gneisses, amphibolites and an impressive volume of migmatites.
Its inner margin is a thin strip of preserved sedimentary helvetic cover. The Argentera massif, similar to the northern massifs (Pelvoux, Belledonne, Grandes Rousses, Mont Blanc, Aiguilles Rouges, Aar-Gotthard-Gastern), is an axial culmination of the crystalline basement of the external sector of the chain (Schmid et al., 2004).
Argentera deposits are Pb-Zn dominated hydrothermal veins with subordinate chalcopyrite, pyrite, arsenopyrite and pyrrhotite, in quartz and fluorite gangue.

2.2 Ligurian Apennines

Unit Ligurian nappes comprise oceanic units (Ligurides) that paleogeographically belong to the Piedmont-Liguria ocean. However, in contrast to the Alps, in the Apennines the remnants of this ocean presently form the upper plate in relation to units attributed to the Apulian plate (Laubscher 1971; Marroni et al. 2002). This is because the Ligurides were "back-thrust" (in respect to the polarity of the Alpine movements), i.e. thrust north- and north-eastward onto the Po Basin during Mid-Miocene and later times (Finetti et al. 2001).
The ore deposits studied here, are hosted in the flyschoid sequence of ophiolite-bearing argilloschists. This sequence, of Jurassic-Cretaceous age, is a thick complex of the Ligurian domain and is established at lower tertiary formations (like "macigno"), and covered by syn- and post-orogenic sediments. The ore deposits have an exhalative hydrothermal oceanic origin and are of Jurassic age (Mastrangelo et al., 1975).

The ore deposits hosted by the Eastern Ligurian ophiolites show different mineral assemblages in relation to their origin and the enclosing rock types (fig. 2.2):

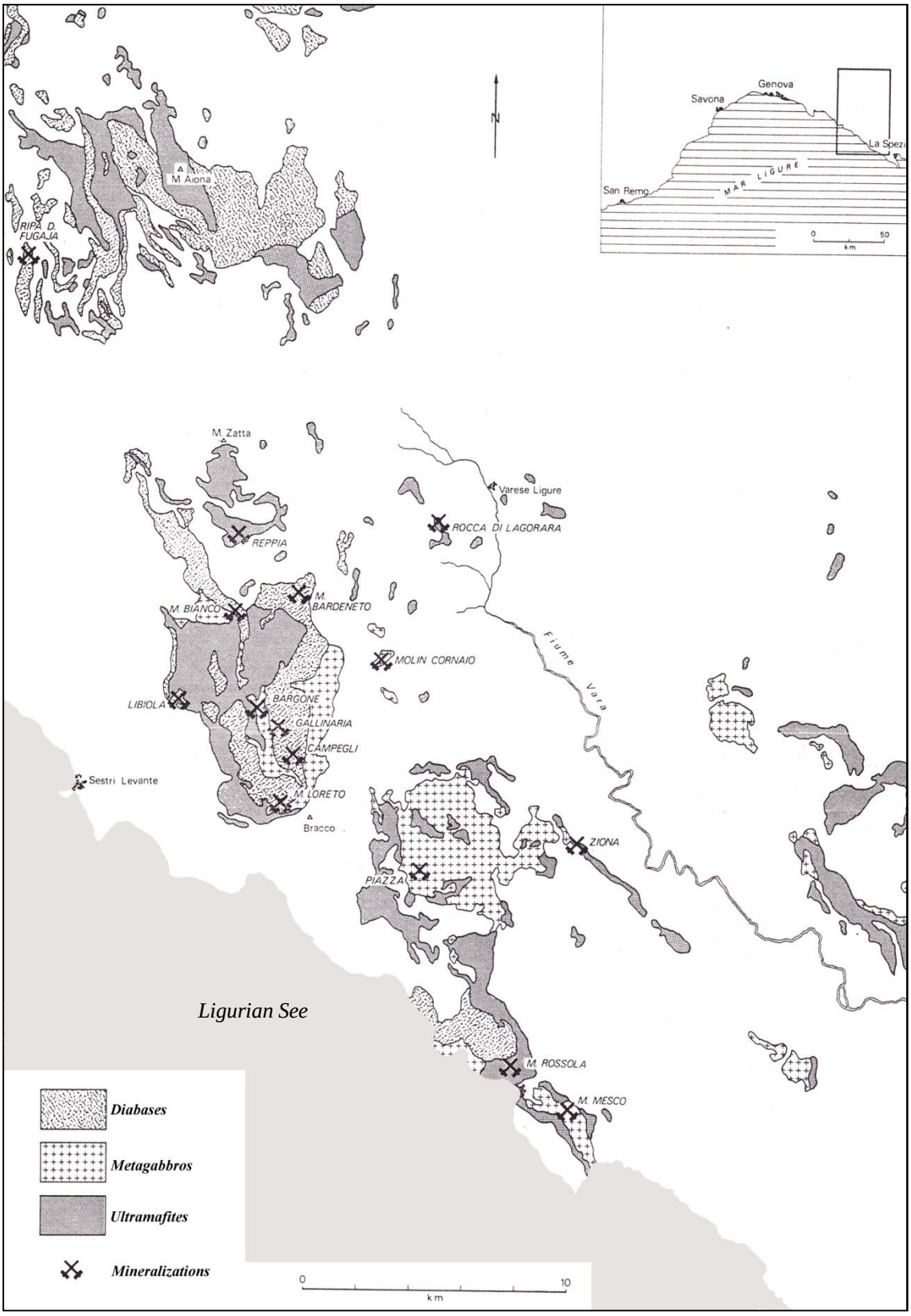

2.2 – Deposits distribution in Ligurian Ophiolites, modified by Brigo and Ferrario (1974)

- In ultramafic rocks (more or less serpentinized): pyrrhotite, chalcopyrite-pyrite-pentlandite orthomagmatic ores (Bonassola-Monte Rossola); chalcopyrite-pyrite-pyrrothite-Ni minerals “stockworks” (Rocca di Lagorara); chalcocite-covellite-

chalcopyrite ores in remobilization veins and veinlets (Reppia, Libiola, Gallinaria);

- In metagabbros: the ore bodies are veins and have a constant mineralogical assemblage defined by bornite, chalcopyrite, quartz and calcite (Molin Cornaio, Bragone, Piazza and Monte Mesco;

- In pillow or sheeted spilitic diabases: massive, disseminated and "stockwork" structures (similiar in all the deposits) with pyrite, chalcopyrite and sphalerite (Libiola, Gallinaria, Casali, Monte Loreto).

Because of stratigraphic-structural considerations, ophiolites of Eastern Liguria can be divided in two distinct units: a "lower unit" formed by ultramafites and metagabbros, that represent the "basement" where pillow or spilitc diabases and the sedimentary cover of Jurassic-Cretaceous age took place. Space and time relationships beween ore deposits and ophiolitic rocks confirmed the geological setting: Cu-Ni-Fe-Cr-(P) are present in ultramafic rocks and metagabbros, and Fe-Cu-Zn-(Au) in spilitc diabases (Brigo and Ferrario, 1974).

2.3 Southern Tuscany-Elba

Northern Apennine evolution had many dislocative phases from Mesozoic begin up to the end of Tertiary, and it caused the overlapping of many tectonic units belonging to different domains and paleogeographical zones. Tectonic units that form Apennines chain belong to four domains that, form W to E: 1. Ligurian domain; 2.Australpine domain; 3. Tuscan domain; 4. Umbro-marchigiano domain. The last one will not considered because is not present in Southern Tuscany area (Costantini et al., 1989).
Tectonic units in Southern Tuscany ("Colline metallifere" and Elba) area are seven, that are overlapped by trasgressive neogenic and Quaternary deposits. Here units are reported from the bottom to the top.
Tuscan domain:

1. Boccheggiano unit – It consititutes the deeper unit so far known in Tuscan South of the Arno river; it consists of grey-black phyllites with quartzites. Its age is upper Silurian-Devonian age.
2. Monticiano-Roccastrada unit – In this unit are distinguished two groups; the first one is a group of Paleozoic formations and second one is the Verrucano group, that is a three formations group in continuous succession ranging in age from Ladinian to the lower Triassic. In this unit we found Elba deposits, Boccheggiano and Campiglia Marittima (which belong to "Colline metallifere").
   Elba deposits are concentrated in the eastern part of island and are hosted in Paleozoic-Triassic formations of Monticiano-Roccastrada unit. Deposits are

constituted by iron oxides with pyrite and sulfides (Cu, Zn, Pb, As) (Tanelli et al., 2001).

In the Boccheggiano area, some pyrite deposits and most polymetallic mineralizations are spatially associated with the late extensional structures, particularly the Boccheggiano fault (Benvenuti et al., 1997). Other pyrite deposits are located at the contact between basement rocks of the Monticiano–Roccastrada unit and the overlying Calcare Cavernoso formation of the Tuscan Nappe (Tanelli and Lattanzi 1983). The Campiglia district has Cu-Pb-Zn ilvaitic-hedembergitic skarn deposits, Cu-Fe diopsidic skarn deposits and iron oxides with cassiterite deposits (Chiarantini, 2005).

3. Tuscan nappe – this unit in Southern Tuscany is in form of discontinuous and isolated fragments having a lenticular shape. The age is from upper Trias to upper Oligocene.

Austroalpine domain:

4. "Argille e calcari" unit/S. Fiora unit – the first one is made up of argillites with turbiditic calcarenite intercalations of Paleocene-Eocene age. The second unit is characterized by turbiditic calcarenites of Cretaceous age.

Ligurian domain:

5. Monteverdi Marittimo unit – consists of argillites and siltstones with calcarenites and sandstones as intercalation. The age is Cretaceous-upper Paleocene.
6. Lower ophiolites unit – constituted by serpentinites, gabbros, diabases and sedimentary rocks that are relative to upper Jurassic-lower Cretaceous. In this unit is located Montecatini Val di Cecina copper deposit with a primary mineralization (chalcopyrite and pyrite with bornite in quartz-chlorite gangue) that is oxidized by descending sulfated water and enriched copper amount in two secondary mineralizations (chalcocite, bornite, tetrahedrite, and native copper).
7. Upper ophiolites unit – is made up of argillites those intercalate with siliceous limestones, limestones and sandstones, from the lower to the upper part.

2.4 Eastern Alps

2.4.1 Central-Eastern Southern Alps

In the ***Western Dolomites*** region (eastern Southalpine), a large pop-up related synclinorium is limited to the north by the dextral Periadriatic Lineament and to the south by the Neogenic south-vergent Valsugana overthrust system (Doglioni, 1987) (Fig. 2.3). The synclinorium allows exposure of the pre-Alpine (Variscan) metamorphic basement along its northernmost and southernmost limbs. This basement mainly consists of phyllites and "porphyroid" gneisses, with subordinate metabasites, and represents a former Early-Mid Paleozoic sequence of sediments with volcanic intercalations. The sequence is formed of three complexes (Sassi & Zirpoli, 1990): a lower pelitic-psammitic

complex with Late Cambrian acritarchs (Kalvacheva et al., 1986; Vecoli et al., 2008), an intermediate volcano-sedimentary complex with intercalations of basic and Late Ordovician acidic volcanic and volcanoclastic rocks ("porphyroids") (Meli & Klötzli, 2001), and an upper pelitic-psammitic complex of probable Early Silurian to possibly Devonian age (cf. Dieni et al., 2005). The three complexes underwent greenschist-facies metamorphism during the Variscan event. The metamorphic rocks are intruded by Permian, post-Variscan granitoids with high-K calc-alkaline affinity, which were emplaced in an extensional, post-orogenic tectonic regime (Rottura et al., 1998; Dal Piaz & Martin, 1998). In the less eroded central portion of the Dolomites region, the metamorphic basement is hidden under a thick Permian–Jurassic volcanic and sedimentary sequence. The base of this sequence consists of a pile of Early Permian rhyolites, dacites and andesites (Atesino Volcanic District1), which are consanguineous with the post-Variscan intrusives (Rottura et al., 1998) and reach a maximum thickness of over 2000 m in its central portion between Bolzano and Trento. The rest of the sequence mainly consists of carbonatic platform and terrigenous sediments, cut by and partly heteropic with Ladinian igneous rocks (Fig. 2.3).

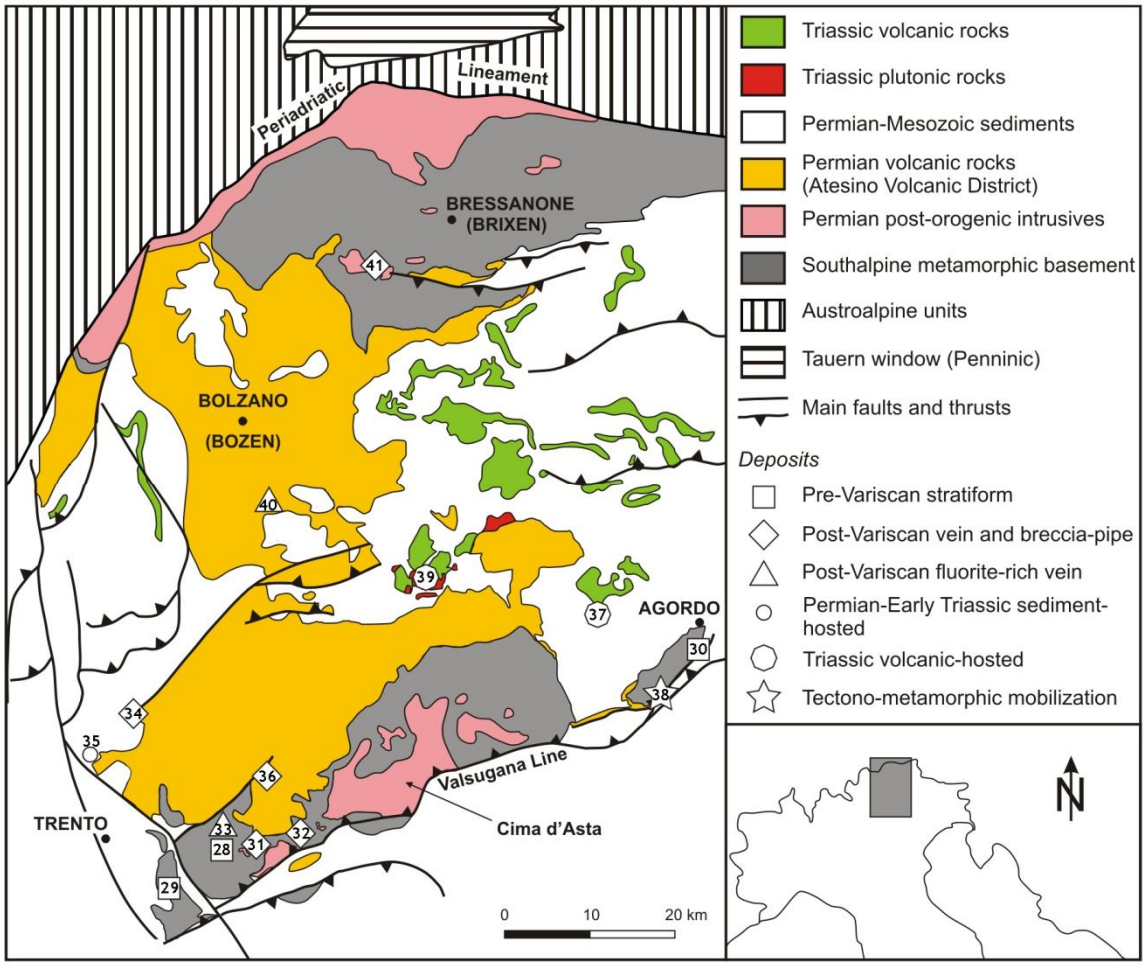

Fig.2.3 – Ore deposits of Central-Eastern Southern alps here studied. For mines number in the map please, see table 2.1

[1] Also reported in the literature as Atesina Volcanic District or Athesia Volcanic District.

The Ladinian igneous rocks are represented by mafic to intermediate volcanic rocks with shoshonitic affinity erupted in a transcurrent tectonic regime (Bonadiman et al., 1994), and by associated intrusives with high-K calc-alkaline to sodic alkaline affinity (Predazzo–Monzoni plutonic complex; Lucchini et al., 1982; Visonà, 1997).

The metallogenic sequence of the region can be summarized as follows:

1. *Pre-metamorphic, hydrothermal-exhalative, stratiform deposits within the crystalline basement (Late Ordovician–Early Silurian).* These deposits are mostly distributed along a belt extending for about 100 km along the Valsugana Line, from the high Valsugana Valley south-east of Trento to the Agordo area north-east of Belluno (Agordo–Valsugana Zone; Frizzo & Ferrara, 1994). The deposits are localized within a metamorphosed volcano-sedimentary unit (phyllites, porphyroid gneisses, chloritoschists, metabasalts) corresponding to the "intermediate complex" of Sassi and Zirpoli (1990). The deposits are pyrite-dominated, with subordinate sphalerite, galena, chalcopyrite, arsenopyrite, tetrahedrite and traces of Au and Ag (Frizzo, 2004a). Similar deposits are also reported in the northern sector of the metamorphic basement within the Bressanone Phyllite (Brigo, 1971). Variscan greenschist facies metamorphism determined moderate to intense recrystallization and, sometimes, remobilization of metals, with formation of chalcopyrite-enriched veinlets within the brecciated massive sulphides.

2. *Deposits connected with post-Variscan magmatism (Early-Mid Permian)*. They are mainly represented by copper and polymetallic (Pb, Zn, Cu, Ag ± Au) veins with quartz gangue and, possibly, by fluorite-rich, sulphide-bearing veins, which cut the lower and intermediate units of the Permian volcanic sequence (andesites to rhyodacites) and the underlying metamorphic sole (Cavinato, 1968; Fellerer, 1968; Brigo, 1971; Bakos et al., 1972; Omenetto & Brigo, 1974; Frizzo, 2004a) (Fig. 2.3). The sulphide-rich deposits are associated with significant propylitic and potassic alteration of the host-rocks. The dominant copper mineral is chalcopyrite. Also connected with the post-Variscan magmatism is a magnetite + pyrrhotite deposit (Fig. 2.3) with minor Cu, Zn, Co, Bi, As, which is developed in the form of a breccia pipe at the margin of the Roncegno subvolcanic granodiorite intrusion, at the south-western end of the Cima d'Asta plutonic complex (Omenetto, 1968b). Only one sulphide-rich vein deposit (Fig. 2.3) is known from the upper, rhyolitic volcanic sequence; it is distinguished from the other sulphide-rich deposits by its peculiar galena + tetrahedrite + chalcopyrite paragenesis (Dessau & Duchi, 1970). The Permian age of this deposit is proven by stratigraphic relations with the overlying Upper Permian Val Gardena (Gröden) Sandstone (Maucher, 1955). All deposits are believed to be connected with the post-Variscan magmatism (Bakos et al., 1972).

3. *Stratabound polymetallic deposits in Permian–Early Triassic sediments.* These deposits include Pb–Zn–Cu–U–fluorite–barite mineralizations in terrigenous sediments intercalated with (Tregiovo Fm.) and overlying (Val Gardena Sandstone, Upper Permian) the upper, rhyolitic Permian volcanic units, and Pb-rich mineralizations in Early Triassic carbonatic sediments of the Werfen Formation (Dessau & Perna, 1966; Brusca et al., 1972; Brusca & Perna, 1995). The deposits in the sandstones are typical low-temperature, red bed-type, diagenetic mineral concentrations, related to shallow groundwater circulation (Wopfner et al., 1983). The ores consist of galena (sphalerite, pyrite) and

covellite–chalcocite ± Cu-sulphosalts. The deposits in the carbonatic sediments have been economically the most important. Most of them are clustered in the south-western portion of the studied area, around Mt. Calisio north-east of Trento (Fig. 2.3), and are bound to a transgressive, oolitic–bioclastic horizon at the base of the Early Triassic Werfen Formation (Tesero Member, formerly assigned to the Upper Permian Bellerophon Fm.; cf. Brusca & Perna, 1995). They consist of impregnations, veinlets and irregular replacement bodies dominated by silver-rich galena, with subordinate barite, sphalerite, pyrite and chalcopyrite. The proposed genesis involves a sequence of synsedimentary, epigenetic-sedimentary, and metasomatic stages (Zanella & Brigo, 1997). One deposit characterized by localized enrichments in copper minerals has been studied here.

4. *Fluorite-rich vein deposits of Triassic age*. This group includes fluorite (barite, calcite, quartz)-dominated, sulphide-poor deposits, which are found in the upper, rhyolitic units of the Permian volcanic sequence (Bakos et al., 1972; Omenetto & Brigo, 1974). No hydrothermal alteration is observed in the host-rocks. A regional geochemical zoning is reported, with dominant fluorite in the core of the Atesino Volcanic District and barite enrichments towards its margins (Bakos et al., 1972). Based on several geological evidences (e.g. cross-cutting relations of some veins with upper Permian sediments and Ladinian mafic dykes; distinct thermal and geochemical zoning), the group is believed to be distinct from fluorite deposits in underlying basement and volcanic units and probably related to a hydrothermal–magmatic event of mid-Triassic age (Bakos et al., 1972).

5. *Deposits associated with Triassic magmatic rocks.* These deposits include both high- and low-temperature hydrothermal associations. High-temperature veins are characterized by tourmaline, scheelite and chalcopyrite as dominant minerals and are spatially associated with Triassic intrusives of the Predazzo–Monzoni igneous complex (Bianchi & di Colbertaldo, 1956). Based on scarce existing reports (Omenetto, 1968a; Cavinato, 1968) and own field observations, the low-temperature deposits are represented by several minor chalcopyrite ± bornite (galena)-bearing impregnations and mineralized breccias with calcitic cement in the Ladinian volcanic rocks, and by impregnations and replacement bodies in the underlying carbonates. For these low-temperature deposits, a genetic link with the Triassic magmatism is as yet unproven. One deposit representative of the low-T type (Valbona) has been studied here.

The ore mineralizations of Monte Mulat are developed at the contact between monzonitic intrusion and a mass of Triassic augitic-plagioclasic porphyrites, alongside veins of tinguaitic porphyries and teralitic-camptonitic porphyrites. The form of the mineral body is that of a stockwork, and the origin of the fractures within which it is lodged mineralization is attributed to the upward pressure determined by the emplacement of granite or contraction of the mass during its porphyritic consolidation (Bianchi and Di Colbertaldo, 1956).

6. *Deposits related to tectono-metamorphic mobilization.* These are represented by a few small siderite (barite) + tetrahedrite and pyrite + chalcopyrite occurrences located within the metamorphic basement in the Agordo area close to the Valsugana Line (Pattine in Fig. 2.3). These deposits have been interpreted as the products of selective remobilization of pre-Variscan deposits during prolonged tectono-metamorphic activity along the Valsugana Line (Fellerer, 1968; Omenetto & Brigo, 1974).

2.4.2 Carnic Alps

Devonian carbonates crop out, more or less continuously, along 100 Km of the Paleocarnic chain; carbonates occur within a fossiliferous Paleozoic sequence. Carnic Alps are cut by some regionally important lineaments (see fig. 2.4), which separate zones of different mineralizations as well as areas displaying different stratigraphic gaps. The orientation of these elements and their function as the limits of subsided basins or uplifted block are the consequence of large-scale transcurrent regional tectonics. West of the Val Bordaglia lineament and within northern Austrian slope, the Paleozoic sequence is weackly metamorphosed (fig 2.4).

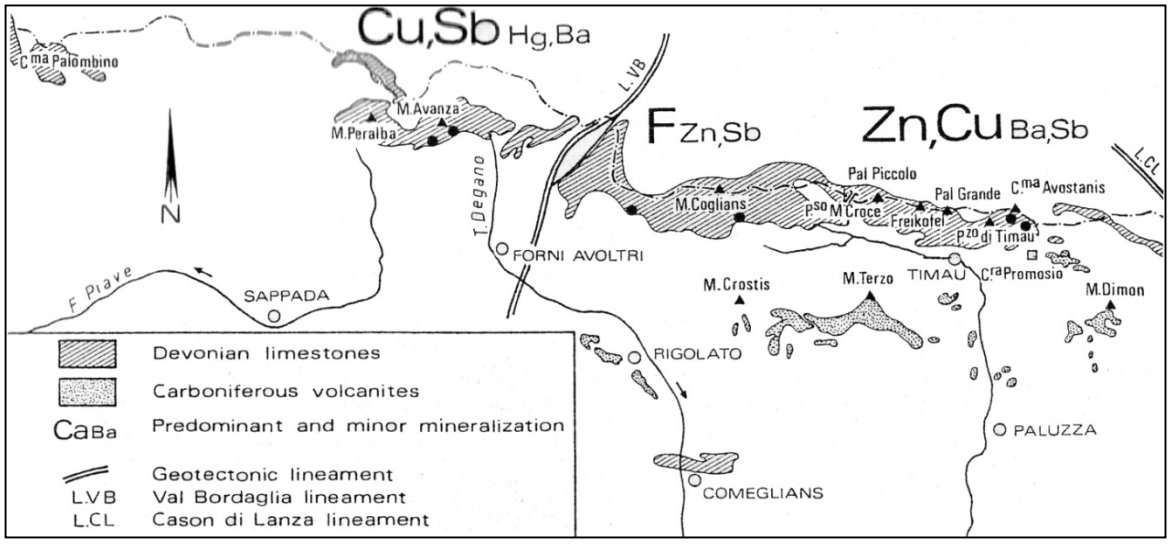

Fig. 2.4 Geological sketch map of Carnic Alps area, modified after Brigo et al., 1988.

Base metal deposits associated with barite and/or fluorite extend over large, and paleogeographically well-limited areas of carbonates. Mineralizations are linked to a paleorelief of Devonian limestones overlain by Lower Carboniferous to Lower Permian clastic sediments. The mainly compressive alpine orogeny has only partially obliterated the old structures. Deposits are stratabound to a carbonate sequence of middle to upper Devonian age and consist of a few sulfides associated to gangue in regionally varying proportions. With reference to their abundance, we have: tetrahedrite, sphalerite, chalcopyrite, pyrite and marcasite, locally with galena, cinnabar, boulangerite and skutterudite. The ore parageneses vary regionally as you can see in figure 2.4. In Monte Avanza zone there are chalcopyrite, Hg-fahlore, sphalerite and barite; in Casera Pramosio area we have chalcopyrite, sphalerite, tetrahedrite, barite and siderite. Comeglians area is rich in tetrahedrite, sphalerite, barite (Brigo et al., 2001; Brigo et al., 1988).

2.4.3 Tauern Window

The Tauern window exposes Penninic tectonic units which are overridden by the Austroalpine units and that comprise continental basement and cover sequences (Neubauer et al., 1999). The Penninic units include the Europe-related basement and

passive continental margin sequences, and the Mesozoic ophiolite of the Glockner nappe that were obducted onto the top of the former (fig.2.5). The Penninic basement is thought to represent upper to middle crust which was detached from the European plate during the final stages of continent-continent collision and loaded on the European plate as a duplex.

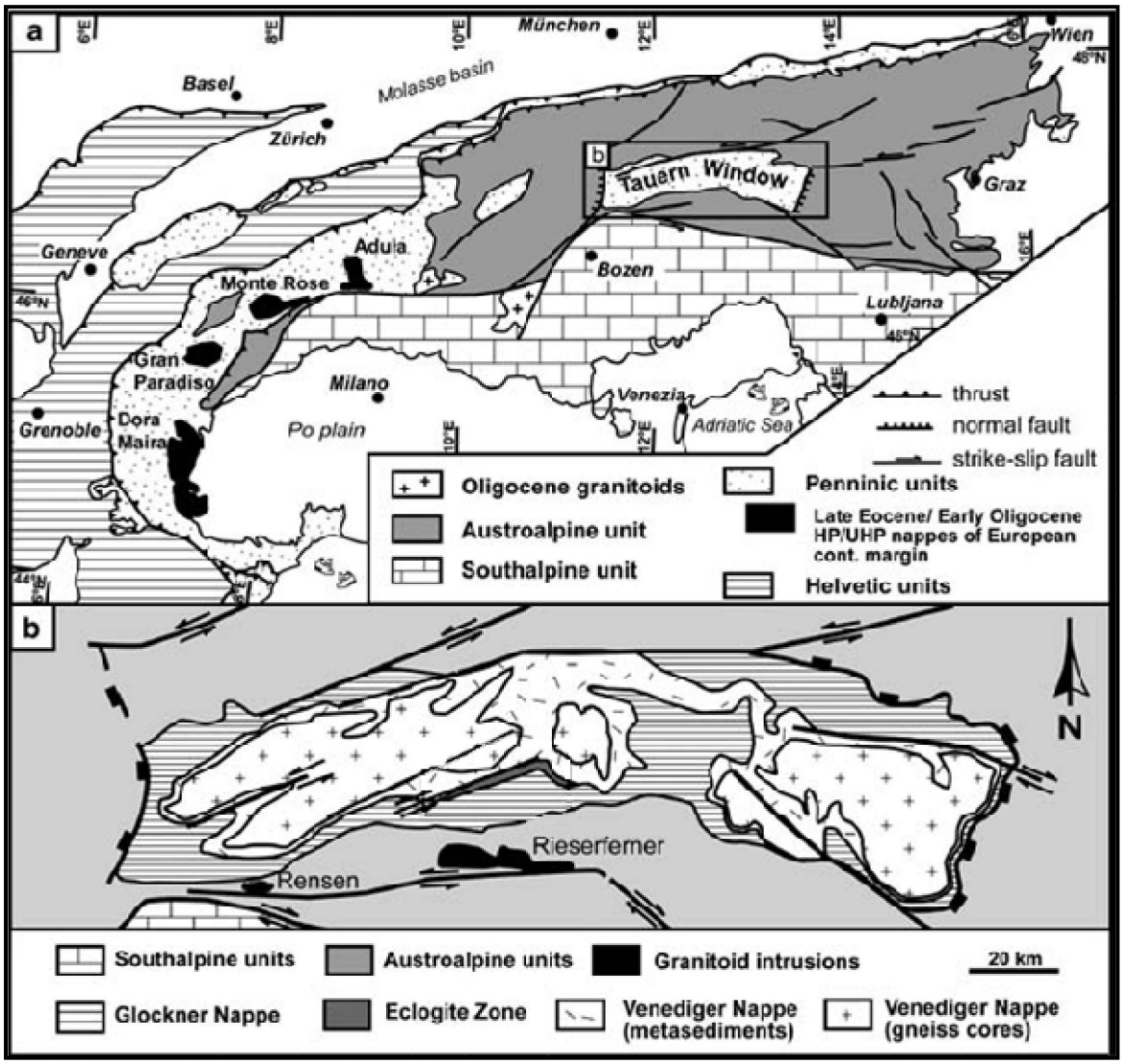

Fig. 2.5 Geological and tectonic sketch maps modified from Godny et al., 2005. a) Location of the Tauern Window within the Alpine belt. b) Tectonic map of the Tauern Window area (modified from Frisch et al. 2000).

The Predoi deposit in the Tauern Window is a stratiform mineralization that is syngenetic with the host Mesozoic formation, which consist of chloritic schists. The paragenesis is given by dominant pyrite, with chalcopyrite, magnetite, pyrrhotite, ilmenite, sphalerite in a chlorite-quartz-carbonates gangue.

2.5 Sampling

Both geological and archaeological reasons drove the mine selection. From the geological point of view they represent rather different geological settings. Archaeological reasons are mainly related to the well-documented chalcolithic mining activities in some cases (Bourgarit et al., 2008; Franceschi et al., 1997), and to the widespread knowledge of copper smelting techniques in the Alps. Minerals were hand collected by the research team during the doctorate activities at the mines trying to capture all the ore mineralogical variability. From this point of view, at each mine the samples were distinguished between (a) primary copper bearing ore mineralization (Cu-Fe and polymetallic sulfides); (b) secondary copper-based minerals produced by alteration (usually malachite, brochantite, native copper etc.) (see table 2.1). See table 2.2 for minerals name abbreviations.
Forty-nine copper deposits in the Alps and the Apennines were selected and sampled. In total 175 samples were analyzed in this work. 18 mines are in western alps, 5 in Ligurian Apennines, 4 in Southern Tuscany, 21 in Central-Eastern Southern Alps and 1 in Modenese Apennine. For each sampling area I analyzed: 35 samples for Western alps, 18 samples for Ligurian Apennines, 16 for Southern Tuscany, 90 for Central-Eastern Southern Alps and 3 samples for Modenese Apennine.

	WESTERN ALPS				
Catalogue n°	**Deposit**	**Deposit type**	**Metallic minerals**	Number of samples	
				(a)	**(b)**
	Piedmont zone				
1	Chialamberto	stratiform massive sulfides	py (cpy-sp-bn-po)	2	0
2	Mont Ros-Ayas	stratiform massive sulfides	py (cpy)	1	0
3	Alagna-Fabbriche	stratiform massive sulfides	py (cpy)(mag-po)	2	0
4	Chuc-Servette	stratiform massive sulfides	py (cpy)	1	0
5	Petit monde	stratiform massive sulfides	py (cpy)	1	0
6	Hèrin-Champ de Praz	stratiform massive sulfides	py (cpy)(sp-po)	1	0
7	Usseglio	Sulfide-rich veins	Co-Ni solfoarsenides (asp-tr-py)	1	0
8	Cruvino	Sulfide-rich veins	Co-Ni arsenides (asp-tr-py)	1	0
9	Ciabraressa	stratiform massive sulfides	py (cpy)	1	0
	Gran Paradiso internal massif				
10	Colle della Borra	stratiform massive sulfides	py-cpy tr-jm-asp	1	0
11	Valprato Soana	Sulfide stockwork	po-cpy-gal-tr-jm-asp-	2	0
	Ligurian Briançonnais zone				
12	Saint Verain	Sulfide-rich veins	bn-cpy (py-gal)	6	4
13	via fiorcia	Sulfide-rich veins	cpy-bn (py-gal)	3	0
14	Salbertrand	stratiform massive sulfides	cpy-py	1	0
15	Murialdo-Pastori	stratiform massive sulfides		3	0

16	Elva	stratiform massive sulfides		1	0
17	Valgrana	stratiform massive sulfides		1	0
	Argentera massif				
18	Argentera-Vinadio	sub-vertical veins	sp-gal (py-asp-po)	1	0
	LIGURIAN APENNINES				
catalogue number	**Deposit**	**deposit type**	**minerals**	Number of samples	
				(a)	**(b)**
19	Libiola	massive, disseminated and stockwork	py-cpy (sp)	3	5
20	Monte Loreto	massive, disseminated and stockwork	py-cpy (sp)	3	1
21	Bonassola	Orthomagmatic stratiform deposit	po-cpy-py-pn	2	0
22	Reppia	remobilization veins	cc-cv-cpy	0	2
23	Piazza	sulfide-rich veins	bn-cpy	2	0
	SOUTHERN TUSCANY				
catalogue number	**Deposit**	**deposit type**	**minerals**	Number of samples	
				(a)	**(b)**
24	Elba	veins , impregnations and replacement masses	Fe oxides (py)(Cu-Zn-Pb-As sulfides)	0	3
25	Montecatini V. di C.	Sulfide-bearing veins	cpy-py (bn)	2	0
26	Boccheggiano	Sulfide-bearing quartz vein	polymetallic sulfides	1	0
27	Campiglia M.ma	skarn deposit	Cu-Pb-Zn sulfides	10	0
	CENTRAL-EASTERN SOUTHERN ALPS				
catalogue number	**Deposit**	**deposit type**	**minerals**	Number of samples	
				(a)	**(b)**
28	Vetriolo	Stratiform massive sulphide	Py (sp-cpy-gal-asp)	5	3
29	Calceranica	Stratiform massive sulphide	Py (sp-cpy-gal-asp)	5	0
30	Valle Imperina	Stratiform massive sulphide	Py (sp-cpy-gal-asp)	8	3
31	Cinque Valli	Sulphide-rich vein system	Cu(Bi) / Zn, Pb, Sb, Cu, Ag sulfides and sulfosalts	2	0
32	Pamera	Breccia pipe	Mt (cpy(Bi), py, Co-Ni sulphides) / Po (cpy, Bi, Te).	4	0
33	Tingherla/Tingerhof	Fluorite-rich vein	gal (sp-cpy-py)		2
34	Mondagiò	Sulphide-rich vein	Gal, tr, cpy, sp, py (Co, Ni, Ag)	3	0
35	Maso Furli (Lavis)	Stratabound veinlets/disseminated	Gal, sp, py, cpy, tr	2	0
36	Maso Erdemolo	Sulphide-rich vein stockwork	Pb-Zn-Cu ore (Bi-Ag sulfides)	4	2
37	Valbona	Mineralized breccia	Cc-cpy-bor (gal)	4	1
38	Pattine-Pian delle loppe	Remobilization veins	Py, cpy (qz, sid, bar, fl)	8	0
39	Bedovina	stockwork structure	sch-cpy(py-stbn)	5	0
40	Vallarsa	Fluorite-rich vein	cc (gal with tr/cpy inclusions)	3	0
41	Montefondoli	Sulphide-rich vein system	Sp, gal(Ag), cpy, (Cu)-Sb-Ag sulfides and sulfosalts	6	2
42	Stelvio	Remobilized sedex	Sp-(Ag)gal (po,cpy, py)	1	0

43	Oris	Remobilized sedex	Sp-(Ag)gal (po,cpy, py)	1	0
44	Val Martello	Remobilized sedex	Sp-(Ag)gal (po,cpy, py)	3	0
45	Predoi	stratiform massive sulfides	py (cpy-mgn-po-sp-cub)	4	4
	CARNIC ALPS				
46	Monte Avanza	Carbonate-hosted stratabound	tr (sp-gal-cpy)	4	0
47	Casera Pramosio	Carbonate-hosted stratabound	tr (sp-gal-cpy)	2	0
48	Comeglians	Carbonate-hosted stratabound	tr (sp-gal-cpy)	2	1
	MODENESE APENNINE				
catalogue number	**Deposit**	**deposit type**	**minerals**	Number of samples	
				(a)	**(b)**
49	Valdragone	quartz veins with disseminated sulfides	cpy-py (sp)	3	0

Table 2.1 – Collected mines and number of samples analyzed. Catalogue number is reffered to fig. 2.1

Samples were taken from both underground works and mining dumps. For Pb–Zn dominated deposits (some post-Variscan veins and the Triassic stratabound deposit), whenever possible samples were taken from their copper-rich portions.

A portion of each sample was gently crushed and primary copper-bearing minerals (chalcopyrite, bornite, tetrahedrite or "cupriferous" pyrite) were separated by handpicking under a binocular microscope.

For some deposits, mixtures of secondary (malachite, azurite, native copper) minerals were analyzed. For some poorly mineralized samples, sulfide concentrates were preliminarily obtained by gravimetric separation; copper-bearing minerals were then handpicked under a binocular microscope. During separation procedures, special care was taken to prevent sample contamination from external sources.

Mineral name	Abbreviation
arsenopyrite	asp
bornite	bn
boulangerite	boul
cassiterite	cst
chalcocite	cc
chalcopyrite	cpy
covellite	cv
galena	gal
jamesonite	jm
magnetite	mt
malachite	mal
marcasite	mr
pentlandite	pn
pyrite	py
pyrrhotite	po
sphalerite	sp
stibnite	stbn
tennantite	tn
tetrahedrite	tr

Table 2.2 – Abbreviations of mineral names

3. Analytical methods and Results

Samples were first selected, prepared and characterized mineralogically and petrologically (XRD, RL-OM); then they were analysed via mass spectrometer (ICP-MC-MS and ICP-Q-MS) for geochemical and isotopic measurements (trace elements, rare earth elements, $^{206}Pb/^{204}Pb$, $^{207}Pb/^{204}Pb$, $^{208}Pb/^{204}Pb$, and $^{65}Cu/^{63}Cu$ isotopic ratios).

3.1 Analytical methods

3.1.1 Samples preparation and minero-petrographic characterization

Most representative samples were chosen for each mine, both primary phases and alteration phases, where possible.

Samples were taken from both underground works and mining dumps. In many cases, samples came from Museums or private collections: in these cases, total amount of samples for a mine is lower and we didn't have a representative sampling of deposit.

A portion of each sample was cut with diamond blade buzz saw to obtain a 2 x 2 x 1 cm ca. piece of material; then the piece was mounted in epoxy resin and polished to make the surface smooth. Samples were cleaned several times to remove the oil and polishing material. Petrological observation was made using a NIKON light reflected microscope, model: Eclipse ME600L.

Another portion of each sample was gently crushed and hand grinded with an agate mortar to obtain mineral powder for mineralogical and geochemical analysis.
Primary copper-bearing minerals (chalcopyrite, bornite, tetrahedrite or "cupriferous" pyrite) and alteration phases were separated by handpicking under a binocular microscope ZEISS, model STEMI 2000-C.
For Pb–Zn dominated deposits (some post-Variscan veins and the Triassic stratabound deposit), whenever possible samples were taken from their copper-rich portions.
For some deposits, mixtures of primary and secondary (malachite, azurite) minerals were analyzed. For some poorly mineralized samples, sulfide concentrates were preliminarily obtained by gravimetric separation; copper-bearing minerals were then handpicked under the microscope. During separation procedures, special care was taken to prevent sample contamination from external sources.
I picked at least 10 mg of material for each sample, up to 100 mg where possible; then they were cleaned several times with distilled water in an ultrasonic bath.

The powder-X Ray Diffrattometer used for characterize mineralogically mines samples was a Panalytical X'Pert PRO-MPD, equipped with X'Celerator detector.
This detector gives ultrafast data collection through RTMS (Real Time Multiple Strip) detection technology: a high-quality powder diffractogram is obtained in only a few minutes of time. The X'Celerator does not need cooling water, a flow of liquid nitrogen, counting gas, or time-consuming positional or intensity calibrations
Zero background sample holders for high accuracy measurements from small quantities of powder were used.
Measurements were made using Philips diffractometer X'Change parafocalizzante Bragg-Brentano geometry and X-ray tube with copper anode, with a vertical goniometer 2theta PW1050/37 theta-installed on a Philips PW3830 generator and diffractometer controlled by a controller PW3710. The data acquisition was performed by scanning continues with steps of 0.02 [° 2Th] per second, and working at 20 kV and 40 mA. Angle interval investigated was from 5 to 80°. X-ray tube is Ceramic Long Fine Focus (LFF Ceramic Tube Cu) with copper anode. Monochromator is a curved crystal of graphite PW3123/10.
The diffractograms obtained were then interpreted with special software X'Pert HighScore Plus 3.0, using the ICDD database and using the RIR protocol for the qualitative determination of mineral phases present and the semi-quantitative estimates of their percentage by weight.

*3.1.*2 Lead isotopic analysis

In order to perform a Pb isotopic analysis, the Pb must be brought from the sample into the mass spectrometer and be ionized. It sounds trivial, but is not, that only Pb from the sample, possibly all of it, and certainly nothing else, should be analyzed (Villa, 2009).

Most ore minerals are soluble in aqua regia. Therefore, dissolution by aqua regia is the method of choice when doing bulk analyses. The dissolved sample contains small (or large) amounts of Pb mixed with all other elements contained before dissolution.

It is necessary to chemically remove all these interfering elements, as experience directly shows that the measurement accuracy depends on Pb purity. This is normally done with cation or anion exchange resins, which retain or release specific elements with specific acids of specific concentration. In the Bern laboratory, Pb is separated from other metals with the Sr•Spec™ resin (EIChroM Industries) described by Horwitz et al. (1992). Its use for Pb was reported by Gale (1996). Because that paper contains a number of errors, the corrected procedure is detailed here. About 200 µL of Sr•Spec™ resin are filled in a 3-mm diameter hand-made PTFE column. The height/width ratio is approximately 4. The sample solution is loaded in 0.5 mL 1 M HNO_3, 1.5 mL of which is also used to wash out the matrix metals, while Pb is very strongly retained on the resin. Pb is then eluted with 3 mL 0.01 M HNO_3 and is ready for analysis. Use of a laser has the great advantage of allowing a reduction of the analyzed sample size. This reduction comes at a price, as the small total number of counted ions entails a loss of precision (see above). Moreover, one important cause of concern that needs to be examined on a case-by-case basis is the presence of interfering ions. Because no chemical separation can be performed on the laser evaporates, elements such as Hg (which also has a ^{204}Hg isotope) are analyzed at the same time as Pb. Mercury can be corrected by measuring the ^{202}Hg isotope and assuming a constant Hg isotopic ratio; this may or may not be an accurate assumption, and as a rule, it is prudent to avoid large corrections lest a small inaccuracy in the amount or isotopic composition of Hg is amplified and produces a large systematic inaccuracy on the 204Pb.

Lead isotope analyses were performed using a Nu Instruments™ multicollector inductively coupled plasma mass spectrometer.

In the ICP-MC-MS (Ion Coupled Plasma-Multicollector-Mass Spectrometry), the sample solution is ionized by introducing it into a 9000-K plasma. All elements are ionized simultaneously, and this has important analytical implications. Mass fractionation can be monitored by adding a small quantity of a tracer element to the element to be analyzed. In Pb analysis, it is usual to add a few nanograms of Tl. The reasoning, accepted by the majority of research groups after extensive tests, is that the ^{203}Tl/^{205}Tl ratio is a known constant; because Tl and Pb are ionized together and fractionated by the same mechanism and because neither mass 203 nor mass 205 interfere with a Pb isotope, the fractionation of the Tl isotopic ratio provides a rapid and accurate correction for the Pb fractionation as well. This ensures about 10–50 times smaller fractionation-derived analytical uncertainties than TIMS analyses. However, a drawback of the simultaneous plasma ionization is that whatever impurities have not been removed by the chemical separation can interfere with the analysis. Such effects can be either direct isobaric interference (such as ^{204}Hg, ^{188}Os^{16}O+, etc. with ^{204}Pb) or a much more subtle artifact whereby the focusing of the ion beam in the source is modified by extraneous ions having multiple oxidation states, such as Fe^{2+}/Fe^{3+}, resulting in irreproducible analytical conditions. Preventing this requires a very thorough chemical purification procedure of Pb from all other elements (Villa, 2009).

3.1.3 Copper isotopic analysis

NIST SRM 976 was used as copper isotopic reference material. A 100 mg/L Cu solution prepared from the NIST SRM 976 standard (63Cu/65Cu 2.2440 _ 0.0021) was used as the primary standard. The dissolution of SRM 976 was carried out as reported in the literature. To test matrix effect and isobaric interferences, test solutions were prepared from single standard solutions of Zn, Na, Fe (Certipur, Merck), Ti and Rh (Aldrich). All the solutions were prepared with ultra pure water (18.2 MU cm^{-1} - TOC 4 mg/L - MilliQ Millipore) and a nitric acid solution (TraceSelect ¼ 69.0% - Fluka).

An appropriate amount of powdered separated minerals (about 2–6 mg) were finally prepared for the dissolution with 2 mL of concentrated aqua regia in order to approximately reach a final Cu concentration of 10 mg/L. According to the literature, aqua regia solution was used for copper ores instead of nitric acid to ensure complete sulfides digestion. The dissolution was carried out by microwave digestion using a sealed PTFE vessel. Ad hoc dilutions were performed for each specimen in order to have the same signal level of the bracketing standard. All the solutions were prepared with ultra pure water: nitric acid solution was added to each sample and standard solutions to reach a 2% HNO_3 concentration. Isotope ratio measurements were performed with a Thermo Electron ICP-QMS system (Mod. X series II) equipped with a collision cell (CC) and a Peltier-cooled spray chamber. Instrumental operating conditions were optimized to obtain maximum sensitivity and signal stability for a 100 mg/L copper solution (Marelli et al., 2010). The instrument was operated in the CC mode to reduce polyatomic isobaric interferences, using the gas mixture indicated by the manufacturer (Shields et al., 1964; Chrastný and Komàrek, 2009).

For every sample a proper dilution factor was adopted in order to keep the analyte concentration at the same level of standard reference concentration. This concentration balancing compensates for mass bias fluctuations along the bracketing sequence.

Moreover it eliminates any possible influence of dead time miscorrection. After every sample or standard measurement, a 60 s wash step was performed using a part of the incoming sample solution. Before every measurement and wash step a 30 s uptake step was performed. Between every batch, a blank solution is monitored to check the level of blank counts on the two copper channels (Marelli et al., 2010).

Every ensemble of replicated measurements is treated separately as follows:

i) the mass uncorrected raw counts are corrected by subtracting the blank solution signals. Blank signals are determined as the mean value of blank solution measurements that bracket the reference and sample.

ii) the blank-corrected ratio values are filtered to reject potential outliers using the Huber outlier test (Devies, 1988; Meier and Zünd, 2000).

iii) instrumental drift and mass bias is corrected using a linear law. Then, a corrected Rsm ratio is obtained for each sample s belonging to a specific batch m.

iv) the final reported sample ratio RSC is obtained as the average of Rsm values determined in every batch. According to this, it is possible to calculate the standard deviation of sample ratio RSC as the mean standard deviation (sx,mean) of the Rsm data

set. In order to have a direct comparison with data reported in literature, δ^{63}% displacement units will be used whenever necessary.
The obtained data was validating with an independent cross-checking carried out by the Laboratorie de Science de la Terre, ENS Lyon, France by Multi Collector Inductive Coupled Plasma Mass Spectrometer (MC-ICP-MS) technique. The two techniques gave the same reliability in accuracy terms. Details are reported in Marelli, 2010.

3.1.4 Traces and Rare Earth Elements analysis

Dried powdered mineral specimens (2-6 mg) were dissolved into aqua regia solution (TraceSelect grade HCl 37% and HNO_3 65% - in a 3:1volumetric ratio) in high pressure microwave sealed PTFE vessels In order to digest silicates contaminated samples, 0.250 mL of hydrofluoridric acid (HF) 47-51% (trace select grade) were added. The thermal program of the microwave unit was the following: 250 W for 2 min, 0 W for 1 min, 400 W for 3 min, 0 W for 1 min, 600 W for 10 min, and a 20 min final cooling. The temperature was kept under 180°C.
Samples were properly diluted (final volume 50 mL – ultrapure water) obtaining a mother solution. Prior to the dissolution step, early bronze objects were observed by optical microscopy to evaluate the corrosion state and the presence of oxide coatings. They were then cleaned with a weak HCl solution (0.1M) followed by a washing with a weak HNO_3 solution (0.1M) in ultrasonic bath and dried under flowing N_2 to avoid any further contamination.

Group	Elements	Commercial reference standard
1	52Cr. 55Mn. 59Co. 60Ni. 66Zn. 69Ga. 72Ge. 107Ag. 111Cd. 115In. 125Te. 137Ba. 205Tl. 208Pb. 209Bi. 238U	ICP multi-element standard solution XXI (Merck)
	47Ti. 118Sn. 121Sb. 193Ir	ICP multi-element standard solution XVI (Merck)
2	75As. 80Se	ICP multi-element standard solution XXI (Merck)
3	89Y. 103Rh. 105Pd. 139La. 140Ce. 141Pr. 146Nd. 147Sm. 153Eu. 157Gd. 159Tb. 163Dy. 165Ho. 166Er. 169Tm. 159Tb. 175Lu. 195Pt. 197Au. 232Th	REE Multi-element standard solution (Carlo Erba) + single standard solution (Fluka) 1000 mg/L for 103Rh. 105Pd. 195Pt and 197Au

Tab. 3.1 Trace elements analysis: groups and standard solutions used for the calibration

Trace analysis were performed through external calibration by Inductively Coupled Plasma Quadrupolar Mass Spectrometer (ICP-QMS, X series II, Thermo Electron). Minor and trace elements, including REE (rare earth elements), were separately analyzed in three main groups (Tab.3.1). The selection of the isotope for every element is a compromise between sensitivity (isotopic abundance) and lack of isobaric interferences, as suggested by the manufacturer. Arsenic and Selenium were analyzed in the collision cell mode (CCT) (Feldmann et al.,1999), in order to reduce the isobaric interferences on mass channel 75 and 80 (by $ArCl^+$ and $ArAr^+$ respectively). A linear calibration was performed for each group, using at least 4 standard solutions (blank included) obtained by a proper dilution of the standard solutions indicated in Table 3.1. A control calibration block was inserted every 9 samples. Each sample was diluted 1:10 from the mother solution with UltraPure water. Concentrated HNO3 was added to these solutions in order to have always a 2% final HNO_3 concentration.

3.2 Results and discussion

In table 3.2 are reported analysis made for each sample.

Tab. 3.2 Analysis carried out on ore deposit samples

	WESTERN ALPS						
cat. N°	**Deposit**	**Sample**	**XRD**	**RL-OM**	**Pb isotopes**	**Cu isotopes**	**Traces and REE**
	Piedmont zone						
1	Chialamberto	CHIAL67	X	X	X		X
1	Chialamberto	CHIAL68	X	X	X		
2	Mont Ros-Ayas	Q20-7	X	X	X		
3	Alagna-Fabbriche	ALA_Ap1	X	X	X	X	X
3	Alagna-Fabbriche	L87'	X	X	X		X
4	Chuc-Servette	46/5	X	X	X		X
5	Petit monde	A5b	X	X	X		X
6	Hèrin-Champ de Praz	46/11	X	X	X		
7	Usseglio	M/U 3761	X	X	X		X
8	Cruvino	M/U 9748	X	X	X		X
9	Ciabraressa	MOR119	X	X	X		
	Gran Paradiso internal massif						
10	Colle della Borra	MOR43-GP36	X	X	X		
11	Valprato Soana	MOR42-GP21	X	X	X		
11	Valprato Soana	MOR42-GP23	X	X	X		
	Ligurian Briançonnais zone						
12	Saint Verain	SVE - Ap1	X	X	X	X	X

12	Saint Verain	SVE - Ap2	X		X	X	X
12	Saint Verain	SVE - Ap3	X		X	X	X
12	Saint Verain	SVE - Ap4	X		X	X	X
12	Saint Verain	SVE- Ar1	X		X	X	X
12	Saint Verain	SVE- Br1	X		X	X	X
12	Saint Verain	SVE- Bp1	X	X	X	X	X
12	Saint Verain	SVE- Bs1	X	X	X	X	X
12	Saint Verain	SVE- Cp1	X	X	X	X	X
12	Saint Verain	SVE- Cs1	X		X	X	X
13	via fiorcia	VF5b B	X	X	X		
13	via fiorcia	VF5b C	X	X	X		
13	via fiorcia	VF2a	X	X	X		X
14	Salbertrand	R96/2	X	X	X		
15	Murialdo-Pastori	MUR-1	X		X		X
15	Murialdo-Pastori	PAS-1	X	X	X		X
15	Murialdo-Pastori	PAS-2	X	X	X		
16	Elva	EL-1	X		X		
17	Valgrana	GR-1	X		X		
	Argentera massif						
18	Argentera	AR 1	X	X	X		

LIGURIAN APENNINES

cat. N°	Deposit	Sample	XRD	RLM	Pb isotopes	Cu isotopes	traces and REE
19	Libiola	LIB_L2p1	X	X	X	X	X
19	Libiola	LIB_Fs1	X		X	X	X
19	Libiola	LIB_Bp1	X	X	X	X	X
19	Libiola	LIB_Gs1	X		X	X	X
19	Libiola	LIB_Ep1	X		X	X	X
19	Libiola	LIB-Ag1	X		X		
19	Libiola	LIB-Ag2	X		X		
20	Monte Loreto	LOR_As1	X		X	X	X
20	Monte Loreto	LOR_Bp1	X		X	X	X
20	Monte Loreto	LOR_M2P1	X		X	X	X
20	Monte Loreto	LOR_M3p1	X		X	X	X
21	Bonassola	BON_Ap1	X		X	X	X
21	Bonassola	BON_Ap2	X		X	X	X
22	Reppia	REP_As1	X		X	X	X
22	Reppia	REP_As2	X		X	X	X
23	Piazza	PIA_Bp1	X		X	X	X
23	Piazza	PIA_Bp2	X		X	X	X

SOUTHERN TUSCANY

cat. N°	Deposit	Sample	XRD	RLM	Pb isotopes	Cu isotopes	traces and REE
24	Elba	ELB_Cs1	X		X	X	X
24	Elba	ELB_Ar1	X		X	X	X

24	Elba	ELB_Br1				X	X
25	Montecatini V. di C.	MB3	X		X	X	X
25	Montecatini V. di C.	MB1	X		X	X	X
26	Boccheggiano	BCpy	X		X	X	X
27	Campiglia M.ma	T31	X		X	X	X
27	Campiglia M.ma	T32	X		X	X	X
27	Campiglia M.ma	T42	X		X	X	X
27	Campiglia M.ma	T41	X		X	X	X
27	Campiglia M.ma	T3A	X		X	X	X
27	Campiglia M.ma	T4B	X		X	X	X
27	Campiglia M.ma	CT2	X		X	X	X
27	Campiglia M.ma	MT1c				X	X
27	Campiglia M.ma	MT1a	X		X	X	X
27	Campiglia M.ma	CT1	X		X	X	X

CENTRAL-EASTERN SOUTHERN ALPS

cat. N°	Deposit	Sample	XRD	RLM	Pb isotopes	Cu isotopes	traces and REE
28	Vetriolo	VET2sp	X		X		
28	Vetriolo	VET2s-neo	X		X		
28	Vetriolo	VET-0	X		X		
28	Vetriolo	VET-p3c	X		X		
28	Vetriolo	VET-s1	X		X		
28	Vetriolo	VET-p3s	X		X		
28	Vetriolo	VET-2p	X		X		
28	Vetriolo	VET-2s	X		X		
29	Calceranica	CALC-2	X	X	X		
29	Calceranica	CALC-1	X	X	X		
29	Calceranica	CALC-4	X		X		
29	Calceranica	CALC-3	X		X		
29	Calceranica	M1200	X		X		
30	Valle Imperina	VI01p1	X	X	X	X	X
30	Valle Imperina	VI03p1	X	X	X	X	X
30	Valle Imperina	VI04p1	X	X	X	X	X
30	Valle Imperina	VI-09	X	X	X		
30	Valle Imperina	VI-06	X	X	X		
30	Valle Imperina	VI-02	X		X		
30	Valle Imperina	VI-08	X		X		
30	Valle Imperina	VI-05	X		X		
30	Valle Imperina	VI-10	X		X		
30	Valle Imperina	VI-07	X		X		
30	Valle Imperina	VIMP_Cunat					X
31	Cinque Valli	5VA 1p	X		X	X	X
31	Cinque Valli	50411	X		X		
32	Pamera	PA6	X		X		
32	Pamera	P3	X		X		

32	Pamera	P28	X		X		
32	Pamera	PAM-1	X		X		
33	Tingherla	TING-2	X		X		
33	Tingherla	TING-1	X		X		
34	Mondagiò	MOND-2	X	X	X		
34	Mondagiò	MOND-1	X	X	X		
34	Mondagiò	MOND-3	X	X	X		
35	Furli di Lavis	LAV-1	X		X		
35	Furli di Lavis	LAV2	X		X		
36	Grua	GRUA_Ddxp1	X		X	X	X
36	Grua	GRUA_Cp1	X		X	X	X
36	Grua	GRUA_Ep1	X		X	X	X
36	Grua	GRUA_Gs1	X		X	X	X
36	Grua	GRUA_As1	X		X	X	X
36	Grua	GRUA_Dsxp1	X		X	X	X
37	Valbona	VBO1Ap1	X	X	X	X	X
37	Valbona	VBO1As1	X	X	X	X	X
37	Valbona	VBO2p1	X	X	X	X	X
37	Valbona	VBE1Ap1	X		X	X	X
37	Valbona	VBE2Ap1	X		X	X	X
38	Pattine	PA04p1	X	X	X	X	X
38	Pattine	PAT_P1	X	X	X		X
38	Pattine	PAT_P2	X	X	X		X
38	Pattine	PAT_P3	X		X		X
38	Pattine	PA05i	X		X		
38	Pattine	PA-09i	X		X		
38	Pattine	PA-02i	X		X		
38	Pattine	PAT-SID	X		X		
	Pattine	PAT-BOR	X		X		
39	Bedovina	BED-2	X	X	X		
39	Bedovina	BED-1	X	X	X		
39	Bedovina	BED-MM1	X	X	X		
39	Bedovina	BED-MM2	X	X	X		
39	Bedovina	BED-MM3	X	X	X		
40	Vallarsa	VAL-p1	X		X		
40	Vallarsa	VAL-p3	X		X		
40	Vallarsa	VAL-2	X		X		
41	Montefondoli	MFO_Ap1	X	X	X	X	X
41	Montefondoli	MFO_Ap2	X	X	X	X	X
41	Montefondoli	MFO_Ap3	X		X	X	X
41	Montefondoli	MFO-MU	X		X		
41	Montefondoli	MFO-KW	X		X		
41	Montefondoli	CD-a-11	X		X		

41	Montefondoli	AF-s1	X		X		
41	Montefondoli	TIL-As	X		X	X	X
42	Stelvio	STE_1p1	X		X	X	X
43	Val Martello	VVN_2p1	X		X	X	X
43	Val Martello	VVN_3p	X		X	X	X
43	Val Martello	VVN_5p	X		X	X	X
44	Oris	ORI_1p1	X		X	X	X
45	Predoi	PRE_IDp1	X	X	X	X	X
45	Predoi	PRE_IICp1	X		X	X	X
45	Predoi	PRE_IIIAs1	X		X	X	X
45	Predoi	PRE_IGS1	X		X	X	X
45	Predoi	PRE_IHs1	X		X	X	X
45	Predoi	PRE_ICp1	X		X	X	X
45	Predoi	PRE_Cu				X	X
45	Predoi	PRE_Cu-S	X		X	X	X

CARNIC ALPS

cat. N°	Deposit	Sample	XRD	RLM	Pb isotopes	Cu isotopes	traces and REE
46	monte avanza	MA-4pBIS	X		X		
46	monte avanza	MA-5pBIS	X		X		
46	monte avanza	MA-1p	X		X		
46	monte avanza	MA-3p	X		X		
47	Casera Pramosio	PN0912	X	X	X		
47	Casera Pramosio	PN0913	X		X		
48	Comeglians	PN091	X	X	X		
48	Comeglians	PN095a-p	X		X		
48	Comeglians	PN095a-s	X		X		

MODENESE APENNINE

cat. N°	Deposit	Sample	XRD	RLM	Pb isotopes	Cu isotopes	traces and REE
49	Valdragone	VD-r1				X	X
49	Valdragone	VD-p1	X		X	X	X
49	Valdragone	VD-p2	X		X	X	X

3.2.1 Ore deposits outline and minerographic analysis

Ophiolite-related metamorphosed stratiform massive sulfides (Piedmont Zone and Tauern window)

The samples studied mainly consist of massive chalcopyrite with porphyroblastic pyrite and subordinate sphalerite in interstitial position or as tiny inclusions (fig 3.1-a). Only in Chialamberto samples I observed strates (between anfibolites and prasinites) of recrystallized pyrite with interstitial chalcopyrite, that cementate pyrites fractures and sphalerite at the phases contact (fig. 3.1-b).

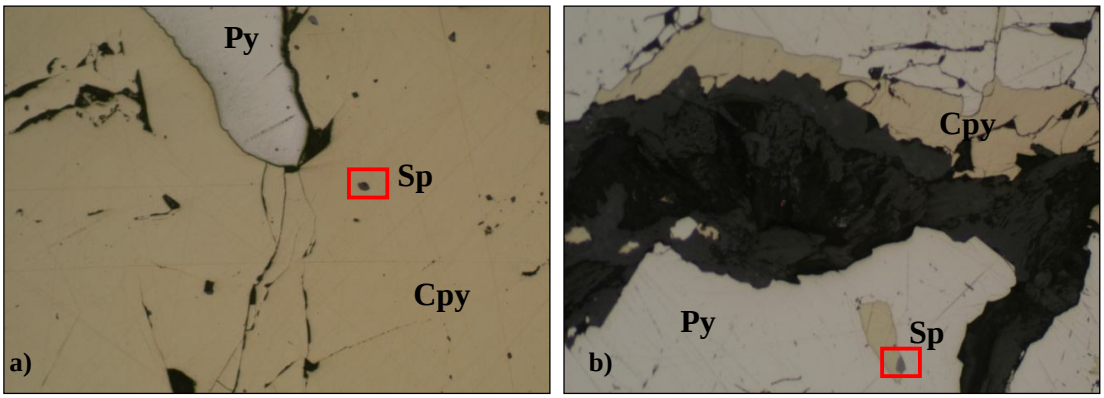

Fig 3.1 Piedmont zone microphotos. Magnification: 5X. a) Sample 46/11-Herin Champ de Praz; b) Sample MOR 41-122 (67) from Chialamberto deposit.

Metamorphosed stratiform and vein hydrothermal deposits of the Gran Paradiso massif and Briançonnais Zone

These deposits have stratiform nature with the exception of La reale-Valprato Soana and Saint Verain, those are filonian deposits. Salbertand and Colle della Borra deposits present massive pyrite with interstitial chalcopyrite in veinlets shape, that is very abundant and associated to sphalerite and tetrahedrite (fig 3.2-a).

La reale mine presents large amount of galena, pyrrhotite and siderite in addition to chalcopyrite and pyrite with sphalerite (fig 3.2-b). Phases are stockwork veinlets in quartz.

Both Via Fiorcia and Saint Verain mineralization are associated to quartzites (with glaucophane in first one and riebeckite in the second one), and are characterized by large amounts of bornite (fig. 3.2-c), with subordinated chalcopyrite, pyrite and sphalerite.

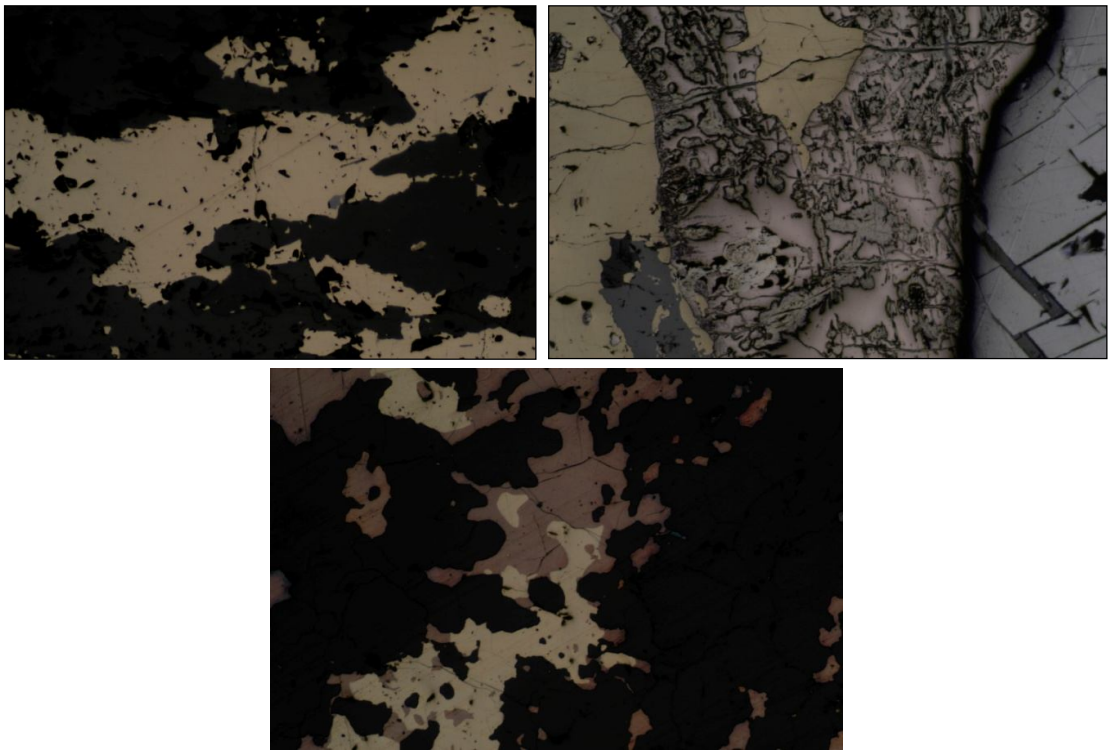

Fig 3.2 Briançonnais and Gran Paradiso microphotos. Magnification: 5X. a) Sample R96/2-Salbertrand; b) Sample MOR42-GP21 from La Reale-Valprato Soana; c) Sample VF5b from Via Fiorcia deposit.

Metamorphosed hydrothermal vein deposits in the Argentera external massif

The Argentera deposits are Pb-Zn-dominated veins with chalcopyrite, pyrite and subordinate arsenopyrite and pyrrhotite, in quartz and fluorite gangue. The samples studied here consist of quartz veins with interstitial chalcopyrite and subordinate sphalerite and tetrahedrite (fig. 3.3).

Ophiolite-hosted VMS deposits in Northern Apennines

Libiola and Monte Loreto minerals are: fine grained compact pyrite with chalcopyrite and sphalerite, and subordinated pyrrhotite. In libiola deposit high concentrations of chalcopyrite with pyrite are frequent along contact surfaces with serpentinites and gabbros (Ferrario and Garuti, 1980).

Typical composition of Reppia mine is constituted by bornite veinlets with chalcocite, chalcopyrite, quartz and carbonates.

Bonassola minerals are oriented veins of pyrrhotite, chalcopyrite with pyrite, pentlandite and sphalerite.

3.2.2 Lead isotope data

In Table 3.3 lead isotopic data are reported for each sample analyzed. I respected the division made on the basis of geographical setting. Archaeological ratios are reported in the third part of this work, together with archaeological artifacts.

Tab. 3.3 Lead isotopes data with relative Standard Error

WESTERN ALPS							
Deposit	**Sample**	**206Pb/204Pb**	**±2SE**	**207Pb/204Pb**	**±2SE**	**208Pb/204Pb**	**±2SE**
Piedmont zone							
Chialamberto	CHIAL67	18.194	0.002	15.657	0.004	38.363	0.01
Chialamberto	CHIAL68	18.351	0.004	15.671	0.005	38.503	0.007
Mont Ros-Ayas	Q20-7	18.177	0.005	15.523	0.005	37.877	0.01
Alagna-Fabbriche	ALA_Ap1	18.241	0.003	15.587	0.003	38.152	0.008
Alagna-Fabbriche	L87'	18.522	0.008	15.613	0.006	38.421	0.01
Chuc-Servette	46/5	18.259	0.002	15.654	0.003	38.361	0.007
Petit monde	A5b	18.174	0.04	15.657	0.01	38.243	0.08
Hèrin-Champ de Praz	46/11	18.106	0.01	15.619	0.01	38.024	0.08

Usseglio	M/U 3761	18.303	0.004	15.664	0.003	38.45	0.008
Cruvino	M/U 9748	18.483	0.006	15.672	0.005	38.621	0.01
Ciabraressa	MOR119	18.406	0.004	15.676	0.003	38.536	0.008
Gran Paradiso internal massif							
Colle della Borra	MOR43-GP36	18.746	0.01	15.667	0.01	38.671	0.2
Valprato Soana	MOR42-GP21	18.756	0.002	15.663	0.002	38.747	0.006
Valprato Soana	MOR42-GP23	18.72	0.005	15.665	0.004	38.709	0.01
Ligurian Briançonnais zone							
Saint Verain	SVE - Ap1	24.534	0.1	15.889	0.08	38.276	0.2
Saint Verain	SVE - Ap2	20.051	0.04	15.807	0.04	38.539	0.08
Saint Verain	SVE - Ap3	18.028	0.002	15.654	0.002	38.173	0.005
Saint Verain	SVE - Ap4	18.463	0.008	15.619	0.007	38.406	0.01
Saint Verain	SVE- Ar1	18.356	0.01	15.61	0.01	38.314	0.02
Saint Verain	SVE- Br1	18.154	0.003	15.608	0.002	38.107	0.006
Saint Verain	SVE- Bp1	18.072	0.006	15.614	0.005	38.095	0.009
Saint Verain	SVE- Bs1	18.172	0.01	15.603	0.01	38.116	0.02
Saint Verain	SVE- Cp1	18.215	0.004	15.545	0.002	37.989	0.008
Saint Verain	SVE- Cs1	18.508	0.002	15.608	0.002	38.382	0.004
via fiorcia	VF5b B	18.477	0.002	15.622	0.002	38.452	0.005
via fiorcia	VF5b C	18.482	0.004	15.628	0.004	38.441	0.1
via fiorcia	VF2a	18.56	0.02	15.613	0.02	38.426	0.04
Salbertrand	R96/2	18.438	0.004	15.607	0.004	38.346	0.006
Murialdo-Pastori	MUR-1	18.338	0.003	15.651	0.003	38.419	0.009
Murialdo-Pastori	PAS-1	18.376	0.002	15.67	0.002	38.481	0.008
Murialdo-Pastori	PAS-2	18.359	0.003	15.67	0.004	38.483	0.01
Elva	EL-1	19.071	0.006	15.732	0.006	38.826	0.008
Valgrana	GR-1	17.63	0.004	15.56	0.004	37.596	0.008
Argentera massif							
Argentera	AR 1	19.108	0.006	15.705	0.006	38.485	0.008

LIGURIAN APENNINES

Deposit	Sample	206Pb/204Pb	±2SE	207Pb/204Pb	±2SE	208Pb/204Pb	±2SE
Libiola	LIB_L2p1	18.04	0.005	15.489	0.004	37.64	0.01
Libiola	LIB_Fs1	18.832	0.003	15.602	0.003	37.926	0.006
Libiola	LIB_Bp1	18.152	0.002	15.537	0.003	37.824	0.006
Libiola	LIB_Gs1	18.333	0.02	15.557	0.01	37.814	0.04
Libiola	LIB_Ep1	18.16	0.01	15.508	0.01	37.733	0.02
Libiola	LIB-Ag1	18.34	0.004	15.848	0.004	38.779	0.006
Libiola	LIB-Ag2	18.359	0.003	15.992	0.003	39.259	0.006
Monte Loreto	LOR_As1	18.29	0.06	15.841	0.05	38.502	0.1
Monte Loreto	LOR_Bp1	18.24	0.004	15.632	0.004	38.277	0.008
Monte Loreto	LOR_M2P1	17.976	0.01	15.521	0.01	37.65	0.1

Monte Loreto	LOR_M3p1	18.155	0.003	15.652	0.002	38.048	0.007
Bonassola	BON_Ap1	18.297	0.004	15.659	0.004	38.481	0.01
Bonassola	BON_Ap2	18.425	0.005	15.647	0.005	38.478	0.01
Reppia	REP_As1	18.261	0.003	15.662	0.003	38.442	0.008
Reppia	REP_As2	18.861	0.01	15.614	0.008	38.163	0.02
Piazza	PIA_Bp1	18.103	0.002	15.504	0.003	37.759	0.008
Piazza	PIA_Bp2	18.087	0.002	15.499	0.002	37.726	0.006

SOUTHERN TUSCANY

Deposit	Sample	206Pb/204Pb	±2SE	207Pb/204Pb	±2SE	208Pb/204Pb	±2SE
Elba	ELB_Cs1	18.677	0.004	15.693	0.004	38.928	0.01
Elba	ELB_Ar1	18.663	0.03	15.682	0.03	38.725	0.06
Elba	ELB_Br1	no sample					
Montecatini V. di C.	MB3	18.138	0.006	15.503	0.006	37.754	0.01
Montecatini V. di C.	MB1	18.121	0.002	15.505	0.002	37.745	0.007
Boccheggiano	BCpy	18.757	0.004	15.704	0.003	39.004	0.01
Campiglia M.ma	T31	18.731	0.003	15.7	0.003	38.972	0.008
Campiglia M.ma	T32	18.701	0.006	15.681	0.005	38.879	0.01
Campiglia M.ma	T42	18.757	0.002	15.694	0.003	38.986	0.008
Campiglia M.ma	T41	18.77	0.004	15.702	0.004	39.013	0.01
Campiglia M.ma	T3A	18.756	0.002	15.696	0.002	38.993	0.006
Campiglia M.ma	T4B	18.757	0.003	15.693	0.003	38.994	0.008
Campiglia M.ma	CT2	18.768	0.002	15.699	0.002	39.011	0.007
Campiglia M.ma	MT1c	no sample					
Campiglia M.ma	MT1a	18.767	0.003	15.703	0.003	39.031	0.008
Campiglia M.ma	CT1	18.767	0.002	15.703	0.002	39.027	0.008

CENTRAL-EASTERN SOUTHERN ALPS

Deposit	Sample	206Pb/204Pb	±2SE	207Pb/204Pb	±2SE	208Pb/204Pb	±2SE
Vetriolo	VET2sp	17.887	0.002	15.643	0.002	38.1	0.006
Vetriolo	VET2s-neo	17.891	0.001	15.638	0.002	38.09	0.004
Vetriolo	VET-0	17.883	0.001	15.64	0.002	38.094	0.004
Vetriolo	VET-p3c	17.886	0.002	15.643	0.002	38.106	0.006
Vetriolo	VET-s1	17.989	0.01	15.672	0.01	38.22	0.2
Vetriolo	VET-p3s	17.885	0.002	15.642	0.002	38.101	0.006
Vetriolo	VET-2p	17.88	0.001	15.64	0.001	38.097	0.004
Vetriolo	VET-2s	17.989	0.001	15.66	0.001	38.159	0.003
Calceranica	CALC-2	17.911	0.002	15.641	0.002	38.119	0.006
Calceranica	CALC-1	17.905	0.002	15.646	0.002	38.125	0.005
Calceranica	CALC-4	17.972	0.002	15.64	0.002	38.145	0.006
Calceranica	CALC-3	17.922	0.002	15.641	0.002	38.136	0.008
Calceranica	M1200	17.897	0.002	15.64	0.001	38.099	0.004
Valle Imperina	VI01p1	18.319	0.003	15.676	0.003	38.562	0.007

Valle Imperina	VI03p1	17.985	0.002	15.663	0.002	38.158	0.006
Valle Imperina	VI04p1	17.973	0.002	15.659	0.002	38.145	0.006
Valle Imperina	VI-09	18.067	0.002	15.677	0.002	38.283	0.005
Valle Imperina	VI-06	18.029	0.004	15.661	0.004	38.208	0.008
Valle Imperina	VI-02	19.489	0.002	15.765	0.002	38.611	0.006
Valle Imperina	VI-08	18.054	0.002	15.661	0.002	38.243	0.007
Valle Imperina	VI-05	18.029	0.003	15.672	0.003	38.227	0.007
Valle Imperina	VI-10	18.715	0.006	15.701	0.004	39.013	0.01
Valle Imperina	VI-07	17.972	0.002	15.651	0.002	38.12	0.007
Valle Imperina	VIMP_Cunat	18.229	0.004	15.715	0.004	38.293	0.006
Cinque Valli	5VA 1p	18.061	0.003	15.661	0.003	38.252	0.008
Cinque Valli	50411	18.27	0.002	15.679	0.002	38.519	0.008
Pamera	PA6	18.209	0.002	15.662	0.002	38.443	0.005
Pamera	P3	18.283	0.002	15.666	0.002	38.537	0.006
Pamera	P28	18.2	0.003	15.655	0.006	38.365	0.006
Pamera	PAM-1	18.092	0.002	15.659	0.002	38.291	0.006
Tingherla	TING-2	18.465	0.002	15.671	0.002	38.738	0.006
Tingherla	TING-1	18.372	0.002	15.671	0.002	38.633	0.006
Mondagiò	MOND-2	18.417	0.003	15.676	0.004	38.682	0.008
Mondagiò	MOND-1	18.405	0.001	15.677	0.002	38.672	0.006
Mondagiò	MOND-3	18.405	0.002	15.677	0.003	38.676	0.008
Furli di Lavis	LAV-1	18.4	0.002	15.676	0.002	38.557	0.007
Furli di Lavis	LAV2	18.277	0.002	15.668	0.002	38.511	0.006
Grua	GRUA_Ddxp1	18.246	0.002	15.663	0.002	38.472	0.004
Grua	GRUA_Cp1	18.2377	0.002	15.661	0.002	38.458	0.006
Grua	GRUA_Ep1	18.253	0.001	15.669	0.002	38.493	0.004
Grua	GRUA_Gs1	18.25	0.002	15.663	0.002	38.482	0.006
Grua	GRUA_As1	18.232	0.002	16.661	0.002	38.451	0.005
Grua	GRUA_Dsxp1	18.249	0.001	15.666	0.002	38.479	0.004
Valbona	VBO1Ap1	18.438	0.002	15.664	0.002	38.578	0.008
Valbona	VBO1As1	18.639	0.008	15.69	0.006	38.778	0.02
Valbona	VBO2p1	18.386	0.002	15.666	0.002	38.548	0.006
Valbona	VBE1Ap1	18.391	0.003	15.661	0.002	38.519	0.008
Valbona	VBE2Ap1	18.458	0.001	15.668	0.001	38.597	0.004
Pattine	PA04p1	18.202	0.004	15.671	0.004	38.514	0.008
Pattine	PAT_P1	18.5	0.008	15.667	0.008	38.587	0.01
Pattine	PAT_P2	18.522	0.002	15.669	0.002	38.606	0.004
Pattine	PAT_P3	18.329	0.002	15.681	0.002	38.485	0.004
Pattine	PA05i	18.419	0.008	15.681	0.008	38.545	0.01
Pattine	PA-09i	18.496	0.002	15.674	0.002	38.615	0.004
Pattine	PA-02i	18.8	0.002	15.681	0.002	38.84	0.004

Pattine	PAT-SID	18.31	0.002	15.668	0.003	38.527	0.008
Pattine	PAT-BOR	18.038	0.002	15.676	0.002	38.25	0.007
Bedovina	BED-2	18.354	0.003	15.674	0.004	38.557	0.008
Bedovina	BED-1	18.348	0.003	15.658	0.002	38.477	0.008
Bedovina	BED-MM1	18.373	0.002	15.663	0.002	38.524	0.008
Bedovina	BED-MM2	18.347	0.001	15.663	0.002	38.492	0.006
Bedovina	BED-MM3	18.354	0.002	15.659	0.002	38.494	0.008
Vallarsa	VAL-p1	19.886	0.004	15.758	0.003	39.361	0.006
Vallarsa	VAL-p3	18.756	0.002	15.69	0.002	38.629	0.006
Vallarsa	VAL-2	18.825	0.003	15.703	0.002	38.867	0.006
Montefondoli	MFO_Ap1	18.253	0.002	15.673	0.002	38.52	0.005
Montefondoli	MFO_Ap2	18.276	0.003	15.676	0.003	38.55	0.008
Montefondoli	MFO_Ap3	18.286	0.002	15.675	0.003	38.5	0.008
Montefondoli	MFO-MU	18.269	0.002	15.674	0.002	38.514	0.006
Montefondoli	MFO-KW	18.281	0.001	15.67	0.001	38.518	0.002
Montefondoli	CD-a-11	18.259	0.002	15.672	0.002	38.501	0.005
Montefondoli	AF-s1	19.033	0.002	15.722	0.002	39.561	0.008
Montefondoli	TIL-As	20.259	0.002	15.776	0.002	38.587	0.006
Stelvio	STE_1p1	18.639	0.003	15.699	0.003	38.595	0.008
Val Martello	VVN_2p1	18.844	0.001	15.700	0.002	39.024	0.007
Val Martello	VVN_3p	18.003	0.004	15.638	0.004	38.144	0.01
Val Martello	VVN_5p	17.964	0.003	15.638	0.003	38.12	0.008
Oris	ORI_1p1	19.537	0.002	15.74	0.002	39.018	0.005
Predoi	PRE_IDp1	18.262	0.005	15.644	0.004	38.41	0.008
Predoi	PRE_IICp1	18.309	0.01	15.585	0.01	38.043	0.04
Predoi	PRE_IIIAs1	18.257	0.01	15.648	0.01	38.381	0.02
Predoi	PRE_IGS1	18.41	0.02	15.598	0.02	38.219	0.06
Predoi	PRE_IHs1	19.019	0.01	15.741	0.01	38.791	0.03
Predoi	PRE_ICp1	18.666	0.004	15.683	0.003	38.9	0.008
Predoi	PRE_Cu	18.286	0.002	15.638	0.002	38.35	0.005
Predoi	PRE_Cu-S	18.238	0.003	15.662	0.004	38.375	0.01

CARNIC ALPS

Deposit	Sample	206Pb/204Pb	±2SE	207Pb/204Pb	±2SE	208Pb/204Pb	±2SE
monte avanza	MA-4pBIS	18.646	0.01	15.7	0.01	38.88	0.02
monte avanza	MA-5pBIS	18.261	0.004	15.667	0.004	38.478	0.01
monte avanza	MA-1p	18.654	0.004	15.7	0.004	38.687	0.01
monte avanza	MA-3p	18.473	0.01	15.694	0.01	38.565	0.02
Casera Pramosio	PN0912	18.365	0.002	15.669	0.002	38.431	0.006
Casera Pramosio	PN0913	18.404	0.003	15.678	0.004	38.459	0.01
Comeglians	PN091	18.443	0.002	15.688	0.002	38.496	0.007
Comeglians	PN095a-p	18.469	0.002	15.69	0.002	38.509	0.007

Comeglians	PN095a-s	18.464	0.002	15.687	0.003	38.5	0.008
MODENESE APENNINE							
Deposit	**Sample**	**206Pb/204Pb**	**±2SE**	**207Pb/204Pb**	**±2SE**	**208Pb/204Pb**	**±2SE**
Valdragone	VD-r1	18.076	0.006	15.659	0.006	38.273	0.008
Valdragone	VD-p1	18.109	0.002	15.534	0.003	37.84	0.006
Valdragone	VD-p2	18.244	0.004	15.632	0.004	38.302	0.006

Mineralization observed and analyzed have been considered separately. To understand the interpretations of data from one point of view of their age and their source, cf. Figures 1.5.2 to 1.5.7. Table 1.5.1 summarizes the different ages of mineralization evaluated by the model and TOLSTIKHIN Kramers (1997). The interpretation of these data is somewhat subjective. That proposed in the following pages shows a possibility among others: better knowledge of regional geology and other tests performed with other methods could provide details. First I considered ofhiolites related mineralization and then sulphide deposits from the central-eastern Southalpine region were analysed.
Only primary phases samples are plotted in diagrams.

Ophiolites related deposits

Here are presented three distinct diagrams that describe three different deposits group.
Group A (fig. 3.4): it's constituted by Ligurian and Modenese Apennines, and Montecatini Val di Cecina deposits, that is related to non metamorphic ophiolites. Samples are below (with exceptions) of Young Upper Crust, indicating a strong mantellic contribution. Two samples of Monte Loreto in black and Bonassola samples indicate a crustal contribution probably related to a metamorphic event.

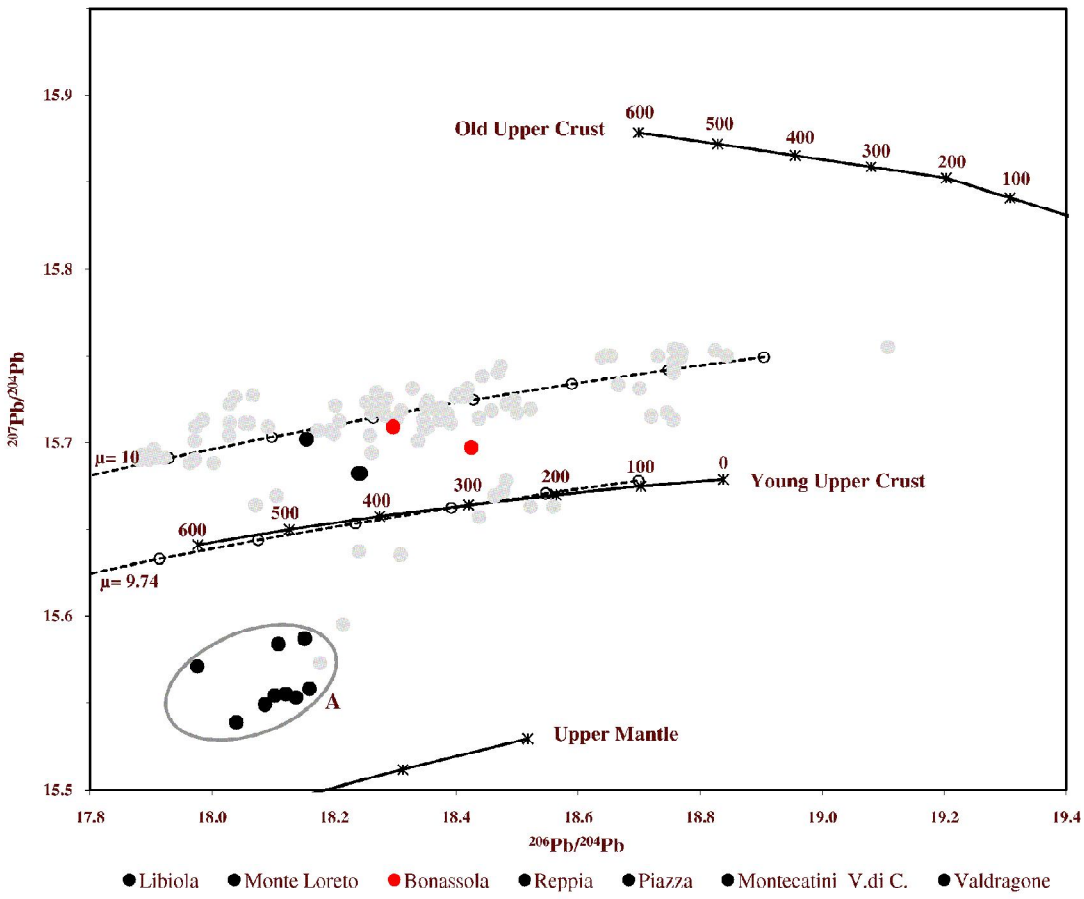

Fig. 3.4Lead isotope data for deposits of non metamorphosed ophiolites of Ligurian and Modenese Apennines and of Montecatini Val di Cecina. μ=9.74 and μ=10 lead growth curves according to Stacey and Kramers (1975); growth curves for upper crust and upper mantle after Kramers and Toltsikhin (1997).

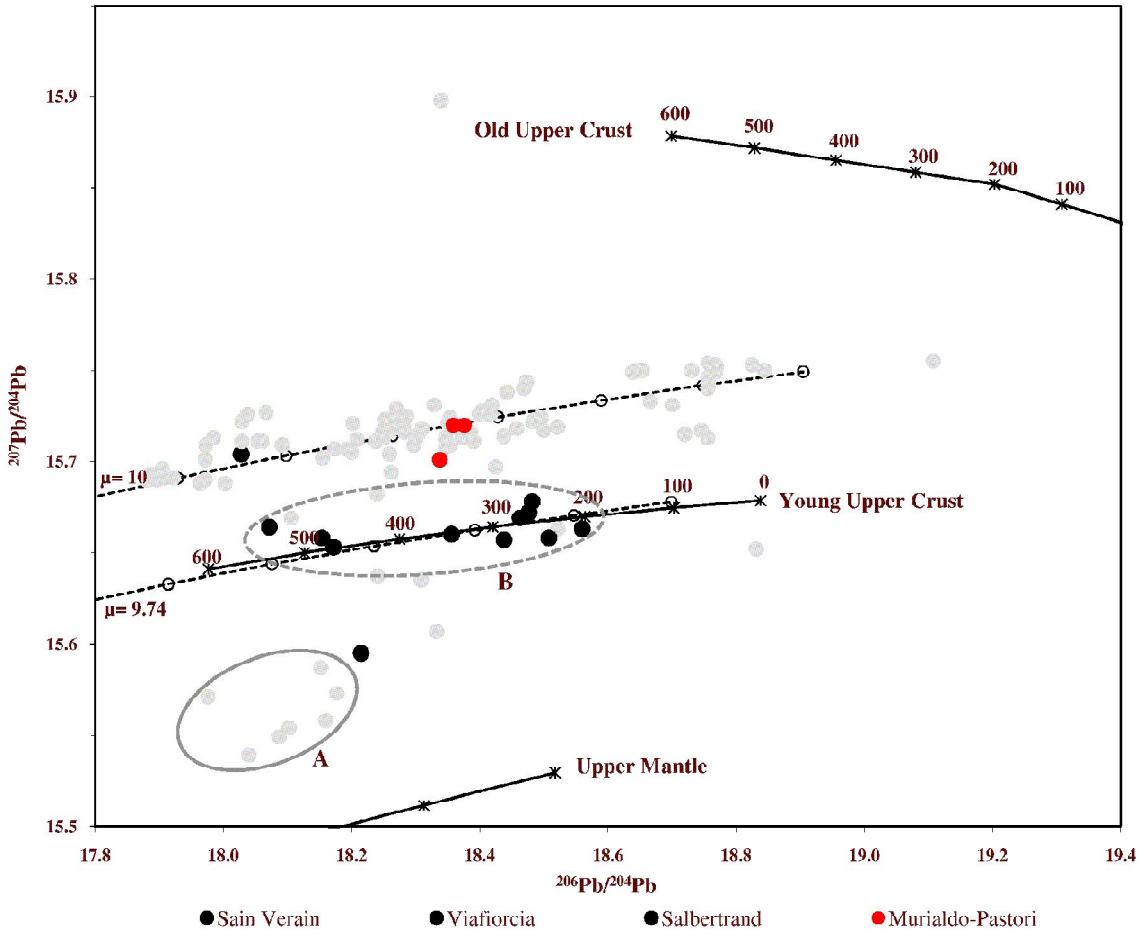

Fig. 3.5 Lead isotope data for deposits of low metamorphosed ophiolites of Briançonnais. μ=9.74 and μ=10 lead growth curves according to Stacey and Kramers (1975); growth curves for upper crust and upper mantle after Kramers and Toltsikhin (1997).

Group B – ophiolites in blueschists (fig 3.5): this group is charactrerized by a light grade of metamorphism (low Temperature) and samples fit along the young upper crust curve. Only bornite samples coming from Saint Verain show different isotopic composition that would suggest a mixing phenomenon.

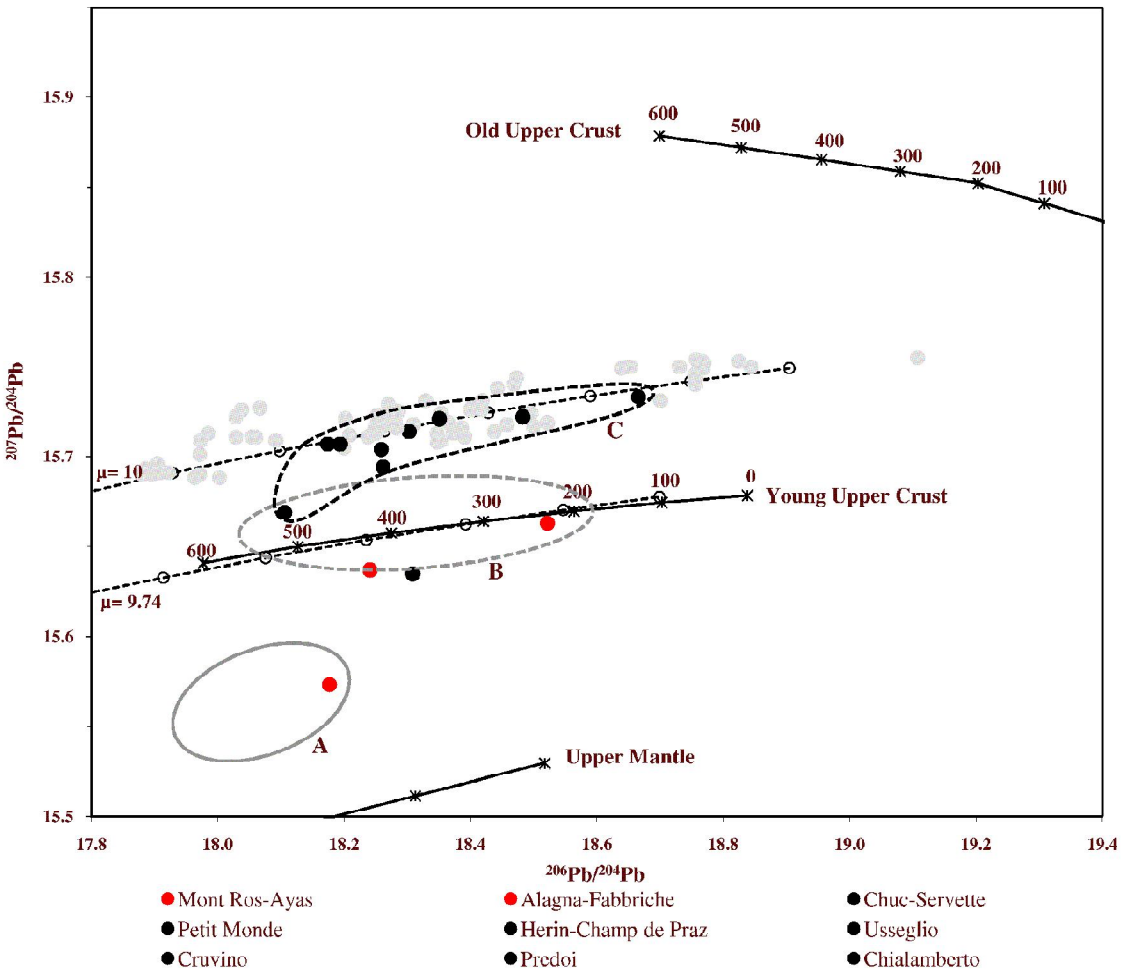

Fig. 3.6Lead isotope data for deposits of high metamorphosed ophiolites of Piedomont zone. μ=9.74 and μ=10 lead growth curves according to Stacey and Kramers (1975); growth curves for upper crust and upper mantle after Kramers and Toltsikhin (1997).

Group C- Piedmontese Zone - metamorphic ophiolites in greenschist facies (fig3.6): range of Piedmontese Zone samples follows the Stacey and Kramers curve with μ=10 and indicate the high metamorphic grade. Mont Ros-Ayas and Alagna Fabbriche samples show a different isotopic imprint, that indicate the belonging of the first deposit to the group A. Alagna instead, seems to belong to group B. The two deposits are located in a very small area of piedmont Zone at the edge with Sesia-Lanzo Zone and near the Arcesa-Brusson Window (Monte Rosa nappe).

Gran Paradiso internal massif and Argentera are plotted in figure 3.7

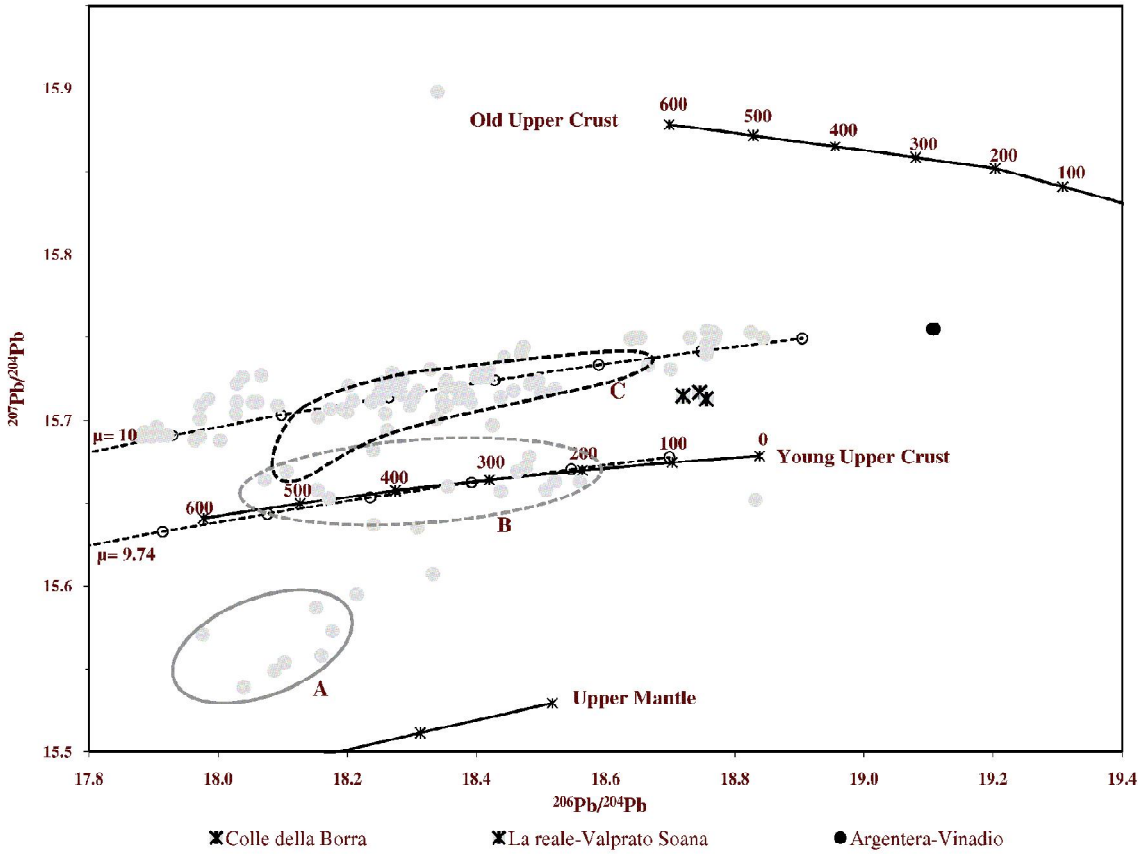

Fig. 3.7 Lead isotope data for deposits of Gran Paradiso and Argentera massif. μ=9.74 and μ=10 lead growth curves according to Stacey and Kramers (1975); growth curves for upper crust and upper mantle after Kramers and Toltsikhin (1997).

Eastern Alps

A progressive relative increase in radiogenic lead is observed from (i) pre-Variscan deposits (fig. 3.x) to (ii) post-Variscan sulphide-rich veins in the Variscan metamorphic basement and in the lower–intermediate units of the Early Permian volcanic sequence (fig. 3.x) to (iii) post-Variscan sulphide-rich and fluorite-rich veins in the upper units of the Early Permian volcanic sequence (fig. 3.8) to (iv) post-Variscan fluorite-rich veins cutting the overlying Late Permian sediments and mid-Triassic mafic dikes (fig. 3.9).

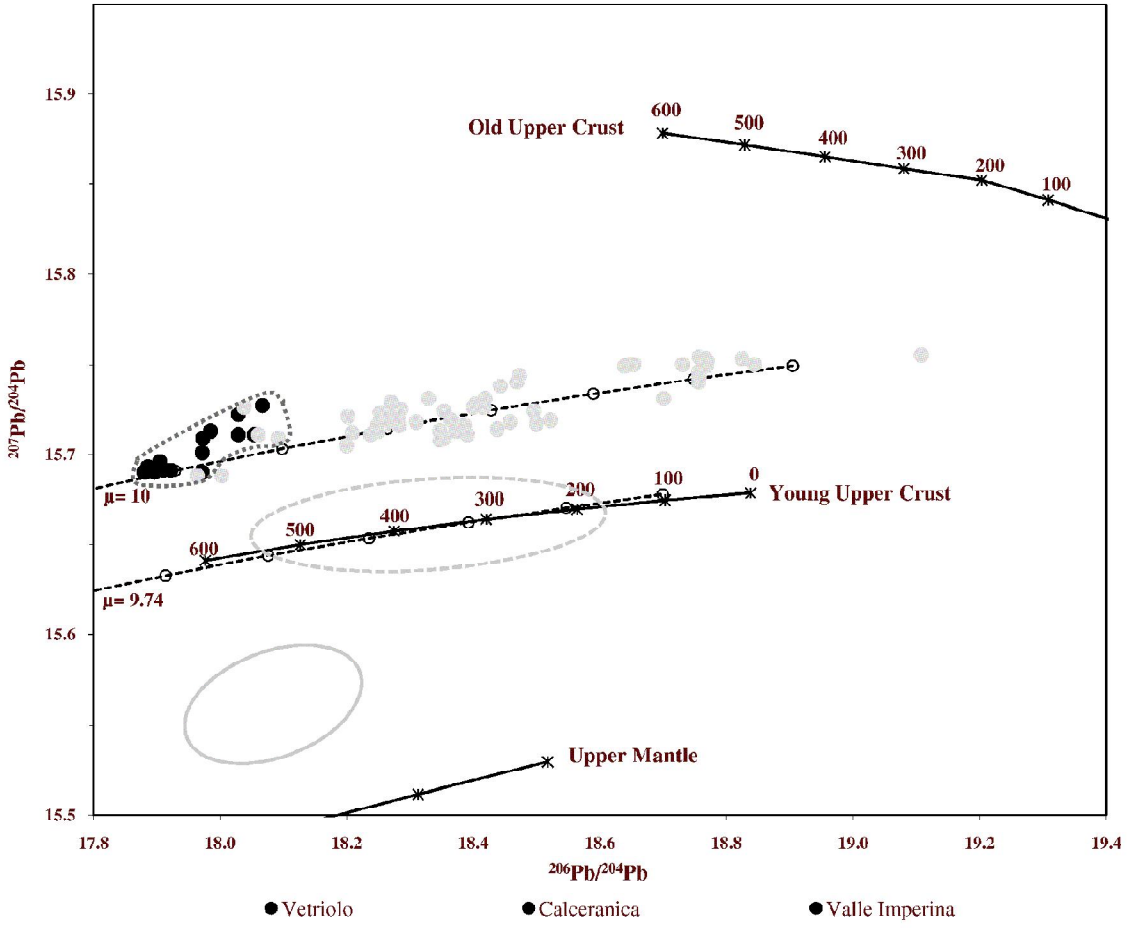

Fig. 3. 8 Lead isotope data for the pre-Variscan stratiform deposits. Reference curves as in Fig. 3.4.

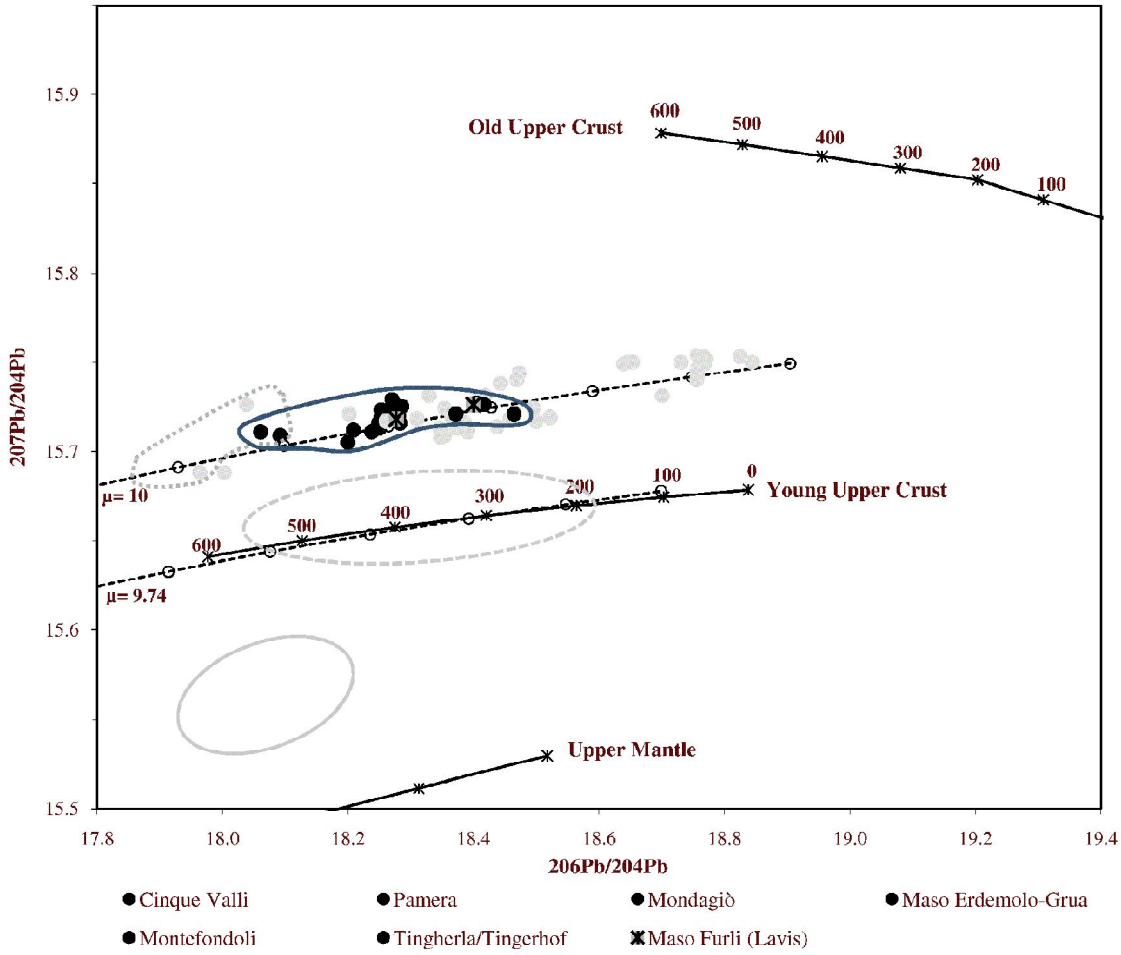

Fig. 3.9 Lead isotope data for the post-Variscan vein deposits. Moreover Maso Furli (Lavis) samples are plotted. Fields: pre-Variscan stratiform deposits (Fig 3.8). Other reference curves as in Fig. 3.4.

The dominant lead sources for all these deposits were Cambrian–Devonian (meta)sediments of the Variscan basement. Contributions from Permian and Triassic igneous rocks were of minor importance, if any, even for vein deposits which were evidently related to Permian magmatism. The isotopic compositions of some of the Permian vein deposits are consistent with, although they do not unequivocally prove, remobilization of metals from the pre-Variscan stratiform deposits. Permian sediments contributed a variable fraction of lead to stratabound deposits in Permian and Early Triassic sediments. Deposits in Triassic magmatic rocks are displaced to slightly lower μ and W values, suggesting lead contribution from Triassic magmatism. For more details see Appendix 1.

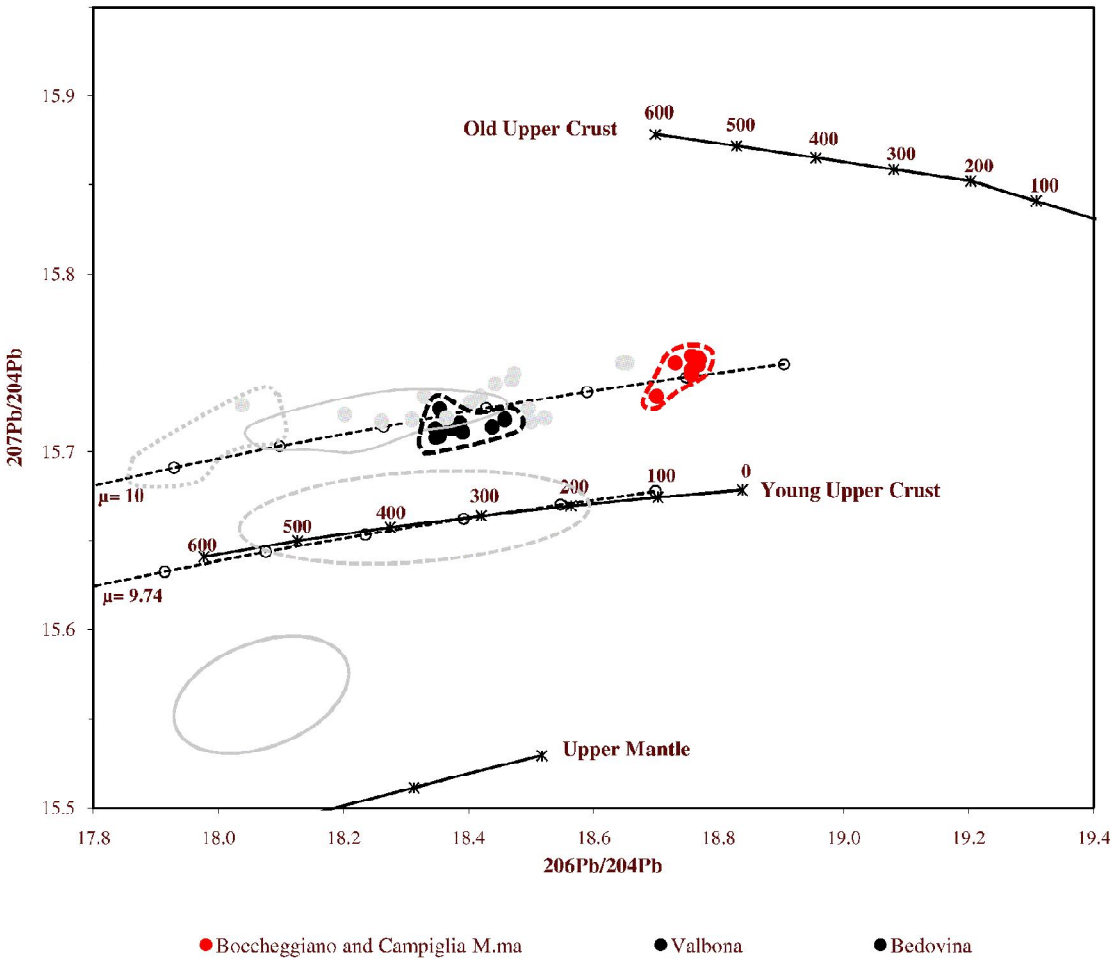

Fig. 3.10. Lead isotope data for deposits in Triassic volcanics (black symbols). Moreover in red, Boccheggiano and Campiglia Marittima samples are also plotted. Reference curves as in Fig. 3.4.

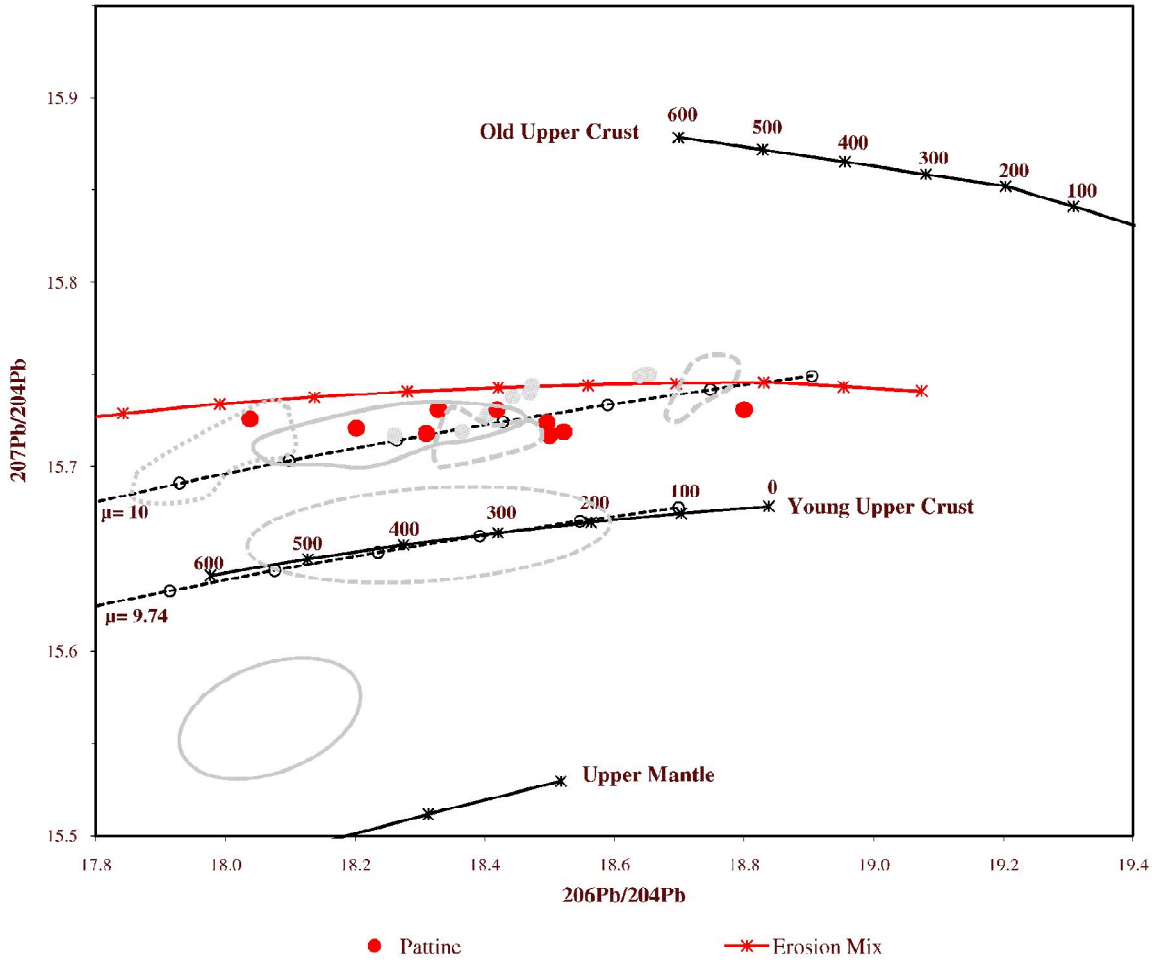

Fig. 3.11. Lead isotope data for stratabound deposits in Permian to Early Triassic sediments. Reference curves as in Fig. 3.4.

Carnic Alps

Here we can see carbonate-hosted deposit of Carnic Alps. Mineralizations are linked to a paleorelief of Devonian limestones overlain by Lower Carboniferous to Lower Permian clastic sediments. The mainly compressive alpine orogeny has only partially obliterated the old structures. Deposits are stratabound to a carbonate sequence of middle to upper Devonian age.

Monte Avanza samples are at the extremes of the field. Samples at 206Pb/204Pb=18.7 are very anomalous and suggest an alpine overprint.

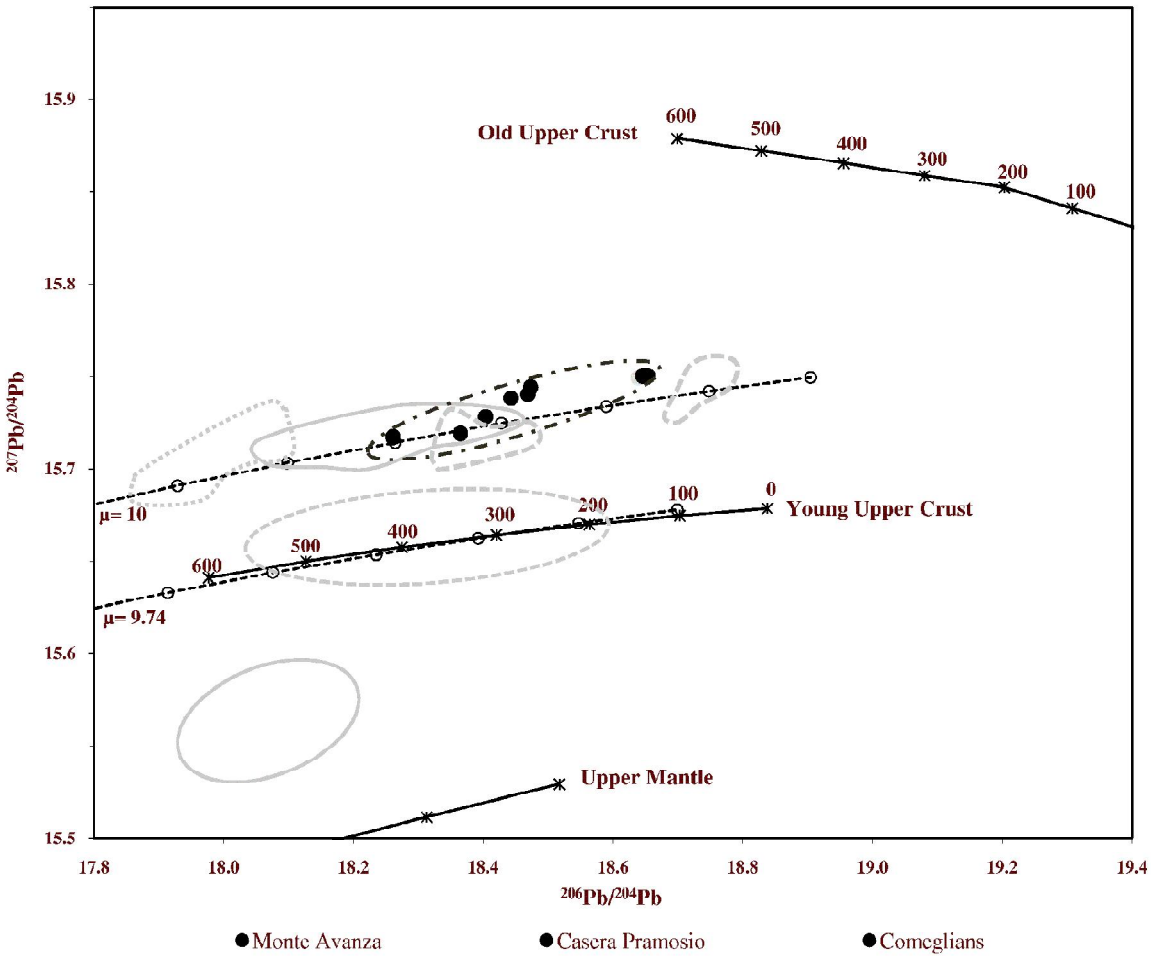

Fig. 3.12. Lead isotope data for carbonate-hosted stratabound of Carnic alps deposits. Reference curves as in Fig. 3.4.

3.2.3 Copper isotopes data

In order to validate the developed protocol, a batch of real samples was analyzed by our methodology and by a well know and calibrated analytical methodology[13,14] as external reference.

The collected data are then compared to each other. Reference data were collected by a MC-ICP-SF-MS at Ecole Normale Superieure de Lyon, Lyon (Francia). The copper isotope ratios here reported refers to 3 different real samples. Samples were chalcopyrites minerals ($CuFeS_2$) collected at Mount Predoi and Libiola mine and a native copper from Elba Island. These samples were digested as reported in the experimental section and each concentrated mother solution was split in two sub-samples. The first one was analyzed by the MC-ICP-SFMS and the second by our ICP-QMS developed protocol. To obtain the reported copper isotopic ratios we used r ¼ 10 and n ¼ 3 and four total bracketing cycles, thus implying that each ratio value represents an average of three values.

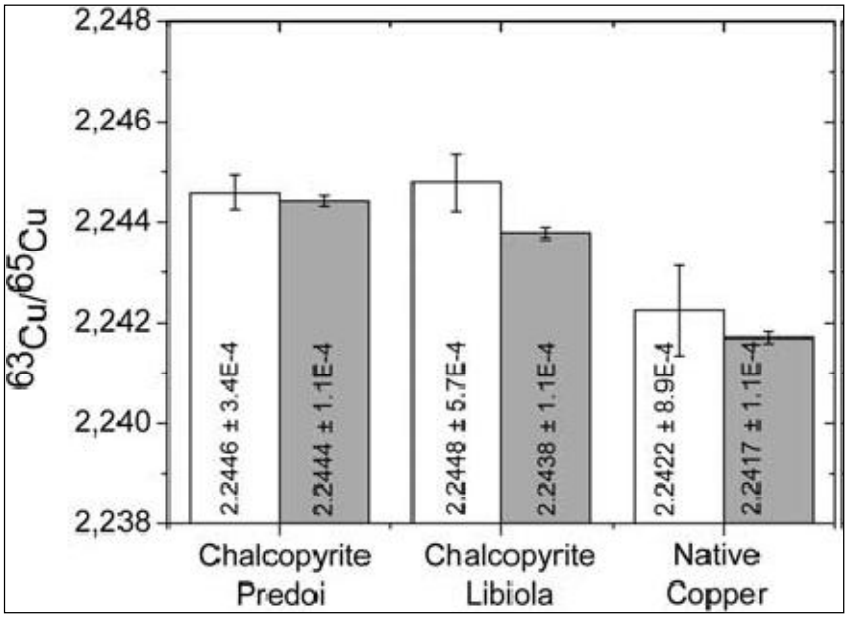

Fig. 3.13 Copper isotopic ratios determined for three real samples: open bars ¼ ICP-CC-QMS, solid bars ¼ MC-ICP-SF-MS. In both cases error bars and numerical uncertainties represent 1s values.

Fig 3.13 clearly shows that accurate results are obtained with the developed protocol, as the results of ICP-CC-QMS are not significantly different from the MC-ICP-SF-MS ones. The means values determined by ICP-CC-QMS on real samples are perfectly in accordance with the mean s values expected for r ¼ 10 and n ¼ 3 (40 min. per sample). Of course, the precision attainable with the multi collector is superior (0.005% vs. 0.025%), but the accurate evaluation of the ICP-QMS behavior and its consequent optimization has markedly lowered the gap between these two techniques.

3.2.4 Trace and Rare Earth Elements

Data and diagram concerning trace and rare earth elements are reported in Appendix 2 and Appendix 3. Data show a great differentiation. In secondary phases samples we can observe a REE enrichment and a negative Eu anomaly, that indicate an oxidizing ambient. Most of native copper samples show a very low concentration of REE.
Predoi series show much more than others the great differentiation between between secondary and primary phases; first ones are strongly enriched in HREE and primary phase samples show a strong enrichment in LREE.

3.3 Conclusions

Lead sources of copper and polymetallic deposits of the central-eastern Southalpine region, particularly pre-Variscan (Late Ordovician–Early Silurian) stratiform, post-Variscan (Permian to Triassic) vein, and stratabound sediment-hosted (Permian to Early Triassic) deposits, are to be sought mainly in the Cambrian–Devonian (meta)sediments of the Variscan basement. Contributions from Permian and Triassic igneous rocks appear to be of minor importance, if any, even for vein deposits which are evidently related to Permian magmatism. The isotopic compositions of some of the Permian deposits are consistent with, although they do not unequivocally prove, remobilization of metals from the pre-Variscan stratiform deposits. Permian sediments contributed a variable fraction of lead to stratabound deposits in Permian to Early Triassic sediments. Triassic magmatism was a probable, but possibly not the sole supplier of lead to the Triassic volcanic-associated deposits. Further data are required to clarify the effective contribution of Triassic magmas and rocks to these deposits. The high μ and W values of the Cu-bearing deposits studied here are consistent with regional isotopic patterns of Pb–Zn-rich deposits in more northerly and easterly sectors of the Eastern Alps (Köppel et al., 1983, 1988; Brigo et al., 2001), which suggested the existence of a high-(μ, W) Southalpine–Austroalpine isotopic province (Köppel, 1983; Koeppel, 1984; Köppel et al., 1993). We further note that other circum-Mediterranean hydrothermal deposits of Paleozoic to Triassic age (e.g. Sardinia, Ludwig et al., 1989; Caron et al., 1997; Betic Cordillera, Arribas et al., 1991) or derived from remobilization of Paleozoic deposits (e.g. Tuscany, Lattanzi et al., 1992) show an identical high-μ and high-W character, which suggests potential persistence southwestwards (present coordinates) of the Southalpine–Austroalpine lead signature across a relatively wide portion of the former north-Gondwanan margin (cf. von Raumer et al., 2002).

Part III

ARCHAEOMETRIC APPLICATIONS

1. Archaeometric applications

The determination of the nature, of the origin, and some origin of the metals is one of the fundamental problems of the archeometallurgy. In the specific case of the objects in copper or I bronze the chemical composition of the elements greatest and smaller contents in the metal you/he/she can sometimes give some indications on the type of mineral used for the extraction of the copper, often fortified by the chemical and mineralogical analyses on the residual phases that are observed what I included in the metal through optic microscopy or electronics. These residual phases and the chemical composition of the metal have commonly spread however in a big number of layers, often distributed on wide geographical, since consequential areas by the same geologic and metallogenic trials. The mineralogical and petrografic indications therefore are often insufficient to propose in non ambiguous way an area of origin of the mineral ones and the metal.
The studies of origin found him therefore mainly on tracing chemists

1.1 Chiusa di Pesio (CN) artifacts

In 2004 was recovered a group of over three hundred pieces of bronze belonging to a storeroom of the early Iron Age, on the basis of the information collected remains of the complex was derived from the Cavanero Mount, Chiusa Pesio (Cuneo), a site whose interest Archaeological was already known from the late nineteenth century for the discovery of graves and materials related to the context of the village, dating from the late Bronze Age and early Iron Age (X-IX century BC).
Part of this findment was analized by Dr. Angelini (see Angelini et al., 2008), with the issue of characterize them by a mineralogical and chemical point of view (SEM-EDS, XRF, EMPA, PIXE, RL-OM). The specimens analyzed belong to each of the functional classes of objects in the closet. In order to have metal not affected and at the same time minimize the aesthetic damage, micro sampling was carried out with a scalpel after a proper study on the stereoscopic microscope.
Despite the large number of objects, many of which belong to functional classes and the variability of types, all the findings are invariably Chiusa Pesio constituent of bronze.
The average content of Sn measured in specimens tested varied from 3 to 19% by weight and shows a bimodal distribution curve with two maxima respectively at around 7-8% and 15-16% by weight.
The archaeometallurgical study of finds from Chiusa di Pesio has allowed us to draw a broad and in-depth picture of the metallurgical realities of North-Western Italy during the X-IX century B.C. The analysis of the finds has found a compositional framework objects are homogeneous as regards the nature of metal, not found: pure copper, copper alloys or arsenic "type Fahlerz" widely present with different evolutionary framework and diffusive, in earlier bronze age. The bronzes, on the other hand, are extremely variable in quantity of Sn and, to a lesser extent, of trace elements. Analytical comparison of specific functional classes of artifacts with contemporary materials and comparable to other typologically from Europe (Heath et al. 2000; Paulin et al. 2003; Giumlia Mair 2008) showed compositional differences that allow alloys therefore distinguish ranges of provenance. It should be noted that even looking in the compositions of all metals studied, a preliminary comparison with contemporary French highlights major differences, particularly for the low content of Pb, As, Sb, Ni and Co of the finds of Chiusa di Pesio (Rychner 1993; Veber et al. 2003; Verney-Bocquet 1998).

This is a very interesting case study, in which my contribution was a provenance study based on lead isotopes. Here below is reported the article that describe Pb isotopes results.

La provenienza del metallo degli oggetti di Monte Cavanero: considerazioni basate sugli isotopi del Pb e sulla geochimica delle mineralizzazioni cuprifere limitrofe

Gilberto Artioli - Ivana Angelini - Ilaria Giunti - Paolo Omenetto - Igor Villa

La determinazione della natura, dell'origine, e della provenienza dei metalli è uno dei problemi fondamentali dell'archeometallurgia. Nel caso specifico degli oggetti in rame o

bronzo la composizione chimica degli elementi maggiori e minori contenuti nel metallo può talvolta dare alcune indicazioni sul tipo di minerali utilizzati per l'estrazione del rame, spesso corroborate dalle analisi chimiche e mineralogiche sulle fasi residue che si osservano quali inclusi nel metallo mediante microscopia ottica od elettronica. Queste fasi residue e la composizione chimica del metallo comunque sono comunemente diffuse in un gran numero di giacimenti, spesso distribuiti su larghe aree geografiche, poiché derivanti dagli stessi processi geologici e metallogenetici. Le indicazioni mineralogiche e petrografiche quindi sono spesso insufficienti per proporre in modo non ambiguo un'area di provenienza dei minerali e del metallo.

Gli studi di provenienza si basano quindi principalmente su traccianti chimici (elementi in tracce) ed isotopici (rapporti isotopici), tra i quali i rapporti isotopici del piombo spiccano sicuramente per diffusione ed importanza (GALE-STOS-GALE 2000). Ovviamente l'utilizzo dei traccianti geochimici deve essere effettuato con cautela (IXER 1999) e fino ad ora l'utilizzo degli elementi chimici maggiori o minori e degli isotopi del Pb è stato applicato con successo limitato, a causa della complessità dei processi in gioco, che includono la variabilità dei giacimenti, l'effetto delle condizioni di estrazione del metallo durante i processi di smelting, e la difficoltà intrinseca di avere databases di riferimento per i minerali ed i metalli (PERNICKA 1999, PERNICKA 2004). Anche l'abbondante utilizzo in letteratura dei rapporti isotopici del Pb quali traccianti per ricostruire la provenienza e diffusione del metallo non è esente da critiche e discussioni (SCAIFE *et al.* 1999, GALE AND STOS-GALE 2000), ed è universalmente accettato che analogie nei rapporti isotopici sono una condizione necessaria ma non sufficiente per l'interpretazione dei giacimenti di provenienza.

Per tale ragione lo studio dei reperti di Monte Cavanero prevede una strategia di ricerca basata sia sulla misura dei rapporti isotopici del Pb e del Cu, sia sull'analisi statistica della suite degli elementi in traccia (COLPANI *et al.* 2007, GIUSSANI *et al.* 2007, ARTIOLI *et al.* 2008). In questa fase si riportano le osservazioni basate sui rapporti isotopici del Pb e sugli elementi minori presenti nel metallo. Le analisi dei rapporti isotopici del Cu sono in corso e serviranno da utile complemento a queste note preliminari.

Inquadramento geologico e campioni giacimentologici delle miniere limitrofe

Senza entrare nel dettaglio della geologia e della tettonica delle Alpi occidentali e delle zone limitrofe, si vuole in questa sede ricordare solamente che, basandosi su semplici considerazioni geografiche, in primo luogo la distanza dal luogo di ritrovamento (Monte Cavanero, Chiusa Pesio) le zone con mineralizzazioni cuprifere significative sono limitate a quattro aree principali (fig. 1):

(1) la zona francese del Queyras, dominata dai calcescisti mesozoici con scaglie di ofioliti, e dove la miniera principale interessa l'importante mineralizzazione a bornite di Saint Veran (BARGE, 1997; ROSTAN *et al.* 1994) sfruttata a larga scala sin

dal Bronzo Antico. Dal punto di vista geologico e minerogenetico Saint Veran si collega strettamente con le mineralizzazioni piemontesi dell'alto Pinerolese, quali Beth-Ghinivert, Salbertrand e soprattutto Viafiorcia (DAL PIAZ *et al.* 1978)

(2) la zona del cosiddetto Brianzonese Ligure, che appartiene alla falda composita medio-Pennidica del Gran San Bernardo ed include complessi misti di vulcaniti calc-alcaline e sedimenti associati di epoca tardo-Ercinica. Non sono segnalate mineralizzazioni consistenti di rame, ma piuttosto modeste concentrazioni a Pb-Zn-Ag con subordinate quantità di Cu, Sb, As, (essenzialmente tetraedrite). Una apparente eccezione è quella del giacimento di Murialdo-Pastori, in Val Bormida, dove alla tetraedrite arsenicale (tennantite) si associano e talora predominano i solfuri di Cu-Fe. Altre manifestazioni sono note più ad ovest in val Tanaro (galene ricche di tetraedrite di Garessio-Priola) e in Val Corsaglia (vene di tetraedrite a Fontane) (PICCOLI 2002, PICCOLI et al. 2007, DEL LUCCHESE 2004, DEL LUCCHESE – DELFINO 2008)

(3) la zona dell'Appennino Ligure, dove nei complessi ofiolitici mesozoici sono note importanti mineralizzazioni a pirite-rame come quelle delle miniere di Libiola e Monte Loreto, sfruttate sin dalla fine del Neolitico (MAGGI - PEARCE 1998, CAMPANA *et al.* 1998)

(4) la vasta zona delle mineralizzazioni pirito-cuprifere nei calcescisti con ofioliti della Falda Piemontese, con giacimenti localizzati principalmente tra la Valle d'Aosta (Chuc-Servette, Champ de Praz, Petit Monde, Ollomont) e la Val Grande Piemontese (Chialamberto, Valli di Lanzo) (Brigo et al., 1976).

Le miniere di Saint Veran e di Libiola/Monte Loreto, oltre ad essere di importanza giacimentologica e per l'estrazione moderna, sono entrambe state assiduamente studiate dal punto di vista archeologico ed hanno prodotto evidenza sicura di sfruttamento nell'antichità. La miniera di Saint Veran mostra evidenze di antiche gallerie che sfruttavano la vena principale di bornite (ROSSI *et al.* 1997) ed anche la sicura presenza di scorie di estrazione del rame risalenti alla metallurgia della Prima Età del Bronzo (BOURGARIT *et al.* 2008). Le miniere liguri sembrano essere state sfruttate perfino in epoche più antiche, sin dalla fine del Neolitico o dall'inizio dell'Eneolitico (MAGGI - PEARCE 1998, CAMPANA *et al.* 1998), anche se non ci sono fino ad ora evidenze sicure di trattamento del minerale e mancano totalmente le scorie di estrazione.

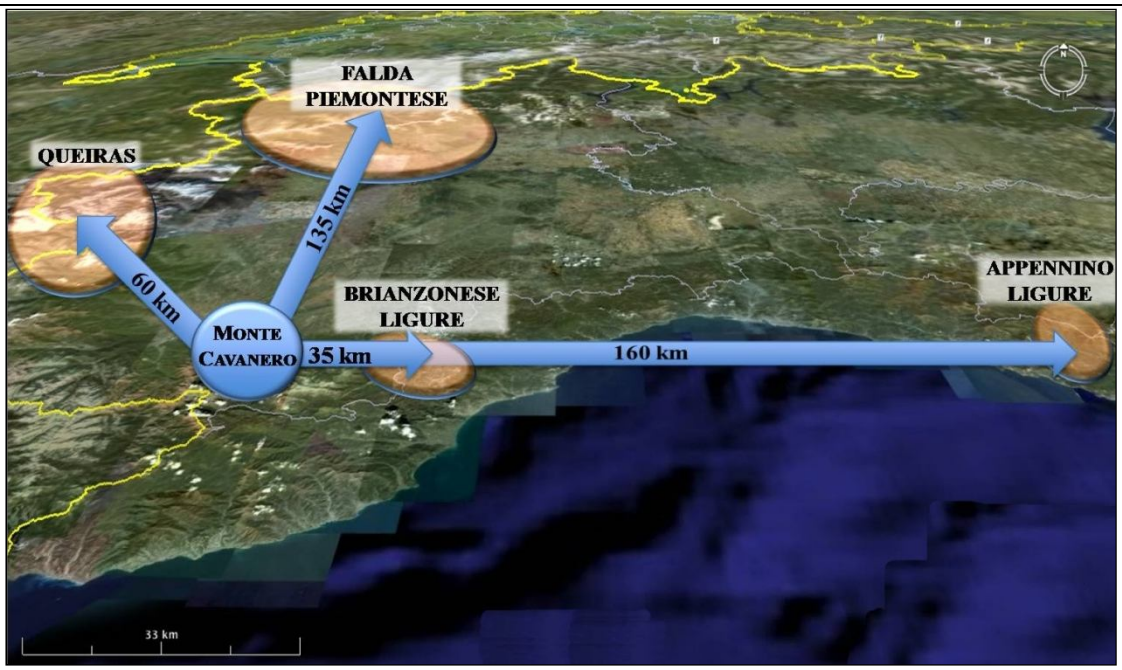

Fig. 1 – Localizzazione geografica di Monte Cavanero e visione generale delle principali mineralizzazioni cuprifere delle Alpi Occidentali e dell'Appennino Ligure.

Tutte le mineralizzazioni principali sono state campionate ed analizzate nell'ambito del presente studio. Per tutte le miniere sono stati ottenuti significativi campioni della mineralizzazione primaria e secondaria. Molti campioni provengono direttamente dalle miniere, per altre di difficile accesso sono stati reperiti campioni da musei, da collezioni giacimentologiche, da precedenti studi esplorativi, o da raccolte mineralogiche private.

Oltre alle località cuprifere caratteristiche delle quattro aree evidenziate, sono stati analizzati alcuni altri campioni di mineralizzazioni di aree limitrofe per ottenere un quadro completo delle mineralizzazioni a rame delle Alpi occidentali. Le mineralizzazioni analizzate sono: (a) alcuni campioni provenienti dalla zona del Gran Paradiso (mineralizzazioni a Cu-Pb-Au della Reale di Valprato Soana, mineralizzazioni a Cu-Au di Colle della Borra nei calcescisti della Falda Piemontese); (b) campioni provenienti dalla più importante mineralizzazione conosciuta nelle ofioliti della Valsesia, Alagna-Fabbriche; (c) campioni provenienti dalla zona del Massiccio dell'Argentera e aree limitrofe (Rio del Nandis-Vinadio, Elva-Stroppo, Valgrana).

Oltre che per i rapporti isotopici del Pb, qui presentati, tutti i campioni sono in corso di analisi anche per il rapporto isotopico del Cu e per gli elementi in traccia. I dati formeranno un data-base di riferimento delle mineralizzazioni a rame delle Alpi occidentali anche per studi futuri.

La fig. 2 e la tab. 1 riportano in dettaglio la localizzazione geografica e le caratteristiche geologiche generali delle miniere analizzate.

Tab. 1. Lista dei campioni delle mineralizzazioni cuprifere analizzate. I numeri delle miniere (colonna 2) sono gli stessi che compaiono in Figura 2.

Miniera	***N° miniera***	***campione***	***Fasi metallifere***	***Area Mineraria***
Saint Veran	1	SVE-Ap1	Bornite	Queyras-Pinerolese
		SVE-Ap2	Calcopirite	
		SVE-Ap3	Calcopirite	
		SVE-Ap4	Bornite	
		SVE-Ar1	Cu nativo	
		SVE-Br1	Cu nativo	
		SVE-Bp1	Bornite	
		SVE-Bs1	Malachite	
		SVE-Cp1	Bornite	
		SVE-Cs1	Malachite	
Viafiorcia	2	VF-2a	Calcopirite	
		VF-5b B	Bornite	
		VF-5b C	Calcopirite	
Salbertrand	3	R-96-2	Calcopirite	
Chialamberto	4	CHIAL67	Calcopirite, Pirite	Falda Piemontese: Valli di Lanzo, Val Grande, Val d'Aosta, Val Pellice
		CHIAL68	Pirite, calcopirite	
Cruvino, Usseglio	5	M/U3761	Tetraedrite	
		M/U9748	Tetraedrite, calcopirite	
Ciabraressa	6	MOR119	Calcopirite	
Petit Monde	7	A5B	Calcopirite	
Chuc-Servette	8	46/5	Calcopirite	
Champ de Praz	9	46/11	Calcopirite	
Fontane	10	FO-1	Tetraedrite, calcopirite	Brianzonese Ligure: Val Corsaglia,Val Bormida
Pastori, Murialdo	11	MUR-1	Calcopirite	
Libiola	12	LIB-Ep1	Calcopirite	Appennino Ligure: ofioliti Liguri
		LIB-Gs1	Crisocolla	
		LIB-Bp1	Calcopirite	
		LIB-L2p1	Calcopirite	
		LIB-Fs1	Crisocolla	
Monte Loreto	13	LOR-Bp2	Calcopirite	
		LOR-As1	Crisocolla	
		M2prph	Calcopirite	
		M3prph3	Calcopirite	
La Reale, Valprato	14	MOR42-GP21'	Calcopirite	Gran Paradiso
		MOR42-GP23	Calcopirite	
Colle della Borra	15	MOR43-GP37	Calcopirite	
Alagna-Fabbriche	16	L-87'	Calcopirite	Valsesia, Val d'Ayas
Mont Ros	17	Q20-7	Calcopirite	
Elva	18	EL-1	Tetraedrite	Argentera-Cuneese
Valgrana	19	GR-1	Malachite, azzurrite	
Argentera	20	AR-1	Calcopirite	

Tab. 2. Dati misurati dei rapporti isotopici del Pb per i campioni giacimentologici.

Campione	$^{206}Pb/^{204}Pb$	$^{207}Pb/^{204}Pb$	$^{208}Pb/^{204}Pb$
SVE-Ap1	18.028	15.654	38.173
SVE-Ap2	18.463	15.619	38.406
SVE-Ap3	18.356	15.610	38.314
SVE-Ap4	18.154	15.608	38.107
SVE-Ar1	24.534	15.889	38.276
SVE-Br1	20.051	15.807	38.539
SVE-Bp1	18.072	15.614	38.095
SVE-Bs1	18.172	15.603	38.116
SVE-Cp1	18.215	15.545	37.989
SVE-Cs1	18.508	15.608	38.382
VF-2a	18.560	15.613	38.426
VF-5b B	18.477	15.622	38.452
VF-5b C	18.482	15.628	38.441
R-96-2	18.438	15.607	38.346
CHIAL67	18.194	15.657	38.363
CHIAL68	18.351	15.671	38.503
M/U3761	18.303	15.664	38.450
M/U9748	18.483	15.672	38.621
46/11	18.106	15.619	38.024
A5B	18.174	15.657	38.243
MOR119	18.406	15.676	38.536
46/5	18.259	15.654	38.361
FO-1	18.308	15.666	38.433
MUR-1	18.338	15.651	38.419
LIB-Ep1	18.160	15.508	37.733
LIB-Gs1	18.333	15.557	37.814
LIB-Bp1	18.152	15.537	37.824
LIB-L2p1	18.040	15.489	37.640
LIB-Fs1	18.832	15.602	37.926
LOR-Bp2	18.240	15.632	38.277
LOR-As1	18.290	15.841	38.502
M2prph	17.976	15.521	37.650
M3prph3	18.155	15.652	38.048
MOR42-GP21’	18.756	15.663	38.747
MOR42-GP23	18.720	15.665	38.709
MOR43-GP37	18.746	15.667	38.671
L-87’	18.522	15.613	38.421
Q20-7	18.177	15.523	37.877
EL-1	19.071	15.732	38.826
GR-1	17.630	15.560	37.596
AR-1	19.108	15.705	38.485

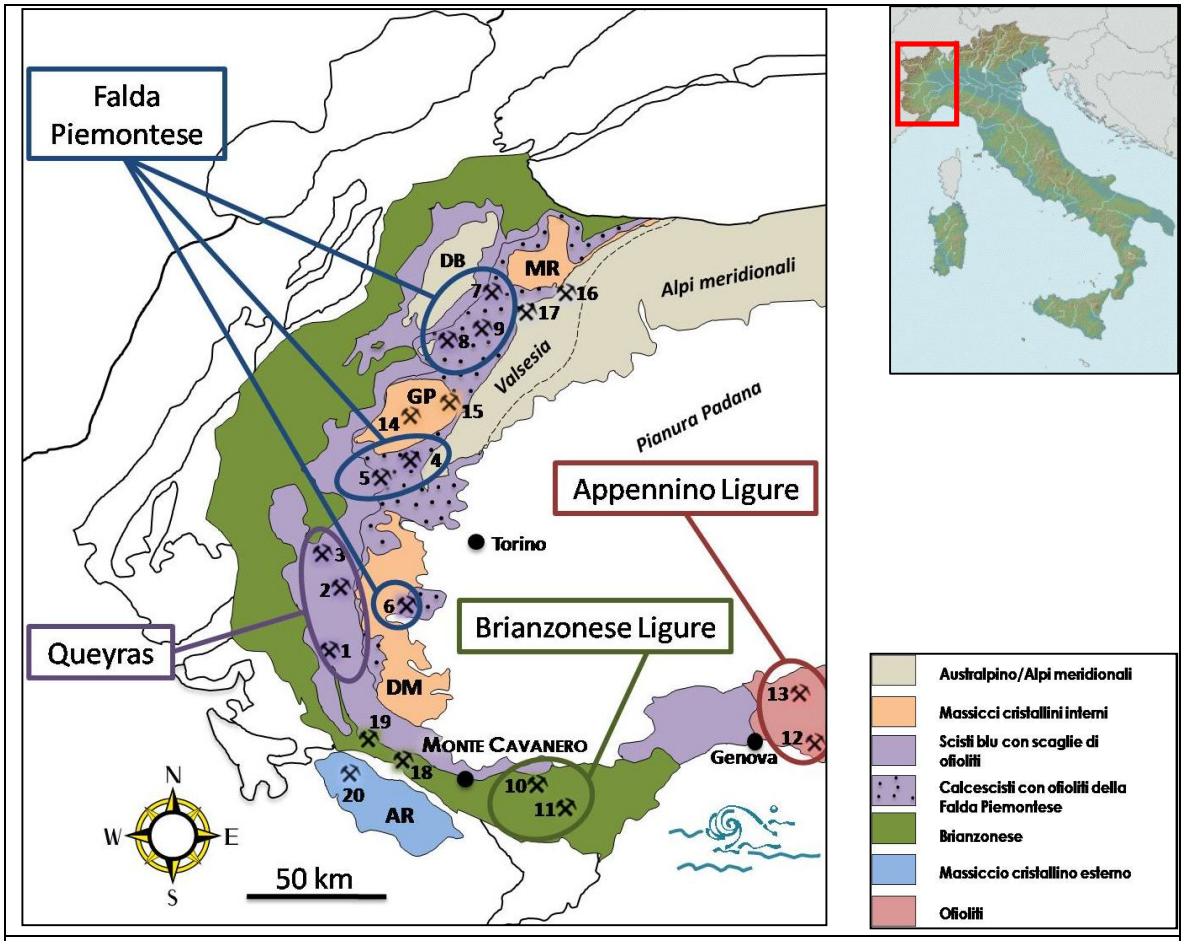

Fig. 2. Schema geologico delle Alpi Occidentali e localizzazione delle mineralizzazioni analizzate. Le sigle in carta sono riferite ai nomi dei massicci principali: AR = Argentera, DM = Dora Maira, GP = Gran Paradiso, MR = Monte Rosa, DB = Dent Blanche.

Metodologie analitiche

Tutti campioni sono stati caratterizzati dal punto di vista mineralogico e petrologico. La identificazione delle fasi minerali è stata effettuata mediante diffrattometria di polveri a raggi-X e microscopia ottica con microscopio polarizzatore in luce riflessa. Le fasi metallifere sono poi state concentrate mediante separazione gravitativa e magnetica, ed una parte del concentrato di fasi metallifere è stato destinato all'analisi chimica ed isotopica mediante spettroscopia di massa.

Lo strumento utilizzato per l'analisi di massa dei rapporti isotopici del Pb è uno spettrometro MC-ICP-MS Nu Plasma HR della Nu Instruments, dotato di 12 gabbie di Faraday come detectors e zoom ottico, utilizzato presso il laboratorio isotopico dell'Institut für Geologie, Universität Bern. La tecnologia mediante zoom ottico a dispersione variabile permette di governare agevolmente le condizioni strumentali modificando un unico parametro meccanico e mantenendo fissi i rivelatori; ciò semplifica notevolmente la complessità del banco di rivelatori e diminuisce le possibilità di errori

strumentali. La calibrazione è stata effettuata sullo standard NIST SRM 981 ($^{204}Pb/^{206}Pb$ = 0.05904 ± 0.00004, $^{207}Pb/^{206}Pb$ = 0.91464 ± 0.00033, $^{208}Pb/^{206}Pb$ = 2.16810 ± 0.00080). In tabella 2 sono riportati i risultati delle analisi isotopiche del Pb sui campioni delle mineralizzazioni.

Sono quindi stati selezionati per le analisi isotopiche 18 campioni tra gli oggetti metallici del ripostiglio di Monte Cavanero, al fine di poter effettuare confronti con i dati dei giacimenti. La tabella 4 riporta le caratteristiche degli oggetti analizzati ed i dati misurati. I campioni sono stati selezionati accuratamente al fine di avere un numero di campioni sufficiente e rappresentativo delle varie tipologie e composizioni osservate. Oltre agli oggetti finiti, è interessante notare la presenza fra gli oggetti rinvenuti nel ripostiglio di un frammento di rame grezzo non lavorato (campione CP-162). Si tratta di un grumo di metallo derivato direttamente dal primo processo di estrazione del rame da minerali con tipologie fahlerz (i.e. polisolfuri misti), non raffinato e con composizione decisamente anomala rispetto agli oggetti finiti (ANGELINI *et al.*, questa pubblicazione). Anche questo campione è stato analizzato ed i risultati saranno discussi separatamente.

Tab. 3. Oggetti metallici del deposito di Monte Cavanero analizzati per i rapporti isotopici del Pb.

Sample label	***Inventario***	***Oggetto***	**$^{206}Pb/^{204}Pb$**	**$^{207}Pb/^{204}Pb$**	**$^{208}Pb/^{204}Pb$**
CP-6	88604	Torquis frammentato	18.158	15.663	38.378
CP-9	88606	Torquis frammentato	18.071	15.67	38.283
CP-34	88640	Pendaglio lanceolato	18.224	15.685	38.523
CP-40	88650	Pendaglio lanceolato	18.179	15.675	38.437
CP-45	88652	Pendaglio lanceolato	18.223	15.640	38.317
CP-51	88594	Armilla frammentaria in lamina spessa	18.220	15.664	38.394
CP-53	88593	Armilla frammentaria in lamina spessa	18.219	15.664	38.407
CP-63	88670/3	Pendaglio circolare con gancio triangolare	18.131	15.663	38.353
CP-94	88614	Sostegno triangolare	18.075	15.656	38.276
CP-156	88661/6	Placchetta in lamina rettangolare	18.053	15.664	38.305
CP-132	88659/12	Spiralina	18.197	15.654	38.379
CP-133	88659/13	Spiralina	18.187	15.67	38.414
CP-161	88680	Frammento di lingotto (?)	17.916	15.651	38.163
CP-162	88681	Scoria di fusione	18.363	15.684	38.482
CP-167	88676/1	Frammento di lama di spada	18.048	15.662	38.234
CP-170/1	88637/1	Frammento di anellino circolare	18.188	15.678	38.442
CP-170/2	88637/2	Frammento di anellino circolare	18.128	15.661	38.352
CP-175CL	88589	Tazza in lamina (corpo)	18.153	15.665	38.385

Risultati e discussione

I risultati giacimentologici, mineralogici, e chimici ottenuti sono il punto di partenza per avere la segnatura geochimica delle mineralizzazioni cuprifere delle Alpi Occidentali, al fine di potere riconoscere prodotti di estrazione (rame semilavorato, scorie) ed eventualmente identificare oggetti prodotti con il rame estratto. Considerando quindi queste premesse di carattere generale, è evidente che i dati ottenuti sui giacimenti selezionati ed analizzati hanno significato solo se relazionati a dati chimici ed isotopici di portata quanto meno regionale, che testimonino la possibile discriminazione rispetto ad altri giacimenti alpini o di aree limitrofe.

Discriminazione dei giacimenti e delle mineralizzazioni

Al fine quindi di mettere in contesto i dati preliminari ottenuti sulle mineralizzazioni studiate, i dati isotopici misurati e riportati nelle Tab. 2 sono stati confrontati con i valori di letteratura disponibili sulle principali mineralizzazioni Alpine (ad es. KÖPPEL 1983, KÖPPEL - SCHROLL 1983) e mediterranee (GALE - STOS-GALE 2000). Per omogeneità e consistenza dei dati, sono stati inclusi solo i giacimenti principali di rame, ed i dati isotopici si riferiscono a minerali cupriferi, escludendo mineralizzazioni a galena o galena/blenda. Questo permette di inquadrare le quattro aree studiate in un coerente quadro evolutivo della tettonica Alpina e della formazione dei giacimenti cupriferi. Dai diagrammi dei rapporti isotopici $^{207}Pb/^{204}Pb$ vs $^{206}Pb/^{204}Pb$ (fig. 3) e $^{208}Pb/^{204}Pb$ vs $^{206}Pb/^{204}Pb$ (fig. 4), che sono fra quelli più utilizzati in archeometria per interpretare i campi discriminanti delle diverse aree minerarie, si osserva che i dati isotopici misurati sulle mineralizzazioni campionate rientrano pienamente nei campi attesi per i giacimenti di origine ofiolitica Appenninica e metaofiolitica Alpina. I dati delle calcopiriti provenienti dalle miniere liguri, soprattutto quelle di Libiola sono nettamente separati da tutti gli altri dati e prossimi ai valori attesi per basalti oceanici che mantengono una consistente componente di mantello, al di sotto della curva evolutiva crostale media con μ_2 = 9.74 di Stacey e Kramer (1976). I valori misurati per i solfuri primari (bornite, calcopirite) dei giacimenti delle Alpi Occidentali sono in prossimità delle curve evolutive con valori di μ_2 = 9.7-10.0. In accordo con i modelli genetici e le età delle mineralizzazioni possiamo evidenziare che, seppur i dati isotopici di alcuni giacimenti delle Alpi Occidentali (figg. 3,4) sono parzialmente sovrapponibili con quelli di alcuni altri giacimenti Europei, soprattutto quelli tedeschi dell'Erzgebirge e quelli spagnoli di Rio Tinto, sono comunque ben distinguibili fra loro e ben connotati dal punto di vista geochimico.

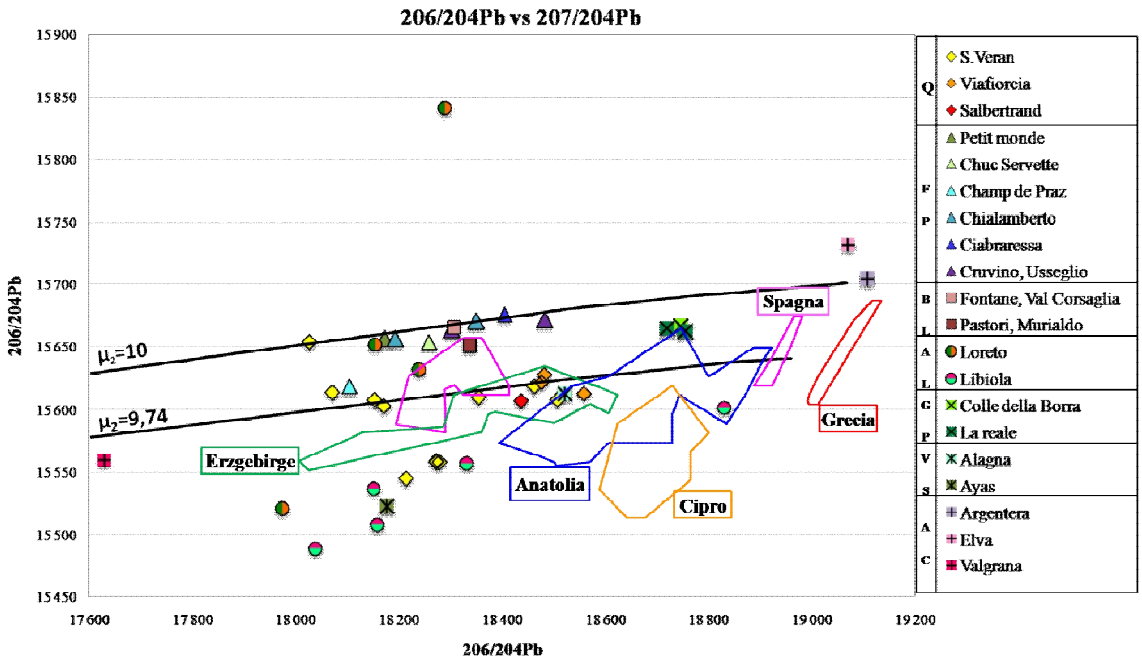

Fig. 3. Diagramma dei rapporti isotopici $^{207}Pb/^{204}Pb$ vs $^{206}Pb/^{204}Pb$ per i campioni giacimentologici (Tab. 2). I campi schematizzati si riferiscono ad alcune delle aree a giacimenti di rame più importanti in Europa e nell'area mediterranea. In didascalia le mineralizzazioni sono divise per aree minerarie: Q = Queyras, FP = Falda Piemontese, BL = Brianzonese Ligure, AL = Appenino Ligure, GP = Gran Paradiso, VS = Val Sesia, AC = Argentera-Cuneese

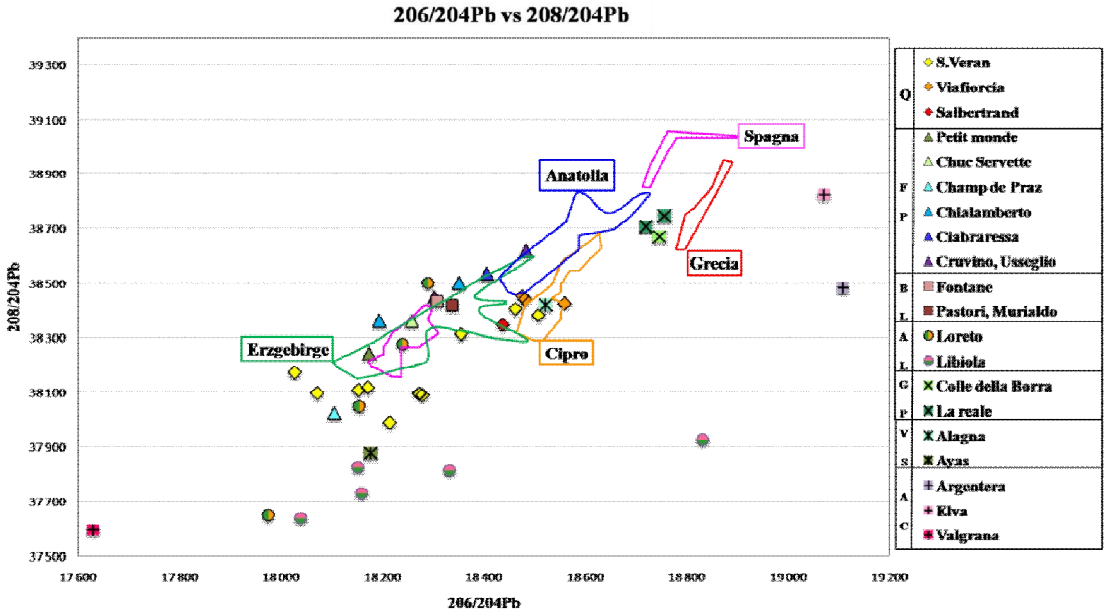

Fig. 4. Diagramma dei rapporti isotopici $^{208}Pb/^{204}Pb$ vs $^{206}Pb/^{204}Pb$ per i campioni giacimentologici (Tab. 2). I campi schematizzati si riferiscono ad alcune delle aree a giacimenti di rame più importanti in Europa e nell'area mediterranea. In didascalia le mineralizzazioni sono divise per aree minerarie: Q = Queyras, FP = Falda Piemontese, BL = Brianzonese Ligure, AL = Appenino Ligure, GP = Gran Paradiso, VS = Val Sesia, AC = Argentera-Cuneese

Discriminazione dei dati isotopici sugli oggetti

Per quanto riguarda gli oggetti, le figg. 5 e 6 riportano i valori misurati dei rapporti isotopici del Pb. Si può immediatamente notare che esiste una sostanziale affinità tra i

dati isotopici misurati sugli oggetti e quelli dei depositi delle Alpi Occidentali, mentre i valori misurati si discostano notevolmente da quelli dei depositi appenninici (Libiola, Monte Loreto), da quelli del Gran Paradiso e da quelli della Valsesia. Si può quindi escludere con sicurezza la provenienza da questi giacimenti.
Le distribuzioni evidenziate dai dati (figg. 5,6) sono condizione necessaria per poter affermare che il rame utilizzato per gli oggetti è compatibile con il rame dei depositi alpini più prossimi. I dati isotopici degli oggetti sono tutti ben raggruppati lungo una curva vicina a μ_2= 10.0, ben compatibile con i depositi piemontesi e valdostani, mentre sembrano essere leggermente separati dai valori relativi ai depositi del Queyras-Pinerolese, soprattutto da quello prevalentemente bornitico di Saint Veran e da tutti quelli con impronta metamorfica molto debole (Viafiorcia, Salbertrand, calcopirite di Saint Veran).
Il rame che compone gli oggetti ha una chiara impronta metamorfica elevata, compatibile quindi sia con molti depositi ofiolitici con metamorfismo in facies eclogitica, sia con le mineralizzazioni del Brianzonese ligure comprese fra la Val Bormida e la Val Corsaglia. Bisogna però tenere ben presente che, sebbene entrambe le aree minerarie abbiano dati isotopici compatibili con gli oggetti, le mineralizzazioni cuprifere sono molto diverse. Infatti mentre nella maggior parte delle mineralizzazioni nei calcescisti con pietre verdi abbiamo giacimenti essenzialmente calcopiritici con blenda associata, nelle miniere del Brianzonese abbiamo pochissima calcopirite, con l'eccezione di Murialdo/Pastori, e in genere il rame è monopolizzato dal minerale tetraedrite (Fahlerz). Il carattere geochimico primario degli oggetti (ANGELINI *et al.* pp.00-00), cha ha tenori molto limitati degli elementi associati a fahlerz (escluso l'oggetto CP-162, che verrà discusso a parte), ma mostra invece contenuti ben individuabili di Zn, indica quindi chiaramente che il rame non proviene dalle mineralizzazioni poste a sud-est di Chiusa Pesio, ma piuttosto dalle mineralizzazioni a calcopirite-blenda poste a nord, cioè in tutta la zona metamorfica che partendo dalla valle d'Aosta (Petit Monde, Chuc Servette), e passando dalle valli piemontesi (Colle della Borra, Chialamberto), arriva fino alla zona prossima alla Francia (Bars de l'Ors/Ciabraressa).

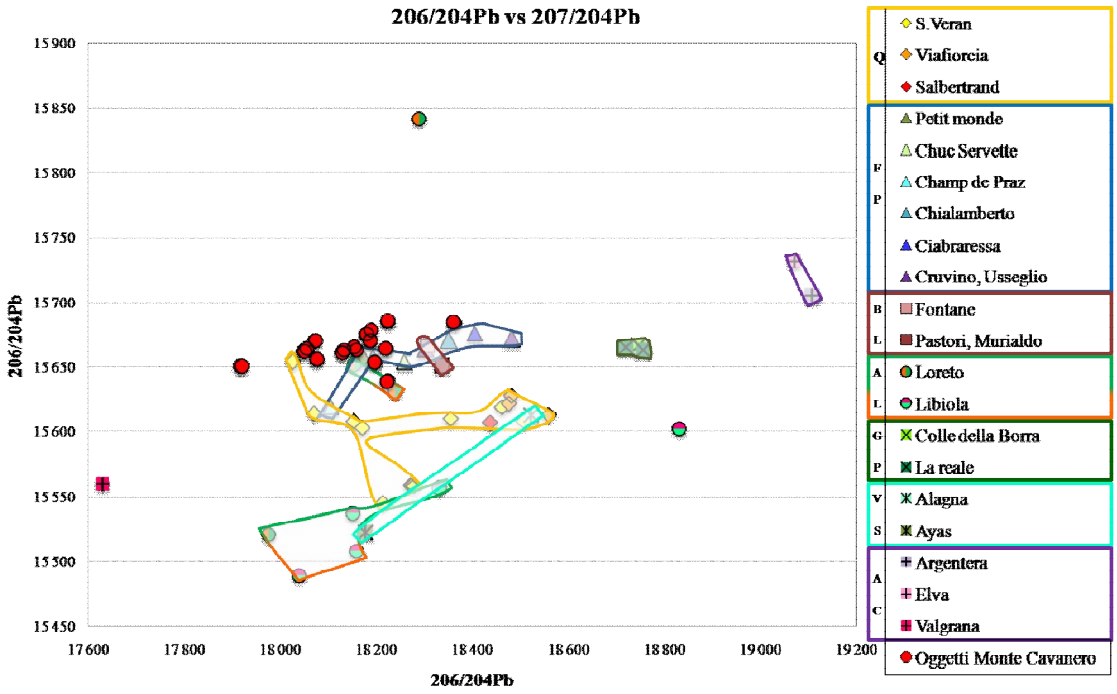

Fig. 5. Diagramma dei rapporti isotopici $^{207}Pb/^{204}Pb$ vs $^{206}Pb/^{204}Pb$ per gli oggetti analizzati (Tab. 3), confrontati con le mineralizzazioni limitrofe, che in didascalia sono divise per aree minerarie e i relativi campi schematizzati sono riportati nel grafico: Q = Queyras, FP = Falda Piemontese, BL = Brianzonese Ligure, AL = Appenino Ligure, GP = Gran Paradiso, VS = Val Sesia, AC = Argentera-Cuneese

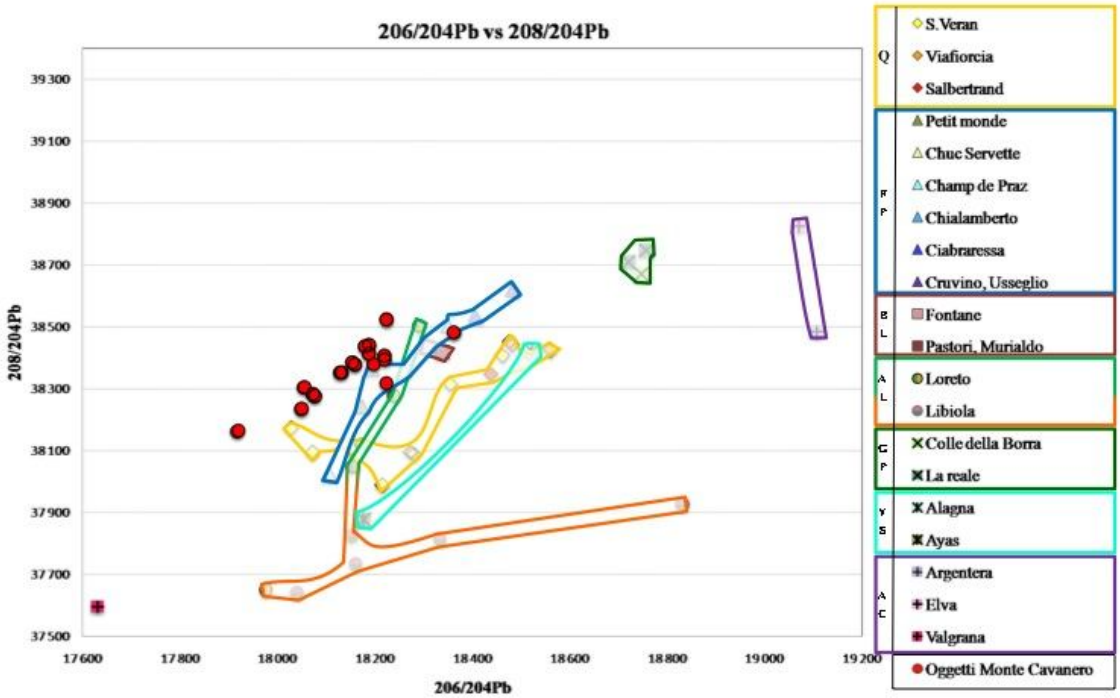

Fig. 6. Diagramma dei rapporti isotopici $^{208}Pb/^{204}Pb$ vs $^{206}Pb/^{204}Pb$ per gli oggetti analizzati (Tab. 3), confrontati con le mineralizzazioni limitrofe, che in didascalia sono divise per aree minerarie e i relativi campi schematizzati sono riportati nel grafico: Q = Queyras, FP = Falda Piemontese, BL = Brianzonese Ligure, AL = Appenino Ligure, GP = Gran Paradiso, VS = Val Sesia, AC = Argentera-Cuneese

Effetti dell'alligazione di stagno

Poiché il rame in tutti gli oggetti ritrovati si trova alligato con tenori di stagno compresi fra 7 e 20 wt% (ANGELINI *et al.* pp.00-00), si pone il problema dell'eventuale contaminazione del segnale isotopico del Pb derivato dai giacimenti per l'estrazione del rame. Questo è un problema di non facile soluzione e raramente affrontato nella letteratura. Per tentare di valutare l'eventuale contributo isotpico dello stagno, abbiamo analizzato il segnale sugli oggetti archeologici dell'Età del Bronzo di stagno puro disponibili. Solo due oggetti di Sn sono noti dall'Italia Settentrionale: (a) un filo di stagno proveniente da Alba (VENTURINO GAMBARI *et al.* 1995), (b) un lingotto di stagno proveniente dalla terramara di Parma (BERNABÒ BREA, comunicazione personale). Entrambi gli oggetti sono stati campionati ed analizzati per il segnale isotopico del Pb. Esistono inoltre numerosi pani di Sn rinvenuti nella Sardegna nuragica, molti dei quali conservati presso il Museo di Nuoro (FADDA, 2006). Anche alcuni di questi lingotti sono stati analizzati per valutare il segnale isotopico.
I dati misurati sono illustrati nelle figg. 7 e 8.
Seppur di provenienza ancora da investigare (analisi degli isotopi dello Sn sono in corso per determinarne la provenienza), il segnale dei rapporti isotopici del Pb di tutti gli oggetti in stagno è variabile, ma allineato con la curva evolutiva degli oggetti. Quindi, seppur di difficile interpretazione geochimica, si può comunque affermare che nessuno dei segnali isotopici del Pb contenuto nello stagno è sufficiente per interferire significativamente con il segnale del Pb contenuto nel rame e, qualsiasi sia la provenienza dello stagno utilizzato per l'alligazione, le variazioni prodotte nel segnale isotopico del rame non incidono sulle ipotesi di provenienza.
A titolo di esempio sono mostrati nelle figure i valori dei rapporti isotopici del Pb degli oggetti di Monte Cavanero corretti per il tenore in Pb dello stagno della lega (ANGELINI *et al.* pp.00-00), assumendo i valori isotopici del Pb misurati sui campioni di stagno disponibili (fig. 7,8).

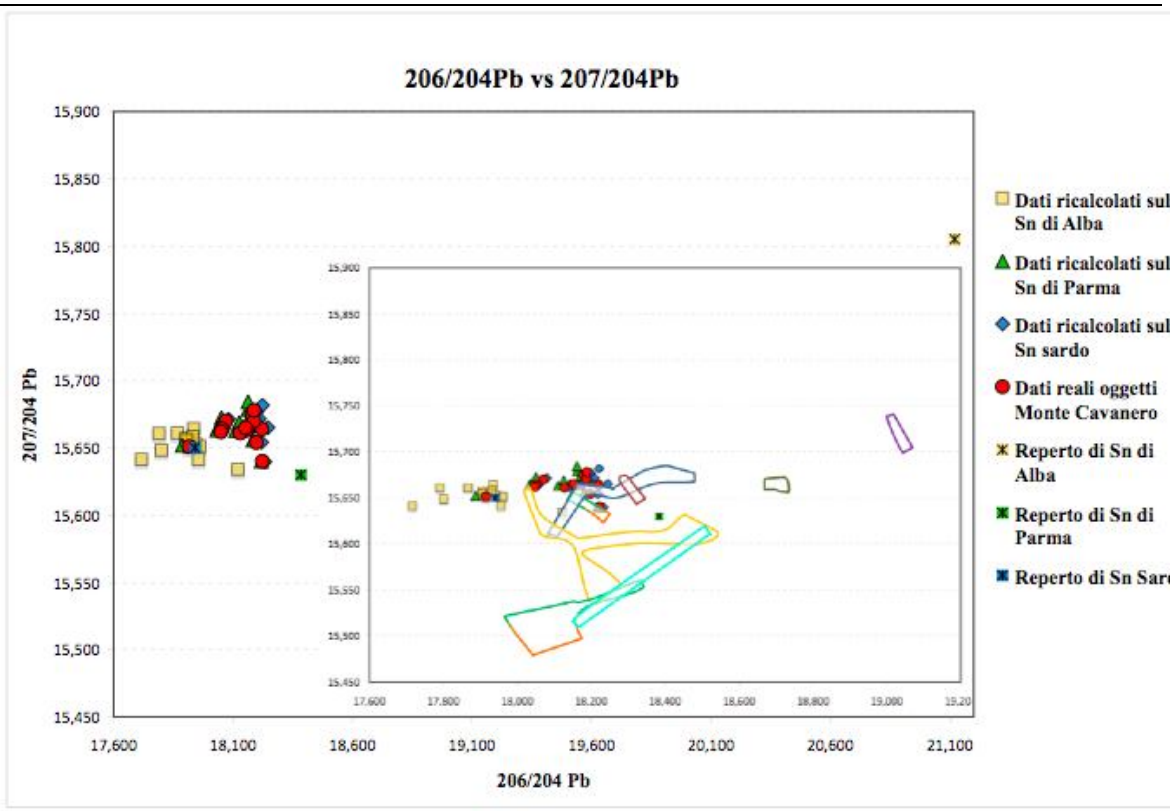

Fig. 7. Diagramma dei rapporti isotopici $^{207}Pb/^{204}Pb$ vs $^{206}Pb/^{204}Pb$ per alcuni campioni di riferimento di stagno dell'Età del Bronzo, confrontati con gli oggetti analizzati (Tab. 3).

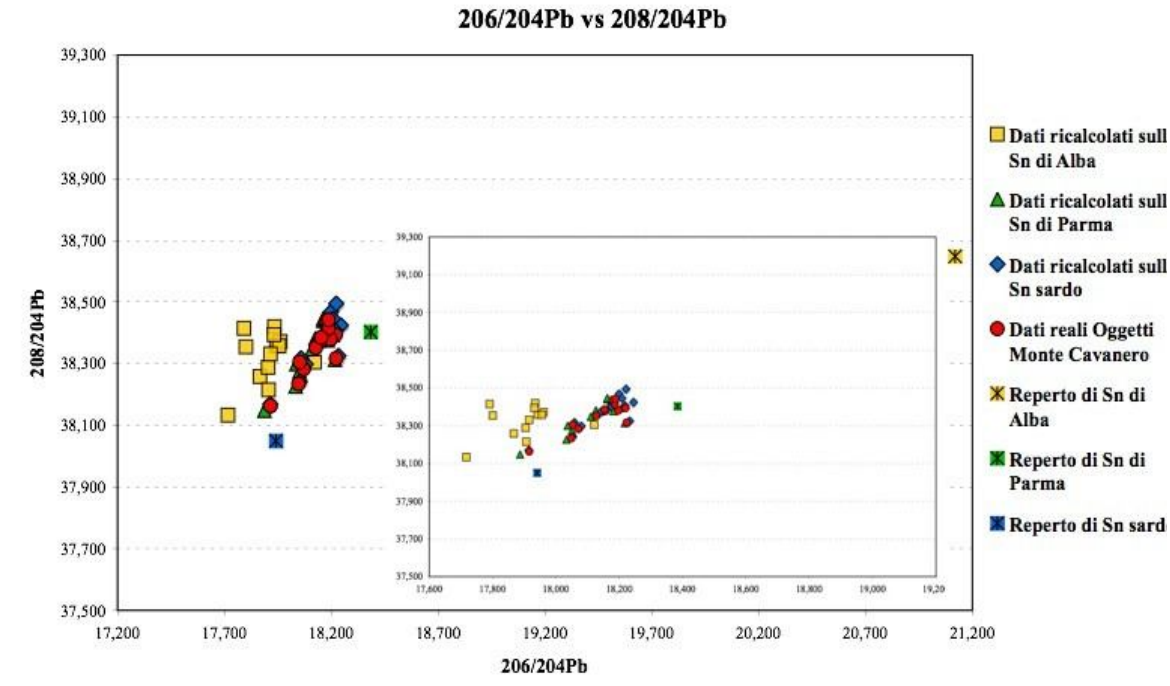

Fig. 8. Diagramma dei rapporti isotopici $^{208}Pb/^{204}Pb$ vs $^{206}Pb/^{204}Pb$ per alcuni campioni di riferimento di stagno dell'Età del Bronzo, confrontati con gli oggetti analizzati (Tab. 3).

Caratterizzazione del rame dell'oggetto CP-162

Fra gli oggetti del ritrovamento di Monte Cavanero ha richiamato la nostra attenzione il grumo di metallo (inventario CP-162), sia perché si tratta di uno dei pochi oggetti non lavorati, sia per la particolare composizione chimica (ANGELINI *et al.* pp.00-00), che mostra il rame alligato con altissimi tenori di Ni (16.33 wt%), Co (7.65 wt%), As (5.75 wt%), e Sb (3.05 wt%). Il frammento è formato da rame di prima estrazione e non totalmente desolforato (tenori in S = 3.04 wt%) e scorificato (Fe = 4.38 wt%). La presenza di Fe e S così elevati esclude anche qualsiasi processo di raffinazione successiva. Si tratta quindi di rame grezzo, la cui composizione assolutamente anomala riflette una carica ricca di minerali misti, ovvero di polisolfuri contenenti As, Sb (probabilmente della serie tetraedrite-tennantite), Co (probabilmente skutterudite o minerali analoghi) e, soprattutto, un elevato tenore di Ni.
Ci si è quindi posti il problema della provenienza del frammento, in primo luogo perché è l'unico oggetto non lavorato, il quale porta quindi un segnale primario della mineralizzazione, ed inoltre per la sua natura curiosa, che denota una carica iniziale in cui la calcopirite è un minerale minoritario.
La ricerca delle eventuali mineralizzazioni utilizzate, cioè di associazioni di tetraedrite, tennantite, skutterudite, calcopirite, ha ovviamente preso in considerazione in primo luogo due aree: l'area mineraria del Brianzonese ligure e l'area mineraria di Cabrières, in Francia. L'area del Brianzonese ligure tra la Val Bormida e la Val Tanaro, comprendente numerose mineralizzazioni di tetraedrite, è compatibile dal punto di vista degli isotopi del Pb, come ampiamente discusso in precedenza, ma in nessun affioramento mostra mineralizzazioni ricche in nichel. Si può quindi escludere con sicurezza una provenienza del minerale da quest'area.L'area mineraria di Cabrières (Hérault, France) comprende una ampia zona mineraria sfruttata fin dall'Eneolitico (AMBERT 1995, MILLE – BOURGARIT 1998, BOURGARIT – MILLE 2005). Le mineralizzazioni a tetraedrite della zona di Cabrières sono le più tardive del ciclo post-Ercinico nella parte meridionale del Massiccio Centrale ed accompagnano invariabilmente mineralizzazioni di barite (HOFFMANN 1969). I rapporti isotopici delle mineralizzazioni (PRANGE – AMBERT 2005) sono in generale compatibili con quelli misurati per il frammento (tab 3), anche se il trattamento delle associazioni di "rame grigio" ad alto tenore di tetraedrite porta ad una composizione del rame estratto molto ricca in antimonio ed argento, e povera di nichel e cobalto (PRANGE – AMBERT 2005). Possiamo quindi sicuramente escludere per il frammento CP-162 anche una provenienza dal sud della Francia.Potendo escludere un'origine alloctona, ed assumendo sulla base delle precedenti considerazioni che la grande maggioranza del rame negli oggetti di Monte Cavanero ha un'origine locale, la nostra attenzione si è quindi focalizzata su alcune mineralizzazioni poco note delle Alpi Occidentali. Si tratta di piccoli affioramenti presenti tra il giacimento cuprifero di Chialamberto e la Val di Susa, presso le località di Cruvino e Bessanetto. Si tratta di modeste mineralizzazioni ricche in Ni-Co-As-Sb coltivate a più riprese dal XVIII sec. per produrre smalto (azzurro di cobalto) e poi definitivamente abbandonate. Note oggi ai collezionisti di minerali per la presenza di specie mineralogiche insolite (safflorite, rammelsbergite, etc.), sono state oggetto di studio nel secolo scorso per valutarne la potenzialità estrattiva (FENOGLIO – FORNASERI 1940). Si tratta a nostra conoscenza delle uniche mineralizzazioni delle Alpi Occidentali che contengono skutterudite con alti tenori di Ni, associata a tetraedrite e poca calcopirite. Sono stati analizzati due campioni di queste mineralizzazioni provenienti da Cruvino e Usseglio. I valori dei rapporti isotopici del Pb misurati su questi campioni sono in perfetto accordo con quelli misurati sul frammentino di Monte Cavanero, indicando quindi una alta probabilità che le mineralizzazioni di questa zona

possano essere state utilizzate per una piccola parte del rame del ripostiglio.Si nota come anche in questo caso i rapporti isotopici del Pb utilizzati come unici parametri discriminanti lascino notevoli ambiguità interpretative, mentre risultino utilissimi se combinati con approfondite analisi chimiche, mineralogiche, e giacimentologiche delle aree studiate.

Conclusioni

In base ai dati chimici, isotopici, mineralogici, e giacimentologici disponibili, è possibile affermare che:

(1) i rapporti isotopici del Pb permettono di indicare con alta probabilità che il rame utilizzato negli oggetti di bronzo di Monte Cavanero è derivato da solfuri primari (calcopirite in primo luogo) compatibili con quelli di miniere prossime al luogo del ritrovamento (Alpi Occidentali), ed in particolare riferibili alle numerose mineralizzazioni cuprifere appartenenti alle formazioni ofiolitiche mesozoiche della Falda Piemontese, e in particolare quelle ricadenti nel settore a metamorfismo eclogitico.

(2) Si possono senz'altro escludere su base isotopica le miniere ofiolitiche di tipo Appenninico (Libiola) e le miniere bornitiche del Queyras (Saint Veran). Si possono escludere su base geochimica le miniere tetraedritiche del Brianzonese ligure (Val Bormida, Val Corsaglia).

(3) Il campione di metallo grezzo (CP-162) ha una composizione molto particolare, estremamente arricchita in Ni-Co-As (con minori Sb-Fe-S) che denota un'origine da polisolfuri complessi in cui la calcopirite è solo una fase minoritaria. Si propone che il minerale per l'estrazione di questo rame provenga dalle mineralizzazioni dell'area a nord della Val di Susa, che sono le uniche note nelle Alpi Occidentali con skutterudite ad alto tenore di Ni, e sono inoltre perfettamente compatibili con i dati misurati dei rapporti isotopici del Pb.

Il quadro dell'estrazione ed utilizzo del rame nell'ultimo scorcio dell'Età del Bronzo che risulta dalle approfondite analisi sugli oggetti di Monte Cavanero è estremamente interessante. I dati sembrano indicare non solo che la totalità del rame degli oggetti veniva estratto da mineralizzazioni locali, ma anche che pare essere frutto della coltivazione prevalente di una ben definita tipologia di giacimenti cupriferi, e cioè gli affioramenti a calcopirite-blenda associati con le metamorfiti ofiolitiche. In modo minoritario o sperimentale venivano sfruttati anche i giacimenti di rame grigio disponibili (tipo Cruvino), come ben dimostrato dal frammento CP-162.

Il quadro ipotizzato apre anche affascinanti problematiche. In primo luogo, se gli oggetti coprono un'arco temporale di alcuni secoli, come desunto dalle analisi tipologiche e stilistiche, l'elevata omogeneità composizionale ed isotopica osservata nei manufatti (rispetto alle mineralizzazioni disponibili) sembrerebbe indicare una inaspettata continuità temporale e localizzazione geografica delle coltivazioni e delle attività metallurgiche. In alternativa, l'alta affinità composizionale degli oggetti potrebbe essere il risultato di una stabile rete di riciclaggio locale, che riutilizza il metallo più volte, omogeneizzandone la composizione. Questo è compatibile con la presenza nel ripostiglio di numerosi oggetti frammentati di età diversa in procinto di essere riprocessati.

Un'altra interessante problematica riguarda i processi di estrazione metallurgica: se le nostre conclusioni sono corrette, il minerale locale utilizzato è principalmente calcopiritico, e la calcopirite richiede imprescindibilmente processi di scorificazione con produzione di scorie fayalitiche. Dove sono le scorie? Le scorie fayalitiche sono praticamente inalterabili e ben riconoscibili, ci dovrebbero quindi essere numerose evidenze di siti di estrazione, presumibilmente non lontani dalle mineralizzazioni, con associazione di forni, scorie, ad altre evidenze di pirotecnologia. A tutt'oggi non ci sono siti metallurgici noti in tutta l'area esaminata.

Infine, si rammenta in questa sede che la "chaine operatoire" della metallurgia del rame, che lega i siti di produzione, i siti di metallurgia estrattiva, ed i manufatti preistorici è ancora alquanto lacunosa. I due esempi più sorprendenti che interessano zone limitrofe a quella esaminata, seppure riferiti a periodi più antichi, sono le miniere bornitiche di Saint Véran, che offrono ampie evidenze di estrazione mineraria nel Bronzo Antico, e le miniere calcopiritiche di Libiola e Monte Loreto, che presentano evidenze di sfruttamento esteso del minerale dalla fine del Neolitico. A tutt'oggi non c'è nessun oggetto coevo che possa essere (sicuramente o tentativamente) riferito a queste mineralizzazioni. Nel caso delle miniere di Saint Veran, seppure in misura molto inferiore alle aspettative, almeno c'è la presenza sul sito di qualche di qualche tuyere e di circa 100 kg di scorie che testimoniano i processi di estrazione del metallo. Nel caso di Libiola e Monte Loreto non c'è neppure questo: non esiste nessuna evidenza di estrazione pirometallurgica, e non si ha ancora nessun indizio della diffusione ed utilizzo del rame in quel periodo.

Le informazioni risultanti dallo studio dei reperti di Monte Cavanero permettono di avere una puntuale ma nitida istantanea della lunga e difficile storia dello sfruttamento minerario delle Alpi. Se riusciremo a recuperare ed interpretare altre fotografie come questa, anche le nostre radici culturali ed il tortuoso rapporto con il territorio saranno più comprensibili.

Ringraziamenti

Si ringraziano le seguenti persone per aver fornito preziosi campioni di mineralizzazioni Piemontesi e Liguri: Gian Carlo Piccoli, Stefano Camarda. I campioni di Saint Veran sono stati studiati in collaborazione con: Pierre Rostan, David Bourgarit, Benoit Mille, Emilen Burger. I campioni di Cruvino e Usseglio provengono dalle Collezioni del Museo di Torino: si ringrazia Piergiorgio Rossetti per averli resi disponibili. Si ringrazia Michael Prange per averci inviato i dati isotopici di Cabrières. Gli oggetti di stagno sono stati analizzati grazie all'autorizzazione di Marica Venturino (Alba), Maria Adelia Bernabò-Brea (Parma), e Maria Ausilia Fadda (Nuoro).

Referenze

AMBERT P. 1995. ***Les mines préhistorique de Cabrières (Hérault): Quinze ans de recherches. État de la question,*** **in** ***Bulletin de la Societé préhistorique Française,*** **9/24, p. 499-508.**

ARTIOLI G., BAUMGARTEN B., MARELLI M., GIUSSANI B., RECCHIA S., NIMIS P., GIUNTI I., ANGELINI I., OMENETTO P. 2008. *Chemical and isotopic tracers in Alpine copper deposits: geochemical links between mines and metal*, in *Geo.Alp* **5**, 139-148.

BARGE H. 1997. Proc. of int. conf. *« Mines et Métallurgie de la préhistoire au Moyen-Âge en Languedoc-Roussillon et régions périphériques »*, Cabriéres 1997. Archéologie en Languedoc 21, pp 99-110.

BOURGARIT D., MILLE B. 2005. *Nouvelles données sur l'atelier métallurgique de la Capitelle du Broum (district minier de Cabrières, Hérault, France) : la transformation de minerais de cuivre à base de sulfures se précise !* In : P.Ambert and J. Vacquer (eds.) *La première métallurgie en France et dans les pays limitrophes* (Carcassonne, 2002), p. 97-108.

BOURGARIT D., ROSTAN P., BURGER E., CAROZZA L., MILLE B., ARTIOLI G. 2008. *The beginning of copper mass production in the Western Alps: the Saint Véran mining area reconsidered. Historical metallurgy*, 42, 1-11.

CAMPANA N., MAGGI R., PEARCE M. 1998. In: C. D'amico, C. Albore Livadie (eds.) *Le Scienze della Terra e l'Archeometria*. Istituto Universitario Suor Orsola Benincasa, Napoli. p.175.

CASTALDO G., STAMPANONI G. 1975. *Memoria illustrativa della carta mineraria d'Italia*. Volume XIV. Servizio Geologico d'Italia. Roma

COLPANI F., MARELLI M., GIUSSANI B., RECCHIA S., ANGELINI I., BAUMGARTEN B., ARTIOLI G. 2007. *Copper isotopic ratio and trace elements spectrometric measurements (ICP-QMS) within Alps and Apennine Cu-ores: Discovering regional geochemical tracers for archaeometrical purposes by advanced chemiometric techniques*, in: D'Amico C. (ed.), *Atti IV Congresso Nazionale di Archeometria. Pisa, 1-3 febbraio 2006*, Pàtron Editore, Bologna, pp 547-559, 2007.

CUMMINGS G.L., RICHARDS J.R. 1975. *Ore lead isotope ratios in a continuously changing Earth*. Earth Plan. Sci. Lett. 28, 155-171.

DEL LUCCHESE A. 2004. Il *Bronzo Finale e l'inizio dell'età del Ferro in Liguria (XII-VIII secolo a.C.)*. In: *I Liguri. Un antico popolo europeo tra Alpi e Mediterraneo*, Catalogo della mostra, a cura di R.C. de Marinis - G. Spadea, Ginevra-Milano. pp. 143-144

DEL LUCCHESE A., DELFINO D. 2008. *Metallurgia preistorica in Val Bormida*, in *Archeologia in Liguria*, I, 2004-2005, pp. 35-55.

FADDA M.A. 2006. *Il Museo Archeologico Nazionale di Nuoro*, in *Sardegna Archeologica* Vol 17., Carlo Delfino Editore. Sassari. Pp. 46-53.

FENOGLIO M., FORNASERI M. 1940. *Periodico di Mineralogia*, Anno XI, n. 1, Gennaio 1940-XVIII.

GALE N.H., STOS-GALE Z. 2000. *Lead isotope analyses applied to provenance studies*, in: E. Ciliberto, G. Spoto (eds.) *Modern analytical methods in art and archaeology*. Wiley-Interscience, New York. Pp. 503-584.

GIUSSANI B., MARELLI M., RECCHIA S., COLPANI F., ANGELINI I., ARTIOLI G. 2007. *Tracing the provenance of ancient copper objects: a multivariate data analysis approach*. Proc. 2nd International Conference *"Archaeometallurgy in Europe 2007", Aquileia, 17-21 giugno 2007.*

HOFFMANN T. 1969. *Barite deposits of the "Montagne Noire", Southern France*, in *Mineralium Deposita* 4., p. 260-274.

KÖPPEL V. 1983. *Summary of lead isotope data from ore deposits of the Eastern and Southern Alps: Some metallogenetic and geotectonic implications*, in: Schneider H.J. (ed.) *Mineral deposits of the Alps and of the Alpine Epoch in Europe*. Springer-Verlag, Berlin, 162-168.

KÖPPEL V., SCHROLL E. 1983. *Lead isotopes of Palaeozoic, strata-bound to stratiform galena bearing sulfide deposits of the Eastern Alps (Austria); implications for their geotectonic setting.* Schweiz. Mineral. Petrogr. Mitt., 63, 347-360.

IXER R.A. 1999. *The role of ore geology and ores in the archaeological provenancing of metals,* in: S.M.M. Young, A.M. Pollard, P. Budd, R.A. Ixer (eds.) *Metals in Antiquity*. BAR International Series n. 792. Archaeopress, Oxford, UK. Pp. 43-52.

MAGGI R., PEARCE M. 1998. *Les mines prehistoriques de Libiola et Monte Loreto (nouvelles fouilles),* In: M.-Ch. Frère-Sautot (ed.) *Paléométallurgie des cuivres.* Monique Mergoil, Montagnac p. 89.

MILLE B., BOURGARIT D. 1998. *Du mineral de cuivre exploité dès le Chalcolithique : les examples de Cabrières (Hérault) et Al Claus (Tarn et Garonne),* in : M.C. Frère-Sautot (ed.), *Paléométallurgie des cuivres (Montagnac),* p. 27-36.

PERNICKA E. 1999. *Trace element fingerprinting of ancient copper: A guide to technology or provenance?,* in: S.M.M. Young, A.M. Pollard, P. Budd, R.A. Ixer (eds.) *Metals in Antiquity*. BAR International Series n. 792. Archaeopress, Oxford, UK. Pp. 163-171.

PERNICKA E. 2004. *Archaeometallurgy: Examples of the application of scientific methods to the provenance of archeological metal objects,* in: M. Martini, M. Milazzo, M. Piacentini (eds) *Physics methods in archaeometry*. SIF, Bologna and IOS Press, Oxford. Pp. 309-329.

PICCOLI G.C. 2002. *Minerali delle Alpi Marittime e Cozie Provincia di Cuneo*. Associazione Amici del Museo "F. Eusebio" Alba, Ed., Alba (Cuneo) 366 pp.

PICCOLI G.C., MALETTO G., BOSIO P., LOMBARDO B. 2007 *Minerali del Piemonte e della Valle d'Aosta*. Associazione Amici del Museo "F. Eusebio" Alba, Ed., Alba (Cuneo) 607 pp.

PRANGE M., AMBERT P. 2005. *Caractérisation géochimique et isotopique des minerais et des métaux base cuivre de Cabrières (Hérault),* in : P.Ambert and J. Vacquer (eds.) *La première métallurgie en France et dans les pays limitrophes* (Carcassonne, 2002), p. 71-81.

ROSSI M., ROSTAN P., GATTIGLIA A. 1997. *Una miniera di rame preistorica nelle Alpi Occidentali,* in *Le Scienze*, 344, 74-80.

ROSTAN P., GATTIGLIA A., ROSSI M. 1994. *Proc. XXXVI Riunione scientifica IIPP, Istituto Italiano di Preistoria e Protoistoria,* Courmayeur, 1994, p. 499-512.

SCAIFE B., BUDD P., MCDONNELL J.G., POLLARD A.M. 1999. *Lead isotope analysis, oxhide ingots and the presentation of scientific data in archaeology,* In: S.M.M. Young, A.M. Pollard, P. Budd, R.A. Ixer (eds.) *Metals in Antiquity*. BAR International Series n. 792. Archaeopress, Oxford, UK. Pp. 122-133.

STACEY J.S., KRAMERS J.D. 1975. *Approximation of terrestrial lead isotope evolution by a two stage model,* in *Earth Plan. Sci. Lett.* 26, 207-221.

VENTURINO GAMBARI M., BARTARELLI L., GIARETTI M., ZAMAGNI B. 1995. *La cultura materiale: L'età del Bronzo,* in: M. Venturino Gambari (ed.) *Navigatori e contadini. Alba e la valle del Tanaro nella preistoria.* Quaderni della Soprintendenza Archeologica del Piemonte. Monografie 4. Famija Albèisa, Alba. Pp. 141-218.

1.2 San Pietro in Tuba and Col del Buson (BL) sites

The project is the result of an agreement between the ARCA Agordo group and the Research Group of Prof. Gilberto Artioli. It was originally planned in three phases:
• A sampling of the mineral phase
• Mineralogical and chemical study of minerals
• Chemical and isotopic study of metal fragments, and semi-finished items
According to the Superintendence of Veneto, were sampled 12 specimens of various types: 6 objects from San Pietro in Tuba (BL) (3 pieces of ingot, two pieces of metal of irregular shape, maybe ingots, a drop of metal) and 6 objects from Col Buson (BL), a proposal dating Eneolithic (a fragment of undefined type axe, an axe-eyed, an axe raised margins, a half pearl ribbon, a tassel and an awl). The micro-samplings were carried out in different parts of objects where there were already signs of cracks or details, so as to minimize the aesthetic damage.

Fig. 1.1 Samples from Col del Buson (CBU-SP and CBU-AX-MR)

On the 11 samples of San Pietro in Tuba and Col of Buson have completed the analysis of isotopes of Pb. Isotope analyses of copper and other chemical tracers commonly used (Artioli et al. 2008) are underway, as can be seen only after the completion of the analysis of geological samples. You are here briefly the preliminary results of the comparison and the statistical analysis carried out in full between the data of the 11 items and copper-bearing mineralizations. Please note that these data are qualitatively and quantitatively in number much higher than those laid down in the original project, which included the simple comparison between objects and deposits of Valsugana area.
Data of Valle imperina deposit (see part II), that is genetically correlated to Calceranica and Vetrioli deposits (High Valsugana), are distinct from all other of the neighbouring mines, including those of Valle del Mis (Pattine), Valbona, Valley of Mocheni (Grua/Tingerhof), and the limited copper deposits along the eastern side by the Adige valley(Calisio, Lavis, Mondagiò). Discrimination among the mining zones has been at the time made with principal component analysis and using all the Pb isotopic ratios measured (fig. 1.3).

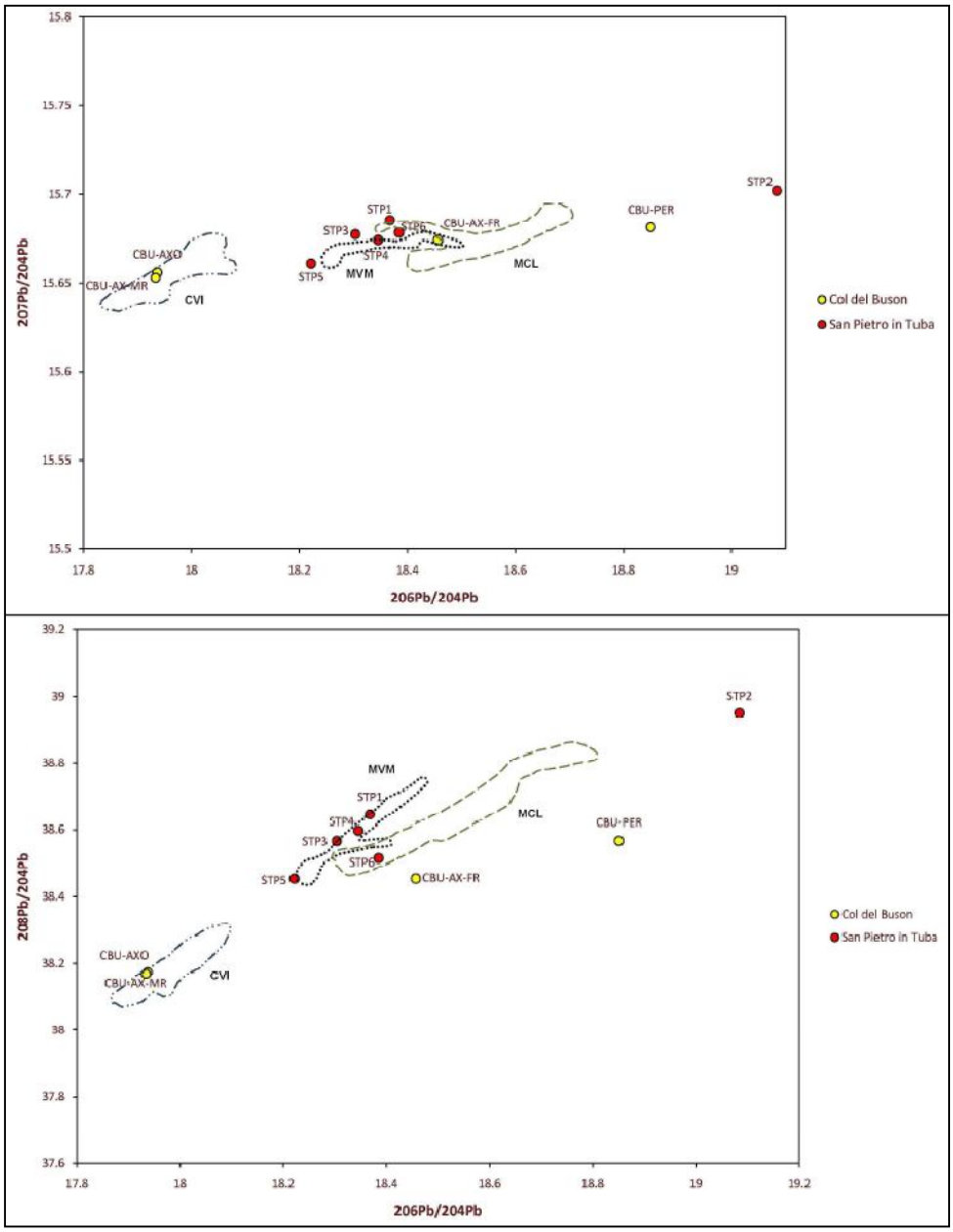

Fig. 1.2 Pb isotopes of archaeological samples of Col del Buson and San Pietro in Tuba. Fields are relating to Central-Eastern Southern Alps and high Valsugana.

Projecting the isotopic data of objects within this model (fig. 1.3), you can clearly see that on the basis of Pb isotopes of only two objects are compatible with the mines of Valle Imperina, Calceranica and Vetriolo, namely the axe-eye (CBU-AXO) and raised margins (CBU-AXMR). All other objects show a substantial isotopic incompatibility with these deposits.

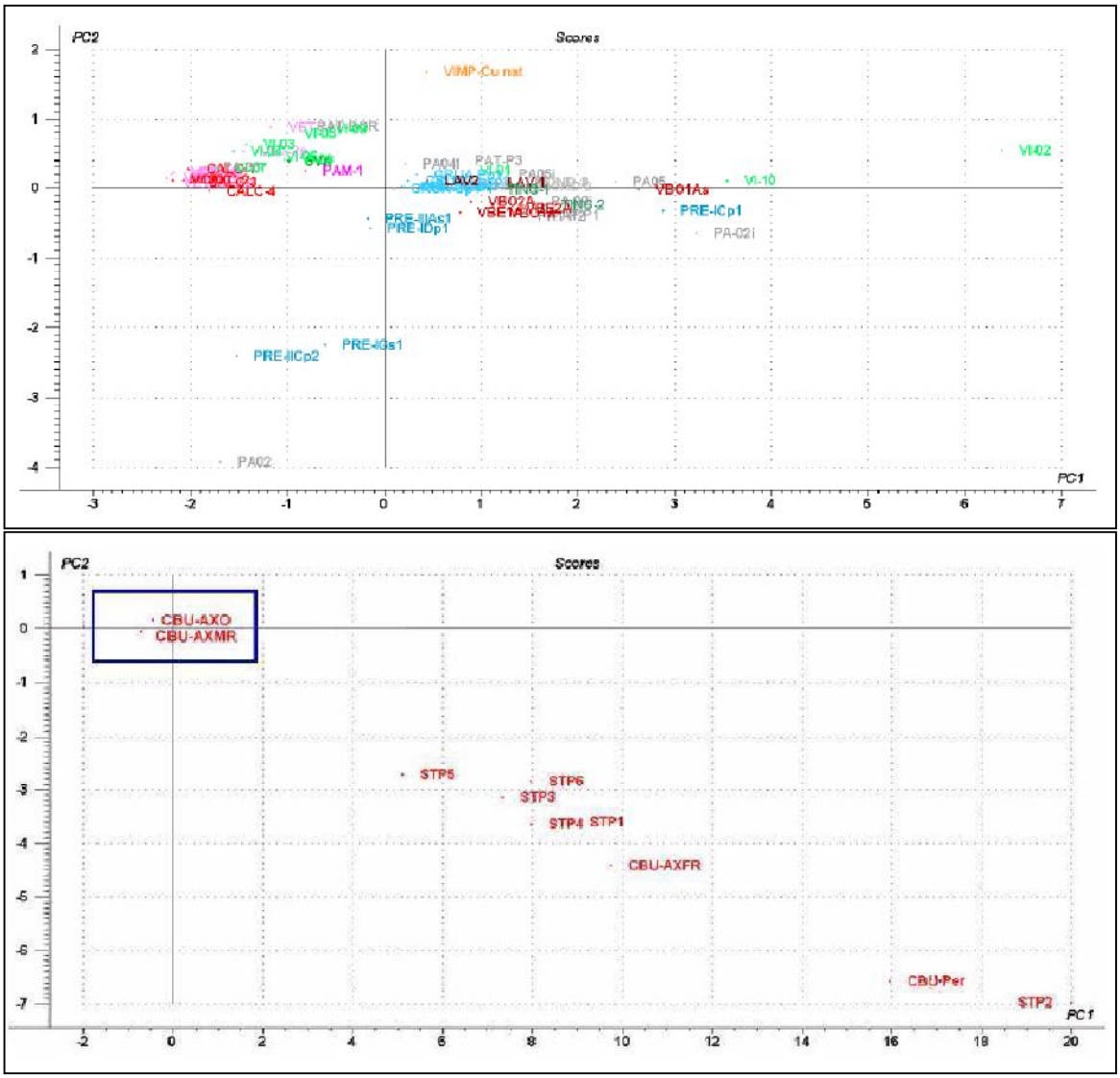

Fig. 1.3 Principal Component Analysis and projection of samples into the model.

Chemically and isotopically objects seem to refer to mineral springs very different. Two axes (CBU, CBU-AXO-AXMR) are compatible with the isotopicamente group mineralizzazioni Trentino and Veneto considered and modeled (Valle Imperina, Calceranica, Vetriolo), even if their obvious derivation from mineral non-sulphides raises some doubt on that interpretation, since they are not mineralizzazioni secondary for now notes consisting of exploited in antiquity.

Other objects on the Col of Buson is certainly incompatible with the three deposits modeled, including that of Valle Imperina. The fragment of axe (CBU-AXFR) can be compatible with some other isotopicamente mineralizzazioni zone (Valbona, Valle del Mis, Valley of Mocheni) even if minor elements would seem to exclude the local origin of the copper (Frizzo 2004), or at least indicate derivation from metal mixing of different origins.

STP2 ingot has a isotopic signature completely alien to the entire area Veneto-Trentino-Alto Adige. Other shards of raw copper have a marking of Pb isotopes of compatible with some deposits in the area (Valbona, Valle del Mis, Valley of Mocheni), even if the minor

suite of elements present in the derived from inclusions and plausibly polymetallic sulfides, deposits seems to differ significantly from these mines list (Frizzo 2004).

1.3 Statistical models

Information on different aspects of ancient life, mining and metallurgic processes of the early Bronze Age can be gained from the accurate study the ancient copper objects. In this context one of the basic questions that archaeologists pose to analytical archaeometry is to unambiguously establish the provenance of the found copper artifacts. To give an adequate answer to this question it is necessary to find a link between objects and the minerals that we suppose were used by ancient metalworkers to produce the object. However, even if we assume that we are able to find such a link, we have firstly to answer to a more challenging question: is it possible to discriminate between each other copper minerals that come from different ores on the basis of their elemental composition? In other words, does every mine posses its own elemental fingerprint and is it sufficiently distinguishable from others? For sure, the key to the provenance matter is concealed in these issues. It must be noticed that the elemental fingerprinting is not the only way to treat the provenance problem: as an example lead isotopes analyzed in minerals and ancient objects proved to be adequate, even if some debates are already ongoing on their general utilization. The utilization of the elemental composition is surely less explored even if very good work can be found in the literature.
The 63Cu/65Cu isotopic ratio was never considered a good tracer since it is well known variations of its value inside every single ore should be expected. However looking carefully to the existing literature data, it can be seen that variations of this ratio between different ore is slightly higher than the in-ore variations. Copper isotopic ratio is also informative because it is in relation with the
minerogenetic processes. Moreover, once the provenance has been assessed, the 63Cu/65Cu ratio could give information concerning the type of mineral used for the object creation (primary, secondary, native) and thus on the adopted smelting process.
We therefore decided to explore the possibility to use the 63Cu/65Cu ratio coupled with the elemental composition to face ore discrimination and hence the provenance problem. It is noteworthy that elements which have never been considered as informative in the past for these issues were also measured here, both in the sampled minerals and in the ancient copper objects for the first time. A carefully selected starting group of Cu-ores (Valle dei Mocheni, Val Venosta, Valle Aurina, Chiusa, Agordo in the Eastern Alps; Queyras in the French Western Alps; Libiola, Monte Loreto, in the Northern Apennine) were sampled in this first stage of the project. Some ancient copper fragments of known provenance (Agordo area) were also available. Before starting with the elemental analysis of specimens and with the consequent data analysis, a preliminary consideration was done. In fact, while for a complete elemental analysis is necessary to have a comprehensive description of a given ore, it is well known that only a subgroup of elements follows the copper phase during the smelting process. Some elements could be found instead almost only in the gangue phase and therefore in slags, after the smelting process. An idea of the behavior of elements could be obtained by the Goldschmidt classification, which groups elements according to their preferred host phases.
As the final goal of this work is to link copper object to their starting ores, we decided then to treat all mineral specimens eliminating the gangue phase by the copper minerals.

From a data analysis point of view, we decided instead to consider all the available information and therefore to use all elements and the isotopic ratio to built the model in an unsupervised way. As we will show, an iterative multi step multivariate data analysis approach which allows considering simultaneously all the information given by the elemental and isotopic data was developed and successfully employed in the copper ore discrimination. This protocol, which is mainly based on Principal Component Analysis, is able to discriminate minerals coming from the different investigated ores starting form 42 variables and the copper isotopic ratio values. This multi step strategy was developed because it was not possible to discriminate all the investigated ores within only one model. The variables selection of this multi step strategy represent the crucial point of the modeling: Partial Least Square-Discriminant Analysis (PLS-DA) was used together with the PCA to found the most relevant discriminant variables. Finally, the optimized protocol here presented was successfully tested on ancient Cu-fragments of known provenance.

The exploratory PCA analysis is an unsupervised method that allows the samples study without imposing any prior knowledge on the model. The original variables are transformed into new orthogonal variables called Principal Components (PC). They are ordered for their explained variance value from the more informative to the less: the last PCs contain only the model noise. Scores and loadings plots are the main results of a PCA calculation. The score plot contains information about samples groups, tendencies and outliers. The loading plot provides information about the relevance of the variables in the PCs construction and about the variables interrelationships. Correlation loadings are also computed for each variable in the chosen PCs space. The correlation loadings plot marks the 50% and 100% explained variance limits for each PC. The outer limit indicates 100% explained variance. The inner limit indicates 50% of explained variance. These limits appear as two ellipses in the bidimensional loading plot. Variables lay between the two ellipses are the more important in the investigate PCs space.

A variable selection was carried out with the aim to detect the variables that mainly distinguish one ore from all the other ones, thus the variables responsible of the elemental fingerprint of each of the investigated ores. This was achieved using a Partial Least Squares – Discriminant Analysis (PLS-DA) strategy. This technique arose as a classification method that models the differences between two classes.

The PLS method calculate a linear regression model between the predictors matrix (X) and the response vector (Y): in this particular case the Y vector is expressed with the binary code. If a sample belongs to the modeled class his code is one, otherwise the value is set to zero. The model provides score and loading plot as well as the regression coefficient for each variable. An estimate of the statistical significance of these regression coefficients is also provided. In this study this technique was employed for the variables selection. Correlation loadings were interpreted: as in the case of PCA, they indicate important variables in the chosen model. Concerning the model coefficient evaluation, higher absolute values indicate important variables for the discrimination of the selected ore from all the others. The statistical relevance of the variables was tested through the Marten's Uncertainty test. This method is based on the Jack-knifing principle working with the cross validation approach. The study of the correlation loadings and the model coefficients led to the definition of a variable subset able to discriminate the samples coming from the different ores.

Two validation procedures were employed in both PCA and PLS-DA models, according to the available number of objects for the model: the test set and the cross-validation. The test set validation method was privileged. This validation method is based on the use of different data sets for calibration (training set) and validation (test set), the former for the

model dimensionality optimization, the latter for the assessment of the particular future prediction strength. From the total matrix a representative set of objects is therefore extracted: it is not used in the model calibration (the phase in which the model is fitted to the available data) but only in the validation step (test set). The external test set samples selection can be done in several ways, among them: a random selection and a manual selection. Ideally it should be approximately as large as the training set, but at the minimum at least 25% of the size of training set if and when samples are in short supply. In case of a limited number of objects, the cross-validation method was used. In this method one (full cross validation) or more samples are kept out of the calibration and used for prediction. This is repeated until all samples have kept out once. Validation residual variance can then be computed from the prediction residuals.

The samples projection method allows to project onto an existing PCA model new samples (not used for the construction of the PCA model). In this way it is possible to visualize the position of these new samples in the scores plot of the already built principal components. In other words this procedure allows comparing their position with the position assumed by the samples used to build the model. Thus the projection of a new sample onto the PCA model is a kind of “prediction” of that sample according to the PCA model. In this work this method was used for the validation of the multiple step exclusion strategy and also to test the protocol on the ancient Cu-objects of known provenance

The first variable study through the box plots and the frequency histogram plots highlighted an asymmetric distribution for the majority of the variables. The logarithmic transformation was then applied. Different measurement unit and number with different magnitude order were also present in the raw data. In order to give all variables the same chance to influence the estimation components the autoscaling was also applied.. A first PCA model was built on the whole data set. The score plot (Fig.1.4.) did not allow differentiating the investigated ores. Instead, the difference between the primary and the secondary minerals emerged as the main information accounted by PC1 and PC2.

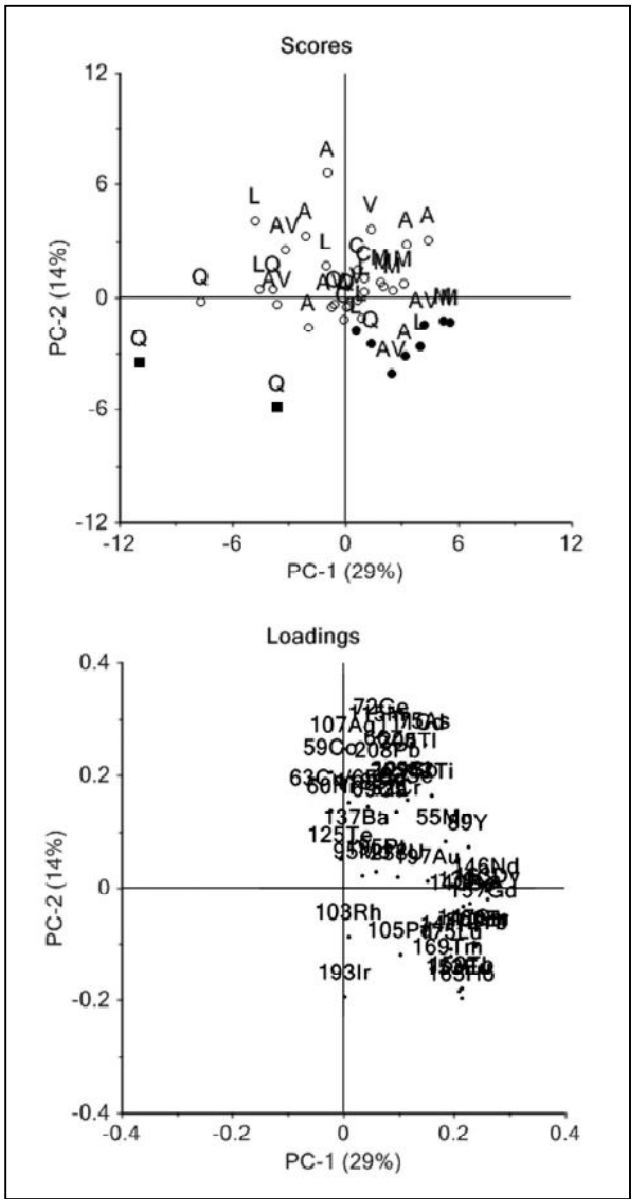

Fig. 1.4. Scores and loadings plot (PC1 29%, PC2 12%) of the model built with all the samples and variables. Samples are labeled according to provenance: Q = Queyras; A = Agordo; L = Libiola - M.te Loreto; AV = Aurina Valley; M = Mocheni Valley; V = Venosta Valley; C = Chiusa. Symbols indicated the type of minerals: empty Circle = primary Cu-minerals; black circle = secondary Cu-minerals; square = native copper samples.

Anyway the study of the following PCs evidenced that samples belonging to a given Cu-ore lies in the same area of the multidimensional space (e.g. PC2 vs. PC3) even if the groups were strongly overlapped. These evidences throw light on route to follow in order to build a separation model between this ore and all the other ones. It was in fact clear from the beginning that a single model is not sufficient and that a multiple step exclusion strategy was necessary. This strategy, which is sketched in Fig.1.5, can be summarized as follows: 1) the whole data set is taken into account and a PCA model was built. Through the study of the score plots generated by the combination of the first principal components (often PC1 to PC4) the better grouped ore is chosen for the exclusion process; 2) the next step concern a variable selection in order to emphasize the differences between the selected ore and all the other ores: the aim is to build a simple discriminant model using only PC1 or no more than two PCs; 3) the minerals belonging to the selected

ore are separated from the original matrix and the whole process is then repeated on this reduced matrix considering again all the variables (repeating also the row data study).

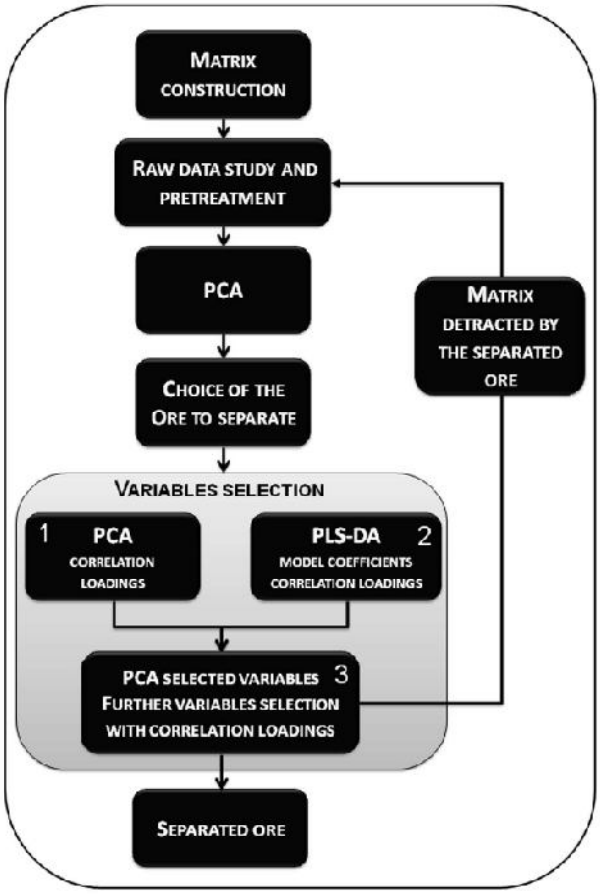

Fig. 1.5. Scheme of the multiple step exclusion strategy

In all the calculated models the main information, often highlighted by PC1 and PC2, was the difference between the primary and the secondary minerals. Thus, as in the very first model considering all the investigated ores (Fig.1.6), the interpretation of the following PCs was always necessary in each step. As it was outlined in the introduction the crucial point of this procedure is the setting up of a strategy to perform the variable selection. Two different approaches were used for this goal and for every single separation model. The first one was based on the PCA modeling and in particular on the correlation loadings plot study (box1). The PCs that gave the better separation of the chosen ore in the score plot (often the PCs following to the first two) were taken into account. Variables lyin between the two limits along the selected PCs in the correlation loading plot were then selected as important variables for the final discriminant model.
The second one was based on the PLS-DA regression modeling (box2). 337 In this case 1) the correlation loadings interpretation was done as in the previous case and 2) the model coefficients study was used for the variables selection. Variables with high coefficient values (absolute values) were important in the discrimination. Anyway, a variable was selected only if its coefficient was statistically significant as well. The next step (box3) was the calculation of a new PCA model with all the selected variables. In the presence of highly correlated variables the less precise one (with respect to ICP-QMS analysis) was kept out. The final model was then obtained with a minimum number of important variables.

As already mentioned, the last step was the elimination of the discriminated ore and the construction of a new data matrix with the remaining ores. This matrix was used as the input matrix for the procedure, indicated in Fig.1.6, which was repeated until all the ores were discriminated. The developed multiple step exclusion strategy is sketched in the discrimination scheme of Fig.1.6..

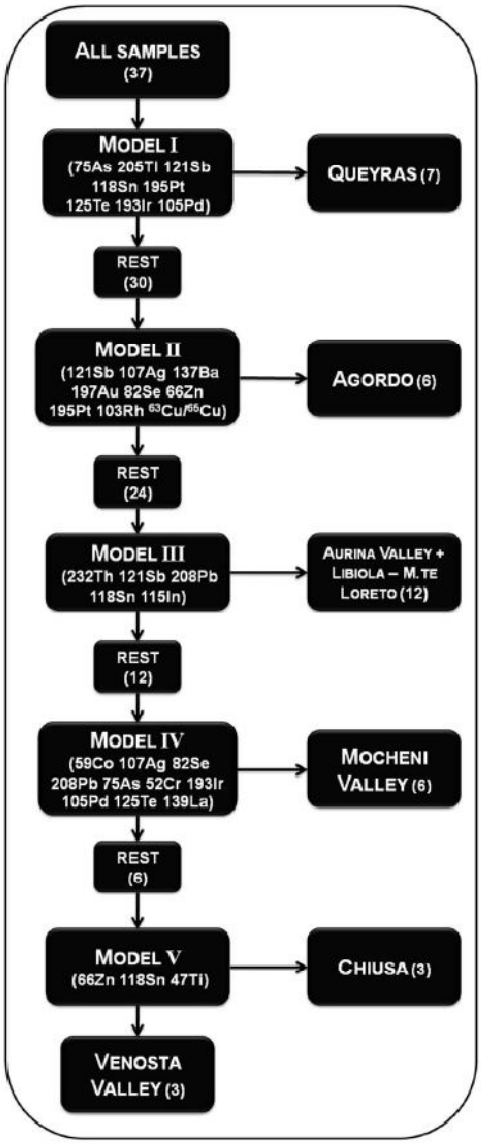

Fig. 1.6 Separation ores schema. Numbers between brackets are the number of samples for each group.

Useful information emerges from the loading plots study. From a geochemical point of view, it is possible to gain information concerning the variables that mainly characterize the investigated ores. Each of the discriminating models describes in fact the differences between a given ore from the other ones and thus highlights the responsible elements for this difference. The geochemical interpretation of the data will be discussed in a more appropriate context. It is worthwhile to note that the copper isotopic ratio is an important variable in one of the built PCA models. Moreover it is very interesting to note that the majority of the elements selected as important variables belong to the category chalcophile according to the Goldschmidt classification. They are: 66Zn, 75As, 82Se, 107Ag, 115In, 118Sn, 121Sb, 125Te, 205Tl and 208Pb. Three of them, 103Rh, 105Pd,

195Pt, are classified as siderophile while the remaining two elements, 137Ba, 232Th, are lithophile.
The protocol was then tested on Cu objects of known provenance. Seven Cu objects founded in Agordo area were available. They were projected in the first separation sequence model (Fig.1.7.), that discriminate the Queyras samples from all the others. They were correctly projected near the bigger group of the minerals samples, far from the Queyras ore samples as showed in Fig.1.7A. Then a projection into the second separation model was performed. In this case 6 of the Cu objects were correctly projected near the Agordo mineral samples while the last Cu object lies far from the group (Fig.1.7B).

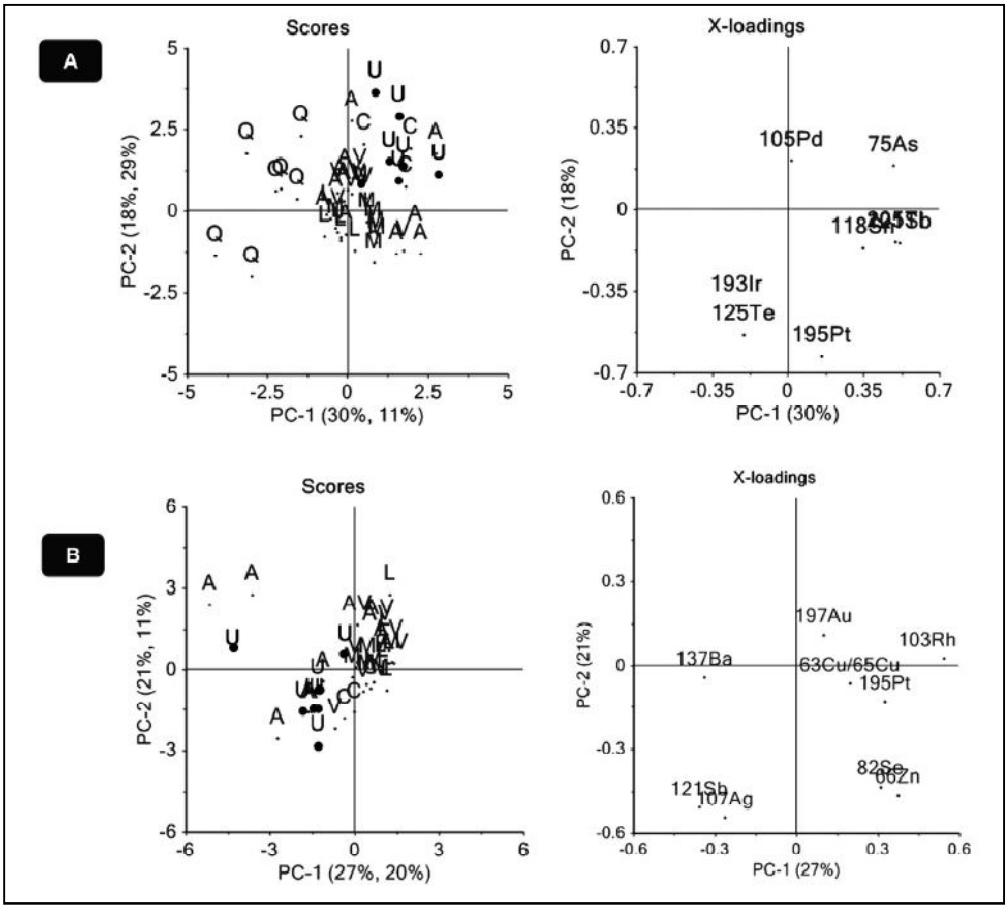

Fig. 3 Agordo Cu-objects (labelled as U) projection into the PCA ores separation sequence (Model I Fig.3A, and Model II Fig.3B).

1.4 Conclusions

A successful strategy to characterize copper ores and to trace the provenance of copper minerals and ancient copper objects was presented in this section. A whole analytical protocol starting from the sampling to the quantitative analysis was developed to ensure good quality analytical data. The measurements of a wide group of elements including the

Rare-Earth Elements (REE) together with the copper isotopic ratio in Cu minerals coming from selected historical ores gave as the first results a fully characterization of the investigated Cu-ores, representing the foundation to the development of a database as the fundamental reference frame for metal extraction and diffusion in the past. This is the first important goal of this project. The second purpose of this work was to use the information coming from the complete elemental and isotopic description of the investigated ore to trace the provenance of ancient copper artifacts. As shown in this work, it was not possible to discriminate all the investigated ores in a single model: the information related to the Cu-mineral type (primary or secondary) was always dominant. Different models were then built selecting the important variables to discriminate a given ore from all the others, leading to a multiple step exclusion protocol. From the results here reported emerges that copper isotopic ratio is an important parameter only in one of the developed models. Another interesting result is that almost all of the selected variables belong to the chalcophile category given by Goldschmidt, confirming the validity of the models also from the geochemical point of view. The complete discrimination of the investigated Cu-ores obtained with this strategy demonstrates that every ore has its specific fingerprint. Moreover this strategy shows the way that can be followed to highlight the most relevant features of each fingerprint. It is noticeably that the multiple step exclusion strategy was able to correctly determine the ancient copper fragments provenance, since they were correctly classified near the minerals sampled in the Agordo Cu-ore. These first results are really encouraging. The geochemical interpretation of the results of this work is now ongoing and lead isotopic ratios will be also determined, in order to improve the performance of this protocol. The coupling of elemental and isotope analysis and chemometrics in the copper minerals and ancient objects study is therefore a very promising way for shedding light on prehistorical metal trades enigmas.

Appendix1

Lead isotope systematics in hydrothermal sulphide deposits from the central-eastern Southalpine (Italy)

Lead isotope systematics in hydrothermal sulphide deposits from the central-eastern Southalpine (Italy)

Nimis P., Omenetto P., Giunti I., Artioli G., Villa I.

Abstract

The isotopic compositions of trace lead in copper-bearing hydrothermal sulphide deposits from the central-eastern Southalpine region were analysed using a Multi-Collector-ICP-MS. The data were combined with existing lead isotope data (ore lead) for hydrothermal polymetallic deposits in the same area and compared with the isotopic compositions of potential lead sources. Copper and polymetallic pre-Variscan (Late Ordovician–Early Silurian) stratiform, post-Variscan (Permian to Triassic) vein, and stratabound sediment-hosted (Permian to Early Triassic) deposits, are characterized by highly variable ratios of radiogenic to non-radiogenic lead, but show very similar, high, time-integrated μ (= $^{238}U/^{204}Pb$) and W (= $^{232}Th/^{204}Pb$) values. A progressive relative increase in radiogenic lead is observed from (i) pre-Variscan deposits to (ii) post-Variscan sulphide-rich veins in the Variscan metamorphic basement and in the lower–intermediate units of the Early Permian volcanic sequence to (iii) post-Variscan sulphide-rich and fluorite-rich veins in the upper units of the Early Permian volcanic sequence to (iv) post-Variscan fluorite-rich veins cutting the overlying Late Permian sediments and mid-Triassic mafic dikes. The dominant lead sources for all these deposits were Cambrian–Devonian (meta)sediments of the Variscan basement. Contributions from Permian and Triassic igneous rocks were of minor importance, if any, even for vein deposits which were evidently related to Permian magmatism. The isotopic compositions of some of the Permian vein deposits are consistent with, although they do not unequivocally prove, remobilization of metals from the pre-Variscan stratiform deposits. Permian sediments contributed a variable fraction of lead to stratabound deposits in Permian and Early Triassic sediments. Deposits in Triassic magmatic rocks are displaced to slightly lower μ and W values, suggesting lead contribution from Triassic magmatism.

The high μ and W values of the deposits studied here are consistent with regional isotopic patterns of Pb–Zn-rich deposits in more northerly and easterly sectors of the Eastern Alps (Austroalpine, eastern Southalpine) and of several circum-Mediterranean Pb–Zn and polymetallic deposits of Paleozoic to Triassic age (Sardinia; Betic Cordillera) or derived from remobilization of Paleozoic deposits (Tuscany). This isotopic uniformity suggests the existence of an isotopic province characterized by the dominance of old (Early Proterozoic to Archean) detrital source material, extending across a relatively wide portion of the former north-Gondwanan margin.

Introduction

The eastern Southern Alps are host to several copper and copper-bearing polymetallic deposits, covering a wide range of types (exhalative stratiform, vein, and sediment-hosted stratabound) and ages (Ordovician to Ladinian) (Brigo et al., 1975; Frizzo, 2004b). The size of these deposits is generally small (<3 Mt at <2% Cu; Frizzo, 2004b, and references

therein), but some of them have been exploited for several centuries and, in some cases, demonstrably since prehistory (Preuschen, 1973; Šebesta, 1992). The most productive area is located in the central-eastern portion of the Southern Alps, between the Periadriatic and Valsugana Lines, east of the Adige Valley (Fig. 1). In historical times, the deposits have been exploited for pyrite (for H_2SO_4 production) and/or Cu, Pb, Zn, Ag, W, barite and fluorite. All mining activities ended by the 1960s (Brigo et al., 1975).

Analysis of lead isotopes is one of the most widely used methods for discrimination of the sources of metals in mineral deposits. Lead isotopes have also become a popular tool in archaeometric studies for provenancing of metal objects and identification of ancient metal sources (see review in Gale & Stos-Gale, 2000). Köppel et al. (1993) reviewed all lead isotope data available at that time for the sulphide deposits of the Alps and their host-rocks and concluded that: (i) sediments forming the pre-Alpine metamorphic basement were the principal lead source for the Southalpine deposits, with mantle lead contributions being restricted to amphibolite-associated deposits from the westernmost sector (Ivrea zone); (ii) a lead isotopic province can be defined which includes the Southalpine and most Austroalpine units and is characterized by the dominance of old (Early Proterozoic to Archean) detrital source material; (iii) a second lead isotopic province, which includes the external massifs, the Penninic realm and some of the most north-westerly Austroalpine units (and extending northwards to central Europe; Koeppel, 1984), shows a dominant input from younger sources. Köppel et al. (1993) admitted that the data used in their study did not cover all major ore- and rock types and were regionally biased. Still today, available data for deposits from the eastern Southalpine region are mostly restricted to Devonian polymetallic stratabound and Permian to Triassic Pb–Zn-rich vein and stratabound deposits from its northernmost sector (Koeppel, 1984; Köppel & Schroll, 1985; Brigo et al., 2001). Extension of the Southalpine–Austroalpine isotopic province to its southernmost sector still lacks adequate analytical support.

In the course of a revisitation of copper metallogeny in the Alps, we have undertaken a lead isotope study of twelve deposits from the central-eastern Southalpine, including pre-Variscan stratiform, and post-Variscan to Triassic vein types. We have investigated deposits where copper was the dominant useful metal as well as a few Pb–Zn- or Fe-dominated deposits in which either copper minerals were a subordinate but significant component or copper-enriched portions could be identified. The results are used here in combination with existing literature data to provide an insight into the sources of metals and verify the consanguinity between individual deposits of the same type and age. The isotopic data presented here will provide a useful basis for provenance studies on ancient copper-bearing artifacts from the studied area and surrounding regions (cf. Artioli et al., 2008, 2009).

Geological outline

In the western Dolomites region (eastern Southalpine), a large pop-up related synclinorium is limited to the north by the dextral Periadriatic Lineament and to the south by the Neogenic south-vergent Valsugana overthrust system (Doglioni, 1987) (Fig. 1). The synclinorium allows exposure of the pre-Alpine (Variscan) metamorphic basement along its northernmost and southernmost limbs. This basement mainly consists of

phyllites and "porphyroid" gneisses, with subordinate metabasites, and represents a former Early-Mid Paleozoic sequence of sediments with volcanic intercalations. The sequence is formed of three complexes (Sassi & Zirpoli, 1990): a lower pelitic-psammitic complex with Late Cambrian acritarchs (Kalvacheva et al., 1986; Vecoli et al., 2008), an intermediate volcano-sedimentary complex with intercalations of basic and Late Ordovician acidic volcanic and volcanoclastic rocks ("porphyroids") (Meli & Klötzli, 2001), and an upper pelitic-psammitic complex of probable Early Silurian to possibly Devonian age (cf. Dieni et al., 2005). The three complexes underwent greenschist-facies metamorphism during the Variscan event. The metamorphic rocks are intruded by Permian, post-Variscan granitoids with high-K calc-alkaline affinity, which were emplaced in an extensional, post-orogenic tectonic regime (Rottura et al., 1998; Dal Piaz & Martin, 1998). In the less eroded central portion of the Dolomites region, the metamorphic basement is hidden under a thick Permian–Jurassic volcanic and sedimentary sequence. The base of this sequence consists of a pile of Early Permian rhyolites, dacites and andesites (Atesino Volcanic District[2]), which are consanguineous with the post-Variscan intrusives (Rottura et al., 1998) and reach a maximum thickness of over 2000 m in its central portion between Bolzano and Trento. The rest of the sequence mainly consists of carbonatic platform and terrigenous sediments, cut by and partly heteropic with Ladinian igneous rocks (Fig. 1). The Ladinian igneous rocks are represented by mafic to intermediate volcanic rocks with shoshonitic affinity erupted in a transcurrent tectonic regime (Bonadiman et al., 1994), and by associated intrusives with high-K calc-alkaline to sodic alkaline affinity (Predazzo–Monzoni plutonic complex; Lucchini et al., 1982; Visonà, 1997).

The metallogenic sequence of the region can be summarized as follows:

1. *Pre-metamorphic, hydrothermal-exhalative, stratiform deposits within the crystalline basement (Late Ordovician–Early Silurian).* These deposits are mostly distributed along a belt extending for about 100 km along the Valsugana Line, from the high Valsugana Valley south-east of Trento to the Agordo area north-east of Belluno (Agordo–Valsugana Zone; Frizzo & Ferrara, 1994) (cf. # 1–3 in Fig. 1). The deposits are localized within a metamorphosed volcano-sedimentary unit (phyllites, porphyroid gneisses, chloritoschists, metabasalts) corresponding to the "intermediate complex" of Sassi and Zirpoli (1990). The deposits are pyrite-dominated, with subordinate sphalerite, galena, chalcopyrite, arsenopyrite, tetrahedrite and traces of Au and Ag (Frizzo, 2004a). Similar deposits are also reported in the northern sector of the metamorphic basement within the Bressanone Phyllite (Brigo, 1971). Variscan greenschist facies metamorphism determined moderate to intense recrystallization and, sometimes, remobilization of metals, with formation of chalcopyrite-enriched veinlets within the brecciated massive sulphides.

2. *Deposits connected with post-Variscan magmatism (Early-Mid Permian).* They are mainly represented by copper and polymetallic (Pb, Zn, Cu, Ag ± Au) veins with quartz gangue and, possibly, by fluorite-rich, sulphide-bearing veins, which cut the lower and intermediate units of the Permian volcanic sequence (andesites to rhyodacites) and the underlying metamorphic sole (Cavinato, 1968; Fellerer, 1968; Brigo, 1971; Bakos et al.,

[2] Also reported in the literature as Atesina Volcanic District or Athesia Volcanic District.

1972; Omenetto & Brigo, 1974; Frizzo, 2004a) (cf. # 5–13 in Fig. 1). The sulphide-rich deposits are associated with significant propylitic and potassic alteration of the host-rocks. The dominant copper mineral is chalcopyrite. Also connected with the post-Variscan magmatism is a magnetite + pyrrhotite deposit (Pamera; cf. # 4 in Fig. 1) with minor Cu, Zn, Co, Bi, As, which is developed in the form of a breccia pipe at the margin of the Roncegno subvolcanic granodiorite intrusion, at the south-western end of the Cima d'Asta plutonic complex (Omenetto, 1968b). Only one sulphide-rich vein deposit (Montagiù; cf. # 8 in Fig. 1) is known from the upper, rhyolitic volcanic sequence; it is distinguished from the other sulphide-rich deposits by its peculiar galena + tetrahedrite + chalcopyrite paragenesis (Dessau & Duchi, 1970). The Permian age of this deposit is proven by stratigraphic relations with the overlying Upper Permian Val Gardena (Gröden) Sandstone (Maucher, 1955). All deposits are believed to be connected with the post-Variscan magmatism (Bakos et al., 1972).

3. *Stratabound polymetallic deposits in Permian–Early Triassic sediments.* These deposits include Pb–Zn–Cu–U–fluorite–barite mineralizations in terrigenous sediments intercalated with (Tregiovo Fm.) and overlying (Val Gardena Sandstone, Upper Permian) the upper, rhyolitic Permian volcanic units, and Pb-rich mineralizations in Early Triassic carbonatic sediments of the Werfen Formation (Dessau & Perna, 1966; Brusca et al., 1972; Brusca & Perna, 1995) (cf. # 16–23 in Fig. 1). The deposits in the sandstones are typical low-temperature, red bed-type, diagenetic mineral concentrations, related to shallow groundwater circulation (Wopfner et al., 1983). The ores consist of galena (sphalerite, pyrite) and covellite–chalcocite ± Cu-sulphosalts. The deposits in the carbonatic sediments have been economically the most important. Most of them are clustered in the south-western portion of the studied area, around Mt. Calisio north-east of Trento (Fig. 1), and are bound to a transgressive, oolitic–bioclastic horizon at the base of the Early Triassic Werfen Formation (Tesero Member, formerly assigned to the Upper Permian Bellerophon Fm.; cf. Brusca & Perna, 1995). They consist of impregnations, veinlets and irregular replacement bodies dominated by silver-rich galena, with subordinate barite, sphalerite, pyrite and chalcopyrite. The proposed genesis involves a sequence of synsedimentary, epigenetic-sedimentary, and metasomatic stages (Zanella & Brigo, 1997). One deposit characterized by localized enrichments in copper minerals (Maso Furli; cf. # 16 in Fig. 1)) has been studied here.

4. *Fluorite-rich vein deposits of Triassic age*. This group includes fluorite (barite, calcite, quartz)-dominated, sulphide-poor deposits, which are found in the upper, rhyolitic units of the Permian volcanic sequence (Bakos et al., 1972; Omenetto & Brigo, 1974) (cf. # 14–15 in Fig. 1). No hydrothermal alteration is observed in the host-rocks. A regional geochemical zoning is reported, with dominant fluorite in the core of the Atesino Volcanic District and barite enrichments towards its margins (Bakos et al., 1972). Based on several geological evidences (e.g. cross-cutting relations of some veins with upper Permian sediments and Ladinian mafic dykes; distinct thermal and geochemical zoning), the group is believed to be distinct from fluorite deposits in underlying basement and volcanic units and probably related to a hydrothermal–magmatic event of mid-Triassic age (Bakos et al., 1972).

5. *Deposits associated with Triassic magmatic rocks.* These deposits include both high- and low-temperature hydrothermal associations. High-temperature veins are characterized by tourmaline, scheelite and chalcopyrite as dominant minerals and are spatially associated with Triassic intrusives of the Predazzo–Monzoni igneous complex (Bianchi & di Colbertaldo, 1956). Based on scarce existing reports (Omenetto, 1968a; Cavinato, 1968) and own field observations, the low-temperature deposits are represented by several minor chalcopyrite ± bornite (galena)-bearing impregnations and mineralized breccias with calcitic cement in the Ladinian volcanic rocks, and by impregnations and replacement bodies in the underlying carbonates. For these low-temperature deposits, a genetic link with the Triassic magmatism is as yet unproven. One deposit representative of the low-*T* type (Valbona; cf. # 25 in Fig. 1) has been studied here.
6. *Deposits related to tectono-metamorphic mobilization.* These are represented by a few small siderite (barite) + tetrahedrite and pyrite + chalcopyrite occurrences located within the metamorphic basement in the Agordo area close to the Valsugana Line (cf. Pattine in Fig. 1). These deposits have been interpreted as the products of selective remobilization of pre-Variscan deposits during prolonged tectono-metamorphic activity along the Valsugana Line (Fellerer, 1968; Omenetto & Brigo, 1974).

Sample material and analytical techniques

The deposits studied in the present work are representative of the six metallogenic types described above. Their location is reported in Figure 1 and individual features for each deposit are reported in Table 1. Samples were taken from both underground works and mining dumps. For Pb–Zn dominated deposits (some post-Variscan veins and the Triassic stratabound deposit), whenever possible samples were taken from their copper-rich portions. The samples were characterized by optical microscopy under reflected light and X-ray powder diffraction. A portion of each sample was gently crushed and primary copper-bearing minerals (chalcopyrite, bornite, tetrahedrite or “cupriferous” pyrite) were separated by handpicking under a binocular microscope. For one deposit (Maso Furli, two samples) mixtures of primary (tetrahedrite, barite) and secondary (malachite, azurite) minerals were analyzed. For some poorly mineralized samples, sulphide concentrates were preliminarily obtained by gravimetric separation; copper-bearing minerals were then handpicked under a binocular microscope. During separation procedures, special care was taken to prevent sample contamination from external sources.

The sulphide separates were dissolved in aqua regia. The dissolved lead was separated from other metals using the Sr•Spec™ resin (EIChroM Industries; Horwitz et al., 1992), following the same procedure described in Villa (2009). About 100µL of Sr•Spec™ resin are filled in a 3-mm diameter hand-made PTFE column. The height to width ratio is approximately 4. The sample solution is loaded in 0.5 mL 1 M HNO_3, 1.5 mL of which is also used to wash out the matrix metals, while Pb is very strongly retained on the resin. Pb is then eluted with 3 mL 0.01 M HNO_3 and is ready for analysis. Lead isotope analyses were performed with a Multi-Collector-ICP-MS (Nu Plasma II). The sample solution was ionized by introducing it into a 9000 K plasma. All elements were ionized simultaneously. Mass fractionation was monitored by adding a small quantity of Tl,

which has a known $^{203}Tl/^{205}Tl$ ratio, is ionized together with and fractionated by the same mechanism as Pb, and does not interfere with Pb isotope measurements.

Results

The new isotopic data are reported in Table 2 and illustrated in Figures 2 to 6 together with previous data reported in Köppel and Schroll (1985) for galenas in deposits from the same area[3] (see Fig. 1 and Table 1 for locations and descriptions of these deposits). The deposits have variable contents of radiogenic lead and show higher $^{207}Pb/^{204}Pb$ and $^{208}Pb/^{204}Pb$ ratios than average young upper crust (Kramers & Tolstikhin, 1997) (Fig. 2). Although superseded by the more sophisticated "plumbotectonic" models, the two-stage model of Stacey and Kramers (1975) provides a simple and widely used reference that facilitates comparison of the different isotopic signatures. According to this model, our samples show time-integrated μ (= $^{238}U/^{204}Pb$) and W (= $^{232}Th/^{204}Pb$) values near 10 and 40.5, respectively, i.e. significantly higher than the assumed average crustal values (μ = 9.74; W = 37.19) (Fig. 2). The isotope patterns allow to recognize five main isotopic groups, which correspond to the above described metallogenic types 1, 2 and 4, 3, 5, and 6, respectively.

Group 1. The *pre-Variscan stratiform deposits* have the least radiogenic compositions, with $^{206}Pb/^{204}Pb$ in the range 17.88–18.09 (Figs. 2 and 3). The $^{207}Pb/^{206}Pb$ model ages relative to the Stacey and Kramers (1975) model are older than true ages.

Group 2. The *post-Variscan vein and breccia-pipe deposits* and the *Triassic fluorite-dominated deposits* show a wide range of isotopic compositions ($^{208}Pb/^{204}Pb$ = 38.25–39.01; $^{206}Pb/^{204}Pb$ = 18.06–18.68), which are distributed roughly parallel to model lead growth curves (Figs. 2 and 4). Three subgroups are distinguished, which are characterized by different overall enrichment in radiogenic lead. The least radiogenic subgroup ($^{206}Pb/^{204}Pb < 18.29$) corresponds to sulphide-rich deposits in the metamorphic basement and in the lower–intermediate units of the Permian volcanic sequence (Cinque Valli, Pamera, Maso Erdemolo, Quadrate, Terlano, and, excluding one outlier, Montefondoli) (Fig. 4). Their isotopic compositions partly overlap those of the most radiogenic pre-Variscan samples and tends to show much too old $^{207}Pb/^{206}Pb$ model ages. The intermediate subgroup ($18.29 < ^{206}Pb/^{204}Pb < 18.50$) includes all fluorite-rich veins in the basement (Vignola, Tingerhof, Corvara), and the relatively late Pb–Cu (Zn, Sb, Ag) deposit of Montagiù, which is hosted in the upper rhyolites. For these deposits the model ages tend to approach the geological ages. The most radiogenic group ($^{206}Pb/^{204}Pb > 18.50$) corresponds to the youngest (Triassic) fluorite-dominated deposits (Vallarsa, Nova Ponente), for which the model ages are close to or even younger than the assumed geological ages (Figs. 2 and 4).

[3] Note that the same data had been previously reported by Koeppel (1984) in plot form (cf. his Fig. 8) and loosely referred to as "deposits from the Bolzano area". In fact, the data also included single analyses for vein deposits from the Valsugana area (Quadrate, Vignola, Cinque Valli) and two analyses for a Pb–Zn–Cu vein deposit from the more southerly Schio-Recoaro basement (Val Mala; cf. Köppel and Schroll, 1985). The latter deposit is outside the region investigated here and has not been reported in Figures 2 and 4. We note, however, that the isotopic composition of this deposit ($^{206}Pb/^{204}Pb$ = 18.234–18.273; $^{207}Pb/^{204}Pb$ = 15.666–15.690; $^{206}Pb/^{204}Pb$ = 38.504–38.588) is comparable with that of the post-Variscan sulphide-rich deposits studied here.

Group 3. The *Permian–Early Triassic sediment-hosted deposits* are poorly covered by our data set (Maso Furli), but they were extensively studied by Köppel and Schroll (1985). They show a restricted range of $^{206}Pb/^{204}Pb$ values (18.25–18.40) and too old $^{207}Pb/^{206}Pb$ model ages (Fig. 2). They largely overlap the field of post-Variscan vein deposits, but shifted on average to slightly lower $^{207}Pb/^{206}Pb$ and $^{207}Pb/^{206}Pb$ values (Fig. 2).

Group 4. The *deposits associated with Triassic magmatic rocks* (represented by the Valbona low-*T* deposit) are characterized by $^{206}Pb/^{204}Pb$ values similar to the intermediate subgroup of post-Variscan deposits, but shifted to slightly lower $^{207}Pb/^{204}Pb$ and $^{208}Pb/^{204}Pb$ ratios (Fig. 2). Preliminary data on the high-*T* deposit of M. Mulat (Bedovina Mine; cf. # 24 in Fig. 1) also confirm this trend (Nimis et al., in prep). The $^{207}Pb/^{206}Pb$ model ages are older than the geological ages.

Group 5. The *deposit related to tectono-metamorphic mobilization* of Pattine shows an anomalous isotopic trend which cross-cuts model lead growth curves at essentially constant $^{207}Pb/^{204}Pb$ and reaches highly radiogenic compositions (Fig. 2). The least radiogenic sample falls within the field of the pre-Variscan deposits.

Origin of lead

Pre-Variscan stratiform deposits

The isotopic compositions of the pre-Variscan stratiform deposits studied here are similar to those of galenas from Paleozoic stratiform pyrite-rich (Cu, Zn, Pb) deposits of the Austroalpine domain of the Eastern Alps (Köppel & Schroll, 1983) (Fig. 3). The high μ and *W* values are compatible with those reported for feldspars[4] in metasediments of the Variscan basement from the western part of the Southalpine and from the eastern Austroalpine units (Cumming et al. 1987) (Fig. 3). Assuming the isotopic compositions of the rocks studied by Cumming et al. (1987) are representative also for the eastern Southalpine basement, the metasediments may have represented the only source of lead to these deposits. The moderate spread in isotopic values shown by the Calceranica and Valle Imperina deposits (Fig. 3) suggests mixing of basement-derived lead components characterized by slightly different isotopic compositions.

Other metamorphosed acidic and basic igneous rocks associated with the metasediments from the Southalpine–Austroalpine regions (orthogneisses and amphibolites) have significantly lower μ and *W* values (Cumming et al., 1987) and are thus incompatible with the deposits (Fig. 3). In this respect, the deposits studied here are unlike stratiform deposits in the western Southalpine Variscan basement (cf. Omenetto & Brigo, 1974), which indicate a major lead contribution from these rocks (Köppel & Schroll, 1983) (Fig. 3).

Post-Variscan sulphide-rich and fluorite-rich vein deposits

[4] As discussed by Köppel and Schroll (1988), correction of feldspar lead isotopic data for the in-situ decay of uranium and thorium is not necessary for comparative purposes, owing to the low U/Pb and Th/Pb ratios typical for this mineral. Typical changes over, say, 200 Ma would be ≤0.032 for $^{206}Pb/^{204}Pb$ and ≤0.05 for $^{208}Pb/^{204}Pb$. Whole-rock U–Pb systems are more sensitive than feldspars to mild metamorphic or hydrothermal overprints and are therefore less reliable for the present purposes.

Our isotopic data (trace-lead) for post-Variscan sulphide- and fluorite-rich vein deposits are in very good agreement with previous data (ore-lead) for polymetallic and fluorite-rich vein deposits in Permian volcanics and basement rocks of the same area reported by Köppel and Schroll (1985) (Fig. 4). The data are distributed roughly parallel to model lead growth curves and show a similar trend as feldspars from the Southalpine–Austroalpine metasediments (Fig. 4). As already pointed out by Koeppel (1984), the sulphides have too high μ and *W* values to be compatible with Permian sediments and post-Variscan igneous rocks (Fig. 4).

The wide compositional range and the linear relations between the isotopic ratios suggest mixing of variably radiogenic leads characterized by metasediment-like μ and *W* values. The least radiogenic lead source could be the same metasediments from which the pre-Variscan lead was extracted or the pre-Variscan deposits themselves. The latter hypothesis would be consistent with observations by Frizzo and Ferrara (1994), who found microtextural and chemical clues of a post-Variscan thermal and hydrothermal overprint on some pre-metamorphic stratiform deposits (enrichments in quartz, Pb, In, Ag), probably connected with the emplacement of the Cima d'Asta pluton.

Given the highly variable compositions of metasediment-hosted feldspars (Fig. 3), the more radiogenic lead sources could simply consist of metasediments with more radiogenic character. The apparent scarcity of such lead component in the pre-Variscan stratiform deposits would imply that more radiogenic material was available in the upper section of the metasediments, which were deposited after formation of the stratiform massive sulphides. Available data do not allow us to independently test this hypothesis. Alternatively, the more radiogenic components could derive from selective leaching of higher-U/Pb minerals coexisting with feldspars in the same basement rocks. This would imply a significant increase of radiogenic lead in deposits of younger age. Consistently, the sulphide-rich deposit cutting the latest Permian volcanics (Montagiù) and the fluorite-deposits of interpreted Triassic age (Vallarsa, Nova Ponente; cf. Bakos et al. 1972) show a progressive enrichment in radiogenic lead (Fig. 4).

In this light, the distinctively more radiogenic character (ore- and trace-lead) of the basement-hosted, fluorite-rich deposits relative to the sulphide-rich deposits in the basement and in the lower–intermediate units of the Permian volcanic sequence (Fig. 4) may reflect (i) a relatively young age of the basement-hosted fluorite-rich deposits, possibly similar to that of the Montagiù deposit (possibly Late Permian) or (ii) a greater selective involvement of non-feldspar minerals as lead sources, possibly owing to specific physico-chemical properties of fluorite's parent hydrothermal fluids.

Permian–Early Triassic sediment-hosted deposits

Köppel and Schroll (1988) attribute the relatively homogeneous isotopic composition of both Permian- and Triassic-hosted stratabound deposits (Figs. 2 and 5) to a common source of lead. Significant overlap with the post-Variscan veins (Fig. 2) suggests that a major part of the lead was supplied by remobilization of Permian sulphides or by leaching of the same metasediments from which the Permian lead was extracted. Sulphide remobilization, involving pedogenetical pre-concentration of Early Permian ores during

prolonged exposure in the Late Permian, followed by chemical reworking during Early Triassic transgression, was favoured by Zanella and Brigo (1997) for the Early Triassic carbonate-hosted deposits. In contrast, based on stratigraphic, sedimentological and hydrological constraints, Wopfner et al. (1983) concluded that no reasons exist to attribute the origin of the metals in the Permian sandstone-hosted deposits to either the post-Variscan veins or the Permian volcanics. Their model involved a source within a northeasterly Variscan basement, which had experienced documented widespread pedogenesis and, presumably, preconcentration prior to the Permian transtension, and metal transport by southwest-directed, low-temperature, shallow groundwaters. Köppel and Schroll (1988) independently came to a similar conclusion for all stratabound deposits in Permian–Triassic sediments (including the large carbonate-hosted Pb–Zn deposits of the Eastern Alps) from their lead isotope data.

We strongly favour a metasediment lead source for the following reasons: (i) the restricted isotopic variability of the stratabound deposits, which contrasts with the large isotopic variability of the post-Variscan veins (Fig. 2), would require unlikely selective remobilization of a particular subgroup of these deposits across the whole investigated area; (ii) the restricted scatter in isotopic data, which according to Köppel and Schroll (1988) is evidence for isotopic homogenization during large-scale, long-term leaching/transport processes, is instead perfectly consistent with the scenario invoked by Wopfner et al. (1983), which allows for a main metal source outside the studied area, possibly in the Austroalpine. As suggested by Köppel and Schroll (1988), the shift of isotopic data to lower $^{208}Pb/^{204}Pb$ and $^{207}Pb/^{204}Pb$ values indicates variable additional contribution of lead from Permian sediments (Fig. 5). Derivation of metals from the Permian volcanic rocks, an hypothesis put forward by Klau and Mostler (1983), is inconsistent with isotopic data (Fig. 5).

Deposits associated with Triassic igneous rocks

The isotopic compositions of the volcanic-associated Triassic deposits are not directly compatible with those of Triassic magmatic rocks in the Southalpine and eastern Austroalpine units, which show even lower μ values (Köppel & Schroll, 1985, 1988) (Fig. 6). If the data reported by Köppel and Schroll (1985, 1988; 11 samples) are truly representative of the Triassic igneous rocks in the Dolomites region (only three samples were from a locality within the area studied here), such rocks may have supplied only part of the lead. It is unclear whether the observed isotopic mismatch is due to insufficient sampling coverage of the Triassic igneous rocks or reflects the existence of a distinct additional component of yet uncertain nature.

Deposits related to tectono-metamorphic mobilization

The Pattine deposit shows an anomalous isotopic trend which cross-cuts model lead growth curves (Fig. 2). The linear trend is interpreted to reflect mixing of two distinct lead components. The first end-member of the mixing line lies in the field of pre-Variscan deposits; the second end-member has much higher $^{208}Pb/^{204}Pb$ and $^{206}Pb/^{204}Pb$, but essentially identical $^{207}Pb/^{204}Pb$ ratios. The isotopic composition of the radiogenic end-

member is unlike that of feldspars in the metasediments, but compatible with those of the Permian volcanic rocks (cf. Fig. 4). The particular location of the Pattine deposit in a strongly tectonized zone, very close to the Neogenic Valsugana Line (Fig. 1), also suggests possible recent addition of highly radiogenic lead from circulating Alpine fluids. The present data are consistent with the interpretation of these deposits as products of late-Variscan tectono-metamorphic remobilizations of pre-Variscan deposits, with possible Alpine overprinting, as proposed by Fellerer (1968) and Omenetto and Brigo (1974).

Conclusions

Lead sources of copper and polymetallic deposits of the central-eastern Southalpine region, particularly pre-Variscan (Late Ordovician–Early Silurian) stratiform, post-Variscan (Permian to Triassic) vein, and stratabound sediment-hosted (Permian to Early Triassic) deposits, are to be sought mainly in the Cambrian–Devonian (meta)sediments of the Variscan basement. Contributions from Permian and Triassic igneous rocks appear to be of minor importance, if any, even for vein deposits which are evidently related to Permian magmatism. The isotopic compositions of some of the Permian deposits are consistent with, although they do not unequivocally prove, remobilization of metals from the pre-Variscan stratiform deposits. Permian sediments contributed a variable fraction of lead to stratabound deposits in Permian to Early Triassic sediments. Triassic magmatism was a probable, but possibly not the sole supplier of lead to the Triassic volcanic-associated deposits. Further data are required to clarify the effective contribution of Triassic magmas and rocks to these deposits.

The high μ and W values of the Cu-bearing deposits studied here are consistent with regional isotopic patterns of Pb–Zn-rich deposits in more northerly and easterly sectors of the Eastern Alps (Köppel et al., 1983, 1988; Brigo et al., 2001), which suggested the existence of a high-(μ, W) Southalpine–Austroalpine isotopic province (Köppel, 1983; Koeppel, 1984; Köppel et al., 1993). We further note that other circum-Mediterranean hydrothermal deposits of Paleozoic to Triassic age (e.g. Sardinia, Ludwig et al., 1989; Caron et al., 1997; Betic Cordillera, Arribas et al., 1991) or derived from remobilization of Paleozoic deposits (e.g. Tuscany, Lattanzi et al., 1992) show an identical high-μ and high-W character, which suggests potential persistence southwestwards (present coordinates) of the Southalpine–Austroalpine lead signature across a relatively wide portion of the former north-Gondwanan margin (cf. von Raumer et al., 2002).

Table 1. List of deposits studied

Deposit[§]	Host unit	Deposit type	Main minerals[†]	Reference
Calceranica	Basement	Stratiform massive sulphide	Py-dominated, sph, cpy, gal, aspy.	Ogniben (1966)
Vetriolo	Basement	Stratiform massive sulphide	Py-dominated, sph, cpy, gal, aspy.	Frizzo (2004b)
Valle Imperina	Basement	Stratiform massive sulphide	Py-dominated, cpy, sph, gal, aspy, tet.	Ogniben (1967)
Pamera	Basement	Breccia pipe	Magnetite ore (cpy(Bi), py, Co-Ni sulphides) / Pyrrhotite ore (cpy, Bi, Te).	Omenetto (1968b)
Cinque Valli	Basement and Permian intrusives	Sulphide-rich vein system	Early Cu(Bi) / Zn, Pb, Sb, Cu, Ag sulphides and sulphosalts / Late fluorite veins.	Barillari et al. (1966)
Montefondoli/Pfundererberg	Basement and Permian intrusives	Sulphide-rich vein system	Sph, gal(Ag), cpy, qz. Abundant (Cu)-Sb-Ag sulphides and sulphosalts. Traces Au in py/sph.	Brigo (1971)
Maso Erdemolo	Permian volcanics (basal andesites)	Sulphide-rich vein stockwork	Qz, chl. Pb-Zn-Cu ore / Cu-dominated ore with Bi-Ag sulphides. Traces Au.	Murara (1966)
Quadrate	Permian volcanics (basal andesites)	Sulphide-rich vein	Gal > sph, py, cpy, qz. Tet and Ag-carriers (stefanite, argentite) in gal.	Omenetto & Detomaso (1970)
Terlano/Terlan	Permian volcanics (intermediate rhyodacites)	Sulphide-rich vein	Sph, gal with tet, cpy, py, qz.	Barnaba (1964)
Montagiù	Permian volcanics (upper rhyolites)	Sulphide-rich vein	Gal, tet = cpy, sph, py (Co, Ni, Ag).	Dessau & Duchi (1970)
Tingerhof/Tingherla	Basement	Fluorite-rich vein	Qz, abundant gal, minor sph, cpy, py.	Vuillermin (1964)
Vignola	Basement	Fluorite-rich vein	Accessory sph > gal(Ag), traces cpy, tet.	Di Colbertaldo (1965)
Corvara/Rabenstein	Basement	Fluorite-rich vein	Accessory gal, sph. Minor cpy, bar.	Morgante (1940)
Vallarsa	Permian volcanics (upper rhyolites)	Fluorite-rich vein	Qz, bar, cc. Abundant accessory gal with tet/cpy inclusions.	Vuillermin (1966)
Nova Ponente/Deutschnofen *	Permian volcanics (upper rhyolites)	Fluorite-rich vein	Bar, qz. Minor gal, traces sph.	Dessau and Perna (1966)
Tregiovo	Permian shales (Tregiovo Fm.)	Stratabound disseminated red-bed type	Gal, sph, py.	Dessau and Perna (1966)
Bletterbach	Upper Permian Val Gardena Sandstones	Stratabound disseminated red-bed type	Gal, sph (py, chc, tet–ten)	Wopfner et al. (1983)
Ortisei/St. Ulrich	Upper Permian Val Gardena Sandstones	Stratabound disseminated red-bed type	Gal, sph (py, chc, tet–ten)	Wopfner et al. (1983)
Rio Frassineto/Verschneidbach	Upper Permian Val Gardena Sandstones	Stratabound disseminated red-bed type	Gal, sph (py, chc, tet–ten)	Wopfner et al. (1983)
Rio Meltina/Möltnerbach	Upper Permian Val Gardena Sandstones	Stratabound disseminated red-bed type	Gal, sph (py, chc, tet–ten)	Wopfner et al. (1983)
Monti della Mendola/Mendelzug **	Upper Permian Val Gardena Sandstones	Stratabound disseminated red-bed type	Gal with sph microinclusions, py.	Brondi et al. (1970)
Schwarzwaldbach °	Upper Permian Val Gardena Sandstones	Stratabound disseminated red-bed type	Data not available.	Köppel and Schroll (1985)
Val di Non/Nonstal ***	Early Triassic carbonates (Werfen Fm.)[#]	Stratabound disseminated	Gal ± bar.	Dessau and Perna (1966)
Doss de le Grave	Early Triassic carbonates (Werfen Fm.)[#]	Stratabound disseminated	Gal (Ag), subordinate bar, traces of Cu carbonates.	Dessau and Perna (1966)
Maso Furli	Early Triassic carbonates (Werfen Fm.)[#]	Stratabound veinlets/disseminated	Gal, sph, py, cpy, tet, bar.	Brusca et al. (1972)
Valbona	Ladinian volcanics	Mineralized breccia	Cc, disseminated cpy, bor, minor gal.	Cavinato (1968)
Pattine	Basement	Remobilization veins	Py, cpy, with qz, sid, bar, fl.	Fellerer (1968)

Notes:
[§]: Names in *italic* indicate deposits for which lead isotope data were taken from Köppel and Schroll (1985).
*: exact location not specified; probably corresponding to the "S. Elena-Case a Prato" veins of Dessau and Perna (1966).
**: exact location not specified; probably corresponding to mineralizations north of Mendel Pass (e.g. Rio del Bavaro) reported in Brondi et al. (1970).
***: exact location not specified; probably corresponding to mineralization in the Lauregno–Marcena area reported in Dessau and Perna (1966).
° : unknown location.
[#]: formerly assigned to the upper Permian Bellerophon Fm. (cf. Brusca and Perna 1995)
[†]: aspy – arsenopyrite, bar – barite, bor – bornite, cc – calcite, chc – chalcocite, cpy – chalcopyrite, fl – fluorite, gal – galena, mcs – marcasite, py – pyrite, qz – quartz, sid – siderite, sph – sphalerite, tet – tetrahedrite, ten – tennantite.
The notation "/" separates subsequent mineralization stages.

Table 2. Lead isotope data.

Deposit	Sample	$^{206}Pb/^{204}Pb$	±2σ	$^{207}Pb/^{204}Pb$	±2σ	$^{208}Pb/^{204}Pb$	±2σ
Calceranica	CALC-1	17.905	0.002	15.646	0.002	38.125	0.005
	CALC-2	17.911	0.002	15.641	0.002	38.119	0.006
	CALC-3	17.922	0.002	15.641	0.002	38.136	0.008
	CALC-4	17.972	0.002	15.640	0.002	38.145	0.006
	M1200	17.897	0.002	15.640	0.001	38.099	0.004
Vetriolo	VET2sp	17.887	0.002	15.643	0.002	38.100	0.006
	VET-0	17.883	0.001	15.640	0.002	38.094	0.004
	VET-p3c	17.886	0.002	15.643	0.002	38.106	0.006
	VET-p3s	17.885	0.002	15.642	0.002	38.101	0.006
	VET-2p	17.880	0.001	15.640	0.001	38.097	0.004
Valle Imperina	VI-03	17.985	0.002	15.663	0.002	38.158	0.006
	VI-04	17.973	0.002	15.659	0.002	38.145	0.006
	VI-05	18.029	0.003	15.672	0.003	38.227	0.007
	VI-06	18.029	0.004	15.661	0.004	38.208	0.008
	VI-07	17.972	0.002	15.651	0.002	38.120	0.007
	VI-08	18.054	0.002	15.661	0.002	38.243	0.007
	VI-09	18.067	0.002	15.677	0.002	38.283	0.005
Pamera	PAM-1	18.092	0.002	15.659	0.002	38.291	0.006
	PA6	18.209	0.003	15.662	0.003	38.443	0.008
	P3	18.283	0.002	15.666	0.002	38.537	0.006
	P28	18.200	0.003	15.655	0.006	38.365	0.006
Cinque Valli	5VA	18.061	0.003	15.661	0.003	38.252	0.008
Montefondoli	MFO_Ap1	18.253	0.002	15.673	0.002	38.520	0.005
	MFO_Ap2	18.276	0.003	15.676	0.003	38.550	0.008
	MFO_Ap3	18.286	0.002	15.675	0.003	38.500	0.008
	MFO-MU	18.269	0.002	15.674	0.002	38.514	0.006
	MFO-KW	18.281	0.001	15.670	0.001	38.518	0.002
	CD-a-11	18.259	0.002	15.672	0.002	38.501	0.005
Maso Erdemolo	GRUA-Cp1	18.238	0.002	15.661	0.002	38.458	0.006
	GRUA-Ddxp1	18.246	0.002	15.663	0.002	38.472	0.004
	GRUA-Dsxp1	18.249	0.001	15.666	0.002	38.479	0.004
	GRUA-Ep1	18.253	0.001	15.669	0.002	38.493	0.004
Montagiù	MOND-1	18.405	0.001	15.677	0.002	38.672	0.006
	MOND-2	18.417	0.003	15.676	0.004	38.682	0.008
	MOND-3	18.405	0.002	15.677	0.003	38.676	0.008
Tingherhof	TING-1	18.372	0.002	15.671	0.002	38.633	0.006
	TING-2	18.465	0.002	15.671	0.002	38.731	0.006
Maso Furli	LAV-1	18.400	0.002	15.676	0.002	38.557	0.007
	LAV-2	18.277	0.002	15.668	0.002	38.511	0.006
Valbona	VBE2A	18.458	0.001	15.668	0.001	38.597	0.004
	VBO1A	18.438	0.002	15.664	0.002	38.578	0.008
	VBO2A	18.386	0.002	15.666	0.002	38.548	0.006
	VBE1A	18.391	0.003	15.661	0.002	38.519	0.008
	VBE1a-r	18.466	0.002	15.670	0.002	38.612	0.007
Pattine	PA05i	18.419	0.008	15.681	0.008	38.545	0.010
	PA-09i	18.496	0.002	15.674	0.002	38.615	0.004
	PA-02i	18.800	0.002	15.681	0.002	38.840	0.004
	PAT-P2	18.500	0.003	15.667	0.003	38.587	0.006
	PAT-P1	18.522	0.002	15.669	0.003	38.606	0.007

PAT-P3	18.329	0.002	15.681	0.002	38.485	0.006
PAT-BOR	18.038	0.002	15.676	0.002	38.248	0.007

Figure captions

Fig. 1. Location of mineral deposits discussed in this work.

Fig. 2. Lead isotope data for deposits of the central-eastern Southalpine. SK: lead growth curves according to Stacey and Kramers (1975); KT: growth curve for young crust after Kramers and Toltsikhin (1997).

Fig. 3. Lead isotope data for the pre-Variscan stratiform deposits. Data for pre-Variscan stratiform deposits in Austroalpine (Köppel and Schroll, 1983) and western Southalpine (Ivrea–Ceneri zone; Cumming et al., 1987) units are shown for comparison. Fields for Southalpine–Austroalpine metasediments, amphibolites and orthogneisses after Köppel and Schroll (1988) and Cumming et al. (1987). Reference curves as in Fig. 2.

Fig. 4. Lead isotope data for the post-Variscan vein deposits. Fields: Southalpine–Austroalpine metasediments – Köppel and Schroll (1988), Cumming et al. (1987); Permian sandstones and volcanics – Köppel and Schroll (1985); pre-Variscan stratiform deposits – this work (Fig. 2). Thick dashed lines separate three subgroups of deposits characterized by increasing radiogenic character and decreasing geological age (see text for further explanation). Other reference curves as in Fig. 2.

Fig. 5. Lead isotope data for stratabound deposits in Permian to Early Triassic sediments. Fields: Southalpine–Austroalpine metasediments – Köppel and Schroll (1988), Cumming et al. (1987); Permian–Early Triassic sandstones and Permian volcanics – Köppel and Schroll (1985). Reference curves as in Fig. 2.

Fig. 6. Lead isotope data for deposits in Triassic volcanics (blue symbols: Maso Furli). Fields: Southalpine–Austroalpine metasediments – Köppel and Schroll (1988), Cumming et al. (1987); Permian–Early Triassic sandstones, Permian and Triassic volcanics – Köppel and Schroll (1985). Reference curves as in Fig. 2.

References

Arribas A.J., Tosdal R.M., Wooden J.L. (1991) Lead isotope constraints on the origin of base- and precious-metal deposits from southeastern Spain. *In* Pagel M., Leroy J.L. (Ed.) Source, Transport and Deposition of Metals. Balkema, Rotterdam, p. 241-244

Artioli G., Nimis P., Gruppo ARCA, Recchia S., Marelli M., Giussani B. (2009) Geochemical links between copper mines and ancient metallurgy: the Agordo case study. *Rend. Online Soc. Geol. It.* 4:15-18

Artioli G., Baumgarten B., Marelli M., Giussani B., Recchia S., Nimis P., Giunti I., Angelini I., Omenetto P. (2008) Chemical and isotopic tracers in Alpine copper deposits: geochemical links between mines and metal. *Geo. Alp.* 5:139-148

Bakos F., Brondi A., Perna G. (1972) The age of mineral deposits in the Permian volcanites of Trentino-Alto Adige (northern Italy). *In* Proceedings 2Nd ISMIDA, Ljubljana, p. 181-194

Barillari A., Jobstraibizer P.G., Omenetto P. (1966) Il giacimento a piombo, zinco e rame di Cinquevalli in Valsugana (Trentino). *In* Atti del Symposium Internazionale sui Giacimenti Minerari delle Alpi, vol. 3. Regione Trentino-Alto Adige, p. 769-792

Barnaba P.F. (1964) Il giacimento piombo-zincifero di Terlano in Alto Adige (studio geo-minerario). *L'Industria Mineraria nel Trentino-Alto Adige, Economia Trentina* 13:133-158

Bianchi A. & di Colbertaldo D. (1956) Osservazioni paragenetiche sul giacimento a rame e tungsteno della Bedovina presso Predazzo. *Rend. Soc. Min. It.* 12:55-65

Bonadiman C., Coltorti M., Siena F. (1994) Petrogenesis and T-fO_2 estimates of Mt. Monzoni complex (central Dolomites, southern Alps): a Triassic shoshonitic intrusion in a transcurrent geodynamic setting. *European Journal of Mineralogy* 6:943-966

Brigo L. (1971) Mineralizzazioni e metallogenesi nell'area della Fillade quarzifera di Bressanone nelle Alpi Sarentine. *St. Trent. Sc. Nat.* A48:80-125

Brigo L., Brusca C., Omenetto P., Perna G. (1975) Alpi Centro-Orientali. *In* Castaldo G., Stampanoni G. (Ed.) Memoria Illustrativa Della Carta Mineraria d'Italia Scala 1: 1.000.000, Memorie per Servire alla Descrizione della Carta Geologica d'Italia Volume XIV. Ministero dell'Industria del Commercio e dell'Artigianato, Servizio Geologico d'Italia, Roma, p. 40-70

Brigo L., Camana G., Rodeghiero F., Potenza R. (2001) Carbonate-hosted siliceous crust type mineralization of Carnic Alps (Italy-Austria). *Ore Geology Reviews* 17:199-214

Brondi A., Polizzano C., Anselmi B., Benvegnù F. (1970) Rinvenimento di una mineralizzazione a galena nelle arenarie permiane di Nalles (Bolzano). *L'Industria Mineraria nel Trentino-Alto Adige, Economia Trentina* 3:171-182

Brusca C. & Perna G. (1995) Inquadramento e genesi dei giacimenti di galena argentifera del Monte Calisio (Trento). *In* Brigo L., Tizzoni M. (Ed.) Il Monte Caliso e l'Argento Nelle Alpi Dall'Antichità Al XVIII Secolo. Atti del Convegno Europeo Promosso e Organizzato dai Comuni di Civezzano e Fornace e dalla SAT Società Alpinisti Trentini - Sezione Di Civezzano, Civezzano-Fornace (Trento), p. 19-30

Brusca C., Dessau G., Lery Jensen M., Perna G. (1972) The deposits of argentiferous galena within the Bellerophon Formation (Upper Permian) of the Southern Alps. *In* Proc. 2nd Int. Symp. Min. Dep. Alps, Ljubljana, p. 159-179

Caron C., Lancelot J., Omenetto P., Orgeval J.-. (1997) Role of the Sardic tectonic phase in the metallogenesis of SW Sardinia (Iglesiente): lead isotope evidence. *Eur. J. Mineral.* 9:1005-1016

Cavinato A. (1968) Ricerche minerarie nelle Alpi Bellunesi. *In* Atti Della Giornata Di Studi Geominerari, 7 Ottobre 1967, Centenario Dell'Istituto Tecnico Industriale Minerario Statale «U. Follador», Agordo, p. 43-62

Cumming G.L., Köppel V., Ferrario A. (1987) A lead isotope study of the northeastern Ivrea Zone and the adjoining Ceneri zone (N-Italy): evidence for a contaminated subcontinental mantle. *Contrib. Mineral. Petrol.* 97:19-30

Dal Piaz G. & Martin S. (1998) Evoluzione litosferica e magmatismo nel dominio Austro-Sudalpino dall'orogenesi varisica al rifting mesozoico. *Mem. Soc. Geol. It.* 53:43-62

Dessau G. & Perna G. (1966) Le mineralizzazioni a galena e blenda nel Trentino-Alto Adige e loro contenuto in elementi accessori. *Atti del Symposium Internazionale sui Giacimenti Minerari delle Alpi* 3:587-687

Dessau G. & Duchi G. (1970) Mineralizzazioni a solfuri nelle vulcaniti del Montagiù (Trento). *L'Industria Mineraria nel Trentino-Alto Adige, Economia Trentina* 3:115-123

Di Colbertaldo D. (1965) Il giacimento a fluorite, blenda e galena di Vignola in Valsugana (Trento). *L'Industria Mineraria nel Trentino-Alto Adige, Economia Trentina* 2:135-154

Dieni I., Giordano D., Loydell D.K., Sassi F.P. (2005) Discovery of Llandovery (Silurian) graptolites and probable Devonian corals in the Southalpine Metamorphic Basement of the Eastern Alps (Agordo, NE Italy). *Geol. Mag.* 142:1-5

Doglioni C. (1987) Tectonics of the Dolomites (Southern Alps, Northern Italy). *J. Struct. Geol.* 9:181-193

Fellerer R. (1968) Geologische und lagerstättenkundliche Untersuchungen zwischen Passo Cereda und Forcella Aurine (südliche Pala-Gruppe/Norditalien). Inaug.-Dissert. Universität München, 73 p.

Frizzo P. (2004a) Il distretto metallifero dell'alta Valsugana. *In* Passardi P., Zammatteo P. (Ed.) Le Miniere del Mandola in Valsugana, *Monografie I Mus. Trid. Sci. Nat.*, p. 131-155

Frizzo P. (2004b) La miniera di Calceranica e i giacimenti a solfuri massicci della zona Agordino-Valsuganese. *In* Passardi P., Zammatteo P. (Ed.) Le Miniere del Mandola in Valsugana, *Monografie I Mus. Trid. Sci. Nat.*, p. 157-180

Frizzo P. & Ferrara E. (1994) I giacimenti a solfuri massivi del Distretto Agordino-Valsuganese (basamento sudalpino). Alpi Orientali. *In* Giornata di Studio in Ricordo del Prof. Zucchetti, Torino 12 Maggio 1994,. Politecnico di Torino, p. 147-156

Gale N.H. & Stos-Gale Z. (2000) Lead isotope analyses applied to provenance studies. *In* Ciliberto E., Spoto G. (Ed.) Modern Analytical Methods in Art and Archaeology. Wiley-Interscience, New York, p. 503-584

Horwitz E.P., Chiarizia R., Dietz M.L. (1992) A novel strontium-selective extraction chromatographic resin. *Solv. Extr. Ion. Exch.* 10:313-336

Kalvacheva R., Sassi F.P., Zanferrari A. (1986) Acritarch evidence for the Cambrian age of phyllites in the Agordo area (South-alpine basement of eastern Alps, Italy). *Rev. Palaeobot. Palynol.* 48:311-326

Klau W. & Mostler H. (1983) Zn-Pb-F mineralization in middle Permian of Tregiovo (Province of Bozen/Trient, Italy). *In* Mineral Deposits of the Alps and of the Alpine Epoch in Europe. Springer-Verlag, Berlin Heidelberg New York Tokio, p. 70-80

Koeppel V. (1984) Lead isotopes as tracers of the origin of metals in ore deposits and of the evolution of continental crust: examples from western and central Europe. *In* Metallogenesis and Mineral Ore Deposits, *Proc. 27th Int. Geol. Congress*, vol. 12, p. 53-82

Köppel V. (1983) Summary of lead isotope data from ore deposits of the Eastern and Southern Alps: Some metallogenetic and geotectonic implications. *In* Schneider H.J. (Ed.) Mineral Deposits of the Alps. Proc. IV ISMIDA 1981. Springer Verlag, Berlin Heidelberg, p. 162-168

Köppel V. & Schroll E. (1983) Lead isotopes of Paleozoic, strata-bound to stratiform galena bearing sulphide deposits of the Eastern Alps (Austria): implications for their geotectonic setting. *Schweiz. Mineral. Petrograph. Mitt.* 63:347-360

Köppel V. & Schroll E. (1985) Herkunft des Pb der triassichen Pb-Zn-Vererzungen in den Ost- und Südalpen. *Arch. Lagerst. Forsch. Geol. B. -A.* 6:215-222

Köppel V., Neubauer F., Schroll E. (1993) Pre-Alpidic ore deposits in the Central, Eastern and Southern Alps. *In* von Raumer J., Neubauer F. (Ed.) Pre-Mesozoic Geology in the Alps. Springer-Verlag, Berlin, p. 145-162

Kramers J.D. & Tolstikhin I.N. (1997) Two terrestrial lead isotope paradoxes, forward transport modelling, core formation and the history of the continental crust. *Chem. Geol.* 139:75-110

Lattanzi P., Hansmann W., Koeppel V., Costagliola P. (1992) Source of metals in metamorphic ore-forming processes in the Apuane Alps (NW Tuscany, Italy): Constraints by Pb-isotope data. *Mineral. Petrol.* 45:217-229

Lucchini F., Rossi P.M., Simboli G., Cristofolini R. (1982) Confronto geochimico fra i prodotti magmatici basici del Trias-Giura nell'area Tetidea. *In* Castellarin A., Vai G.B. (Ed.) Guida alla Geologia del Sudalpino Centro-Orientale. Guide Geologiche Regionali. Soc. Geol. It., p. 133-141

Ludwig K.R., Vollmer R., Turi B., Simmons K.R., Perna G. (1989) Isotopic constraints on the genesis of base-metal ores in Southern and Central Sardinia. *Eur. J. Mineral.* 1:657-666

Maucher A. (1955) Erzmikroskopische Untersuchungen an Blei-Zink-Lagerstätten im Raume von Trento (Norditalien). *Mitt. Geol. Ges. Wien* 48:131-140

Meli S. & Klötzli U.S. (2001) Evidence for Lower Paleozoic magmatism in the Eastern Southalpine basement: zircon geochronology from Comelico porphyroids. *Schweiz. Mineral. Petrograph. Mitt.* 81:147-157

Morgante S. (1940) Il giacimento di Corvara in Val Sarentino. *Mem. Ist. Geol. Univ. Padova* 14:3-68

Murara G. (1966) Le mineralizzazioni a solfuri misti nelle vulcaniti atesine, formazione andesitica, dell'alta Val Fersina (Trentino). *In* Atti del Symposium Internazionale sui Giacimenti Minerari delle Alpi, vol. 2. Regione Trentino-Alto Adige, p. 471-494

Ogniben L. (1966) Nota sul Cristallino Antico e il giacimento di pirite di Calceranica (Trento). *In* Atti Del Symposium Internazionale Sui Giacimenti Minerari Delle Alpi, vol. 3-4. Regione Trentino-Alto Adige, p. 911-927

Ogniben L. (1967) Il Cristallino antico e il giacimento di pirite di Agordo (Belluno) (Nota riassuntiva). *In* Atti della Giornata di Studi Geominerari, 7 Ottobre 1967, Centenario dell'Istituto Tecnico Industriale Minerario Statale «U. Follador», Agordo, p. 63-65

Omenetto P. (1968a) Le risorse minerarie della regione di Belluno. *In* Atti Della Giornata Di Studi Geominerari, 7 Ottobre 1967, Centenario dell'Istituto Tecnico Industriale Minerario Statale «U. Follador», Agordo, p. 31-42

Omenetto P. (1968b) Il giacimento ferrifero della Pamera, presso Roncegno (Valsugana). *Mem. Ist. Geol. Min. Univ. Padova* 26:38

Omenetto P. & Detomaso G. (1970) Le mineralizzazioni filoniane a solfuri misti della zona di Piné (Trento). *L'Industria Mineraria nel Trentino-Alto Adige, Economia Trentina* 3:143-169

Omenetto P. & Brigo L. (1974) Metallogenesi nel quadro dell'orogene ercinico delle Alpi (con particolare riguardo al versante italiano). *Mem. Soc. Geol. It.* 13:1-24

Preuschen E. (1973) Estrazione mineraria dell'età del bronzo nel Trentino. *Preistoria Alpina, Rendiconti* 91:113-150

Rottura A., Bargossi G.M., Caggianelli A., Del Moro A., Visonà D., Tranne C.A. (1998) Origin and significance of the Permian high-K calc-alkaline magmatism in the central-eastern Southern Alps, Italy. *Lithos* 45:329-348

Sassi F.P. & Zirpoli G. (1990) The lithostratigraphic sequence in the Southalpine Basement of the Eastern Alps. *In* Sassi F.P., Zanferrari A. (Ed.) Pre-Variscan and Variscan Events in the Alpine-Mediterranean Belts, *Rend. Soc. Geol. It.*, vol. 12, p. 397-402

Šebesta G. (1992) La via del rame. Economia Trentina, Supplemento 3/1992, 221 p.

Stacey J.S. & Kramers J.D. (1975) Approximation of terrestrial lead isotope evolution by a two-stage model. *Earth Planet. Sci. Lett.* 26:207-221

Vecoli M., Dieni I., Sassi F., Servais T. (2008) Cambrian Acritarchs from the Col di Foglia (Agordo) southalpine metamorphic basement, Italian Eastern Alps: the oldest biostratigraphic record in the alps. *Rendiconti Lincei* 19:45-55

Villa I.M. (2009) Lead isotopic measurements in archeological objects. *Archaeol. Anthropol. Sci.* 1:149-153

Visonà D. (1997) The Predazzo multipulse intrusive body (Western Dolomites, Italy). Field and mineralogical studies. *Mem. Sc. Geol.* 49:117-125

von Raumer J.F., Stampfli G.M., Borel G., Bussy F. (2002) Organization of pre-variscan basement areas at the north-Gondwanan margin. *Int. J. Earth Sciences* 91:35-52

Vuillermin F. (1964) Nota preliminare su alcuni filoni quarzoso-fluoritici in Trentino-Alto Adige. *L'Industria Mineraria nel Trentino-Alto Adige, Economia Trentina* 13:305-321

Vuillermin F. (1966) Il giacimento fluoritico "Vallarsa Sud" nella Vallarsa di Laives (Bolzano). *In* Atti del Symposium Internazionale sui Giacimenti Minerari delle Alpi, vol. 2. Regione Trentino-Alto Adige, p. 505-525

Wopfner H., Griesecke S., Koch J., Fels H. (1983) New aspects on metal deposits of the Groeden Sandstone (South Tyrol, Italy). *In* Schneider H.-J. (Ed.) Mineral Deposits of the Alps and of the Alpine Epoch in Europe. Springer-Verlag, Berlin Heidelberg New York Tokio, p. 60-69

Zanella M. & Brigo L. (1997) Le mineralizzazioni argentifere nello Scitico a nord di M. Calisio (Trento, Italia): relazioni fra assetto paleogeografico e chimismo. *In* Brigo L., Tizzoni M. (Ed.) Atti Convegno Europeo "Il M. Calisio e l'argento Nelle Alpi dall'antichità Al XVIII Secolo. Giacimenti, Storia e Rapporti Con La Tradizione Mineraria Mitteleuropea", 12-14 Ottobre 1995. Comune di Civezzano, Comune di Fornace, p. 31-41

Appendix 2

Cu isotopes, traces and REE data

WESTERN ALPS

Deposit	Sample	^{139}La	^{140}Ce	^{141}Pr	^{146}Nd	^{147}Sm	^{153}Eu	^{157}Gd	^{159}Tb	^{163}Dy	^{165}Ho	^{166}Er	^{169}Tm	^{172}Yb	^{175}Lu	^{89}Y
Piedmont zone																
Chialamberto	CHIAL67	2.0191	6.5622	1.3915	8.8245	3.1098	0.6964	3.0754	0.9273	6.4479	1.3780	3.9068	0.4090	3.0213	0.2481	29.7097
Alagna-Fabbriche	ALA_Ap1	0.1223	0.2894	0.0358	0.1654	0.0983	0.0135	0.0840	0.0204	0.1552	0.0245	0.0659	0.0095	0.0566	<LOD	0.5253
Alagna-Fabbriche	L87'	1.8483	4.7548	0.6976	4.4537	1.2502	1.5969	1.3455	0.4200	3.0667	0.3827	1.7447	0.1257	1.2060	0.1340	14.8364
Chuc-Servette	46/5	0.1367	0.2782	0.0855	0.2362	0.0590	0.0233	<LOD	0.0684	0.2471	0.1103	0.1088	0.1010	0.0264	<LOD	0.3263
Petit monde	A5b	0.0259	0.0790	0.0530	0.1369	0.0469	<LOD	<LOD	0.0543	0.1912	0.0876	0.0975	0.0814	0.0543	<LOD	0.1530
Usseglio	M/U 3761	22.4302	0.4520	0.0975	0.3960	0.1925	9.0379	0.1389	0.0621	0.2230	0.0938	0.0975	0.0902	0.0682	0.0219	0.2010
Cruvino	M/U 9748	0.1789	0.0672	0.0466	0.1160	0.0423	<LOD	<LOD	0.0466	0.1604	0.0748	0.0683	0.0694	0.0108	<LOD	0.1767
Ligurian Briançonnais zone																
Saint Verain	SVE - Ap1	<LOD	0.5171	0.1372	0.8617	0.3379	0.1315	0.3785	0.0813	0.5506	0.1283	0.3965	0.0281	0.3006	0.0378	3.3026
Saint Verain	SVE - Ap2	0.1093	0.1710	<LOD	<LOD	<LOD	<LOD	<LOD	<LOD	<LOD	<LOD	<LOD	<LOD	<LOD	<LOD	<LOD
Saint Verain	SVE - Ap3	3.7847	7.8312	0.8757	3.7286	0.6229	0.1619	0.8522	0.1199	0.7543	0.1137	0.3341	0.0343	0.2421	<LOD	3.5650
Saint Verain	SVE - Ap4	0.3195	0.4682	0.0437	0.1511	<LOD	<LOD	<LOD	<LOD	0.0417	<LOD	<LOD	<LOD	<LOD	<LOD	0.2050
Saint Verain	SVE- Ar1	0.6392	1.2370	0.1392	0.4627	0.1303	<LOD	0.1235	0.0190	0.1201	0.0209	0.0598	<LOD	<LOD	<LOD	0.8056
Saint Verain	SVE- Br1	0.2947	0.4729	0.0443	0.2040	<LOD	<LOD	<LOD	<LOD	<LOD	<LOD	<LOD	<LOD	<LOD	<LOD	0.1236
Saint Verain	SVE- Bp1	2.2405	4.0730	0.5194	2.1933	0.5056	0.1159	0.5935	0.0656	0.5139	0.0993	0.3279	<LOD	0.3249	<LOD	2.9304
Saint Verain	SVE- Bs1	1.4715	2.9950	0.5071	2.4347	0.7671	0.1892	0.8370	0.1578	0.9744	0.2037	0.6326	0.0910	0.5959	0.0796	5.3219
Saint Verain	SVE- Cp1	0.3101	0.4915	0.0601	0.1762	<LOD	<LOD	<LOD	0.0093	0.0872	0.0071	0.0310	<LOD	0.0383	<LOD	0.3933
Saint Verain	SVE- Cs1	3.1219	7.2550	0.9733	4.6116	1.1902	0.3733	1.3980	0.2396	1.4127	0.2836	0.8139	0.1075	0.6420	0.0862	7.3091
via fiorcia	VF2a	0.0557	0.1574	0.0696	0.2256	0.0836	0.0376	0.0209	0.0641	0.2437	0.1017	0.1058	0.0905	0.0390	<LOD	0.4095
Murialdo-Pastori	MUR-1	0.0732	0.1055	0.0633	0.1632	0.0633	0.0113	<LOD	0.0619	0.2195	0.1027	0.0957	0.0929	0.0253	<LOD	0.1365
Murialdo-Pastori	PAS-1	0.5484	1.0784	0.2260	0.8657	0.3656	0.0615	0.2094	0.1379	0.5484	0.1595	0.2160	0.1196	0.0980	<LOD	1.1964

LIGURIAN APENNINES

Deposit	Sample	^{139}La	^{140}Ce	^{141}Pr	^{146}Nd	^{147}Sm	^{153}Eu	^{157}Gd	^{159}Tb	^{163}Dy	^{165}Ho	^{166}Er	^{169}Tm	^{172}Yb	^{175}Lu	^{89}Y
Libiola	LIB_L2p1	0.2470	0.1235	<LOD	0.1235	<LOD	<LOD	<LOD	<LOD	0.1235	<LOD	<LOD	<LOD	<LOD	<LOD	0.4941
Libiola	LIB_Fs1	6.4551	31.6887	6.3084	39.4642	15.1108	5.5749	20.0989	3.5210	21.5659	4.2545	11.4432	1.4671	8.6557	1.1737	101.3746
Libiola	LIB_Bp1	3.0485	7.1131	0.8256	3.1755	0.6351	0.2540	1.0797	0.1905	1.3972	0.3175	0.9526	0.1270	0.8256	0.1270	10.7966
Libiola	LIB_Gs1	3.2569	19.9574	4.5736	30.3519	15.1759	6.5139	19.7495	3.8806	24.8774	4.6429	12.6120	1.7324	10.8103	1.5245	97.7773
Libiola	LIB_Ep1	0.2548	0.3567	0.0510	0.2548	0.0510	0.0510	0.1019	<LOD	0.0510	<LOD	0.0510	<LOD	0.0510	<LOD	0.8153
Monte Loreto	LOR_As1	0.9282	4.4555	0.8354	4.5483	1.2995	0.2785	1.0211	0.1856	0.7426	0.0928	0.2785	<LOD	0.1856	<LOD	2.8775
Monte Loreto	LOR_Bp1	0.1715	0.1715	<LOD	0.0857	<LOD	<LOD	<LOD	<LOD	<LOD	<LOD	<LOD	<LOD	<LOD	<LOD	0.1715
Monte Loreto	LOR_M2P1	0.8387	1.6774	0.2097	1.6774	0.6290	0.2097	0.8387	0.2097	1.0484	0.2097	0.4193	<LOD	0.4193	<LOD	5.0321
Monte Loreto	LOR_M3p1	0.9844	1.5751	0.1969	0.7876	0.1969	<LOD	0.3938	<LOD	0.3938	<LOD	0.1969	<LOD	0.1969	<LOD	3.1502
Bonassola	BON_Ap1	0.0620	0.1562	0.0151	0.0824	0.0224	<LOD	0.0268	0.0045	0.0193	0.0056	0.0136	<LOD	0.0228	0.0044	0.1247
Bonassola	BON_Ap2	0.1522	0.2901	0.0321	0.1407	0.0469	<LOD	0.0312	0.0061	0.0376	0.0074	0.0170	<LOD	0.0189	<LOD	0.1725
Reppia	REP_As1	3.6783	3.1504	2.9945	19.7875	8.6420	2.0420	10.2499	1.7891	10.0929	1.8218	4.7962	0.6687	4.3969	0.5670	35.3183
Reppia	REP_As2	14.9952	39.4097	12.9153	77.7705	32.1391	8.6289	37.7820	7.0120	41.7609	7.2164	18.7011	2.5501	15.5396	1.9117	104.8274
Piazza	PIA_Bp1	0.0924	0.1925	<LOD	0.0761	0.0165	<LOD	<LOD	<LOD	<LOD	<LOD	<LOD	<LOD	0.0076	<LOD	0.0829

Piazza	PIA_Bp2	0.1281	0.2619	0.0187	<LOD	0.0156	<LOD	<LOD	<LOD	<LOD	<LOD	<LOD	<LOD	0.0174	<LOD	0.0606

SOUTHERN TUSCANY

Deposit	Sample	^{139}La	^{140}Ce	^{141}Pr	^{146}Nd	^{147}Sm	^{153}Eu	^{157}Gd	^{159}Tb	^{163}Dy	^{165}Ho	^{166}Er	^{169}Tm	^{172}Yb	^{175}Lu	^{89}Y
Elba	ELB_Cs1	0.9078	0.5188	0.1297	0.5188	0.1297	<LOD	0.1297	<LOD	0.1297	<LOD	0.1297	<LOD	0.1297	<LOD	2.3344
Elba	ELB_Ar1	0.4754	0.4754	<LOD	0.4754	<LOD	<LOD	<LOD	<LOD	<LOD	<LOD	<LOD	<LOD	<LOD	<LOD	<LOD
Elba	ELB_Br1	10.9107	13.6384	<LOD	5.4554	<LOD	<LOD	<LOD	<LOD	<LOD	<LOD	<LOD	<LOD	<LOD	<LOD	5.4554
Montecatini V. di C.	MB3	0.0882	0.1205	<LOD	<LOD	<LOD	0.0134	<LOD	<LOD	<LOD	<LOD	<LOD	<LOD	<LOD	<LOD	0.0536
Montecatini V. di C.	MB1	0.3529	0.6432	0.0627	0.2108	<LOD	0.0162	0.0713	0.0065	0.0326	0.0099	0.0161	<LOD	0.0158	<LOD	0.1960
Boccheggiano	BCpy	0.4716	0.8683	0.0737	0.2393	<LOD	0.0082	0.0322	<LOD	0.0188	<LOD	<LOD	<LOD	0.0145	<LOD	0.1049
Campiglia M.ma	T31	0.0997	0.2607	0.0261	0.0848	<LOD	0.0077	<LOD	0.0030	0.0138	0.0029	<LOD	<LOD	0.0090	<LOD	0.0869
Campiglia M.ma	T32	0.1293	0.2681	0.0266	0.0774	<LOD	<LOD	<LOD	<LOD	0.0269	<LOD	<LOD	<LOD	0.0097	0.0025	0.0987
Campiglia M.ma	T42	0.0424	0.1028	0.0133	0.0366	<LOD	<LOD	<LOD	<LOD	0.0119	<LOD	<LOD	<LOD	<LOD	<LOD	0.0477
Campiglia M.ma	T41	0.1296	0.2181	0.0167	0.0700	<LOD	<LOD	<LOD	<LOD	0.0153	<LOD	<LOD	<LOD	<LOD	<LOD	0.0408
Campiglia M.ma	T3A	0.1408	0.3219	0.0295	0.1141	<LOD	0.0067	0.0238	0.0044	0.0219	0.0059	0.0113	<LOD	0.0128	0.0029	0.1474
Campiglia M.ma	T4B	0.0896	0.1791	0.0167	0.0532	<LOD	0.0058	<LOD	<LOD	0.0199	0.0035	0.0098	<LOD	<LOD	0.0024	0.0797
Campiglia M.ma	CT2	2.6230	0.6214	0.3940	1.7304	0.3660	0.1650	0.5673	0.0809	0.5742	0.1497	0.4768	0.0539	0.3968	0.0609	6.4788
Campiglia M.ma	MT1c	0.7699	0.8693	0.1671	0.5837	0.1086	0.0398	0.1696	0.0234	0.1285	0.0327	0.0765	0.0129	0.0603	<LOD	1.3920
Campiglia M.ma	MT1a	0.6467	0.8094	0.1297	0.5889	0.1020	0.0506	0.1280	0.0224	0.0898	0.0268	0.0699	0.0137	0.0635	0.0167	1.0016
Campiglia M.ma	CT1	0.9775	0.8329	0.2115	0.7706	0.1570	0.0838	0.3669	0.0619	0.3552	0.0879	0.3022	0.0434	0.2652	0.0485	3.3372

CENTRAL-EASTERN SOUTHERN ALPS

Deposit	Sample	^{139}La	^{140}Ce	^{141}Pr	^{146}Nd	^{147}Sm	^{153}Eu	^{157}Gd	^{159}Tb	^{163}Dy	^{165}Ho	^{166}Er	^{169}Tm	^{172}Yb	^{175}Lu	^{89}Y
Valle Imperina	VI01p1	1.2323	2.3970	0.3126	1.2702	0.4205	0.1391	0.5642	0.1070	0.6278	0.1309	0.3440	0.0405	0.2709	0.0407	3.0119
Valle Imperina	VI03p1	1.0924	1.8177	0.1863	0.6984	0.1687	0.1203	0.1825	0.0289	0.1819	0.0314	0.0692	<LOD	0.0636	<LOD	1.0032
Valle Imperina	VI04p1	0.4650	0.8411	0.0871	0.2985	0.0756	0.0513	0.0716	0.0095	0.0473	<LOD	<LOD	<LOD	<LOD	<LOD	0.2000
Valle Imperina	VIMP_Cunat	0.2541	0.6210	0.0697	0.4468	0.1762	0.0430	0.1373	0.0307	0.1414	0.0266	0.0779	0.0143	0.0594	0.0143	0.5902
Cinque Valli	5VA 1p	1.5316	2.5145	0.3190	1.3625	0.3262	0.0684	0.3002	0.0296	0.1542	0.0191	0.0481	0.0068	0.0204	<LOD	0.5842
Grua	GRUA_Ddxp1	5.3205	11.0621	1.3014	5.0909	1.2249	0.3828	1.3780	0.2297	1.3397	0.2297	0.6124	0.0766	0.4976	0.0766	6.5454
Grua	GRUA_Cp1	2.6935	5.7136	0.6802	2.6663	0.6802	0.1905	0.7346	0.1360	0.7890	0.1632	0.4081	0.0544	0.3537	0.0544	4.1083
Grua	GRUA_Ep1	15.0401	35.1716	3.3943	12.8163	2.6335	0.5267	2.2823	0.2926	1.3460	0.2341	0.4682	0.0585	0.4097	0.0585	5.1499
Grua	GRUA_Gs1	31.3028	93.0296	16.0358	79.1905	26.5799	7.6884	24.6029	4.3934	25.4816	4.1737	10.5441	1.4278	9.5556	1.0983	75.5660
Grua	GRUA_As1	40.3523	106.8983	12.3181	50.8298	13.3092	4.5308	13.8755	2.4070	15.2914	2.6902	7.3625	0.9911	6.7962	0.8495	68.8113
Grua	GRUA_Dsxp1	8.9496	17.3112	1.9598	7.3164	1.4372	0.3266	1.3065	0.1960	0.9146	0.1307	0.3920	0.0653	0.3266	<LOD	4.3768
Valbona	VBO1Ap1	2.2448	4.9226	0.4314	2.5423	<LOD	<LOD	0.5655	<LOD	0.2553	<LOD	0.2509	<LOD	0.1561	<LOD	1.5911
Valbona	VBO1As1	12.3187	29.2860	3.6386	15.0509	3.5760	0.8011	3.0861	0.4295	2.2531	0.3995	1.1827	0.1706	1.0104	0.1644	9.1915
Valbona	VBO2p1	5.4901	13.4947	1.6894	7.5667	1.4857	0.3851	1.3248	0.1580	1.0814	0.1949	0.5001	0.0506	0.5179	0.0550	3.9228
Valbona	VBE1Ap1	29.0405	57.3048	6.7373	28.9327	6.0625	1.3764	6.1660	0.8417	4.4779	0.8712	2.3155	0.3053	1.9798	0.2984	23.9094
Valbona	VBE2Ap1	2.5836	5.7980	0.4991	1.9317	<LOD	0.0276	0.1955	0.0251	0.0994	0.0268	0.0530	<LOD	0.0511	<LOD	0.5411
Pattine	PA04p1	7.5628	17.0181	2.1923	9.2932	2.1806	0.6491	2.1827	0.3316	1.7318	0.3223	1.0065	0.1221	0.8587	0.1172	7.4801
Pattine	PAT_P1	1.4750	3.3697	0.3611	1.6486	0.4940	0.1528	0.5664	0.1399	0.8412	0.1786	0.4077	0.0555	0.2688	0.0268	4.4856
Pattine	PAT_P2	0.6909	1.3272	0.1693	0.9103	0.1848	0.0592	0.3150	0.0856	0.5835	0.1147	0.3268	0.0319	0.1939	0.0173	3.5866

Pattine	PAT_P3	0.0483	0.0801	<LOD	0.0954	0.0294	0.0177	0.0742	0.0177	0.1072	0.0165	0.0589	0.0059	0.0377	0.0012	0.5289
Montefondoli	MFO_Ap1	1.2730	2.6840	0.3569	1.4280	0.4156	0.0949	0.4562	0.0877	0.5488	0.1009	0.2182	0.0285	0.1571	0.0201	2.3490
Montefondoli	MFO_Ap2	1.4819	4.5445	0.5377	2.2902	0.5452	0.1236	0.4450	0.0647	0.3050	0.0476	0.0925	0.0108	0.0677	0.0074	0.7751
Montefondoli	MFO_Ap3	0.4446	1.0931	0.1471	0.6433	0.2127	0.0956	0.3567	0.0592	0.4879	0.0988	0.3007	0.0479	0.3723	0.0531	2.2419
Montefondoli	TIL-As	202.7866	303.8326	61.6003	284.1792	72.9853	13.0327	73.2235	10.3031	55.3470	10.5215	29.4403	4.0428	27.0481	3.8920	208.9407
Stelvio	STE_1p1	0.2117	0.6352	<LOD	0.2117	<LOD	<LOD	<LOD	<LOD	<LOD	<LOD	<LOD	<LOD	<LOD	<LOD	0.2117
Val Martello	VVN_2p1	1.0062	0.8049	<LOD	0.6037	0.4025	<LOD	0.8049	0.2012	1.2074	0.2012	0.6037	0.2012	0.8049	<LOD	7.2445
Val Martello	VVN_3p	2.6904	5.2504	0.7053	2.8302	0.5884	0.1075	0.4962	0.0713	0.2949	0.0548	0.1187	0.0169	0.1241	0.0163	1.0594
Val Martello	VVN_5p	7.2232	15.5236	1.8216	7.0776	1.3818	0.2161	1.1211	0.1374	0.5093	0.0689	0.1445	0.0142	0.0750	0.0101	1.0819
Oris	ORI_1p1	1.4847	0.9898	0.2475	0.7424	0.4949	<LOD	0.9898	0.2475	1.4847	0.2475	0.7424	<LOD	0.7424	<LOD	8.4135
Predoi	PRE_IDp1	1.1480	2.4503	0.2742	1.0795	0.2228	0.0514	0.2228	0.0343	0.1713	0.0343	0.0857	0.0171	0.0857	0.0171	0.8910
Predoi	PRE_IICp1	0.0378	0.0662	0.0095	0.0378	0.0189	<LOD	0.0378	0.0095	0.0567	0.0095	0.0378	0.0095	0.0378	0.0095	0.3593
Predoi	PRE_IIIAs1	4.3272	4.2423	1.8666	12.2180	6.5332	3.0545	17.5633	4.3272	34.1933	8.4847	26.3025	3.7333	22.3147	3.4787	232.9895
Predoi	PRE_IGS1	4.1694	4.0121	1.8094	11.6429	6.3721	2.9894	16.8350	4.2481	33.5913	8.3388	25.7245	3.6187	22.1844	3.3827	224.9123
Predoi	PRE_IHs1	1.0612	4.3415	1.0612	7.3322	4.9203	2.0260	7.7182	1.8331	13.9892	3.0873	10.2266	1.7366	13.6033	2.0260	58.1756
Predoi	PRE_ICp1	0.3237	0.6473	0.1618	0.4855	0.1618	<LOD	0.1618	<LOD	0.1618	<LOD	<LOD	<LOD	<LOD	<LOD	0.4855

WESTERN ALPS

Deposit	Sample	$^{63}Cu/^{65}Cu$	δ63	^{47}Ti	^{52}Cr	^{55}Mn	^{59}Co	^{60}Ni	^{66}Zn	^{107}Ag	^{111}Cd	^{137}Ba	^{193}Ir	^{103}Rh	^{105}Pd	^{195}Pt	^{197}Au
Piedmont zone																	
Chialambert o	CHIAL67			30.7045	<LOD	<LOD	16.7032	432.9334	<LOD	22.7213	0.4913	<LOD	<LOD	36.3418	74.4891	0.7369	17.5016
Alagna-Fabbriche	ALA_Ap1	2.243966	-0.0157	165.1447	104.7371	81.3091	137.8120	77.1747	5119.7154	93.9418	21.3609	8.4984	0.2297	1.6484	3.7323	<LOD	0.3229
Alagna-Fabbriche	L87'			10.9132	<LOD	731.4592	26.7994	573.1490	10121.6265	76.1160	42.5476	40.1992	<LOD	30.3635	61.4039	0.6783	12.6607
Chuc-Servette	46/5			17.8700	<LOD	<LOD	45.6850	94.4779	663.0546	9.3235	3.2632	4.9725	<LOD	2.4505	5.3066	0.5532	1.0085
Petit monde	A5b			21.3423	<LOD	153.3438	47.9893	458.6743	445.7209	18.0114	11.1029	2.2206	<LOD	3.1693	5.8352	0.1727	1.1239
Usseglio	M/U 3761			4.9953	11.0872	12.6710	<LOD	48.7347	601.1429	46.5417	<LOD	24879.0784	<LOD	2.8449	3.6868	0.3716	2.8205
Cruvino	M/U 9748			7.0461	<LOD	<LOD	2575.6344	8434.7691	92.9006	22.1140	<LOD	<LOD	<LOD	0.1453	0.7014	0.2244	28.3038
Ligurian Briançonnais zone																	
Saint Verain	SVE - Ap1	2.24091	-1.379	1165.4167	242.9418	124.9918	10.5627	169.4431	<LOD	9.2424	<LOD	8.3621	<LOD	<LOD	3.3281	<LOD	0.5180
Saint Verain	SVE - Ap2	2.2411468	-1.2714674	<LOD	146.8239	16.2504	68.4228	111.1870	<LOD	6.8423	<LOD	9.9783	7.6006	<LOD	3.3755	<LOD	0.7438
Saint Verain	SVE - Ap3	2.2434512	-0.244558	545.2589	298.7654	177.4369	37.4056	158.7341	20894.3961	33.0896	90.1571	19.6619	<LOD	<LOD	1.0090	0.4592	<LOD
Saint Verain	SVE - Ap4	2.2424404	-0.6950105	<LOD	177.8276	22.0071	9.8653	108.2649	592.9274	10.3712	4.5532	4.0473	14.5652	<LOD	0.9066	0.1324	1.2400
Saint Verain	SVE-Ar1	2.241837	-0.9639103	258.5375	276.5517	41.6996	17.0134	189.4830	494.3904	17.3470	3.0024	8.6735	3.9798	<LOD	0.9508	0.4524	2.9814
Saint Verain	SVE-Br1	2.2409686	-1.3508958	<LOD	191.7207	84.7358	16.0951	106.9849	473.8579	80.4754	<LOD	11.8346	<LOD	<LOD	1.0561	0.3940	<LOD
Saint Verain	SVE-Bp1	2.2418007	-0.9800757	<LOD	344.9769	240.5830	50.8722	201.8989	8531.6879	87.4366	48.7525	4.2393	<LOD	<LOD	1.7556	<LOD	4.7820

Saint Verain	SVE-Bs1	2.23583	-3.6405	464.3802	1013.0579	600.6198	62.8512	552.2727	2426.0331	12.7686	14.1322	16.1157	6.9273	<LOD	1.3091	<LOD	3.3955
Saint Verain	SVE-Cp1	2.24087	-1.3933	246.3611	121.0459	84.1294	39.6790	114.0142	52963.8789	58.0116	278.2550	19.3372	17.2403	<LOD	1.6708	<LOD	0.4312
Saint Verain	SVE-Cs1	2.2367857	-3.2149448	1145.2171	639.0485	872.7634	37.5995	398.2125	2150.5756	6.5514	13.2453	29.9087	3.1219	<LOD	0.9829	0.0377	1.9782
via fiorcia	VF2a			11.2813	<LOD	3.3426	339.4154	501.2539	1091.0873	5.5710	5.4318	4.0390	<LOD	2.7423	4.9248	0.1643	1.1240
Murialdo-Pastori	MUR-1			6.1919	3.0959	<LOD	<LOD	2.6738	1718.2464	92.8782	25.3304	11.6801	<LOD	5.0520	9.1823	0.2632	1.5747
Murialdo-Pastori	PAS-1			9.3055	<LOD	7.8099	3.4896	<LOD	599.3719	1824.5365	33.5662	1.1632	<LOD	1.2961	3.0043	0.3390	1.0934

LIGURIAN APENNINES

Deposit	Sample	$^{63}Cu/^{65}Cu$	δ63	^{47}Ti	^{52}Cr	^{55}Mn	^{59}Co	^{60}Ni	^{66}Zn	^{107}Ag	^{111}Cd	^{137}Ba	^{193}Ir	^{103}Rh	^{105}Pd	^{195}Pt	^{197}Au
Libiola	LIB_L2p1	2.2430173	-0.4379102	273.8508	409.9733	109.0709	726.9338	355.2526	7263.1615	45.8271	42.8625	3.2116	<LOD	0.8647	2.5940	4.8174	8.6466
Libiola	LIB_Fs1	2.2430063	-0.442838	2177.1335	710.9427	687.7629	578.3194	397.4296	35664.4982	4.2545	99.1740	4.1078	<LOD	0.5868	6.8952	1.6138	3.0808
Libiola	LIB_Bp1	2.2486331	2.0646509	599.1489	350.5726	326.6295	30.3576	65.0338	1442.3015	31.7548	9.5264	3.2390	4.0646	0.1905	1.7148	1.0162	2.7309
Libiola	LIB_Gs1	2.2426243	-0.6130523	337.8204	291.6689	139.8403	45.5971	113.0226	25660.4874	3.1183	21.9670	8.1077	4.8508	0.4851	6.5832	0.2079	3.5341
Libiola	LIB_Ep1	2.242937	-0.4736953	193.5352	326.6352	143.8520	473.3407	137.1256	513.6478	4.9938	3.4651	<LOD	1.9873	<LOD	0.6115	0.2038	3.3122
Monte Loreto	LOR_As1	2.2431708	-0.3695396	497.3474	564.7371	325.0673	15.9656	53.8375	676.5893	2.1349	2.5991	7.9828	6.1263	0.8354	3.8058	2.5991	8.3541
Monte Loreto	LOR_Bp1	2.2411135	-1.2863049	275.2791	484.8889	211.3245	92.2455	48.5232	1946.9285	14.3169	16.3744	3.7721	3.0863	1.2002	4.3722	0.5144	4.8009
Monte Loreto	LOR_M2P1	2.2441836	0.0818121	1746.7736	879.5721	913.9582	51.5792	71.0787	1267.4644	13.6286	12.7900	10.2739	10.2739	0.8387	3.7741	1.0484	7.7578
Monte Loreto	LOR_M3p1	2.2464397	1.0871957	793.0655	843.4689	429.2162	42.1341	164.5985	576.4886	11.0257	10.4351	8.6631	11.2226	0.7876	3.3471	2.9533	6.1035
Bonassola	BON_Ap1	2.244048	0.0213942	121.6842	123.2355	44.4682	637.3772	107.5509	1814.9221	3.4471	5.5154	3.6195	<LOD	1.1758	20.2972	4.4994	0.9323
Bonassola	BON_Ap2	2.2440286	0.0127456	123.1662	136.2947	128.6940	3947.1923	811.2042	2580.7901	5.8733	2.4184	11.2283	<LOD	1.1116	2.6280	<LOD	0.7386
Reppia	REP_As1	2.24342	-0.2576	78.9277	220.7905	210.4356	79.7331	263.3609	413.6227	0.3452	4.8323	4.2570	0.1151	0.1597	0.8975	0.0195	0.0572
Reppia	REP_As2	2.24285	-0.5133	149.4432	252.3616	9217.2297	2977.8983	479.5027	2058.3684	1.5665	4.8561	8.4590	<LOD	2.3928	6.8510	0.0388	0.0573
Piazza	PIA_Bp1	2.2435	-0.2221	201.3842	258.4523	52.9525	9.8772	76.5480	572.8751	180.5325	4.3898	<LOD	0.2744	1.9778	4.2336	<LOD	0.5632
Piazza	PIA_Bp2	2.24448	0.2154	242.2659	311.7371	47.9822	30.3200	109.5054	990.8470	178.0934	5.5930	10.8917	<LOD	2.6349	5.5215	<LOD	0.0528

SOUTHERN TUSCANY

Deposit	Sample	Cu63/65	δ63	47Ti	52Cr	55Mn	59Co	60Ni	66Zn	107Ag	111Cd	137Ba	^{193}Ir	103Rh	105Pd	195Pt	197Au
Elba	ELB_Cs1	2.2448967	0.3996155	440.6836	526.2784	137.7298	19.0643	46.1693	405.7973	8.6892	4.0204	10.7642	6.2251	1.4266	5.8360	5.8360	3.7610
Elba	ELB_Ar1	2.2416347	-1.0540634	1643.9792	3123.9409	172.5750	52.2955	110.7713	<LOD	145.4765	13.3116	10.9345	14.2624	3.8033	15.6886	0.4754	15.6886
Elba	ELB_Br1	2.2445947	0.2650275	14516.7051	18793.7050	1721.1651	3093.1874	2351.2589	7331.9999	392.7857	100.9241	286.4062	444.6116	19.0937	90.0134	32.7321	177.2991
Montecatini V. di C.	MB3	2.2411679	-1.2620547	38.7740	25.3425	9.6301	8.1096	<LOD	38.2671	526.1093	4.0548	2.0274	0.2534	5.3422	10.7731	<LOD	1.0588
Montecatini V. di C.	MB1	2.2406059	-1.4888697	9.9888	41.8283	23.3073	11.0294	49.9442	181.4641	509.0151	9.1564	5.4106	0.2081	5.2774	13.1853	<LOD	0.2649
Boccheggiano	BCpy	2.2417901	-0.9848041	33.9087	30.9458	25.5138	3.4567	26.5014	96.9525	65.6775	3.9505	4.7736	<LOD	2.8230	12.8639	0.3404	0.3039
Campiglia M.ma	T31	2.2460829	0.9281879	78.8694	61.4065	110.3599	365.8623	54.3927	6316.7065	582.8604	26.9101	8.0158	0.0997	1.1168	4.7250	<LOD	0.1777
Campiglia M.ma	T32	2.2458074	0.8054415	121.6916	81.7156	46.4427	220.4558	117.3805	7903.0949	657.8401	28.4143	1.9596	0.1293	1.4013	5.3419	<LOD	1.0538
Campiglia M.ma	T42	2.2447122	0.3173637	83.4289	42.6108	290.4152	33.9231	66.4673	7722.3427	985.8398	30.0620	1.5169	0.0424	1.2932	4.9051	<LOD	0.3600

Campiglia M.ma	T41	2.245647 8	0.7343165	95.1586	61.0451	403.2569	38.4225	85.1041	9020.3144	1018.3763	36.4475	1.9750	0.1296	1.2931	5.9519	<LOD	0.2400
Campiglia M.ma	T3A	2.243215 9	-0.3494287	112.6649	70.5456	62.3990	383.7540	83.0254	7285.0859	651.8965	25.3063	3.9866	0.1408	1.3948	5.6714	<LOD	0.2481
Campiglia M.ma	T4B	2.244695	-0.309696	107.6169	64.2258	334.7316	38.0533	83.8551	11004.4731	1152.9644	42.7024	4.6490	0.0896	1.4853	6.4054	<LOD	0.2384
Campiglia M.ma	CT2	2.242388 3	-0.71822	12.9626	35.3295	96.8385	4.8292	39.6504	4969.0080	<LOD	26.9419	7.1167	0.2542	0.6738	1.3339	<LOD	0.5421
Campiglia M.ma	MT1c	2.242544	0.6488439	18.0747	42.4253	451.3647	6.7780	7.7822	4661.7590	70.0394	70.2904	6.2759	<LOD	4.3153	7.9026	<LOD	0.4765
Campiglia M.ma	MT1a	2.238872 6	-2.2849317	23.4007	43.8190	732.5341	14.2240	34.8717	3321.9839	<LOD	49.7839	6.4237	<LOD	2.9205	5.7974	<LOD	0.2008
Campiglia M.ma	CT1	2.243632 6	-0.1637154	14.8002	43.2071	117.9243	3.8194	49.6523	7459.7833	<LOD	60.8718	6.6840	0.4774	1.3308	2.5423	<LOD	0.1317

CENTRAL-EASTERN SOUTHERN ALPS

Deposit	Sample	Cu63/65	δ63	47Ti	52Cr	55Mn	59Co	60Ni	66Zn	107Ag	111Cd	137Ba	193Ir	103Rh	105Pd	195Pt	197Au
Valle Imperina	VI01p1	2.2429842	-0.4526693	393.0542	201.5130	1098.9728	43.2110	60.6616	<LOD	175.3371	<LOD	28.2534	40.2818	<LOD	2.9201	0.2319	2.7132
Valle Imperina	VI03p1	2.2417679	-0.9946868	<LOD	100.0879	463.6195	352.1227	150.0022	45013.6173	201.7315	288.2064	98.4025	3.4862	0.2383	0.4914	0.2883	6.0584
Valle Imperina	VI04p1	2.2518712	3.5076721	150.2938	129.8305	50.5565	11.0055	67.2367	10529 1.6646	115.2138	327.9295	6.3626	<LOD	<LOD	13.2685	0.2352	29.6289
Valle Imperina	VIMP_Cunat			104.1066	<LOD	27.2563	1.4345	<LOD	65.5790	150.4218	0.2049	8.4023	0.4099	6.9678	13.9683	0.2213	0.4836
Cinque Valli	5VA 1p	2.2424434	-0.6936702	<LOD	6.1499	3.0749	4.4726	24.5994	710.8678	76.5937	<LOD	6.4294	<LOD	1.5551	3.4216	0.0988	0.6919
Grua	GRUA_Ddxp1	2.2444561	0.2032472	100.2482	167.4248	973.3909	82.5258	44.4782	2931.2730	28.7079	19.3300	0.3828	1.9521	0.1914	1.0718	0.4976	3.3684
Grua	GRUA_Cp1	2.2451863	0.528638	104.4768	186.0721	384.7141	83.7175	58.0336	1023.2741	60.0197	8.0262	3.3737	1.2243	0.2449	0.9523	1.9861	4.5981
Grua	GRUA_Ep1	2.2446951	0.3097698	235.7255	351.7156	422.4684	72.2743	45.0617	877.2408	97.9654	7.7249	1.8142	1.8727	0.4682	1.5216	0.2926	3.1602
Grua	GRUA_Gs1	2.2413766	-1.1690744	286.4478	356.5221	1159.8502	32.1814	95.1165	1688.1531	11.7523	15.5965	8.0179	3.6245	1.2082	8.5671	42.5059	26.3602
Grua	GRUA_As1	2.2426207	-0.6146731	423.9118	518.6335	2336.1871	26.6184	58.1923	1758.5117	22.0876	8.3536	11.7517	19.5390	0.5663	5.6635	0.7079	4.9555
Grua	GRUA_Dsxp1	2.2429588	-0.4639755	181.6695	190.8803	509.3408	64.0841	138.6855	2251.7607	43.1147	16.6579	7.7084	4.8994	0.2613	1.3065	0.0653	2.5477
Valbona	VBO1Ap1	2.2435585	-0.1967403	3550.4015	2184.8625	2258.1353	587.0708	695.6478	4589.5434	228.7000	148.5440	246.2411	<LOD	<LOD	<LOD	0.1910	<LOD
Valbona	VBO1As1	2.2447529	0.3355247	13440.9274	2997.6635	1200.3603	237.6118	649.3858	1371.0696	67.1183	29.3508	193.5856	<LOD	<LOD	2.8725	2.5596	3.4422
Valbona	VBO2p1	2.2416171	-1.061892	2597.5203	2562.9482	593.2580	364.6209	1958.1662	5741.2805	62.2299	37.3379	101.6421	6.1239	<LOD	2.2276	1.0853	2.4846
Valbona	VBE1Ap1	2.2391619	-2.1559945	1013.5066	237.8000	2608.6854	140.1360	129.5719	<LOD	9.0549	1.7248	70.7148	18.8019	<LOD	2.9278	0.9445	1.3250
Valbona	VBE2Ap1	2.2411847	-1.2545903	271.7828	170.4820	324.9040	22.2368	72.0636	<LOD	84.0056	2.4708	37.8849	30.8515	<LOD	3.6563	<LOD	11.2007
Pattine	PA04p1	2.2386563	-2.3813172	406.0620	82.3844	2144.4073	1130.2864	133.4007	12212.8837	10.6858	27.5764	81.0056	21.4199	<LOD	1.3488	0.1179	0.5967
Pattine	PAT_P1			5.5549	<LOD	476.0391	17.8552	18.8471	<LOD	11.9035	<LOD	17.5576	0.1984	<LOD	0.3363	0.1914	<LOD
Pattine	PAT_P2			13.2906	<LOD	101.3181	9.1942	<LOD	14.7471	4.2785	0.0910	14.8381	0.1821	<LOD	0.2485	0.0555	<LOD
Pattine	PAT_P3			<LOD	<LOD	164.6718	6.4785	<LOD	59.6022	1.1779	<LOD	3.6515	0.2356	<LOD	<LOD	0.0624	<LOD
Montefondoli	MFO_Ap1	2.24455	0.2465	126.6750	94.5692	371.6012	175.9463	65.6421	10164.1994	177.2179	74.8606	8.9006	<LOD	1.1980	3.4318	0.0686	0.8325
Montefondoli	MFO_Ap2	2.24256	-0.641	97.5904	63.7440	164.6250	430.2251	83.9578	35952.3749	171.4883	200.9159	4.6069	<LOD	0.4397	1.0144	0.0192	1.6405
Montefondoli	MFO_Ap3	2.23889	-2.2787	120.8281	95.7619	1032.9681	73.9979	28.8186	7365.2633	49.8322	57.7874	<LOD	<LOD	0.7029	1.5769	0.0417	0.1618

Montefondoli	TIL-As	2.2385	-2.4497	230.4232	75.1927	790.2222	82.5536	667.1372	4157.4949	0.9318	108.3632	62.4276	0.0932	0.4780	4.0786	1.9971	0.0692
Stelvio	STE_1p1	2.2468362	1.2639117	531.2688	701.3002	53.9950	126.4119	38.3259	1102.1340	325.2407	72.8404	5.7171	4.2349	1.0587	6.7758	2.7527	9.7403
Val Martello	VVN_2p1	2.2412929	-1.2063932	634.0969	846.4016	1346.0724	1081.4461	77.8786	1735.2641	382.3497	91.7639	21.1299	4.6284	1.2074	5.4334	1.4087	13.6841
Val Martello	VVN_3p	2.2434028	-0.2661275	357.0305	122.2740	57.3159	49.6738	80.4811	4262.8728	177.9182	40.1212	4.7763	<LOD	1.3818	3.2052	0.0993	0.3361
Val Martello	VVN_5p	2.2442601	0.1158943	360.4749	73.0007	52.6221	824.4731	147.9034	924.7358	32.5152	4.2569	15.7595	<LOD	0.2947	0.9908	0.1492	0.1546
Oris	ORI_1p1	2.2463851	1.0628902	985.8647	1575.3049	1565.4067	1292.2152	131.1517	2206.3177	448.6377	112.0976	20.2914	50.9759	1.4847	6.6813	9.6508	17.8168
Predoi	PRE_IDp1	2.2423193	-0.7489688	125.5643	117.5623	53.9577	857.9427	91.8600	166.8250	1.8334	2.3646	10.3837	<LOD	0.0685	0.2913	0.0171	0.4284
Predoi	PRE_IICp1	2.2439848	-0.0067685	86.3196	86.7829	24.4520	1239.6203	123.6784	118.0050	3.4418	2.7988	0.5106	1.8722	0.0946	0.3782	0.0756	0.5390
Predoi	PRE_IIIAs1	2.2463983	1.0687627	642.5454	566.3529	431.9554	121.2462	219.0746	2854.2489	2.9696	20.5329	11.3695	<LOD	1.4424	14.6785	0.3394	2.1212
Predoi	PRE_IGS1	2.2448024	0.3575663	490.0240	377.9219	471.6156	114.3048	229.9470	2931.1757	3.7761	19.1164	11.6429	2.9107	1.4947	14.0816	0.3933	2.9107
Predoi	PRE_IHs1	2.2444674	0.2082922	305.5426	458.0727	69.7529	14.2786	56.0531	172.1149	3.4732	<LOD	3.5696	5.8851	0.1930	4.9203	0.8683	6.2710
Predoi	PRE_ICp1	2.2492123	2.3227722	465.7680	540.2133	114.2572	213.4635	119.7597	1018.2809	16.1837	10.5194	4.0459	<LOD	0.6473	3.5604	0.4855	7.2827

WESTERN ALPS

Deposit	Sample	69Ga	72Ge	75As	80Se	115In	118Sn	121Sb	125Te	^{205}Tl	209Bi	208Pb	^{232}Th	238U
Piedmont zone														
Chialamberto	CHIAL67	1.8423	2.4564	<LOD	157.6983	<LOD	7.7375	33.1609	0.9825	<LOD	7.4919	93.0960	1.2159	1.7195
Alagna-Fabbriche	ALA_Ap1	2.2969	23.4280	26.1838	248.9757	3.2156	40.1952	1.3781	3.6750	0.2297	2.2969	35.3717	0.0484	1.1484
Alagna-Fabbriche	L87'	1.2433	8.1503	3.5917	193.5362	<LOD	7.0452	3.3154	1.6577	<LOD	3.4535	253.3515	0.3371	<LOD
Chuc-Servette	46/5	<LOD	9.1681	11.8097	51.1237	<LOD	<LOD	16.9377	0.9323	<LOD	<LOD	166.7349	<LOD	<LOD
Petit monde	A5b	0.6168	9.8693	12.3366	41.6977	<LOD	<LOD	23.6862	<LOD	<LOD	4.1944	29.9779	0.6366	<LOD
Usseglio	M/U 3761	613.5702	1.3402	4326.4254	14.6204	<LOD	<LOD	42411.3966	<LOD	<LOD	182.2679	76221.1138	0.9113	<LOD
Cruvino	M/U 9748	0.8672	4.1193	161085.5529	41.8432	<LOD	<LOD	1570.7467	0.7588	<LOD	385.6947	24.7157	0.6363	13.0083
Ligurian Briançonnais zone														
Saint Verain	SVE - Ap1	14.9638	10.1226	3336.9294	<LOD	<LOD	<LOD	0.8635	11.4429	<LOD	6.1616	10.1226	0.1760	8.8022
Saint Verain	SVE - Ap2	19.6715	23.0927	3746.1469	<LOD	<LOD	<LOD	0.4830	13.6846	<LOD	<LOD	7.6976	<LOD	0.8553
Saint Verain	SVE - Ap3	19.6619	25.8962	46.0377	<LOD	2.3978	<LOD	<LOD	17.7437	<LOD	10.5503	2403.0714	5.3567	0.4796
Saint Verain	SVE - Ap4	16.1891	51.3499	16.9480	111.8063	2.2766	<LOD	<LOD	6.5768	<LOD	0.7589	27.3192	0.0501	1.7707
Saint Verain	SVE- Ar1	26.6877	61.3818	29.6901	<LOD	0.6672	<LOD	<LOD	4.0032	<LOD	<LOD	33.3597	0.4183	0.3336
Saint Verain	SVE- Br1	15.6217	19.8822	14.2015	<LOD	0.9468	<LOD	<LOD	29.8232	<LOD	15.1483	52.0723	<LOD	0.4734
Saint Verain	SVE- Bp1	17.4873	34.4447	33.9148	<LOD	1.0598	<LOD	<LOD	20.6668	1.0598	15.8976	174.3432	1.5013	0.5299
Saint Verain	SVE- Bs1	13.0165	15.0000	11.4050	<LOD	0.3719	<LOD	0.2821	6.4463	<LOD	2.8512	91.1157	0.3288	1.7355
Saint Verain	SVE- Cp1	17.5793	24.1087	15.5702	80.1113	2.2602	<LOD	<LOD	19.8395	<LOD	15.5702	239.3294	0.0702	0.2511
Saint Verain	SVE- Cs1	12.8180	10.6817	86.7351	<LOD	<LOD	<LOD	0.9978	5.4120	<LOD	1.1394	343.9497	0.6059	1.7091
via fiorcia	VF2a	1.2535	7.5209	16.7131	119.0809	2.5070	<LOD	42.4791	0.5571	<LOD	0.9749	19.6379	0.3830	<LOD
Murialdo-Pastori	MUR-1	1.4072	19.7014	558.6764	55.8676	17.3091	74.4433	271.0354	<LOD	<LOD	78.3836	312.5492	2.0912	<LOD

Murialdo-Pastori	PAS-1	<LOD	<LOD	9591.2794	110.3363	4.9851	<LOD	1718.1883	<LOD	<LOD	2535.7402	1122.9707	0.4104	<LOD

LIGURIAN APENNINES

Deposit	Sample	69Ga	72Ge	75As	80Se	115In	118Sn	121Sb	125Te	205Tl	209Bi	208Pb	232Th	238U
Libiola	LIB_L2p1	33.3513	137.3577	134.0226	290.6500	1.2352	<LOD	8.3996	15.3169	4.6939	7.7820	133.4050	<LOD	1.8528
Libiola	LIB_Fs1	46.6529	56.6289	59.5631	96.0932	0.2934	<LOD	2.4940	9.5360	0.4401	2.0539	4.8413	<LOD	35.2097
Libiola	LIB_Bp1	30.4846	117.2386	196.1174	124.1611	23.2445	<LOD	1.8418	4.5092	0.3175	1.1432	31.7548	0.1270	0.8891
Libiola	LIB_Gs1	21.1354	20.9968	28.1344	49.8242	0.4851	<LOD	1.2473	4.9893	0.1386	1.1087	5.1279	0.0693	31.3220
Libiola	LIB_Ep1	23.6441	101.3028	101.9142	119.6473	0.9172	<LOD	1.4268	6.0129	1.0191	4.2294	18.1917	<LOD	1.2739
Monte Loreto	LOR_As1	44.0911	40.1925	47.3399	50.3102	<LOD	<LOD	3.4345	6.4976	0.5569	1.7636	2.4134	0.0928	1.2067
Monte Loreto	LOR_Bp1	32.6631	127.3091	40.9789	572.8479	8.4015	<LOD	1.9718	19.1178	0.3429	2.2290	7.9729	<LOD	1.0288
Monte Loreto	LOR_M2P1	68.5626	127.8996	82.8203	272.9923	6.7095	<LOD	2.9354	12.3706	0.4193	3.7741	3.7741	0.2097	2.3064
Monte Loreto	LOR_M3p1	71.0766	104.7445	84.6619	241.3849	12.2071	<LOD	2.5595	10.2382	0.5907	3.3471	2.3627	0.1969	1.9689
Bonassola	BON_Ap1	2.5854	20.6829	16.8389	103.5681	1.0341	2.9301	0.6894	1.2065	1.3789	0.8618	7.7561	0.0809	0.1724
Bonassola	BON_Ap2	4.4913	17.1016	9.9960	264.0758	5.3551	6.2188	0.5182	7.6007	1.0365	2.4184	31.7848	0.0323	0.1727
Reppia	REP_As1	2.1860	2.8764	22.2057	32.7695	<LOD	1.2656	3.6818	<LOD	0.1151	0.1151	8.8592	0.0228	8.8592
Reppia	REP_As2	3.7596	8.4590	89.3456	64.2059	<LOD	2.5064	2.0364	<LOD	7.6758	0.1566	21.1476	0.0193	0.7832
Piazza	PIA_Bp1	6.0360	23.0467	21.3621	1224.5757	1.0975	12.6208	1.0975	42.5266	<LOD	8.7797	147.6086	1.3161	<LOD
Piazza	PIA_Bp2	7.0649	18.8396	21.8175	1178.8144	0.5887	3.8268	0.8831	45.0385	<LOD	16.7790	133.6437	0.0200	0.2944

SOUTHERN TUSCANY

Deposit	Sample	69Ga	72Ge	75As	80Se	115In	118Sn	121Sb	125Te	205Tl	209Bi	208Pb	232Th	238U
Elba	ELB_Cs1	40.2036	44.0943	101.9356	70.4212	4.4094	<LOD	1.6860	11.9314	0.1297	135.5251	63.4180	0.6484	1.9453
Elba	ELB_Ar1	203.0015	193.0178	272.8872	270.0348	<LOD	<LOD	7.1312	40.4101	0.9508	8.5574	<LOD	<LOD	<LOD
Elba	ELB_Br1	1573.8705	1459.3080	5848.1427	1925.7410	10.9107	<LOD	92.7411	163.6607	8.1830	155.4777	155.4777	2.7277	<LOD
Montecatini V. di C.	MB3	1.5205	6.3356	10.8973	364.1710	0.2534	<LOD	2.0274	5.3219	0.5068	333.2533	17.4863	0.0724	0.2534
Montecatini V. di C.	MB1	2.2891	5.8268	7.6997	342.7424	0.2081	<LOD	1.2486	4.1620	0.4162	320.8918	21.4344	0.0328	0.2081
Boccheggiano	BCpy	1.6461	11.3578	30.1228	22.3863	22.5509	<LOD	5.7612	<LOD	<LOD	1.3168	38.5176	0.0234	0.1646
Campiglia M.ma	T31	2.0039	52.1025	91.7518	11.4511	0.7157	2.2902	0.4706	2.1471	<LOD	90.0342	31.3474	0.0646	<LOD
Campiglia M.ma	T32	1.3717	51.9296	69.5660	13.5213	0.7838	4.3111	0.5591	1.7636	<LOD	13.1294	24.1032	0.0307	<LOD
Campiglia M.ma	T42	1.1032	53.3669	42.7487	<LOD	0.9653	1.6548	0.3762	2.4822	<LOD	20.9606	41.3697	0.0187	<LOD
Campiglia M.ma	T41	1.7954	57.9929	41.4748	<LOD	2.3341	1.7954	0.5297	1.9750	0.1795	22.9817	24.4180	0.0427	<LOD
Campiglia M.ma	T3A	1.3866	51.3059	71.2389	12.8265	0.8667	2.7733	1.1662	1.5600	<LOD	27.5596	36.3994	0.0740	<LOD
Campiglia M.ma	T4B	1.3775	58.0270	46.6627	<LOD	1.3775	5.3378	0.6014	2.0662	<LOD	34.9540	44.5964	0.0710	<LOD
Campiglia M.ma	CT2	2.7959	5.0834	21.6044	19.3169	0.5083	<LOD	3.5584	<LOD	0.7625	2.0334	2826.3616	0.0240	1.7792
Campiglia M.ma	MT1c	3.0124	3.5145	250.7861	90.8754	<LOD	<LOD	1.5062	<LOD	<LOD	316.3067	1396.5194	0.0253	<LOD
Campiglia M.ma	MT1a	2.2942	2.7530	161.0520	59.4195	<LOD	<LOD	2.2942	<LOD	<LOD	244.7898	1006.0013	0.1632	<LOD
Campiglia M.ma	CT1	2.8646	3.3420	18.6196	16.4712	0.4774	<LOD	0.9549	<LOD	0.4774	1.6710	1918.0595	0.0316	3.8194

CENTRAL-EASTERN SOUTHERN ALPS

Deposit	Sample	69Ga	72Ge	75As	80Se	115In	118Sn	121Sb	125Te	205Tl	209Bi	208Pb	232Th	238U
Valle Imperina	VI01p1	40.7181	64.8165	59.4152	<LOD	<LOD	<LOD	25.9682	<LOD	0.4155	80.6052	68.9715	0.5867	5.4014
Valle Imperina	VI03p1	13.8723	46.2842	766.8651	<LOD	262.5362	113.5712	180.8583	1.2965	11.1497	330.6012	55787.3258	0.6759	1.9447

Valle Imperina	VI04p1	14.1008	47.8051	16088.6627	<LOD	10.4896	94.5785	60.9429	<LOD	12.5531	147.0266	39344.6560	3.2587	0.5159
Valle Imperina	VIMP_Cunat	3.2789	0.4099	40.4264	36.8128	<LOD	10.8615	1.4345	0.2049	<LOD	0.6148	3.0740	0.3279	0.2049
Cinque Valli	5VA 1p	<LOD	18.7291	20.6238	26.7552	69.0461	517.1610	9.7578	<LOD	0.5591	115.1701	62.3372	0.0607	0.2795
Grua	GRUA_Ddxp1	16.1147	160.0372	1292.2405	86.0856	20.4401	52.4781	7.9234	3.8660	0.5359	34.6026	1185.4469	0.3445	0.6890
Grua	GRUA_Cp1	12.3250	166.4555	1376.9716	131.6843	18.3923	39.8590	6.4754	3.9995	0.2993	94.9270	3147.9079	0.2449	0.5442
Grua	GRUA_Ep1	25.6910	183.5827	948.0521	159.5302	47.2270	54.3667	7.5493	7.6663	0.3511	220.6855	1907.2233	0.5267	0.9949
Grua	GRUA_Gs1	31.9618	44.7026	137.2929	80.2889	1.8672	5.1622	2.7459	9.8851	2.9655	15.1571	1101.6380	1.7573	3.1852
Grua	GRUA_As1	37.3790	37.9453	77.4481	76.5986	40.6355	<LOD	3.5397	8.3536	0.2832	7.2209	3525.5187	3.8229	8.4952
Grua	GRUA_Dsxp1	14.8288	114.5151	948.5224	92.4352	12.8037	57.6822	11.4319	5.7486	0.1307	26.5220	947.2159	0.5879	0.8492
Valbona	VBO1Ap1	199.8350	821.9879	1648.8606	256.6769	4.6628	53.0673	1440.1441	29.3091	64.8353	1.1102	3743.5753	0.1135	2.8865
Valbona	VBO1As1	224.8787	941.5987	481.6980	449.3258	4.9637	88.6998	555.2907	26.7610	11.4382	1.5107	1211.3668	1.0353	17.2652
Valbona	VBO2p1	175.6265	835.4935	498.9913	364.3904	4.6096	19.3604	518.3517	26.2748	11.2936	1.1524	1728.3767	0.9210	11.0631
Valbona	VBE1Ap1	24.3621	24.1465	35.1418	<LOD	<LOD	<LOD	35.4436	3.2339	0.6468	0.2156	35.7886	1.9666	2.8027
Valbona	VBE2Ap1	32.1198	39.9438	39.9438	<LOD	<LOD	<LOD	96.1947	<LOD	0.8236	0.4118	123.1259	0.3488	<LOD
Pattine	PA04p1	18.2693	10.3411	48.9481	<LOD	1.0341	<LOD	0.5477	<LOD	2.0682	16.8905	66.8727	3.4408	5.1706
Pattine	PAT_P1	1.7855	13.1930	540.0674	3.1605	<LOD	2.9759	85.4073	<LOD	10.5147	0.1984	110.9997	0.3492	0.0992
Pattine	PAT_P2	1.5475	10.7417	280.0678	2.0499	<LOD	2.4579	82.7477	<LOD	6.7363	0.0910	52.9804	0.2276	0.0910
Pattine	PAT_P3	1.0601	14.2527	258.5791	<LOD	<LOD	2.9448	150.1835	<LOD	8.5987	0.4712	21.3202	<LOD	<LOD
Montefondoli	MFO_Ap1	3.9735	22.5694	967.9293	267.0081	15.0993	16.3708	98.8605	<LOD	0.6358	83.7613	8878.3765	0.6046	0.6358
Montefondoli	MFO_Ap2	4.5129	21.7181	2520.5231	235.2126	7.7095	11.0001	482.2169	0.4701	2.4445	237.9588	3250.1925	0.0573	0.0940
Montefondoli	MFO_Ap3	2.1014	19.8128	15.7541	54.6850	3.3021	34.3722	185.9703	<LOD	<LOD	6.7544	1981.2814	0.0195	0.1501
Montefondoli	TIL-As	12.9514	5.2178	115.6370	44.4681	0.0932	2.1430	145.1676	<LOD	2.1430	1.0249	72.3974	2.5698	2474.7437
Stelvio	STE_1p1	63.9471	103.3317	80.6749	165.5848	120.2713	81.5219	25.4094	15.6691	0.6352	7.8346	3.8114	0.2117	40.2316
Val Martello	VVN_2p1	73.2502	113.0950	1404.2298	202.2429	94.5813	123.3581	6246.3875	24.1484	0.8049	14124.8047	14873.4052	0.2012	4.2260
Val Martello	VVN_3p	2.8658	19.3441	8.3857	176.0999	259.5934	868.8141	1.9105	1.6717	<LOD	4.0599	34.6284	1.3438	4.7763
Val Martello	VVN_5p	2.3549	22.1900	27.5016	64.9690	26.8998	63.2190	1.6303	0.3623	0.0906	10.1440	264.8313	1.5227	0.6340
Oris	ORI_1p1	129.6669	170.2497	1710.9108	228.8968	105.1688	133.1313	7101.9872	36.1286	1.4847	15832.2349	16438.5021	0.2475	4.7017
Predoi	PRE_IDp1	6.4256	152.0034	35.2293	171.3315	1.0452	3.8553	0.3598	3.7183	0.0857	1.0624	7.3337	0.4969	0.3427
Predoi	PRE_IICp1	2.1559	127.8388	37.3588	170.7669	0.9739	0.5862	0.1986	3.7728	0.0567	0.6997	2.1842	0.0095	0.1513
Predoi	PRE_IIIAs1	28.5086	47.6839	133.3793	83.3196	0.0848	<LOD	2.2909	13.3210	0.4242	1.6969	8.0605	<LOD	2.6303
Predoi	PRE_IGS1	20.6111	32.1753	107.8541	68.0480	0.0787	<LOD	1.4160	12.7442	0.3933	1.4160	4.8774	<LOD	2.5174
Predoi	PRE_IHs1	31.3550	22.3827	37.0472	53.9306	<LOD	<LOD	1.2542	<LOD	0.5789	2.6049	1.5436	0.0965	1.2542
Predoi	PRE_ICp1	40.1357	100.0155	45.1526	226.5724	3.5604	<LOD	0.8092	12.1378	0.3237	5.1788	3.3986	0.6473	0.4855

Appendix3

REE plots

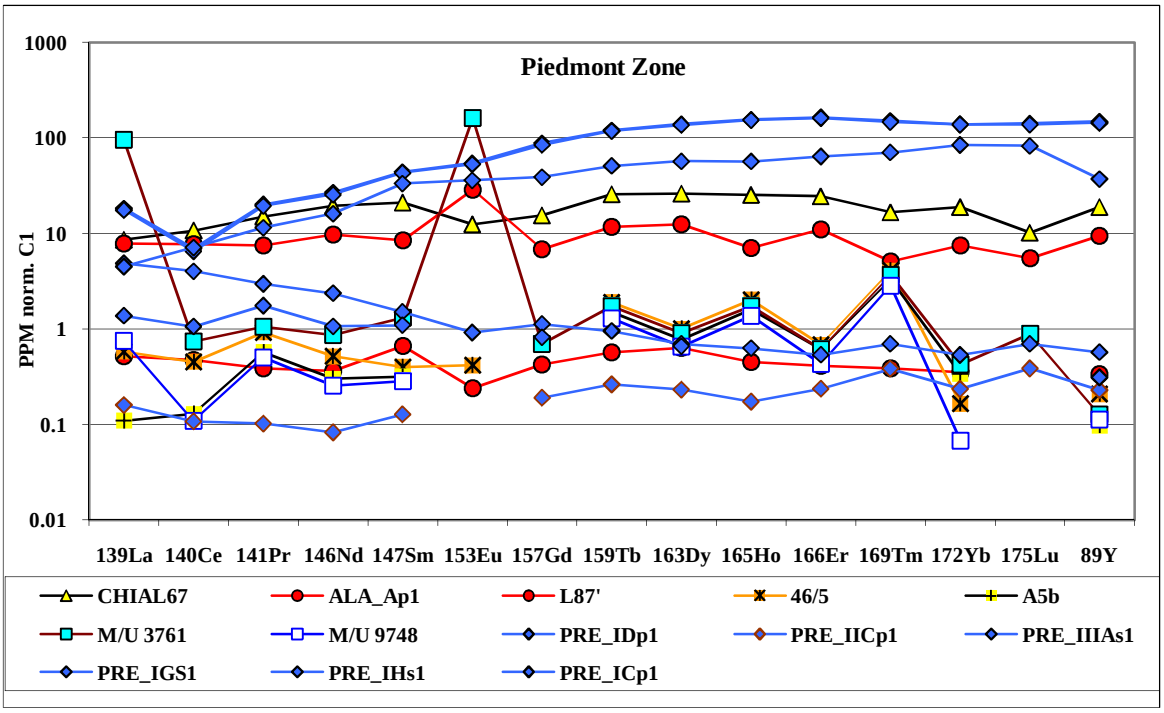
Piedmont Zone
PPM norm. C1
1000
100
10
1
0.1
0.01
139La 140Ce 141Pr 146Nd 147Sm 153Eu 157Gd 159Tb 163Dy 165Ho 166Er 169Tm 172Yb 175Lu 89Y
CHIAL67
ALA_Ap1
L87'
46/5
A5b
M/U 3761
M/U 9748
PRE_IDp1
PRE_IICp1
PRE_IIIAs1
PRE_IGS1
PRE_IHs1
PRE_ICp1

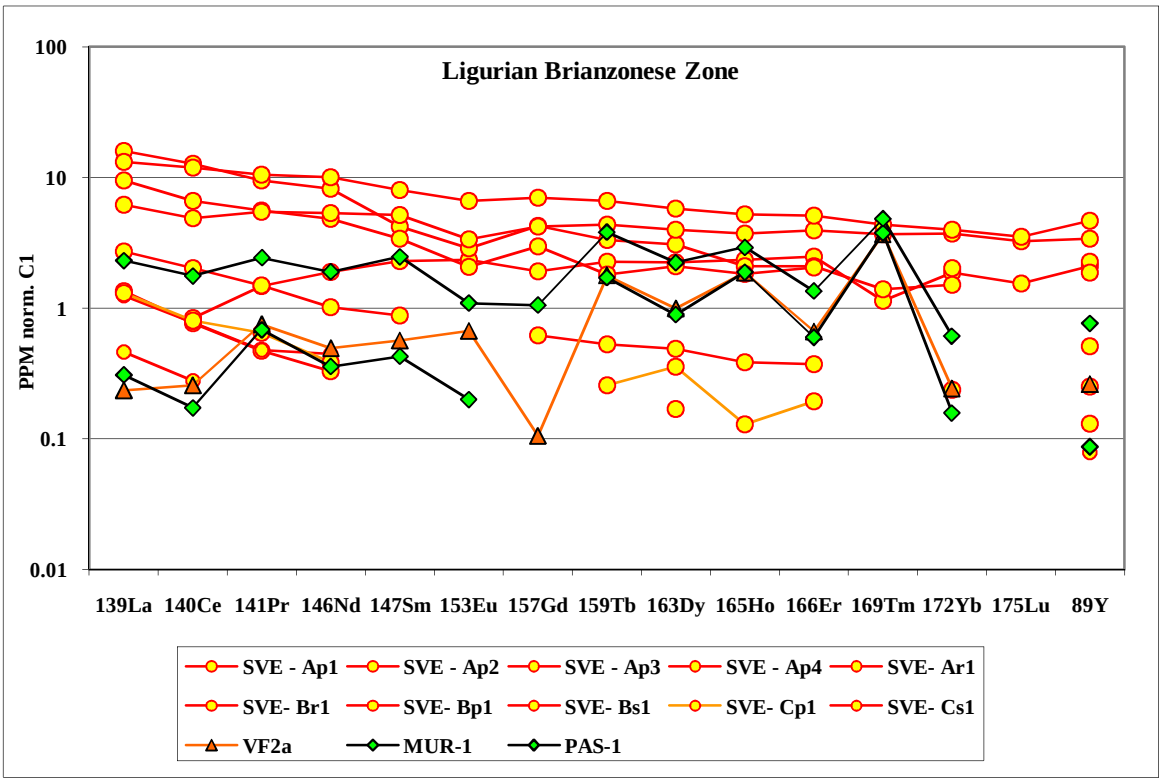
Ligurian Brianzonese Zone
PPM norm. C1
100
10
1
0.1
0.01
139La 140Ce 141Pr 146Nd 147Sm 153Eu 157Gd 159Tb 163Dy 165Ho 166Er 169Tm 172Yb 175Lu 89Y
SVE - Ap1
SVE - Ap2
SVE - Ap3
SVE - Ap4
SVE- Ar1
SVE- Br1
SVE- Bp1
SVE- Bs1
SVE- Cp1
SVE- Cs1
VF2a
MUR-1
PAS-1

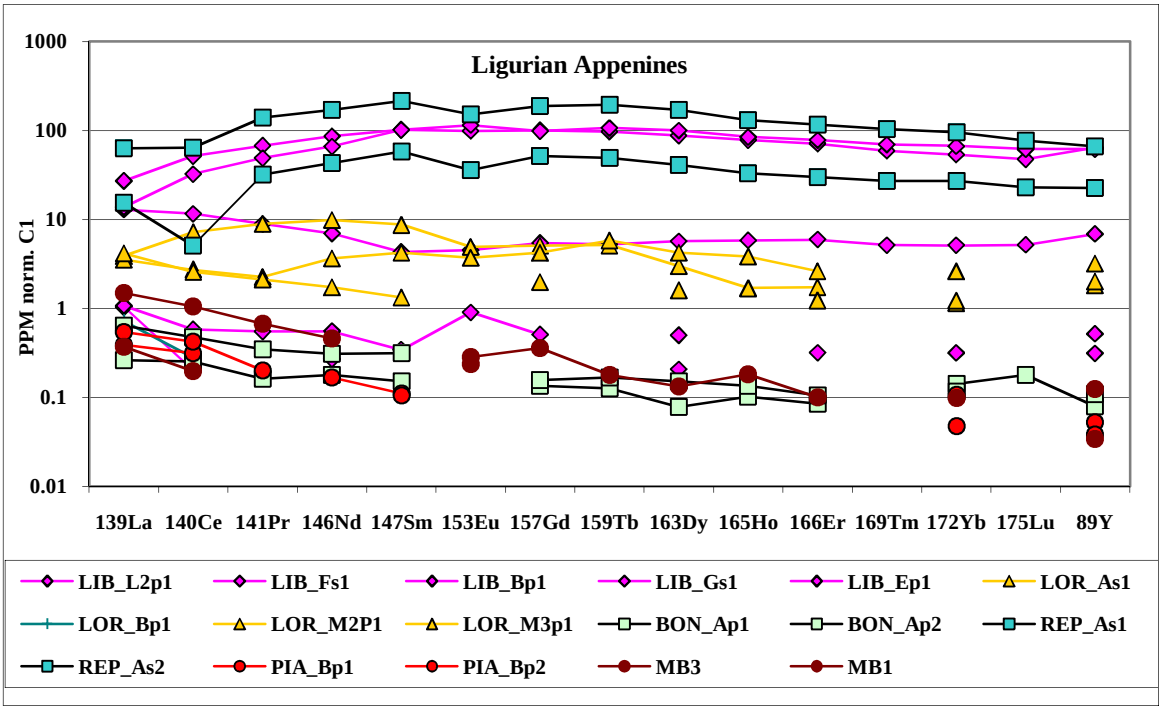
Ligurian Appenines
PPM norm. C1
1000
100
10
1
0.1
0.01
139La 140Ce 141Pr 146Nd 147Sm 153Eu 157Gd 159Tb 163Dy 165Ho 166Er 169Tm 172Yb 175Lu 89Y
LIB_L2p1
LIB_Fs1
LIB_Bp1
LIB_Gs1
LIB_Ep1
LOR_As1
LOR_Bp1
LOR_M2P1
LOR_M3p1
BON_Ap1
BON_Ap2
REP_As1
REP_As2
PIA_Bp1
PIA_Bp2
MB3
MB1

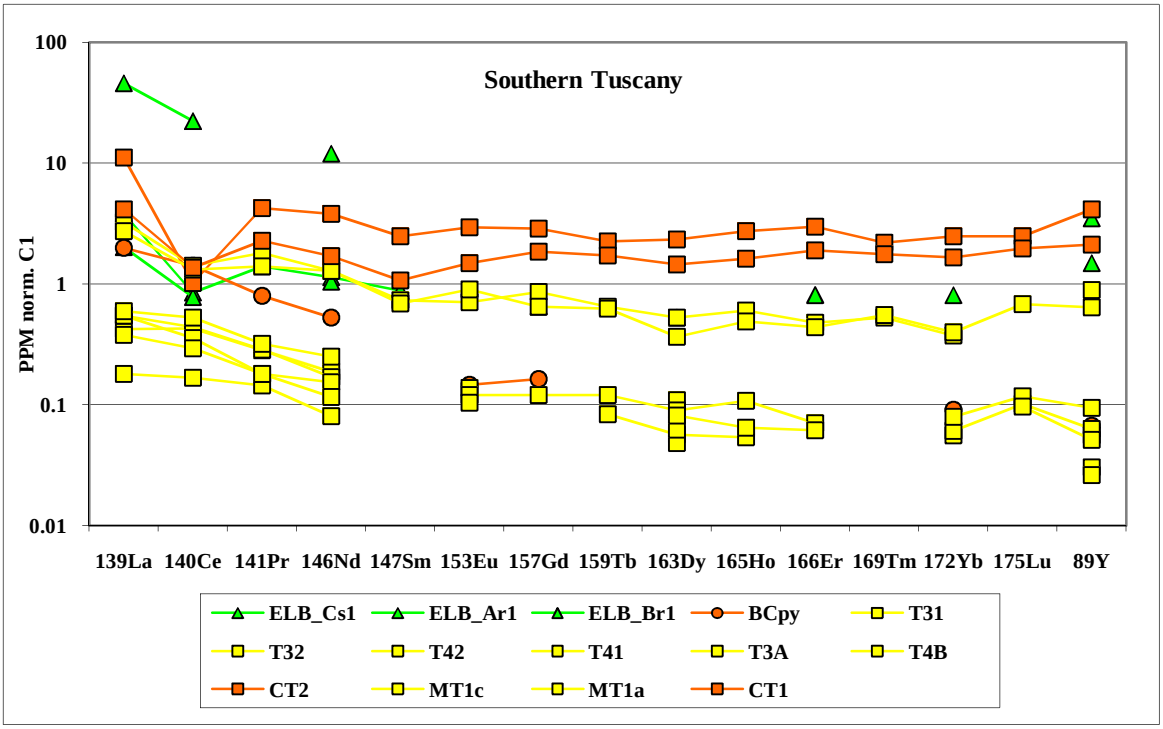
Southern Tuscany
PPM norm. C1
100
10
1
0.1
0.01
139La 140Ce 141Pr 146Nd 147Sm 153Eu 157Gd 159Tb 163Dy 165Ho 166Er 169Tm 172Yb 175Lu 89Y
ELB_Cs1
ELB_Ar1
ELB_Br1
BCpy
T31
T32
T42
T41
T3A
T4B
CT2
MT1c
MT1a
CT1

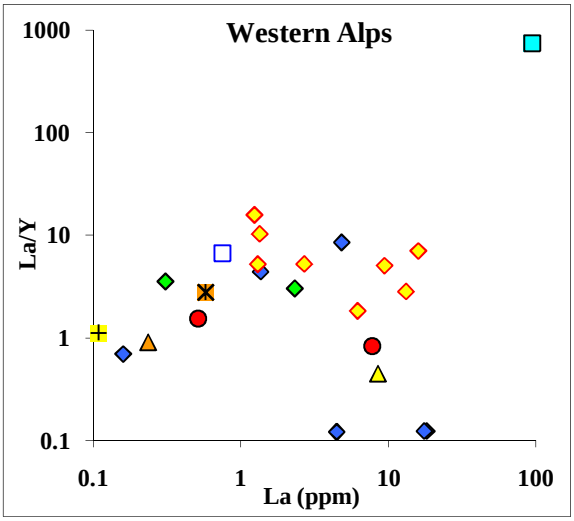
Western Alps
1000
100
10
1
0.1
La/Y
0.1
1
10
100
La (ppm)

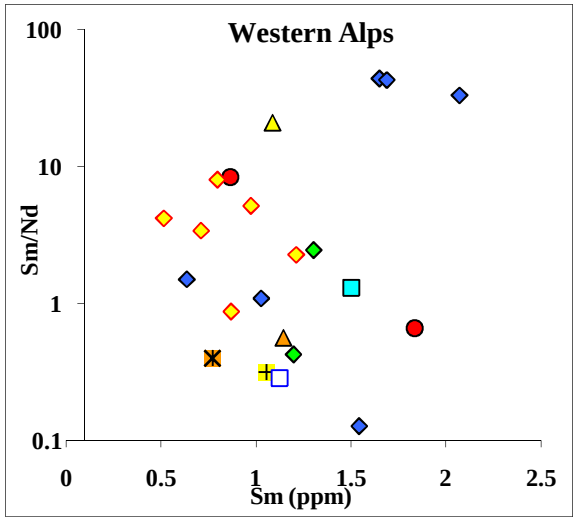
Western Alps
100
10
1
0.1
Sm/Nd
0
0.5
1
1.5
2
2.5
Sm (ppm)

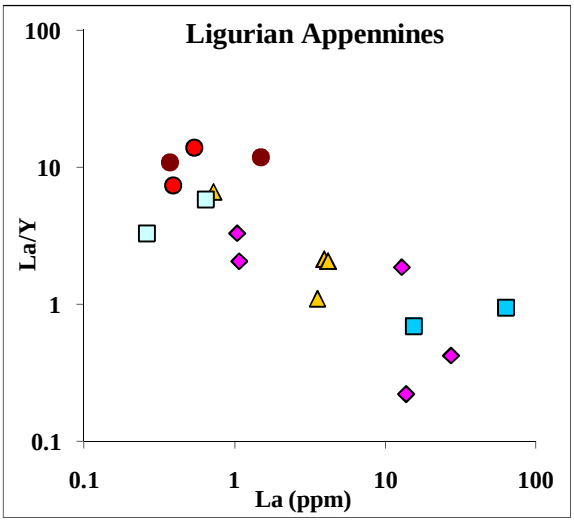
Ligurian Appennines
100
10
1
0.1
La/Y
0.1
1
10
100
La (ppm)

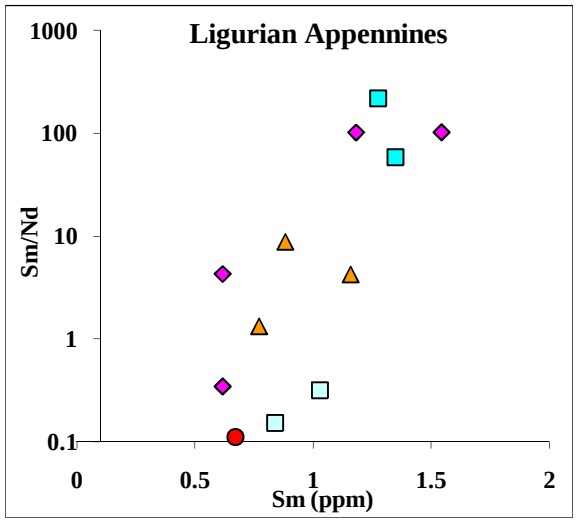
Ligurian Appennines
1000
100
10
1
0.1
Sm/Nd
0
0.5
1
1.5
2
Sm (ppm)

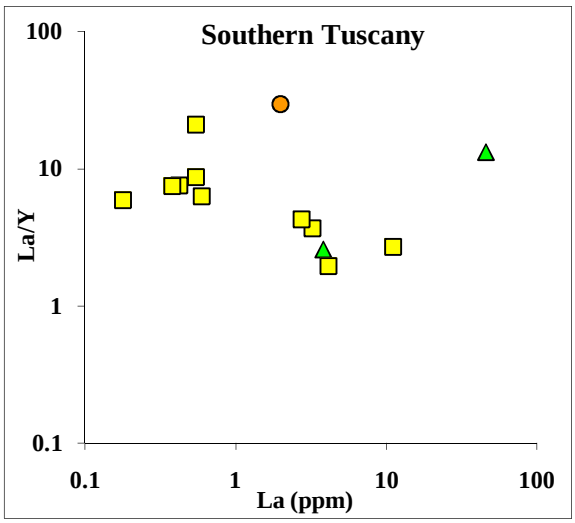
Southern Tuscany
100
10
1
0.1
La/Y
0.1
1
10
100
La (ppm)

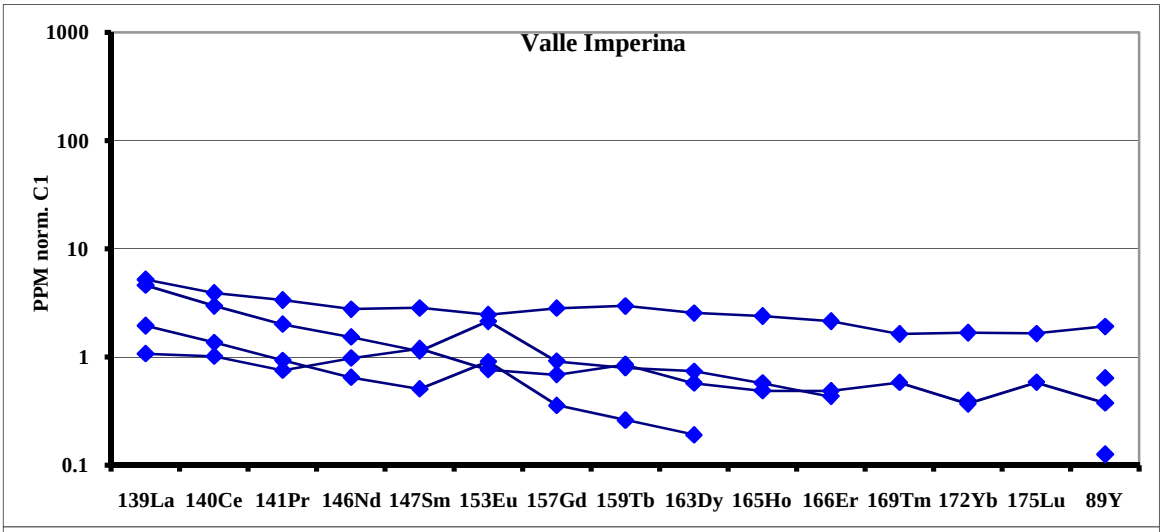
Valle Imperina
PPM norm. C1
1000
100
10
1
0.1
139La 140Ce 141Pr 146Nd 147Sm 153Eu 157Gd 159Tb 163Dy 165Ho 166Er 169Tm 172Yb 175Lu 89Y

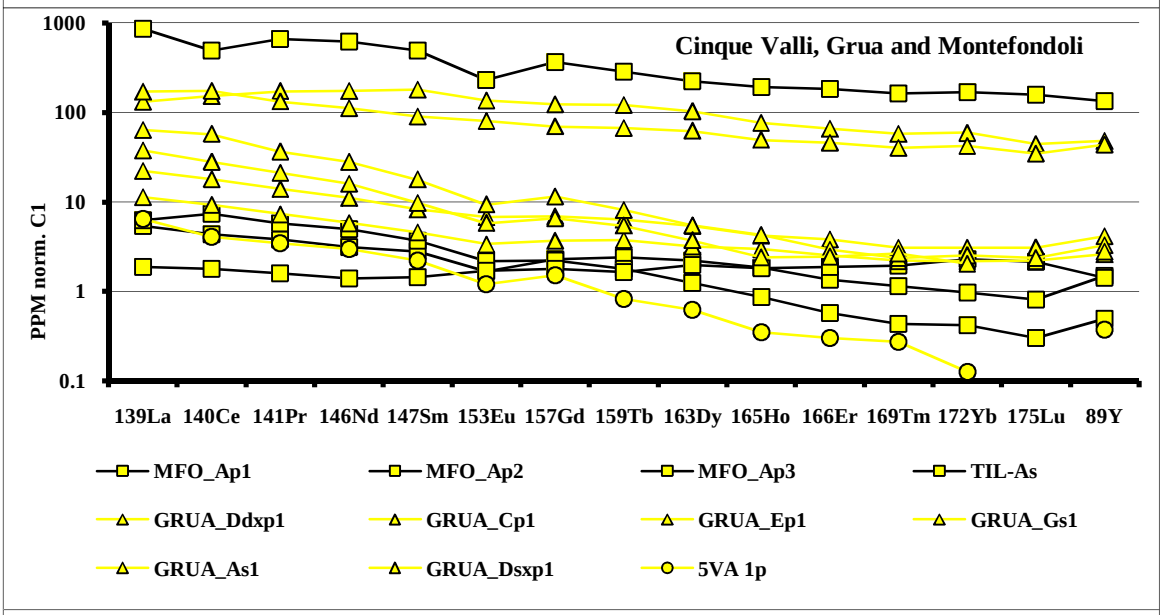
Cinque Valli, Grua and Montefondoli
PPM norm. C1
1000
100
10
1
0.1
139La 140Ce 141Pr 146Nd 147Sm 153Eu 157Gd 159Tb 163Dy 165Ho 166Er 169Tm 172Yb 175Lu 89Y
MFO_Ap1
MFO_Ap2
MFO_Ap3
TIL-As
GRUA_Ddxp1
GRUA_Cp1
GRUA_Ep1
GRUA_Gs1
GRUA_As1
GRUA_Dsxp1
5VA 1p

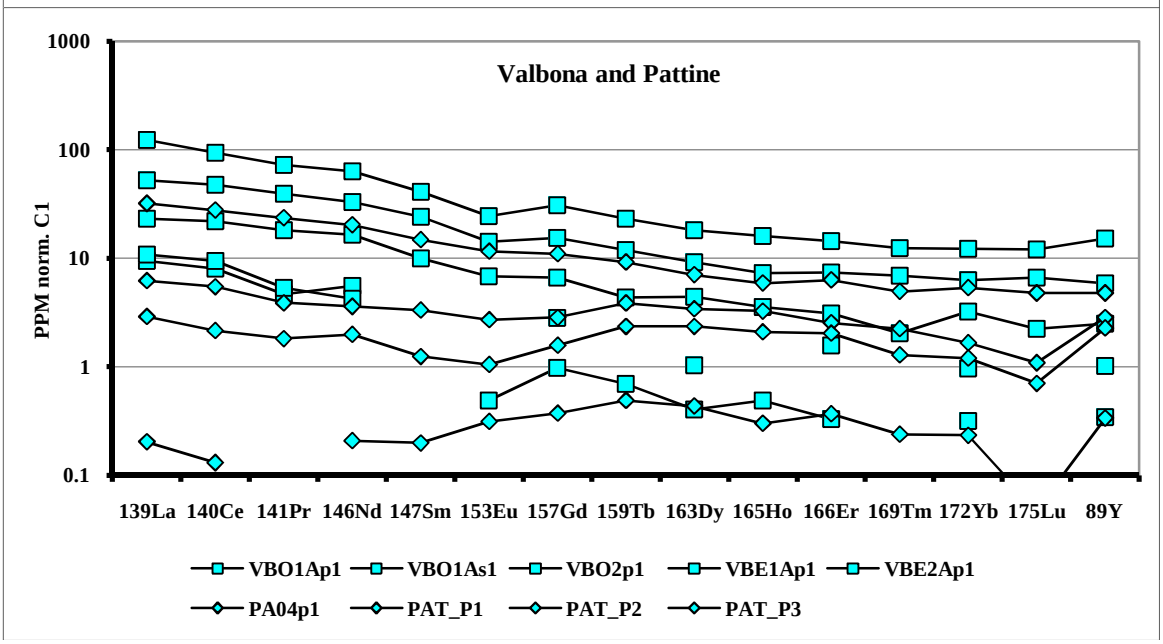
Valbona and Pattine
PPM norm. C1
1000
100
10
1
0.1
139La 140Ce 141Pr 146Nd 147Sm 153Eu 157Gd 159Tb 163Dy 165Ho 166Er 169Tm 172Yb 175Lu 89Y
VBO1Ap1
VBO1As1
VBO2p1
VBE1Ap1
VBE2Ap1
PA04p1
PAT_P1
PAT_P2
PAT_P3

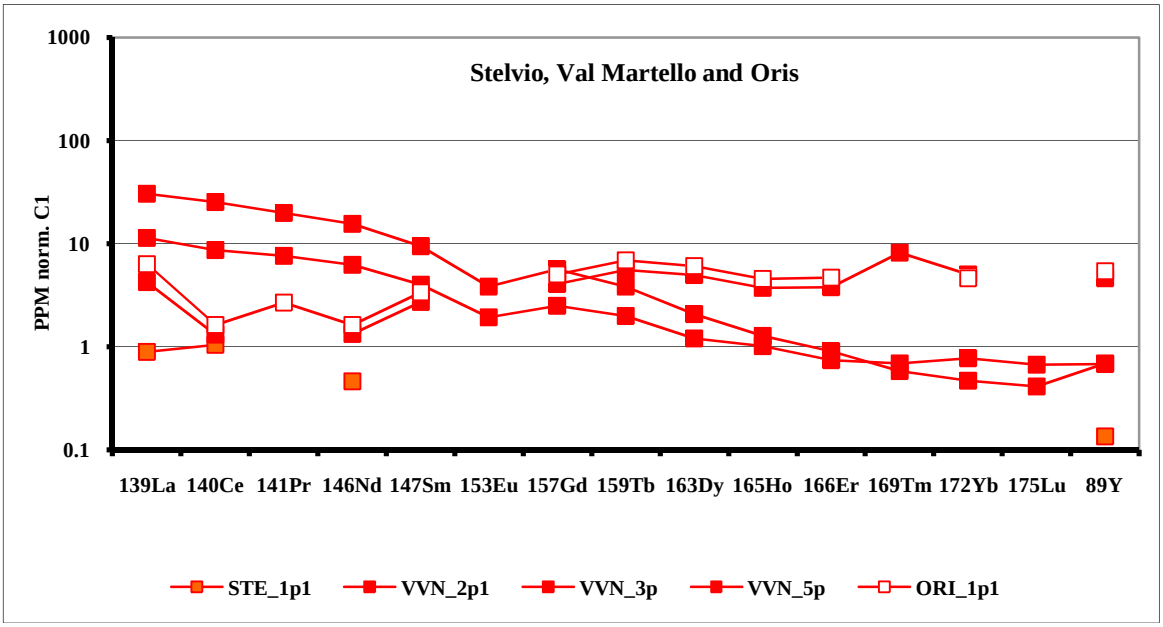
Stelvio, Val Martello and Oris
PPM norm. C1
1000
100
10
1
0.1
139La 140Ce 141Pr 146Nd 147Sm 153Eu 157Gd 159Tb 163Dy 165Ho 166Er 169Tm 172Yb 175Lu 89Y
STE_1p1
VVN_2p1
VVN_3p
VVN_5p
ORI_1p1

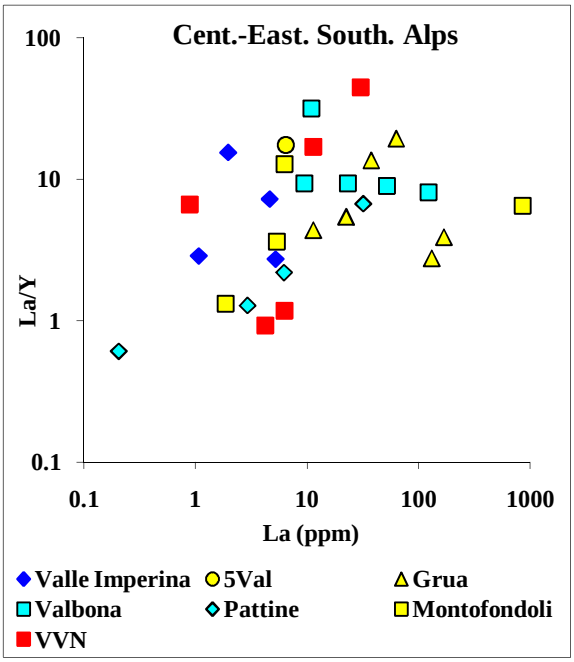
Cent.-East. South. Alps
La/Y
100
10
1
0.1
0.1 1 10 100 1000
La (ppm)
Valle Imperina
5Val
Grua
Valbona
Pattine
Montofondoli
VVN

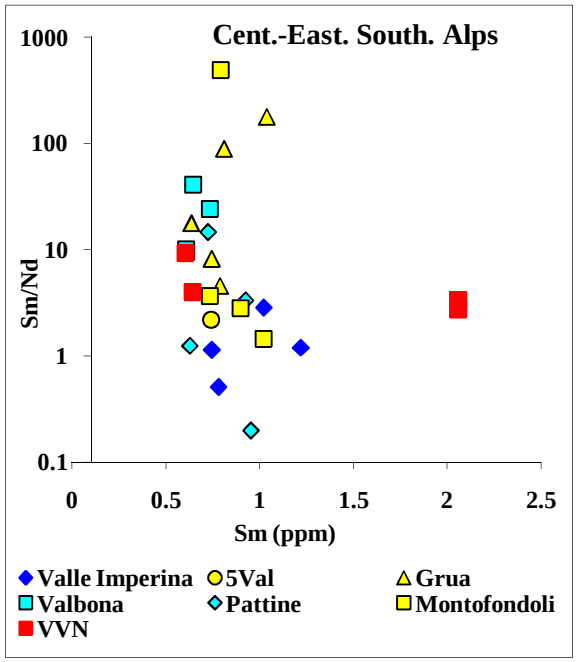
Cent.-East. South. Alps
Sm/Nd
1000
100
10
1
0.1
0 0.5 1 1.5 2 2.5
Sm (ppm)
Valle Imperina
5Val
Grua
Valbona
Pattine
Montofondoli
VVN

Bibliography

F. Albarede, P. Telouk, J. Blichert-Toft and et al, Geochim. Cosmochim. Acta, 2004, 68, 2725.

Artioli G., Baumgarten B., Marelli M., Giussani B., Recchia S., Nimis P., Giunti I., Angelini I., Omenetto P. (2008) Chemical and isotopic tracers in Alpine copper deposits: geochemical links between mines and metal. Geo. Alp. 5:139-148

D. Asael, A. Matthews, M. Bar-Matthews and L. Halicz, Chem. Geol., 2007, 243, 238.

Attanasio, D., Bultrini, G., Ingo, G.M., 2001. The possibility of provenancing: a series of bronze punic coins found at Tharros (Western Sardinia) using the literature lead isotope database. Archaeometry 43, 529–547.

Bakos F., Brondi A., Perna G. (1972) The age of mineral deposits in the Permian volcanites of Trentino-Alto Adige (northern Italy). In Proceedings 2Nd ISMIDA, Ljubljana, p. 181-194

Barnes, I. L., Gramlich, J. W., Diaz, M. G., Brill, R. H. (1978) The Possible Change of Lead Isotope Ratios in the Manufacture of Pigments: A Fractionation Experiment. Archaeological Chemistry—II 1978, 273-277

BAUDIN, T., MARQUER, D. & PERSOZ, F. 1993: Basement-cover relationships in the Tambo nappe (Central Alps, Switzerland): geometry, structure and kinematics. J. Struct. Geol. 15, 543–553
Benvenuti M., Mascaro I., Corsini F., Lattanzi P., Parrini P., Tanelli G. (1997). Mine waste dumps and heavy metal pollution in abandoned mining district of Boccheggiano (Southern Tuscany, Italy). Environmental
Geology 30, 238-243.

Bianchi A., Di Colbertaldo D. (1956) “Osservazioni paragenetiche sul giacimento a rame e tungsteno della Bedovina presso Predazzo”. Rend. Soc. Min. It., Vol XII, pp. 55-65

Bonadiman C., Coltorti M., Siena F. (1994) Petrogenesis and T-fO2 estimates of Mt. Monzoni complex (central Dolomites, southern Alps): a Triassic shoshonitic intrusion in a transcurrent geodynamic setting. European Journal of Mineralogy 6:943-966

Bottino G. 1973. Studio geologico e mineralogico delle argille di Lozzolo (Biellese). Rend. Soc. it. Min. petr., 29, 19-42

Bourgarit D, Rostan P, Burger E, Carozza L, Mille B, Artioli G (2008) The beginning of copper mass production in the western Alps: the Saint-Véran mining area reconsidered. Historical Metallurgy, 42: 1-11

Brigo L. (1971) Mineralizzazioni e metallogenesi nell'area della Fillade quarzifera di Bressanone nelle Alpi Sarentine. St. Trent. Sc. Nat. A48:80-125

BRIGO L. and FERRARIO A., 1974. Le mineralizzazioni nelle ofioliti della Liguria orientale. Società Italiana Mineralogia e Petrologia. Vol. XXX (1), Milano, 305-316

Brigo, L., Dulski, P., Moller, P., Schneider, H.-J., Wolter, R., 1988. Stratabound mineralizations in the Carnic AlpsrItaly. In: Boissonnas, J., Omenetto, P. ŽEds.., Mineral Deposits Within the European Community. Springer, Berlin, pp. 485–498.

Brigo, L. Camana G., Roeghiero F., Potenza R., 2001. Carbonate-hosted siliceous crust type mineralization of Carnic Alps (Italy-Austria) Ore Geology Reviews 17, 199–214

Brondi A., Polizzano C., Anselmi B., Benvegnù F. (1970) Rinvenimento di una mineralizzazione a galena nelle arenarie permiane di Nalles (Bolzano). L'Industria Mineraria nel Trentino-Alto Adige, Economia Trentina 3:171-182

Brusca C. & Perna G. (1995) Inquadramento e genesi dei giacimenti di galena argentifera del Monte Calisio (Trento). In Brigo L., Tizzoni M. (Ed.) Il Monte Calisio e l'Argento Nelle Alpi Dall'Antichità Al XVIII Secolo. Atti Del Convegno Europeo Promosso e Organizzato Dai Comuni Di Civezzano e Fornace e Dalla SAT Società Alpinisti Trentini - Sezione Di Civezzano, Civezzano-Fornace (Trento), p. 19-30

Brusca C., Dessau G., Lery Jensen M., Perna G. (1972) The deposits of argentiferous galena within the Bellerophon Formation (Upper Permian) of the Southern Alps. In Proc. 2nd Int. Symp. Min. Dep. Alps, Ljubljana, p. 159-179

CARON, CH., HOMEWOOD, P. & WILDI, W. 1989: The original Swiss flysch: a reappraisal of the type deposits in the Swiss Prealps. Earth-Science Re- views 26, 1–45.

Cavinato A. (1968) Ricerche minerarie nelle Alpi Bellunesi. In Atti Della Giornata Di Studi Geominerari, 7 Ottobre 1967, Centenario Dell'Istituto Tecnico Industriale Minerario Statale «U. Follador», Agordo, p. 43-62

Chiarantini, L., 2005. Approccio integrato con traccianti multipli allo studio archeometallurgico di antichi siti di estrazione e trattamento di minerali metalliferi della Toscana meridionale. Unpublished PhD thesis, Università degli Studi di Firenze, Florence.

E. Ciceri, S. Recchia, C. Dossi and et al, Talanta, 2008, 74, 642

Costantini A, Elter FM, Pandeli E, Pascucci V, Sandrelli F and Tognani M (1994) Geology of the Boccheggiano and Serrabottini area (Grosseto). Mem Soc Geol Ital 48 :73–78

Cui, J. & Wu, X., 2010. An experimental investigation on lead isotopic fractionation during metallurgical processes . *Archaeometry* *no. doi: 10.1111/j.1475-4754.2010.00548.x *Received 19 September 2009; accepted 19 April 2010

Cumming, G. L. and Richards, J. R. (1975). Ore lead isotope ratios in a continuously changing Earth. Earth Planet. Sci.Lett. 28, 155–71.

Dal Piaz G. & Martin S. (1998) Evoluzione litosferica e magmatismo nel dominio Austro-Sudalpino dall'orogenesi varisica al rifting mesozoico. Mem. Soc. Geol. It. 53:43-62

P. L. Davies, Fresenius' Z. Anal. Chem., 1988, 331, 513.
Dessau G. & Perna G. (1966) Le mineralizzazioni a galena e blenda nel Trentino-Alto Adige e loro contenuto in elementi accessori. Atti del Symposium Internazionale sui Giacimenti Minerari delle Alpi 3:587-687

Dickin A. P. (2005) Radiogenic isotope geology 2nd Edition. Cambridge. Cambridge University Press, pp 100-131

Dieni I., Giordano D., Loydell D.K., Sassi F.P. (2005) Discovery of Llandovery (Silurian) graptolites and probable Devonian corals in the Southalpine Metamorphic Basement of the Eastern Alps (Agordo, NE Italy). Geol. Mag. 142:1-5

Doe, B. R. and Stacey, J. S. (1974). The application of lead isotopes to the problems of ore genesis and ore prospect evaluation: a review. Econ. Geol. 69, 757–76.

Doglioni C. (1987) Tectonics of the Dolomites (Southern Alps, Northern Italy). J. Struct. Geol. 9:181-193

ESCHER, A., J.C. HUNZIKER, M. MARTHALER, H. MASSON, M. SARTORI & A. STECK 1997: Geologic framework and structural evolution of the western Swiss-Italian Alps. In: PFIFFNER A.O. et al. (Eds.): Deep Structure of the Swiss Alps: Results From NRP 20. Birkhäuser, Basel, Switzerland, 205–221.

Faure, G. (1986). The isotope geology of lead. Principles of isotope geology. New York, JohnWiley and sons**:** 309-340.

Fellerer R. (1968) Geologische und lagerstättenkundliche Untersuchungen zwischen Passo Cereda und Forcella Aurine (südliche Pala-Gruppe/Norditalien). Inaug.-Dissert. Universität München, 73 p.

Franceschi, E., A. Del Lucchese, D. Palazzi, M. Rossi. (1997). Aspects of metallurgical activity in Liguria (Italy). The middle and the Late Bronze Age. – J. Thermal Analysis, 49, 1593-1600

FRISCH, W., GOMMERINGER, K., KELM, U. & POPP, F. 1989: The Upper Bünd- ner Schiefer of the Tauern Window – A key to understanding Eoalpine orogenic processes in the Eastern Alps. In: FLÜGEL, W. & FAUPL P. (Eds.): Geodynamics of the Eastern Alps. Deuticke, Vienna, 55–69.

Frizzo P. (2004a) Il distretto metallifero dell'alta Valsugana. In Passardi P., Zammatteo P. (Ed.) Le Miniere Del Mandola in Valsugana, Monografie I Mus. Trid. Sci. Nat., p. 131-155

Frizzo P. & Ferrara E. (1994) I giacimenti a solfuri massivi del Distretto Agordino-Valsuganese (basamento sudalpino). Alpi Orientali. In Giornata Di Studio in Ricordo Del Prof. Zucchetti, Torino 12 Maggio 1994,. Politecnico di Torino, p. 147-156

GALE, N.H., 2009. A response to the paper of A.M. Pollard: what a long, strange trip it's been: lead isotopes and archaeology. In: From mine to microscope. Edited by A.J. Shortland, I.C. Freestone and T. Rehren. Short Run Press, Exeter, UK. 191-196

GALE, N.H. & STOS-GALE, Z. 2000. Lead isotope analyses applied to provenance studies. - In: Ciliberto, E. Spoto, G. (eds). Modern analytical methods in art and archaeology. New York, 503-584.

GEBAUER, D. 1999: Alpine geochronology of the Central and Western Alps: new constraints for a complex geodynamic evolution. Schweiz. Mineral. Petr. Mitt. 79, 191–208.
Glodny, J., Ring, U., Kühn, A., Gleissner, P., Franz, G.2005. Crystallization and very rapid exhumation of the youngest Alpine eclogites (Tauern Window, Eastern Alps) from Rb/Sr mineral assemblage analysis. *Contributions to Mineralogy and Petrology*, 149(6), pp.699-712.

GOUFFON, Y. 1993: Géologie de la nappe du Grand Saint-Bernard entre le Val de Bagnes et la frontière Suisse (Vallée d'Aoste, Italie). Mém. Géol. Lau- sanne 12, 1–147.
Faure, G. & Mensing T.M. (2005) Isotopes: Principles And Applications, 3rd Edition. New York, John Wiley and sons, pp. 214-281

Feldmann I, Jakubowski N, Thomas C, Stuewer D (1999) Application of a hexapole collision and reaction cell in ICP-MS Part II: Analytical figures of merit and first applications. Fresenius, J Anal Chem 365, 422

FINETTI, I.R., BOCCALETTI, M., BONINI, M., DEL BEN, A., GELETTI, R., PIPAN, M. & SANI, F. 2001: Crustal section based on CROP seismic data across the North Tyrrhenian – Northern Apennines – Adriatic Sea. Tectono- physics 343: 135–163.

Frisch W, Dunkl I, Kuhlemann J (2000) Post-collisional orogen- parallel large-scale extension in the Eastern Alps. Tectono- physics 327:239–265
HAUPTMANN, A. 2007. The archaeometallurgy of Copper. Springer, Berlin.

IXER, R.A. 1999. The role of ore geology and ores in archaeological provenancing of metals. In: S.M.M. Young, A.M. Pollard, P.Budd, R.A. Ixer, Metals in Antiquity. BAR International Series n. 792. Archaeopress, Oxford, UK, 43-52.

Holmes, A. (1946). An estimate of the age of the Earth. Nature 157, 680–4.

Houtermans, F.G., (1946). Die Isotopenhäufigkeiten im natürlichen Blei und das Alter des Urans. *Naturwissenschaften*, 33(6), pp.185-186.

Jaffey, A. H., Flynn, K. F., Glendenin, L. E., Bentley, W. C. and Essling, A. M. (1971). Precision measurement of the half-lives and specific activities of U235 and U238. Phys. Rev.C4, 1889–907.

Kalvacheva R., Sassi F.P., Zanferrari A. (1986) Acritarch evidence for the Cambrian age of phyllites in the Agordo area (South-alpine basement of eastern Alps, Italy). Rev. Palaeobot. Palynol. 48:311-326

KELLER, L.M. & SCHMID, S.M. 2001: On the kinematics of shearing near the top of the Monte Rosa nappe and the nature of the Furgg zone in Val Lo- ranco (Antrona valley, N. Italy): tectonometamorphic and paleogeo- graphical consequences. Schweiz. Mineral. Petr. Mitt. 81, 347–367.

KERKHOVE, C. 1969: La zone du flysch dans les nappes de l'Embrunais-Ubaye. Géol. Alpine 45, 5–204.

Kramers J.D. & Tolstikhin I. N. (1997). Two terrestrial lead isotope paradoxes , forward transport modelling , core formation and the history of the continental crust. *Chemical Geology* 139: 75-110

KURZ, W., NEUBAUER, F. & DACHS, E. 1998: Eclogite meso- and microfabrics: implications for the burial and exhumation history of eclogites in the Tauern Window (Eastern Alps) from P-T-d paths. Tectonophysics 285, 183–209.

P. B. Larson, K. Maher, F. C. Ramos and et al, Chem. Geol., 2003, 201, 337.

Laubscher 1971: The large-scale kinematics of the Western Alps and the northern Apennines and its palinspastic implications. Am. J. Science 271, 193–226.

Lucchini F., Rossi P.M., Simboli G., Cristofolini R. (1982) Confronto geochimico fra i prodotti magmatici basici del Trias-Giura nell'area Tetidea. In Castellarin A., Vai G.B. (Ed.) Guida Alla Geologia Del Sudalpino Centro-Orientale. Guide Geologiche Regionali. Soc. Geol. It., p. 133-141
Macfarlane, A., 1999, The lead isotope method for tracing the sources of metal in archaeological artifacts: strengths, weaknesses and applications in theWestern Hemisphere, in *Metals in antiquity* (eds. S. M. M. Young, A. M. Pollard, P. Budd and R. A. Ixer), 310–16, Bar International Series 792, Archaeopress, Oxford.

MANATSCHAL, G. & NIEVERGELT, P. 1997: A continent-ocean transition recorded in the Err and Platta nappes (Eastern Switzerland). Eclogae Geol. Helv. 90, 3–27.

C. N. Marechal, P. Telouk and F. Albarede, Chem. Geol., 1999, 156, 251.

Marcoux, E. (1986). Isotopes du plomb et paragenèses métalliques, traceurs de l'histoire des gîtes français. Applications en recherche minière. BRGM unpublished document.

MARRONI, M., MOLLI, G., OTTIA, G., PANDOLFI, L., TRIBUZIO, R. 2002: The External Ligurian Units (Northern Apennine, Italy): From rifting to con- vergence of a fossil ocean-continent transition zone. Ofioliti 27, 119–132.

Mastrangelo F., Natale P., Zucchetti S., 1975. Liguria, in Memoria illustrativa della carta mineraria d'Italia. 71-77

Mathur, S. Titley, F. Barra and et al, J. Geochem. Explor., 2009,102, 1.

Maucher A. (1955) Erzmikroskopische Untersuchungen an Blei-Zink-Lagerstätten im Raume von Trento (Norditalien). Mitt. Geol. Ges. Wien 48:131-140

P. C. Meier and R. E. Zünd, Statistical Methods in Analytical Chemistry, Wiley-Interscience, 2000

Meli S. & Klötzli U.S. (2001) Evidence for Lower Paleozoic magmatism in the Eastern Southalpine basement: zircon geochronology from Comelico porphyroids. Schweiz. Mineral. Petrograph. Mitt. 81:147-157

T. J. Murphy, E. L. Garner and W. R. Shields, J. Res. Nat. Bur. Stand., 1964, 68A, 386.

Neubauer, F., Genser, J., Kurz, W., and Wang, X., 1999, Exhumation of the Tauern Window, Eastern Alps: Physics and Chemistry of the Earth, ser. A, v. 24, p. 675–680.

OBERHÄNSLI, R. 1978: Chemische Untersuchungen an Glaukophan-führenden basischen Gesteinen aus den Bündnerschiefern Graubündens. Schweiz. Mineral. Petrogr. Mitt. 58, 139–156.

Omenetto P. (1968a) Le risorse minerarie della regione di Belluno. In Atti Della Giornata Di Studi Geominerari, 7 Ottobre 1967, Centenario Dell'Istituto Tecnico Industriale Minerario Statale «U. Follador», Agordo, p. 31-42

Omenetto P. (1968b) Il giacimento ferrifero della Pamera, presso Roncegno (Valsugana). Mem. Ist. Geol. Min. Univ. Padova 26:38

Omenetto P. & Brigo L. (1974) Metallogenesi nel quadro dell'orogene ercinico delle Alpi (con particolare riguardo al versante italiano). Mem. Soc. Geol. It. 13:1-24

Oversby, V.M. (1974). A new look at the lead isotope growth curve. Nature 248, 132–3.

POLLARD A.M., 2009. What a long, strange trip it's been: lead isotopes and archaeology. In: From mine to microscope. Edited by A.J. Shortland, I.C. Freestone and T. Rehren. Short Run Press, Exeter, UK. 191

PERNICKA, E. 1999. Trace element fingerprinting of ancient copper: a guide to technology or provenance? In: S.M.M. Young, A.M. Pollard, P.Budd, R.A. Ixer, Metals in Antiquity. BAR International Series n. 792. Archaeopress, Oxford, UK, 163-171.

Pesarin, F. 2001. Multivariate Permutation Tests With Applications in Biostatistics, Wiley, Chichester.

RENFREW, C. & BAHN, P. 2000. Archaeology: Theories, methods and practice. Thames & Hudson, London.
C.L. Rosenberg, J.-P. Brun and D. Gapais, 2004. Indentation model of the Eastern Alps and the origin of the Tauern Window, Geology;32;997-1000

Rossetti PG and Ferrero S, 2008. The Zn-Pb deposits of Casario (Ligurian Alps, NW Italy): Late Palaeozoic sedimentary-exhalative bodies affected by the alpine metamorphism. Geodinamica acta. 21/3 pp.117-137

Rottura A., Bargossi G.M., Caggianelli A., Del Moro A., Visonà D., Tranne C.A. (1998) Origin and significance of the Permian high-K calc-alkaline magmatism in the central-eastern Southern Alps, Italy. Lithos 45:329-348

Sahl, K., Doe, B., Wedepohl, K. (1973). Lead Handbook of geochemistry. Berlin, Heidelberg, New-York, Springer-Verlag.

Sassi F.P. & Zirpoli G. (1990) The lithostratigraphic sequence in the Southalpine Basement of the Eastern Alps. In Sassi F.P., Zanferrari A. (Ed.) Pre-Variscan and Variscan Events in the Alpine-Mediterranean Belts, Rend. Soc. Geol. It., vol. 12, p. 397-402

Schmid, S.M. et al., 2004. Tectonic map and overall architecture of the Alpine orogen. *Eclogae Geologicae Helvetiae*, 97(1), pp.93-117.

Stacey, J. S., Kramers, J.D. (1975). Approximation of terrestrial lead isotope evolution by a two-stage model. Earth Planet. Sci. Lett. 26: 207-221.

Stanton, R. L. and Russell, R. D. (1959). Anomalous leads and the emplacement of lead sulfide ores. Econ. Geol. 54, 588–607.

Tanelli G (1983) Mineralizzazioni metallifere e minerogenesi della Toscana. Mem Soc Geol Ital 25:91–109

Tanelli G, Benvenuti M, Costagliola P, Dini A, Lattanzi P, Manieri C, Mascaro I, Ruggieri G (2001) The iron mineral deposits of Elba island: state of the art. Ofioliti 26(2a):239–248

G. Tanelli, P.F. Lattanzi, Metallogeny and mineral exploration in Tuscany: state of the art, Mem. Soc. Geol. Ital. 31 (1986) 299–304.

Tatsumoto, M., Knight, R. J. and All`egre, C. J. (1973). Time differences in the formation of meteorites as determined from the ratio of lead-207 to lead-206. Science 180, 1279–83.

Vecoli M., Dieni I., Sassi F., Servais T. (2008) Cambrian Acritarchs from the Col di Foglia (Agordo) southalpine metamorphic basement, Italian Eastern Alps: the oldest biostratigraphic record in the alps. Rendiconti Lincei 19:45-55

Villa, I.M., 2009. Lead isotopic measurements in archeological objects. Archaeological and Anthropological Sciences, 1(3), 149-153.

Visonà D. (1997) The Predazzo multipulse intrusive body (Western Dolomites, Italy). Field and mineralogical studies. Mem. Sc. Geol. 49:117-125

Wopfner H., Griesecke S., Koch J., Fels H. (1983) New aspects on metal deposits of the Groeden Sandstone (South Tyrol, Italy). In Schneider H.-. (Ed.) Mineral Deposits of the Alps and of the Alpine Epoch in Europe. Springer-Verlag, Berlin Heidelberg New York Tokio, p. 60-69

Zanella M. & Brigo L. (1997) Le mineralizzazioni argentifere nello Scitico a nord di M. Calisio (Trento, Italia): relazioni fra assetto paleogeografico e chimismo. In Brigo L., Tizzoni M. (Ed.) Atti Convegno Europeo “Il M. Calisio e l’argento Nelle Alpi dall’antichità Al XVIII Secolo. Giacimenti, Storia e Rapporti Con La Tradizione Mineraria Mitteleuropea”, 12-14 Ottobre 1995. Comune di Civezzano, Comune di Fornace, p. 31-41

X. K. Zhu, R. K. O’Nions, Y. Guo and et al, Chem. Geol., 2000, 163,139.